Advances in Clinical and Experimental Medicine

MONTHLY ISSN 1899-5276 (PRINT) ISSN 2451-2680 (ONLINE) www.advances.umed.wroc.pl

2020, Vol. 29, No. 11 (November)

Impact Factor (IF) – 1.514
Ministry of Science and Higher Education – 40 pts.
Index Copernicus (ICV) – 155.19 pts.

Wroclaw Medical University

Advances
in Clinical and Experimental
Medicine

Advances
in Clinical and Experimental Medicine

ISSN 1899-5276 (PRINT) ISSN 2451-2680 (ONLINE) www.advances.umed.wroc.pl

MONTHLY 2020
Vol. 29, No. 11
(November)

Advances in Clinical and Experimental Medicine is a peer-reviewed open access journal published by Wroclaw Medical University. Its abbreviated title is Adv Clin Exp Med. Journal publishes original papers and reviews encompassing all aspects of medicine, including molecular biology, biochemistry, genetics, biotechnology, and other areas. It is published monthly, one volume per year.

Editorial Office
ul. Marcinkowskiego 2–6
50-368 Wrocław, Poland
Tel.: +48 71 784 11 36
E-mail: redakcja@umed.wroc.pl

Publisher
Wroclaw Medical University
Wybrzeże L. Pasteura 1
50-367 Wrocław, Poland

Online edition is the original version of the journal

Editorial Policy

Advances in Clinical and Experimental Medicine (Adv Clin Exp Med) is an independent multidisciplinary forum for exchange of scientific and clinical information, publishing original research and news encompassing all aspects of medicine, including molecular biology, biochemistry, genetics, biotechnology and other areas. During the review process, the Editorial Board conforms to the "Uniform Requirements for Manuscripts Submitted to Biomedical Journals: Writing and Editing for Biomedical Publication" approved by the International Committee of Medical Journal Editors (www.ICMJE.org/). The journal publishes (in English only) original papers and reviews. Short works considered original, novel and significant are given priority. Experimental studies must include a statement that the experimental protocol and informed consent procedure were in compliance with the Helsinki Convention and were approved by an ethics committee.

For all subscription-related queries please contact our Editorial Office:
redakcja@umed.wroc.pl

For more information visit the journal's website:
www.advances.umed.wroc.pl

Pursuant to the ordinance No. 134/XV R/2017 of the Rector of Wroclaw Medical University (as of December 28, 2017) from January 1, 2018 authors are required to pay a fee amounting to 700 euros for each manuscript accepted for publication in the journal Advances in Clinical and Experimental Medicine.

„Podniesienie poziomu naukowego i poziomu umiędzynarodowienia wydawanych czasopism naukowych oraz upowszechniania informacji o wynikach badań naukowych lub prac rozwojowych – zadanie finansowane w ramach umowy 784/p-DUN/2017 ze środków Ministra Nauki i Szkolnictwa Wyższego przeznaczonych na działalność upowszechniającą naukę".

Indexed in: MEDLINE, Science Citation Index Expanded, Journal Citation Reports/Science Edition, Scopus,
EMBASE/Excerpta Medica, Ulrich's™ International Periodicals Directory, Index Copernicus

Typographic design: Monika Kolęda, Piotr Gil
DTP: Wydawnictwo UMW
Cover: Monika Kolęda
Printing and binding: EXDRUK

Advances
in Clinical and Experimental Medicine

MONTHLY 2020, Vol. 29, No. 11 (November)

ISSN 1899-5276 (PRINT)
ISSN 2451-2680 (ONLINE)
www.advances.umed.wroc.pl

Contents

Original papers

MicroRNA-451 increases vascular permeability and suppresses angiogenesis in pulmonary burn injury in a rat model

*Jie Zhou[1,B,D], *Huibin Lian[2,B,C], Gang Xu[1,A,F], Tianlan Zhao[1,B,C]

[1] Department of Plastic and Cosmetic Surgery, Second Affiliated Hospital of Soochow University, China
[2] Burns and Plastic Surgery, Northern Jiangsu People's Hospital, Yangzhou, China

A – research concept and design; B – collection and/or assembly of data; C – data analysis and interpretation; D – writing the article; E – critical revision of the article; F – final approval of the article

Advances in Clinical and Experimental Medicine, ISSN 1899–5276 (print), ISSN 2451–2680 (online) *Adv Clin Exp Med*. 2020;29(11):1241–1248

Address for correspondence
Tianlan Zhao
E-mail: ztl1965@163.com

Funding sources
The hospital-level Project of Northern Jiangsu People's Hospital (project No. yzucms201322).

Conflict of interest
None declared

*Jie Zhou and Huibin Lian contributed equally to this work.

Received on February 17, 2020
Reviewed on June 8, 2020
Accepted on August 11, 2020

Abstract

Background. Burns are common traumas that cause systemic symptoms by increasing vascular permeability.

Objectives. To investigate the role of miRNA-451 and to clarify the underlying mechanism of the burn process.

Material and methods. We established a heat-induced third-degree burn with acute lung injury (ALI) model in rats. Hematoxylin and eosin (H&E) staining and in situ hybridization were performed. Overexpressed miRNA-451 in human umbilical vascular endothelial cells (HUVEC) were carried out. The migration and proliferation of HUVEC cells were examined.

Results. The H&E staining showed that the burn injury caused by heat went through the dermis and damaged deep tissues. Meanwhile, the heat also induced acute lung injury, characterized by inflammatory exudation in the alveoli and significant enlargement of the alveolar septum. In situ hybridization showed that the expression of miRNA-451 increased in the lung endothelial cells. We overexpressed miRNA-451 in human umbilical vascular endothelial cells (HUVEC) and the results showed that miRNA-451 inhibited the migration and proliferation of HUVEC cells, increased HUVEC cell permeability, inhibited cell adhesion, and induced cell apoptosis. Furthermore, the expression of occludin and ZO-1, 2 key protein molecules in forming tight junction between cells, decreased, and the proteins dispersed in the cytoplasm of HUVEC cells.

Conclusions. MiRNA-451 was upregulated in the lung endothelial cells of the rat model, and contributed to increase lung endothelial cell permeability. It suppresses angiogenesis of lung endothelial cells, indicating their potential as a target in the treatment of burn injuries.

Key words: angiogenesis, burn, endothelial cell, miRNA-451, hyperpermeability

Cite as
Zhou J, Lian H, Xu G, Zhao T. MicroRNA-451 increases vascular permeability and suppresses angiogenesis in pulmonary burn injury in a rat model. *Adv Clin Exp Med*. 2020;29(11):1241–1248. doi:10.17219/acem/126299

DOI
10.17219/acem/126299

Introduction

A burn is a type of injury caused by heat, cold, electricity, chemicals, or radiation to the skin or other tissues.[1] According to the severity of damage to the skin and tissues, burns are divided into 4 types: first-, second-, third-, and fourth-degree burns. One of the physiological characteristics of burns is increased vascular permeability associated with massive release of inflammatory mediators, resulting in immediate and continuous loss of substances ranging from water to macromolecules.[2] This leads to the reduction of blood volume and insufficient blood supply to important organs, such as heart, brain and kidneys. Severe burn is always accompanied by infection, shock and inhalation injury, which may be associated with acute lung injury (ALI). The severe stage of ALI, known as acute respiratory distress syndrome (ARDS), has a high fatality rate. It is important to investigate related molecular mechanisms of vascular hyperpermeability in burn injury in order to develop effective therapeutics.

MicroRNAs (miRNAs) are a group of small non-coding RNA molecules that function in post-transcriptional regulation of gene expression.[3] Recently, the role of miRNAs in regulating the function of endothelial cells has attracted great interests. Son et al. found that murine-specific miRNA-712 is a flow-sensitive microRNA, which is upregulated by disturbed flow in arterial endothelium both in vitro and in vivo. This miRNA activated matrix metalloproteinases (MMP2 and MMP9) and induced endothelial cell inflammation and hyperpermeability.[4] MiRNA-663 is an oscillatory shear (OS)-sensitive miRNA in human umbilical vein endothelial cells (HUVECs), and is involved in OS-induced cellular inflammation by mediating the expression of inflammatory genes. Oscillatory shear-induced monocyte adhesion was blocked by treating HUVECs with miRNA-663 inhibitor.[5] Thus, miRNAs are potential targets for the treatment of vascular dysfunctions during the burn process.

In this study, we established a heat-induced third-degree burn model in rats and detected the expression of miRNA-451 in lung endothelial cells. In order to discover the effects of miRNA-451 on the permeability and angiogenesis of vascular endothelial cells, we upregulated and downregulated miRNA-451 through transfecting miRNA-451 mimic or inhibitor into HUVECs. Phenotypic change of cells, including cell proliferation, cell adhesion, cell migration, and cell apoptosis, in different groups of HUVECs cultured with or without serum from rats in different burn groups were examined. Moreover, we evaluated the change of expression of ZO-1 and occludin, which are very common tight junction associated proteins. Damaged tight junctions will cause increased permeability.[6]

Material and methods

Animals and groupings

The animal experiments were conducted according to the protocols approved by the Animal Experimental Ethics Committee of the Second Affiliated Hospital of Soochow University, China. Healthy male adult Sprague–Dawley (SD) rats were purchased from Shanghai SLCA Laboratory Animal Ltd. (Shanghai, China). The weight of rats ranged from 300 g to 350 g. Eighteen rats were randomly separated into 3 groups: burn group, sham burn group and control group, with 6 rats in each group. The back hair of the rats in the burn group and sham burn group were shaved under anesthesia (urethane, 5 mg/kg body weight). Then, the nude skin of the burn group was scalded with 95°C hot water for 18 s, which caused a third-degree burn consisting nearly 30% of total body surface area (TBSA), while the nude skin of sham burn group was exposed to 37°C water for the same time. After that, the rats from the burn group were injected with physiological saline solution following the Parkland formula (4 mL/kg/1% TBSA). All the rats were kept in individual cages and allowed free access to food and water.

Hematoxylin and eosin staining

Skin and lung samples were collected 12 h after burn and fixed with 4% neutral-buffered formalin for 24 h. After dehydration and embedding, the samples were cut into sections of 3 μm in thickness. The sections were stained with hematoxylin and eosin (H&E).

Colloid osmotic pressure measurements

The plasma samples from each group were collected at different time points: 60 min before burn, and 0 min, 30 min, 60 min, 90 min, 120 min, and 180 min after burn. Colloid osmotic pressure was analyzed using a micro-colloid osmometer (Wescor 4420; Wescor, Logan, USA) with a semipermeable membrane, which had a rejection characteristic of 30 kDa. One to 1.5 μL plasma was applied to the semipermeable membrane in each measurement. All the measurements were performed at room temperature.

Cell culture and grouping

The HUVECs were purchased from American Type Culture Collection (ATCC; Manassas, USA) and cultured in the EGM02 medium (CC03162; Lonza, Cologne, Germany). MiRNA-451 mimic and inhibitor (GenePharma, Shanghai, China) were transfected into the cells using Lipofectamine 2000 (11668027; Thermo Fisher Scientific, Waltham, USA). Then, the HUVECs were divided into 7 groups:

– group 1: cells cultured with medium supplemented with 10% FCS (Gibco, Rockville, USA);

– group 2: cells cultured with medium supplemented with 10% rat serum from burn group;
– group 3: cells cultured with medium supplemented with 10% rat serum from control group;
– group 4: cells transfected with miRNA-451 mimic and cultured with medium supplemented with 10% rat serum from burn group;
– group 5: cells transfected with scramble control for miRNA-451 mimic and cultured with medium supplemented with 10% rat serum from burn group;
– group 6: cells transfected with miRNA-451 inhibitor and cultured with medium supplemented with 10% rat serum from burn group;
– group 7: cells transfected with scramble control for miRNA-451 inhibitor and cultured with medium supplemented with 10% rat serum from burn group.

Real-time PCR

The expression of miRNA-451 in the HUVECs after transfection was examined using real-time polymerase chain reaction (RT-PCR). The total RNA of cells was isolated by lysing the cells with Trizol (15596018; Thermo Fisher Scientific) and reversed transcribed into cDNA. Real-time PCR was carried out using 2 × SYBR Premix Ex Taq (RR820A; Takara Bio, Shiga, Japan) according to the manufacturer's protocol. Primers were purchased from Sangon Biotech (Shanghai, China) as follow: forward: 5'-ACACTCCAGCTGGGAAACCGTTACCATTAC, reverse: 5'-TGGTGTCGTGGAGTCG. The relative gene expression was analyzed using the $2^{-\Delta\Delta CT}$ method.

Cell proliferation

Cell counting kit-8 assay (CCK-8; Dojindo, Kumamoto, Japan) was used to detect the proliferation of the HUVECs from each group. According to the manufacturer's protocol, 5×10^3 cells/well were seeded into 24-well plate and culture for 72 h. After culturing, CCK8 solution was added into each well and the light absorbance of each well was measured at 450 nm using a microplate reader (Multiskan FC; Thermo Fisher Scientific).

Cell apoptosis

Annexin V/PI stain and flow cytometer were used for detecting cell apoptosis. In brief, HUVECs from each group were suspended in binding buffer at a concentration of 3×10^5 and incubated with Annexin V and PI for 15 min at room temperature in the dark. Then the cells were examined with a flow cytometer (LSRFortessa; Becton Dickinson, Franklin Lakes, USA) and the results were analyzed with FlowJo software v. 7.6.1 (www.flowjo.com). The annexin V+/PI– cells and annexin V–/PI+ cells were used to identify apoptotic cells and necrotic cells, respectively. The procedure was repeated 3 times for each sample.

Scratch assay

The HUVECs from each group were culture in six-well plates and wounds were made using a 200 μL tip when cell monolayers were formed. After cell debris was removed, the cells were cultured with serum-free medium, and the wounds were observed and captured at 24 h and 48 h using an inverted light microscope (Olympus BX43; Olympus, Tokyo, Japan). Three independent experiments were performed in each group.

Cell permeability

In vitro cell permeability assay was performed as previously described.[7] In brief, HUVECs from each group were seeded into type I collagen-coated upper chambers (0.4 μm pores; Becton Dickinson) and were grown to confluence. Fifteen microliters of fluorescein isothiocyanate (FITC)-dextran (Sigma-Aldrich, St. Louis, USA) was added to the upper chamber and incubated at 37°C for 30 min. Then, fluorescence intensity in the lower chambers, which diffused from upper chambers, was measured.

Western blotting analysis

The HUVECs from each group were lysed with radioimmunoprecipitation assay buffer (RIPA). The total proteins were loaded to SDS-PAGE gel and separated with electrophoresis. Then, the proteins were transferred to the polyvinylidene fluoride (PVDF) membrane, followed by blocking with 5% non-fat milk. After that, the membrane was blotted with the primary antibodies, including occludin (sc-133256; Santa Cruz Biotechnology, Santa Cruz, USA) and ZO-1 (#5406; Cell Signaling Technology, Danvers, USA), and secondary antibodies. Chemiluminescence was used to detect the specific bands.

Statistical analyses

All the quantitative data of each experiment were expressed as the mean ±standard deviation (SD) and the variables were analyzed using one-way analysis of variance (ANOVA); the Tukey's method was used for the following multiple comparison tests. Apoptosis ratio data was evaluated with the χ^2 test. SPSS software v. 20.0 (IBM Corp., Armonk, USA) was used for all the statistical analyses. A value of $p < 0.05$ was considered to be statistically significant.

Results

Establishment of a burn model in rat

Under a microscope, the epidermis showed nuclear condensation, and necrotic hair follicles and sebaceous glands were observed in the dermis of rats in the burn group.

The lesions were in line with the characteristics of third-degree burn damage. There were no significant abnormal changes in the dermis and epidermis of rats in the sham group and the control group (Fig. 1A).

It was known that local burns could lead to acute injury to the lung by inducing the release of pro-inflammatory cytokines.[7] We collected the lung tissues from rats in each group and performed H&E staining. It was noted that the alveolar septum was significantly widened and there was a large number of neutrophils infiltration in the lung tissue of burned rats. There was also markedly inflammatory exudation in the alveoli, leading to the decrease of alveolar space in the burn group compared to the sham group and the control group. There was no significant abnormal change in the lung tissue of the sham group and the control group, as shown in Fig. 1B.

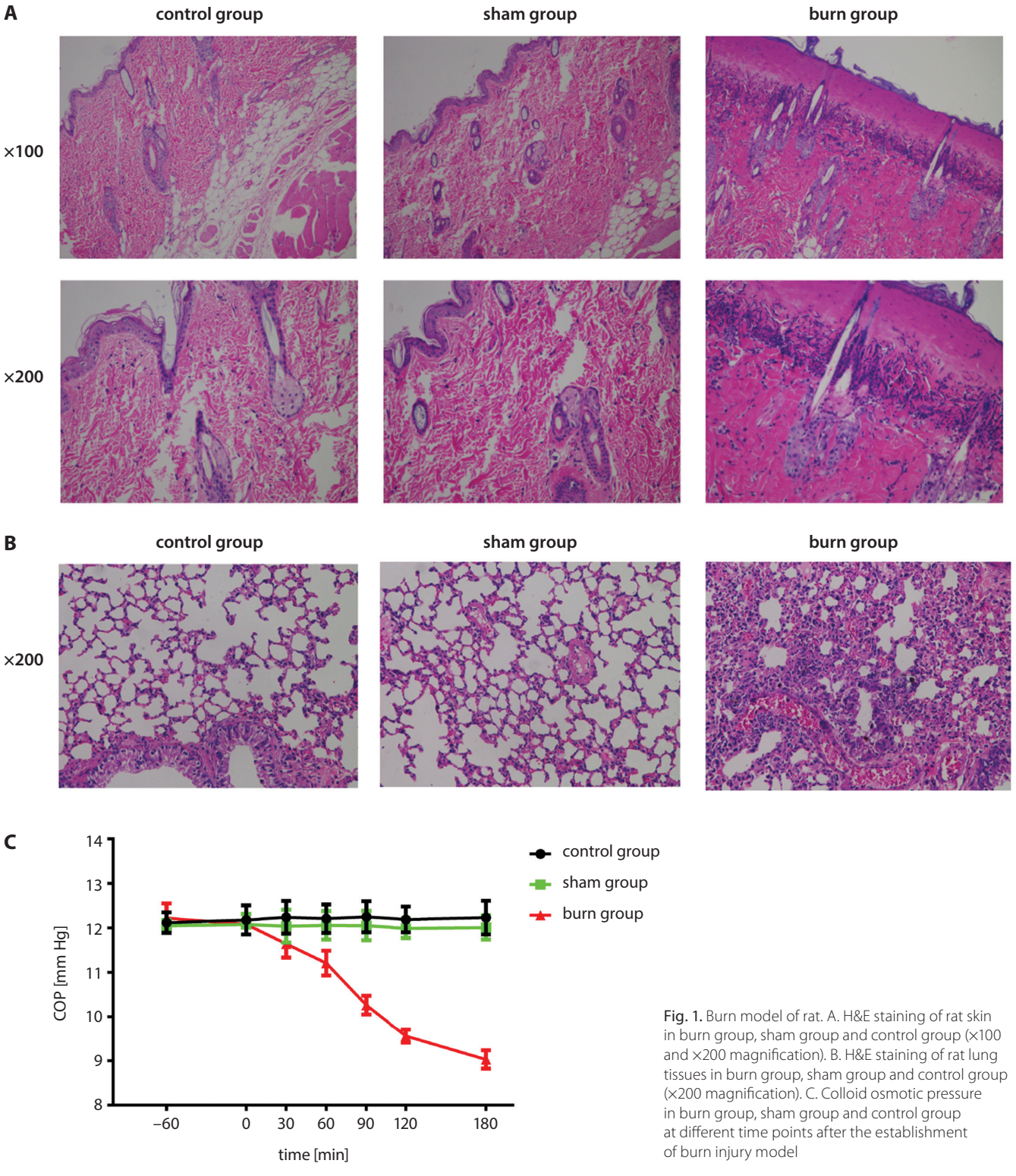

Fig. 1. Burn model of rat. A. H&E staining of rat skin in burn group, sham group and control group (×100 and ×200 magnification). B. H&E staining of rat lung tissues in burn group, sham group and control group (×200 magnification). C. Colloid osmotic pressure in burn group, sham group and control group at different time points after the establishment of burn injury model

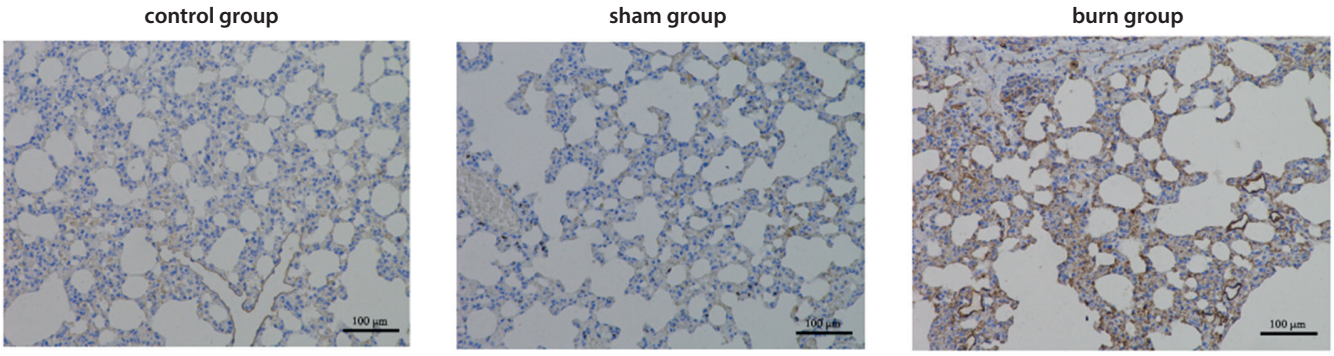

Fig. 2. MiRNA-451 upregulated in the lung microvascular endothelial cells after the establishment of burn injury. In situ hybridization on the expression of miRNA-451 in lung endothelial cell in burn group, sham group and control group (×200 magnification)

We also collected the plasma from each group at different time points to examine the variation of colloidal osmotic pressure. The results showed that colloidal osmotic pressure was continuously decreased from 12.8 ±0.2 mm Hg to 9.4 ±0.3 mm Hg in the burn group after the burn injury was established. However, no significant changes were found in the sham burn group and the control group (around 12.4 mm Hg) (Fig. 1C).

Increased expression of miRNA-451 in the lung microvascular endothelial cells after burn

It was reported that miRNA-451 was upregulated in denatured dermis of severely burned patients.[8] In order to understand the potential role of miRNA-451 in the burn process, we used in situ hybridization to examine its expression of miRNA-451 in the microvascular endothelial cells from each group. It was found that the expression of miRNA-451 was significantly upregulated in the burn group compared with the sham burn group and control group (Fig. 2), indicating that miRNA-451 played a role in regulating the phenotypic and functional changes of endothelial cells during the burn process.

MiRNA-451 promoted apoptosis, and inhibited proliferation and migration of endothelial cells

Because miRNA-451 was upregulated in the microvascular endothelial cells in vivo, we altered the expression of miRNA-451 in HUVECs by transfecting its mimic or inhibitor, and treating the cells with serum separated from the rats of the burn group in order to further clarify its effect on endothelial cells. The RT-PCR results showed that the expression of miRNA-451 increased in the group transfected with mimic (2.86 ±0.27) and decreased in the group transfected with inhibitor (0.26 ±0.06) (Fig. 3A).

We further used CCK8 assay to detect cell proliferation. The results showed that HUVECs treated with the serum from the rats of the burn groups displayed a significant decrease in cell growth when compared to the same cells treated with the serum separated from the control group, which was 1.353 ±0.09 and 1.564 ±0.12, respectively. Importantly, miRNA-451 mimics could work in concert with the serum separated from the rats of the burn group to inhibit the cell proliferation; the result of optical density (OD) 450 nm was 0.576 ±0.07. Furthermore, miRNA-451 inhibitor induced the cell growth in HUVECs (2.011 ±0.11), indicating that miRNA-451 inhibited cell proliferation in burn process (Fig. 3B).

Fluorescence-activated cell sorting (FACS) and scratch assay were used to detect cell apoptosis and cell migration in each group. PI/Annexin V double staining showed that more apoptotic cells were readily seen in the HUVECs transfected with miRNA-451 mimics and treated with the serum separated from the rats of burn group, indicating that miRNA-451 could induce apoptosis in the burn process (Fig. 3C). Meanwhile, miRNA-451 also displayed its ability to inhibit cell migration. The apoptosis rate of group 4 (cells transfected with miRNA-451 mimic and cultured with medium supplemented with 10% rat serum from burn group) was dramatically higher than in group 6 (cells transfected with miRNA-451 inhibitor and cultured with medium supplemented with 10% rat serum from the burn group) (21.35 ±0.93 and 2.37 ±0.38) (Fig. 3D).

MiRNA-451 increased the permeability of HUVEC cells

Hyperpermeability occurs in vascular endothelial cells during the burn process. Cell permeability was evaluated in HUVECs under different conditions. The results showed that upregulation of miRNA-451 in HUVECs displayed an increase in permeability, since the intensity of FITC-dextran increased in the bottom cell culture chamber, which was 55.4 ±6.3%. The opposite effects were found in the HUVECs with the downregulation of miRNA-451 cells (10.35 ±2.43%) (Fig. 4A).

The results of western blot analysis showed that the serum separated from the rats of the burn group downregulated the expression of occludin and ZO-1; the effects

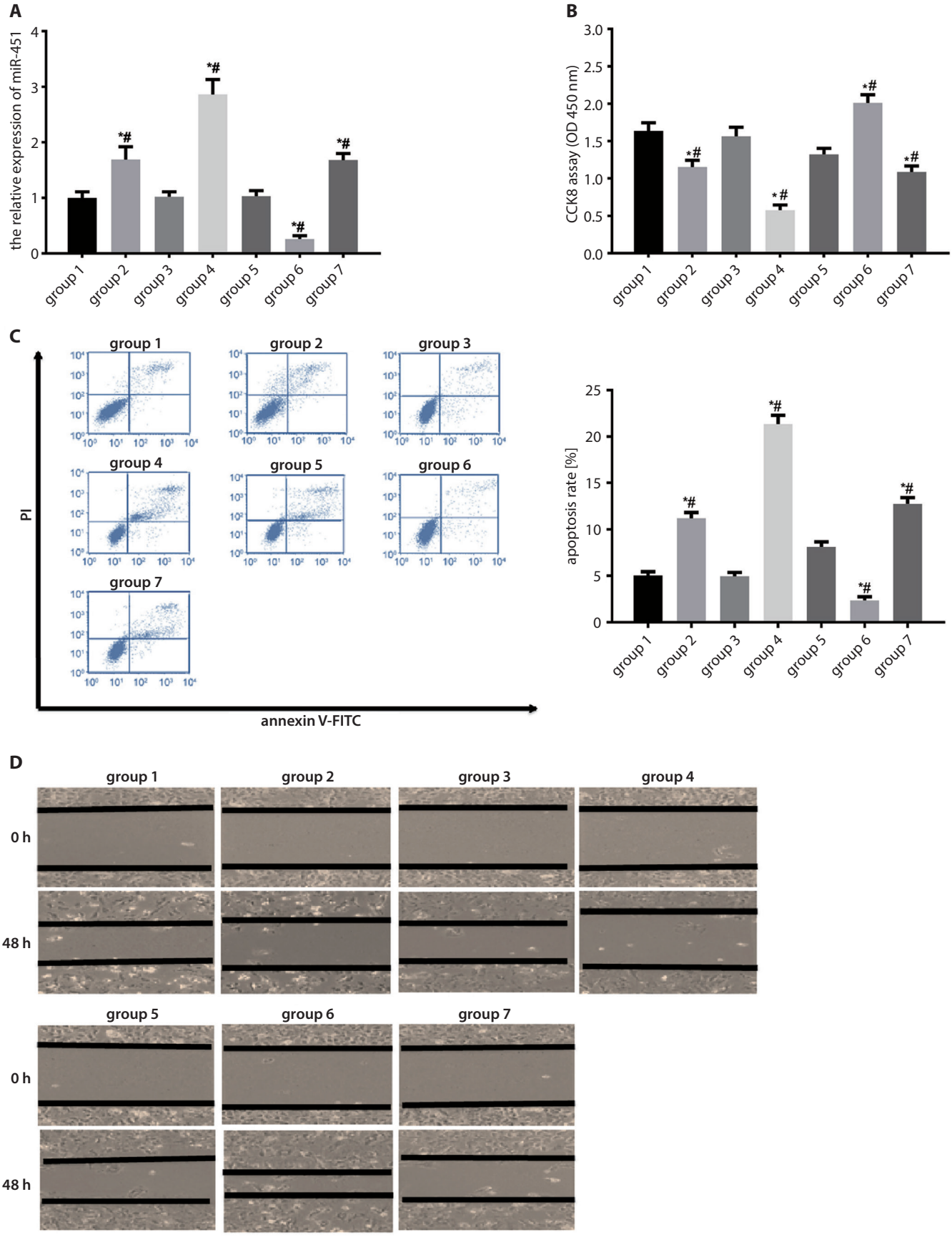

Fig. 3. MiRNA-451 regulated the proliferation, apoptosis and migration of HUVECs. A. RT-PCR on the expression of miRNA-451 expression in HUVECs in different groups after transfection. B. CCK8 assay on the cell proliferation in various groups. C. FACS on the cell apoptosis in various groups. D. Scratch assay on the cell migration in various groups

Compared with control group, * $p < 0.05$. Compared with sham burn group, # $p < 0.05$.

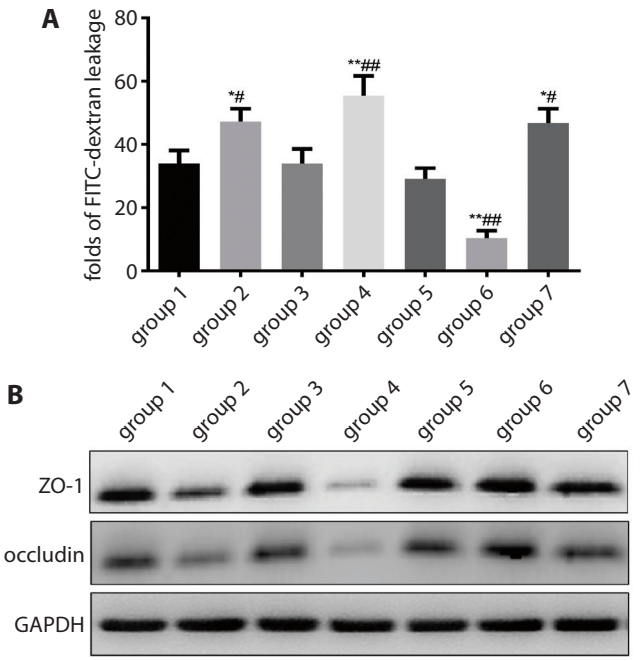

Fig. 4. MiRNA-451 increased the permeability of HUVECs. A. The HUVEC cell permeability in various groups. B. Western blot analysis on the expression of ZO-1 and occludin in HUVECs in various groups

were more obvious in the HUVECs transfected with miRNA-451 mimics. The miRNA-451 inhibitor antagonized the effects caused by the serum separated from the rats of burn group, since the expression of occludin and ZO-1 was not downregulated (Fig. 4B).

Discussion

Vascular hyperpermeability is a critical issue in the burn process, since it results in the release of a number of pro-inflammatory cytokines, including interleukin 1 beta (IL-1β), tumor necrosis factor α (TNF-α) and other inflammatory factors,[9] leading to systemic symptoms. However, the mechanisms of vascular hyperpermeability in burn injury are not completely understood. Recently, the role of miRNAs in regulating the functions of endothelial cells has attracted great interests.[10] In the present study, a third-degree burn model in rats was established. The H&E staining showed that the burn injury went through the dermis and affected deep tissues. Furthermore, the burns on the back skin of rats resulted in ALI, indicating the release of pro-inflammatory factors and the injury of functions of endothelial cells.

In situ hybridization (ISH) is a mature methodology for assessing miRNA expression.[11–13] It could detect specific nucleic acid sequences in cellular level in tissue samples. The ISH technology could provide more information about the cellular origin of expression and on expression levels in different tissue compartments and cell populations, aiding in the detection of individual miRNAs and mRNAs.[12]

The results of ISH showed the overexpression of miRNA-451 in the endothelial cells of burn group, indicating that miRNA-451 played a role in regulating the phenotypic and functional changes of endothelial cells during the burn process. Moreover, this result is consistent with the previous report that miRNA-451 was upregulated in denatured dermis of severely burned patients,[8] demonstrating that miRNA-451 is a factor regulating the permeability of endothelial cells in the burn process.

Cell–cell junctions that provide structural integrity are essential elements in maintaining homeostasis in endothelial cells.[14] In particular, tight junctions control the permeability in endothelial cells.[15] Occludin, a transmembrane protein, is one of the key components of tight junctions which regulates actin assembly.[16] ZO-1 is a protein which plays a role in anchoring occludin to the actin assembly.[17] Thus, occludin along with ZO-1 maintains the integrity and barrier functions of endothelia. However, burns damage the inter-endothelial junctions[18] and lead to the leakage of substances ranging from water to macromolecules. In our study, we found that the serum from the rats of the burn group decreased the expression of ZO-1 and occludin, and the effects were simulated by miRNA-451 mimics in HUVECs, leading to microvascular hyperpermeability. On the other hand, downregulation of miRNA-451 antagonizes the effects caused by the serum from the burn group.

Angiogenesis is a biological mechanism of new capillary formation which supplies oxygen and nutrients to cells in the wound area and regenerates tissues.[19] Angiogenesis is critical in determining the wound-healing outcomes in third-degree burns.[20] Recently, the correlation between miRNAs and angiogenesis has been studied. Soufi-Zomorrod used bioinformatics algorithms to identify that VEGFR2 and FGFR1 were the targets of miRNA-129-1 and miRNA-133. The HUVECs transfected with miRNA-129-1 and miRNA-133 mimics suppressed the angiogenesis properties, including cell proliferation, cell viability and migration.[21] Liu reported that the elevation of miRNA-451 in human hepatocellular carcinoma (HCC) cells mitigated the viability, migration and tube formation of HUVECs by targeting IL-6-STAT3-VEGF signaling. Its overexpression also reduced angiogenesis of HCC cells in vivo.[22] In our study, we transfected HUVECs with miRNA-451 mimic and inhibitor, and the results showed that miRNA-451 mimics could suppress the cell proliferation and migration and induce apoptosis in HUVECs, and the effects were similar to those of the treatment with serum from rats with third-degree burns, indicating that miRNA-451 is a key regulator inhibiting angiogenesis in burn process. Li Q et al. study also shown that miRNA-451 had anti-angiogenic effect, and downregulation of miRNA-451 would promote the migration of HUVEC.[23]

In summary, this study showed that miRNA-451 was overexpressed in lung endothelial cells in rats with

third-degree burns. In vitro experiments suggested that miRNA-451 may play a role in suppressing angiogenesis and increasing permeability of HUVECs. MiRNA-451 could be a potential target for the treatment of burn injury.

ORCID iDs

Jie Zhou https://orcid.org/0000-0002-9217-9516
Huibin Lian https://orcid.org/0000-0003-2846-2779
Tianlan Zhao https://orcid.org/0000-0002-9146-2782
Gang Xu https://orcid.org/0000-0002-9186-7173

References

1. Herndon DN. *Total Burn Care*. 4th ed. New York, NY: Saunders Elsevier; 2012.
2. Turk E, Caliskan M, Karagulle E, et al. A prospective clinical study of flow-mediated dilatation in burn injury. *J Burn Care Res*. 2014;35(2): 169–175.
3. Bartel DP. MicroRNAs: Genomics, biogenesis, mechanism, and function. *Cell*. 2004;116(2):281–297.
4. Son DJ, Kumar S, Takabe W, et al. The atypical mechanosensitive microRNA-712 derived from pre-ribosomal RNA induces endothelial inflammation and atherosclerosis. *Nat Commun*. 2013;4:3000.
5. Ni CW, Qiu H, Jo H. MicroRNA-663 upregulated by oscillatory shear stress plays a role in inflammatory response of endothelial cells. *Am J Physiol Heart Circ Physiol*. 2011;300(5):H1762–H1769.
6. Bazzoni G, Martinez-Estrada OM, Orsenigo F, Cordenonsi M, Citi S, Dejana E. Interaction of junctional adhesion molecule with the tight junction components ZO-1, cingulin, and occludin. *J Biol Chem*. 2000; 275(27):20520–20526.
7. Chen F, Ohashi N, Li W, Eckman C, Nguyen JH. Disruptions of occludin and claudin-5 in brain endothelial cells in vitro and in brains of mice with acute liver failure. *Hepatology*. 2009:50(6):1914–1923.
8. Liang P, Lv C, Jiang B, et al. MicroRNA profiling in denatured dermis of deep burn patients. *Burns*. 2012;38(4):534–540.
9. Ravat F, Payre J, Peslages P, Fontaine M, Sens N. Burn: An inflammatory process [in French]. *Pathol Biol (Paris)*. 2011;59(3):e63–e72.
10. Cheng XW, Wan YF, Zhou Q, Wang Y, Zhu HQ. MicroRNA-126 inhibits endothelial permeability and apoptosis in apolipoprotein E-knockout mice fed a high-fat diet. *Mol Med Rep*. 2017;16(3):3061–3068.
11. Nelson PT, Wilfred BR. In situ hybridization is a necessary experimental complement to microRNA (miRNA) expression profiling in the human brain. *Neurosci Lett*. 2009;466(2):69–72.
12. Nielsen BS. MicroRNA in situ hybridization. *Methods Mol Biol*. 2012; 822:67–84.
13. Li J, Li X, Li Y, et al. Cell-specific detection of miR-375 downregulation for predicting the prognosis of esophageal squamous cell carcinoma by miRNA in situ hybridization. *PLoS One*. 2013;8(1):e53582.
14. Dejana E, Tournier-Lasserve E, Weinstein BM. The control of vascular integrity by endothelial cell junctions: Molecular basis and pathological implications. *Dev Cell*. 2009:16(2):209–221.
15. Steed E, Balda MS, Matter K. Dynamics and functions of tight junctions. *Trends Cell Biol*. 2010;20(3):142–149.
16. Kuwabara H, Kokai Y, Kojima T, Takakuwa R, Mori M, Sawada N. Occludin regulates actin cytoskeleton in endothelial cells. *Cell Struct Funct*. 2001;26(2):109–116.
17. Van Itallie CM, Tietgens AJ, Krystofiak E, Kachar B, Anderson JM. A complex of ZO-1 and the BAR-domain protein TOCA-1 regulates actin assembly at the tight junction. *Mol Biol Cell*. 2015;26(15):2769–2787.
18. Wiggins-Dohlvik K, Suk Han M, Stagg HW, Alluri H. Melatonin inhibits thermal injury-induced hyperpermeability in microvascular endothelial cells. *J Trauma Acute Care Surg*. 2014;77(6):899–905,discussion 905.
19. Gonzalez AC, Fortuna Costa T, de Araújo Andrade Z, Ribeiro Alves Peixoto Medrado A. Wound healing: A literature review. *An Bras Dermatol*. 2016;91(5):614–620.
20. Tredget EE. The basis of fibrosis and wound healing disorders following thermal injury. *J Trauma*. 2007;62(6 Suppl):S69.
21. Soufi-Zomorrod M, Hajifathali A, Kouhkan F, Mehdizadeh M, Hosseini Rad SMA, Soleimani M. MicroRNAs modulating angiogenesis: miR-129-1 and miR-133 act as angio-miR in HUVECs. *Tumor Biol*. 2016; 37(7):9527–9534.
22. Liu XM, Zhang A, Xiang J, Lv Y, Zhang X. miR-451 acts as a suppressor of angiogenesis in hepatocellular carcinoma by targeting the IL-6R-STAT3 pathway. *Oncol Rep*. 2016;36(3):1385–1392.
23. Li Q, Zhang D, Gao H, Gao X. Downregulation of microRNA-451 improves cell migration, invasion and tube formation in hypoxia-treated HUVECs by targeting MIF. *Mol Med Rep*. 2019;20:1167–1177.

Protective and therapeutic effects of pyrrolidine dithiocarbamate in a rat tongue cancer model created experimentally using 4-nitroquinoline 1-oxide

Aysenur Meric Hafız[1,A], Remzi Doğan[2,A,B,D], Zuhal Gucin[3,B,C], Omer Faruk Ozer[4,B,C], Alper Yenigun[2,E], Orhan Ozturan[2,F]

[1] Department of Otorhinolaryngology, Koc University, Istanbul, Turkey
[2] Department of Otorhinolaryngology, Bezmialem Vakif University, Istanbul, Turkey
[3] Department of Pathology, Bezmialem Vakif University, Istanbul, Turkey
[4] Department of Biochemistry, Bezmialem Vakif University, Istanbul, Turkey

A – research concept and design; B – collection and/or assembly of data; C – data analysis and interpretation;
D – writing the article; E – critical revision of the article; F – final approval of the article

Advances in Clinical and Experimental Medicine, ISSN 1899–5276 (print), ISSN 2451–2680 (online) *Adv Clin Exp Med*. 2020;29(11):1249–1254

Address for correspondence
Remzi Doğan
E-mail: dr.remzidogan@gmail.com

Funding sources
None declared

Conflict of interest
None declared

Received on November 3, 2019
Reviewed on June 13, 2020
Accepted on September 20, 2020

Abstract

Background. Tongue tumors, which are oropharyngeal tumors, are increasing in frequency. Pyrrolidine dithiocarbamate (PDTC) is a powerful antioxidant and antitumoral agent.

Objectives. To evaluate the protective and therapeutic effects of PDTC in a tongue cancer model induced with 4-nitroquinoline 1-oxide (4-NQO).

Material and methods. We included 40 rats in the trial and assigned them randomly to 5 groups. Group 1 (cancer, n = 7): 4-NQO (0–12 weeks); group 2 (protection, n = 8): 4-NQO (0–12 weeks) + PDTC (300 mg/kg/day, 0–12 weeks); group 3 (therapy-high dose, n = 10): 4-NQO (0–12 weeks) + PDTC (600 mg/kg/day, weeks 12–30); group 4 (therapy-low dose, n = 10): 4-NQO (0–12 weeks) + PDTC (300 mg/kg/day, weeks 12–30); and group 5 (control). Cardiac blood samples were taken to analyze oxidative stress parameters (total antioxidant status (TAS), total oxidant status (TOS) and oxidative stress index (OSI)). Histopathological assessment was performed under a light microscope.

Results. The results of the histopathological assessment showed that the model we used in group 1 was successful, which was consistent with the literature. The PDTC dose administered in group 2 could not prevent tumor formation. Group 3 demonstrated that PDTC in high doses is effective as a therapeutic agent. Group 4 indicated that PDTC in low doses has no therapeutic effect. The results of the biochemical assessment showed that in group 3, TOS and OSI values were significantly lower than in groups 1, 2 and 4. No significant difference was found in the TOS and OSI values between groups 5 and 3.

Conclusions. Our study demonstrated histopathologically that in an experimentally generated tongue cancer model, application of 600 mg/kg/day of PDTC led to a significant reduction in the size of the tumor. This was supported by the biochemical parameters.

Key words: antioxidant, tongue cancer, antitumoral, pyrrolidine dithiocarbamate, 4-nitroquinoline 1-oxide

Cite as
Hafız AM, Doğan R, Gucin Z, Ozer OF, Yenigun A, Ozturan O. Protective and therapeutic effects of pyrrolidine dithiocarbamate in a rat tongue cancer model created experimentally using 4-nitroquinoline 1-oxide. *Adv Clin Exp Med*. 2020;29(11):1249–1254. doi:10.17219/acem/127682

DOI
10.17219/acem/127682

Introduction

Oral and parapharyngeal cancer represents less than 2% of all deaths from cancer and more than 2% of newly diagnosed cancer cases.[1] The progression of oral cancer proceeds from hyperplastic epithelial lesions to dysplasia and invasive carcinoma.[2] Remission and prognosis are linked to a more detailed understanding of the multi-stage process causing the development of cancer.[3] It is therefore important to repress the carcinogenesis with chemoprotective agents. Many current studies are directed towards identifying currently available chemoprotective agents.[4] Some of these agents are foodstuffs such as vegetables and fruit, and it has been reported that they act as protective agents in carcinoma of the tongue.[5] These chemoprotective agents have anti-proliferative, anti-inflammatory and antioxidant effects.

Pyrrolidine dithiocarbamate (PDTC) is a metal chelator and antioxidant as well as nuclear factor kappa-light-chain-enhancer of activated B cells (NF-κB) inhibitor. It is a thiol compound of low molecular weight. It has a large number of biological activities, including changing the redox state,[6] chelating heavy metal ions[7] and inhibiting enzymes.[8] Principally, PDTC is a powerful inhibitor of NF-κB.[9] It shows an antioxidant effect, preventing the toxic effect of free radicals[10] as well as blocking the pro-inflammatory effects of cytokines.[11] In addition, it increases antioxidant activity by increasing the gene expression of superoxide dismutase (SOD)[12] and glutathione peroxidase (GPX),[13] 2 endogenase antioxidant enzymes. In addition, PDTC affects oxidant-related cell damage by reducing the build-up of malondialdehyde (MDA).[14] Studies have shown that PDTC, particularly through NF-κB inhibition, prevents the development, growth and angiogenesis of tumors.[15,16] We also studied the effectiveness of PDTC in preventing and treating experimentally produced tongue cancer.

Material and methods

Animals, diets and chemicals

Our study was started after obtaining approval from the Ethics Committee for experimental research at Bezmialem Vakif University (Istanbul, Turkey). We included 40 female Sprauge–Dawley rats (8 weeks old). All the animals were kept in cages in groups of 3 or 4, with drinking water and standard feed ad libitum. The day/night rhythm was set to 12/12 h, and the temperature was 23°C.

The animals were randomly assigned to 5 groups:

Group 1 (cancer, n = 7): 20 ppm of 4-nitroquinoline 1-oxide (4-NQO) was added to the drinking water for the first 12 weeks of the study.

Group 2 (protection, n = 8): 20 ppm of 4-NQO was added to the drinking water for the first 12 weeks of the study. In addition, a dose of 300 mg/kg/day of PDTC was administered by gavage for the same 12-week period.

Group 3 (high-dose therapy, n = 10): 20 ppm of 4-NQO was added to the drinking water for the first 12 weeks of the study. Subsequently, a dose of 600 mg/kg/day of PDTC was given by gavage from week 13 until week 30.

Group 4 (low-dose therapy, n = 10): 20 ppm of 4-NQO was added to the drinking water for the first 12 weeks of the study. Subsequently, a dose of 300 mg/kg/day of PDTC was given by gavage from week 13 until week 30.

Group 5 (control, n = 5): Physiological saline (1 cm^3) was administered by gavage for 12 weeks.

Groups 1, 2 and 5 were sacrificed at the end of the 12^{th} week; groups 3 and 4 were sacrificed at the end of the 30^{th} week. After sacrificing the rats, their tongues were excised. Macroscopic photographs were taken.

Histopathological analysis

Each tongue was cut in half longitudinally. Each tissue specimen was fixed in 10% buffered formalin and embedded in paraffin blocks. Each specimen was sliced into multiple transverse sections for histological processing. The histopathological evaluation was performed by light microscopy. The tongue sections were graded as normal, hyperplasia, carcinoma in situ, dysplasia, or carcinoma per animal, as modified from the method described by Ribeiro et al.[17]

Biochemical parameters

At the end of the study, before sacrificing the rats, cardiac blood samples (5 mL) were taken to analyze oxidative stress parameters: total antioxidant status (TAS), total oxidant status (TOS) and oxidative stress index (OSI). The heparinized blood was centrifuged (1500 × g for 10 min) and the serum that was obtained was saved at –80°C for TOS and TAS analysis using commercial kits (Rel Assay Diagnostics, Gaziantep, Turkey); the OSI was the TOS-to-TAS ratio (see below).

Measurement of total oxidant status

Plasma TOS was measured using an automated method developed by Erel.[18] The oxidants present in a sample oxidize the ferrous ion in an o-dianisidine complex to ferric ion. Oxidation is enhanced using glycerol, which is abundant in the reaction medium, and the ferric ion forms a colored complex with xylenol orange under acidic conditions. The color intensity (which can be measured spectrophotometrically) is associated with the total level of oxidants present. Hydrogen peroxide is used to calibrate the assay, and the results are expressed in terms of micromoles of hydrogen peroxide equivalent per liter (mmol H_2O_2 equiv/L).

Measurement of total antioxidant status

Plasma TAS was measured using another automated method developed by Erel.[19] This involves production of the hydroxyl radical, which is a potent biological reactant. A ferrous ion solution (reagent 1) is mixed with hydrogen peroxide (reagent 2). Radicals produced by the hydroxyl radical, including the brown dianisidinyl radical cation, are also potent in biological terms. Thus, it is possible to measure the antioxidative capacity of a sample in terms of the inhibition of free radical reactions initiated by the production of the hydroxyl radical. Variation in the assay data is very low (less than 3%), and results are expressed as mmol Trolox equiv/L.

Measurement of oxidative stress index

The OSI is the TOS-to-TAS ratio, but TAS values were changed to mmol/L. Each OSI was calculated as follows: OSI (arbitrary units) = TOS (mmol H_2O_2/l)/TAS (mmol Trolox/L).[20]

Statistical analysis

The statistical analysis was carried out using the Statistical Package for the Social Sciences v. 13.0 for Windows (SPSS Inc., Chicago, USA). All quantitative variables were assessed using measures of central location (i.e., mean and median) and measures of dispersion (i.e., standard deviation (SD)). Data normality was checked using the Kolmogorov–Smirnov test.

For inter-group comparisons, the one-way analysis of variance (ANOVA) was used. Tukey's honestly significant differences (HSD) post hoc test was used with the Bonferroni correction applied was used to establish between which groups a difference existed ($p < 0.01$ was accepted as statistically significant). To assess qualitative data, the χ^2 test was used; $p < 0.05$ was accepted as significant.

Results

The rats were weighed at the beginning of the study and before sacrificing the animals (Table 1).

Table 1. Body mass of rats range before and after treatment

Group	Before [g]	After [g]
Group 1 (n = 7) cancer	219.7 ±24.9	165.2 ±17.3
Group 2 (n = 8) protection	228.5 ±23.9	201.8 ±10.9
Group 3 (n = 10) high-dose therapy	219. 1 ±27.5	195.3 ±14.7
Group 4 (n = 10) low-dose therapy	226.8 ±20.3	180.1 ±12.5
Group 5 (n = 5) control	216.3 ±25.8	247.4 ±32.8

Histopathological analysis

Group 1 (4-NQO 12 weeks): Of the 7 rats used, after 12 weeks 4 had in situ squamous cell carcinomas (SCC), 2 had high-grade dysplasia and 1 had middle-grade dysplasia (Fig. 1). Group 2 (4-NQO weeks 0–12 + PDTC 300 mg/kg/day weeks 0–12): Of the 8 rats used, after 12 weeks, 1 had superficial invasive SCC, 1 had in situ SCC, 1 had noninvasive SCC, 4 had high-grade dysplasia, and 1 had low-grade dysplasia (Fig. 2). Group 3 (4-NQO weeks 0–12 + PDTC 600 mg/kg/day weeks 12–30): Of the 10 rats used, after 30 weeks, 1 had middle-grade dysplasia, 1 high-grade dysplasia and 5 had low-grade dysplasia, while 3 were healthy (Fig. 3). Group 4 (4-NQO weeks 0–12 + PDTC 300 mg/kg/day weeks 12–30): Of the 10 rats used, after 30 weeks, 4 had invasive SCC, 2 had superficial invasive SCC and 4 had non-invasive SCC (Fig. 4). Group 5 (physiological saline 12 weeks): None of the rats developed tumors (Fig. 5).

Our study found no significant difference between groups 1 and 2 in terms of carcinogenesis ($p > 0.05$). Likewise, there was no significant difference between groups 3 and 5 ($p > 0.05$). Significant differences in terms of carcinogenesis were found between groups 3 and 1 ($p < 0.05$) and between groups 3 and 4 ($p < 0.05$).

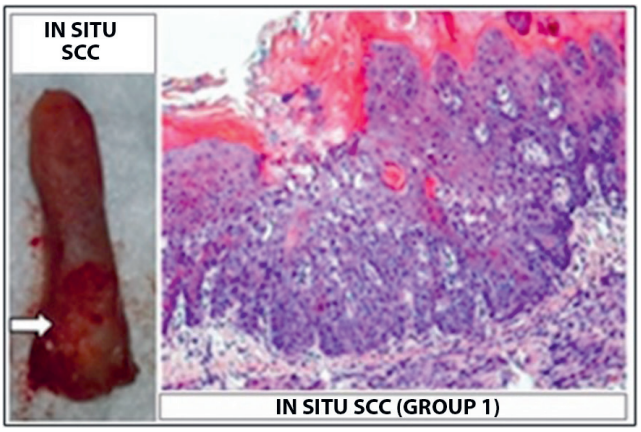

Fig. 1. Macroscopic and histopathological view of group 1 (cancer)

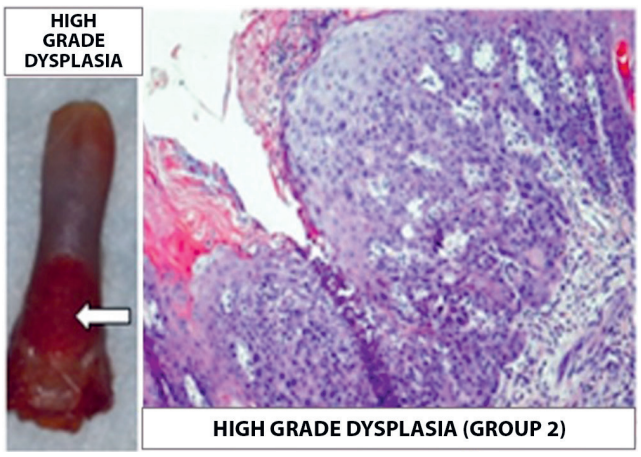

Fig. 2. Macroscopic and histopathological view of group 2 (protection)

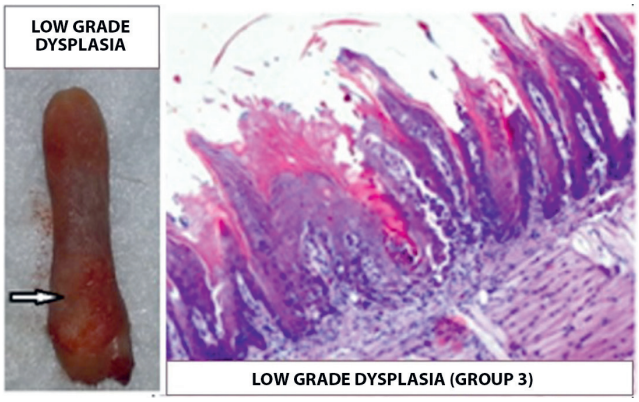

Fig. 3. Macroscopic and histopathological view of group 3 (high-dose therapy)

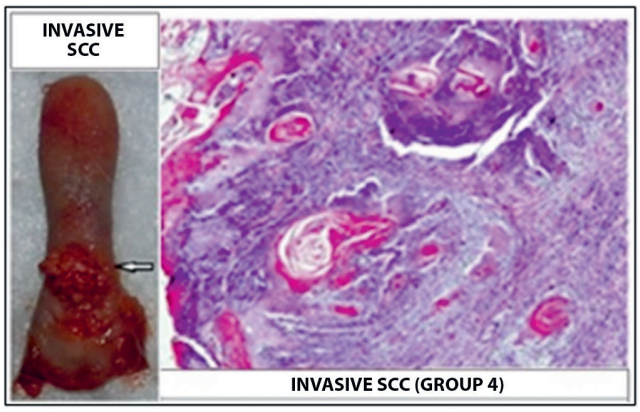

Fig. 4. Macroscopic and histopathological view of group 4 (low-dose therapy)

Biochemical parameters

The TOS and OSI values in group 3 were significantly lower than in group 1 and group 4 ($p < 0.01$) (Table 2). There was no significant difference in the TOS and OSI values between groups 1, 2 and 4 ($p > 0.05$) (Table 1). The TAS values in group 3 were significantly higher than in all the other groups ($p < 0.01$) (Table 2).

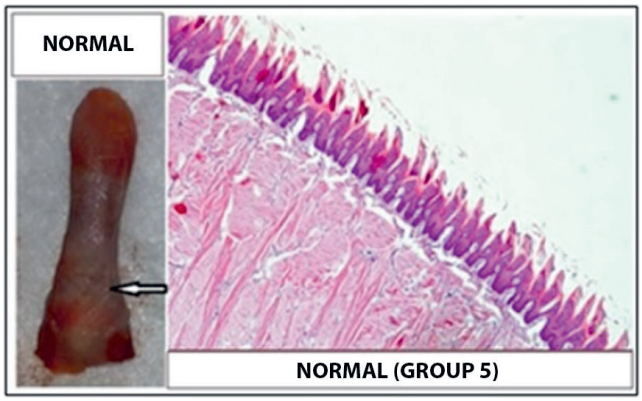

Fig. 5. Macroscopic and histopathological view of group 5 (control)

Discussion

Oral cavity cancers account for about 3% of all malignancies.[21] Squamous cell carcinoma of the tongue is the 2nd most frequent oval cavity cancer.[22] Smoking, alcohol use and chewing tobacco have been shown to be among the most common causes of tongue cancer.[23] In 60–70% of tumors in the oral cavity, diagnosis is made after the tumor has passed the locally advanced stage.[24] It is thus very important to prevent the spread of the tumor by early diagnosis. Despite advanced treatment methods, during the last decades, the prognosis for patients with oral/lingual SCC has not improved significantly.[25]

Today, surgery and chemotherapy (CT) are the treatments most frequently used in cases of tongue cancer. However, even though these methods are now the principal modalities for treating tongue cancer, either of them can lead to a number of defective outcomes. For example, surgical treatment creates a great physiological and psychological burden for the patient and can lead to problems with swallowing and speaking, thereby severely reducing the patient's quality of life. Chemotherapy, on the other hand, involves serious toxicity, which may lead to multi-system risks affecting the patient's health. Radiotherapy (RT), even

Table 2. Biochemical parameters (mean ± standard deviation (SD))

Groups	TOS [μmol H_2O_2Eqv/L]	TAS [μmol TroloxEqv/L]	OSI (TOS/TASX100)
Group 1 (cancer) (4-NQO)	13.28 ±1.07[b]	1.62 ±0.67[a]	0.081 ±0.067[a]
Group 2 (protective) (4-NQO+PDTC (300 mg/kg/day), 12 weeks)	11.93 ±1.76	1.48 ±0.53[c]	0.080 ±0.037
Group 3 (high-dose treatment) (4-NQO+PDTC (600 mg/kg/day), 30 weeks)	7.21 ±0.54[d]	3.14 ±0.71[d,e]	0.022 ±0.012[d]
Group 4 (low-dose treatment) (4-NQO+PDTC (300 mg/kg/day), 30 weeks)	12.57 ±1.19	1.38 ±0.25	0.091 ±0.024
Group 5 (control) (saline, 30 weeks) One-way ANOVA[¥] (between groups)	5.08 ±0.37 p = 0.0001	1.75 ±0.28 p = 0.0021	0.029 ± 0.023 p = 0.0001

TAS – total anti-oxidant status; TOS – total oxidant status; OSI – oxidative stress index; [¥] – one-way analysis of variance (ANOVA) test, $p < 0.05$ significance level obtained; [a–e] $p < 0.01$ significance level obtained (Tukey's HSD post hoc test); [a] – group 1 compared to group 3; [b] – group 1 compared to group 4; [c] – group 2 compared to group 3; [d] – group 3 compared to group 4; [e] – group 3 compared to group 5.

if advanced technology allows a reduction of the affected area, can cause a number of problems, given the close proximity of several structures in the oropharyngeal region. As a result of these treatment methods, several functions (speaking, mastication, swallowing) can become dysfunctional or distorted.[26]

It is therefore important to repress the carcinogenesis with chemoprotective agents, and many current studies are directed towards identifying currently available ones.[4,5] Pyrrolidine dithiocarbamate is an NF-κB inhibitor and is known to be anti-viral, anti-inflammatory, antioxidant and metal-chelating.[27] It has a strong anti-tumoral effect especially because of NF-κB inhibition. The NF-κB mediators produce an anti-apoptotic signal, inhibiting cell apoptosis; thus, the cell loses the normal apoptotic function and, consequently, a tumor can develop.[28] It has been shown that PDTC induces apoptosis in smooth muscle cells and leukemic cells through an apoptotic pathway.[29] In addition, it has been shown that tumor cell growth and proliferation in gastrointestinal stromal (GIS) tumors is inhibited thanks to the anti-tumoral effect of PDTC.[30] In mice, PDTC inhibits tumor formation and reduces tumor angiogenesis in lung cancer through NF-κB inhibition.[28] Thus, we can expect the NF-κB inhibitor PDTC to be an effective tumor drug, but additional research in this area is required. For this purpose, our study assessed the protective and therapeutic effectiveness of PDTC in carcinoma of the tongue.

In our study, we gave group 1 4-NQO (20 ppm) for 12 weeks. According to the literature, 4-NQO is used to generate experimental tongue cancer. Of the 7 rats in group 1, 4 developed in situ carcinoma, 2 developed high-grade dysplasia and 1 developed middle-grade dysplasia (Fig. 1). These results are consistent with the literature[31,32] and show that our cancer model was implemented successfully.

Our study also tested whether PDTC in a low dose was effective in preventing the development of cancer. Therefore, we gave group 2 4-NQO (20 ppm) over 12 weeks along with low-dose PDTC (300 mg/kg/day). After 12 weeks, it could be shown that PDTC inhibits the formation of cancer tissue in rats (Fig. 2). At that time, no significant differences in tumor development could be found between groups 1 and 2 ($p > 0.05$). We think that this was due to the low dose administered. Our intention in setting up this group was to assess whether PDTC has protective effects when applied in pre-malignant carcinomas of the tongue.

We planned group 3 to assess the therapeutic effectiveness of PDTC. In this group, after 12 weeks of 4-NOQ administration, we gave high-dose PDTC (600 mg/kg/day) for the following 18 weeks. At the end of 30 weeks, we found a significant reduction in cancer development in group 3 (Fig. 3). The effectiveness of PDTC applied in high doses in the treatment of tongue tumors was shown macroscopically and histopathologically (Fig. 3). We assume that PDTC produces this effect thanks to its NF-κB inhibition. In the literature, there are only a few studies showing PDTC to be effective in cancer treatment.[28–30]

In group 4, set up to assess the effectiveness of small doses (300 mg/kg/day) of PDTC in cancer treatment, after 30 weeks all the rats had developed cancer (Fig. 4). There was a histological difference between groups 1 and 4, because group 1 was administered 4-NQO for 12 weeks and then was sacrificed, whereas group 4 received low-dose PDTC after 12 weeks of 4-NQO. However, this low dose of PDTC was not effective enough, and cancer development continued.

It is known that oxidative stress plays an important role in carcinogenesis. Reactive oxygen radicals play roles in various places, damaging DNA, interacting with oncogenes, affecting tumor suppressor genes, and affecting immunological mechanisms.[33]

In a study by Doğan et al., oxidative stress parameters were investigated in head and neck tumors. In malignant tumors, TOS values were significantly higher and TAS values lower than in benign tumors.[34] Various studies have shown a strong antioxidant effect of PDTC.[11,12] In order to assess oxidative stress, our study evaluated the TAS, TOS and OSI values in intracardiac serum samples taken from all the rats. In group 3, TOS and OSI values were significantly lower than in groups 1 and 4 (Table 2). No significant difference in the TOS and OSI values was found between groups 3 and 5 (Table 2). The TAS values in group 3 were significantly higher than in other groups (Table 2). These data led us to assume that PDTC is a strong antioxidant that can help prevent tongue cancer.

Conclusions

Our study confirmed a number of general results: 1) that 20 ppm of 4-NQO applied over 12 weeks creates experimental tongue cancer in a rat model; 2) that PDTC applied at a dose of 300 mg/kg/day is not protective against tongue cancer; and 3) that 300 mg/kg/day of PDTC is not sufficient to stop the progress of tongue cancer. At the same time, our study showed that a dose of 600 mg/kg/day of PDTC can stop the progress of tongue cancer and lead to a significant reduction of lesions. Our results indicate that the effects of PDTC are achieved by reducing oxidative stress and inhibiting NF-κB.

The limitations of our study include its experimental nature, the lack of comparisons with other non-surgical treatment methods (CT, RT) and the lack of additional groups that would enable evaluation of tumor sizes and survival.

The primary strength of our study is that it investigates the effects of PDTC on tongue cancer for the first time in the literature, providing both histopathological and biochemical evaluation parameters, using different doses of PDTC and evaluating both preventative and therapeutic effects. We have demonstrated experimentally that PDTC can contribute to the prevention and treatment of tongue cancer. This study is the first in the literature on this subject, and additional experimental and clinical studies are needed.

ORCID iDs

Aysenur Meric Hafız https://orcid.org/0000-0002-3066-6255
Remzi Doğan https://orcid.org/0000-0001-5627-1342
Zuhal Gucin https://orcid.org/0000-0001-5330-2158
Omer Faruk Ozer https://orcid.org/0000-0002-1052-8939
Alper Yenigun https://orcid.org/0000-0001-9722-1333
Orhan Ozturan https://orcid.org/0000-0002-6129-8627

References

1. Balanchaert RH. Epidemiology of oral cancer. In: Ord RA, Balanchaert RH, eds. *Oral Cancer.* Chicago, IL: Quitessence Publishing; 2000:3–8.
2. Partridge M, Emilion G, Pateromichelakis S, Phillips E, Langdon J. Cancerisation of the oral cavity: Comparison of the spectrum of molecular alterations in cases presenting with both dysplastic and malignant lesions. *Oral Oncol.* 1997;33:332–337.
3. Shklar G. Development of experimental oral carcinogenesis and its impact on current oral cancer research. *J Dent Res.* 1999;78(12):1768–1772.
4. Kelloff GJ, Crowell JA, Steele VE, et al. Progress in cancer chemoprevention. *Ann N Y Acad Sci.* 1999;889:1–13.
5. Tanaka T. Chemoprevention of oral carcinogenesis. *Eur J Cancer.* 1995; 31(1):3–15.
6. Orrenius S. Nobel CSI, van den Dobbelsteen DJ, Burkitt MJ, Slater AF. Dithiocarbamates and the redox regulation of cell death. *Biochem Soc Trans.* 1996;24(4):1032–1038.
7. Iseki A, Kambe F, Okumura K, et al. Pyrrolidine dithiocarbamate inhibits TNF-α- dependent activation of NF-κB by increasing intracellular copper level in human aortic smooth muscle cells. *Biochem Biophys Res Commun.* 2000;276(1):88–92.
8. Ross SD, Kron IL, Gangemi JJ, et al. Attenuation of lung reperfusion injury after transplantation using an inhibitor of nuclear factor-κB. *Am J Physiol Lung Cell Mol Physiol.* 2000;279(3):L528–L536.
9. Schreck R, Meier B, Männel DN, Dröge W, Baeuerle PA. Dithiocarbamates as potent inhibitors of nuclear factor κB activation in intact cells. *J Exp Med.* 1992;175(5):1181–1194.
10. Muller DN, Dechend R, Mervaala EMA, et al. NF-κB inhibition ameliorates angiotensin II-induced inflammatory damage in rats. *Hypertension.* 2000;35(1 Pt 2):193–201.
11. Liu SF, Ye X, Malik AB. Inhibition of NF-κB activation by pyrrolidine dithiocarbamate prevents in vivo expression of proinflammatory genes. *Circulation.* 1999;100(12):1330–1337.
12. Borrello S, Demple B. NF kappa B-independent transcriptional induction of the human manganous superoxide dismutase gene. *Arch Biochem Biophys.* 1997;348(2):289–294.
13. Wild AC, Mulcahy RT. Pyrrolidine dithiocarbamate upregulates the expression of the genes encoding the catalytic and regulatory subunits of γ-glutamylcysteine synthetase and increases intracellular glutathione levels. *Biochem J.* 1999;338(Pt 3):659–665.
14. Nathens AB, Bitar R, Davreux C, et al. Pyrrolidine dithiocarbamate attenuates endotoxin-induced acute lung injury. *Am J Resp Cell Mol Biol.* 1997;17(5):608–616.
15. Spiller SE, Logsdon NJ, Deckard LA, Sontheimer H. Inhibition of nuclear factor kappa-B signaling reduces growth in medulloblastoma in vivo. *BMC Cancer.* 2011;11:136.
16. Yang C, Zhang H, Huang W, Lin Q, Wei H. Effect of combined use of PDTC and paclitaxel on proliferation and invasion of human breast cancer cell line MCF-7 [in Chinese]. *Sheng Wu Yi Xue Gong Cheng Xue Za Zhi.* 2010;27:1105–1109.
17. Ribeiro D, Kitakawa D, Domingues MA, Cabral LA, Marques ME, Salvadori DM. Survivin and nitric oxide inducible synthase production during 4NQO-induced rat tongue carcinogenesis: A possible relationship. *Exp Mol Pathol.* 2007;83(1):131–137.
18. Erel O. A new automated colorimetric method for measuring total oxidant status. *Clin Biochem.* 2005;38(12):1103–1111.
19. Erel O. A novel automated method to measure total antioxidant response against potent free radical reactions. *Clin Biochem.* 2004; 37(2):112–119.
20. Vural M, Camuzcuoglu H, Toy H, Aksoy N. Amniotic fluid prolidase activity and oxidative status in neural tube defects. *Fetal Diagn Ther.* 2010;28(1):34–39.
21. Kademani D. Oral cancer. *Mayo Clin Proc.* 2007;82(7):878–887.
22. Bachar G, Hod R, Goldstein DP, et al. Outcome of oral tongue squamous cell carcinoma in patients with and without known risk factors. *Oral Oncol.* 2011;47(1):45–50.
23. Nagpal JK, Patnaik S, Das BR. Prevalence of high-risk human papilloma virus types and its association with P53 codon 72 polymorphism in tobacco addicted oral squamous cell carcinoma OSCC patients of Eastern India. *Int J Cancer.* 2002;97(5):649–653.
24. Lippman SM, Sudbø J, Hong WK. Oral cancer prevention and the evolution of molecular-targeted drug development. *J Clin Oncol.* 2005; 23(2):346–356.
25. Haddadin KJ, Soutar DS, Webster MHC, Robertson AG, Oliver RJ, MacDonald DG. Natural history and patterns of recurrence of tongue tumors. *Br J Plast Surg.* 2000;53(4):279–285.
26. Makita H, Mutoh M, Maruyama T. A prostaglandin E2 receptor subtype EP1-selective antagonist, ONO-8711, suppresses 4-nitroquinoline 1-oxide-induced rat tongue carcinogenesis. *Carcinogenesis.* 2007;28(3):677–684.
27. Ji GQ, Chen RQ, Zheng JX. Macrophage activation by polysaccharides from *Atractylodes macrocephala* Koidz through the nuclear factor-kB pathway. *Pharm Biol.* 2015;53(4):512–517.
28. Gao P, Gao YJ, Liang HL. Effect of NF-κB inhibitor PDTC on VEGF and endostatin expression of mice with Lewis lung cancer. *Asian Pac J Trop Med.* 2015;8(3):220–224.
29. Cheng AC, Huang TC, Lai CS, et al. Pyrrolidine dithiocarbamate inhibition of luteolin-induced apoptosis through upregulated phosphorylation of Akt and caspase-9 in human leukemia HL-60 cells. *J Agric Food Chem.* 2006;54(12):4215–4221.
30. Panizzi L, Catalano S, Miarelli C, Cioni PL, Campeol E. In vitro antimicrobial activity of extracts and isolated constituents of *Geum rivale*. *Phytother Res.* 2000;14(7):561–573.
31. Minicucci EM, Ribeiro DA, da Silva GN, Pardini MI, Montovani JC, Salvadori DM. The role of the TP53 gene during rat tongue carcinogenesis induced by 4-nitroquinoline 1-oxide. *Exp Toxicol Pathol.* 2011;63(5):483–489.
32. Miranda SR, Noguti J, Carvalho JG, Oshima CT, Ribeiro DA. Oxidative DNA damage is a preliminary step during rat tongue carcinogenesis induced by 4-nitroquinoline 1-oxide. *J Mol Histol.* 2011;42(2):181–186.
33. Battisti C, Formichi P, Tripodi SA, Vindigni C, Roviello F, Federico A. Vitamin E serum levels and gastric cancer: Results from a cohort of patients in Tuscany, Italy. *Cancer Lett.* 2000;151(1):15–18.
34. Doğan R, Meriç Hafiz A, Tugrul S, Ozturan O, Keskin S, Kocyigit A. Can oxidative stress parameters be used as biomarkers for the discrimination of malignant head and neck tumors. *J Craniofac Surg.* 2016;27(3):e316–e320.

The effect of serum uric acid levels on the long-term prognosis of patients with non-ST-elevation myocardial infarction

Łukasz Kuźma[1,A–F], Agata Kulikowska[2,B–D], Anna Kurasz[1,B–D], Marta Maria Niwińska[1,B–D], Małgorzata Zalewska-Adamiec[1,C,E,F], Sławomir Dobrzycki[1,E,F], Hanna Bachórzewska-Gajewska[1,3,A–F]

[1] Department of Invasive Cardiology, Medical University of Bialystok, Poland
[2] Department of Anesthesiology and Intensive Therapy, Medical University of Bialystok, Poland
[3] Department of Clinical Medicine, Medical University of Bialystok, Poland

A – research concept and design; B – collection and/or assembly of data; C – data analysis and interpretation; D – writing the article; E – critical revision of the article; F – final approval of the article

Advances in Clinical and Experimental Medicine, ISSN 1899–5276 (print), ISSN 2451–2680 (online) *Adv Clin Exp Med*. 2020;29(11):1255–1263

Address for correspondence
Łukasz Kuźma
E-mail: kuzma.lukasz@gmail.com

Funding sources
None declared

Conflict of interest
None declared

Received on April 30, 2020
Reviewed on August 6, 2020
Accepted on September 1, 2020

Abstract

Background. Cardiovascular diseases (CVD) are the leading cause of death worldwide. Many studies have reported an association between serum uric acid (sUA) and CVD, and its role as a risk marker for mortality.

Objectives. To assess the relationship between sUA levels and the long-term prognosis of patients with non-ST-elevation myocardial infarction (NSTEMI).

Material and methods. The study was conducted at the Clinical Hospital of Białystok (Poland). Based on medical records, 9328 patients were hospitalized between 2011 and 2013, of which 726 had NSTEMI. The exclusion criteria were: any diagnosed neoplasms and estimated glomerular filtration rate (eGFR) <15 mL/min. The average observation time was 2324 days.

Results. A total of 549 patients were qualified for the analysis; men were in the majority (69.03%, n = 379), and the mean age was 68.42 years (standard deviation (SD) = 11.66). The sUA norm was exceeded in 137 of the patients (24.95%). Hyperuricemia is more likely to occur in women (risk ratio (RR) = 1.52, 95% confidence interval (95% CI) = 1.016–2.288, p = 0.042), in patients with chronic kidney disease (CKD) (RR = 3.452, 95% CI = 2.432–4.854, p < 0.001) and in patients with higher body mass index (BMI)s (RR = 1.048, 95% CI = 1.008–1.090, p = 0.018). In the whole study group, during the study, 178 of the patients died (32.41.9%), more often those with hyperuricemia: (60/137 patients (43.8%)) compared to patients with normal sUA values (118/412 values (28.64%)); p < 0.001). There was a significant correlation between an increase in sUA levels and an increase in mortality (p < 0.001). Independent risk factors of death were age (RR = 1.086, 95% CI = 1.065–1.108, p < 0.001), sUA (RR = 1.245, 95% CI = 1.131–1.370, p = 0.041), ejection fraction (EF) (RR = 0.928, 95% CI = 0.910–0.946, p < 0.001) and hemoglobin concentration (RR = 0.685, 95% CI = 0.611–0.768, p < 0.001).

Conclusions. Serum UA concentration is an independent risk factor of long-term mortality in patients who have undergone NSTEMI, and is associated with higher in-hospital death rates. Secondary prevention after NSTEMI should entail management of the patients' sUA levels.

Key words: uric acid, myocardial infarction, mortality, hyperuricemia, gout

Cite as
Kuźma Ł, Kulikowska A, Kurasz A, et al. The effect of serum uric acid levels on the long-term prognosis of patients with non-ST-elevation myocardial infarction. *Adv Clin Exp Med*. 2020;29(11):1255–1263. doi:10.17219/acem/127145

DOI
10.17219/acem/127145

Introduction

Cardiovascular disease (CVD) is the leading cause of death worldwide.[1] Among other conditions, this group of diseases includes acute coronary syndromes (ACS). Their occurrence depends on risk factors that can be divided into modifiable (such as hypertension, diabetes, obesity, dyslipidemia, lack of physical activity, current smoking, moderate alcohol use) and non-modifiable (which include age, gender and family history).[2] In order to prevent the occurrence of ACS more effectively, it is important to identify new modifiable risk factors as well as ways to control them.

The effects of excessive serum uric acid levels (sUA) were an intensely studied subject in recent decades. Although the physiopathological mechanisms leading to an increased risk of CVD are still a matter of debate, numerous studies have shown that uric acid (UA) is significantly associated with essential hypertension, ACS and chronic coronary syndrome, and heart failure, as well as with stroke, chronic kidney disease (CKD) and type 2 diabetes mellitus (DM2). Many researchers indicate that sUA is an independent risk factor for these pathologies.[3–5]

The prognostic value of sUA levels after ACS has also been investigated in several studies in recent years, and high levels of sUA on admission were found to be independently associated with in-hospital and long-term adverse outcomes across the whole spectrum of patients with ACS, including non-ST-segment elevation myocardial infarction (NSTEMI).[6–13]

Due to gradual increases in NSTEMI cases over STEMI and the limited number of studies focused on NSTEMI, we decided to investigate the relationship between sUA levels and the long-term prognosis of patients with NSTEMI in the study population. In addition, our work is novel in presenting very accurate clinical, biochemical, echocardiographic, and angiographic characteristics, which are not included in previous studies. The very long observation time, during which not only total mortality was assessed but also the type of revascularization treatment during the observation period, is also noteworthy.

The aim of the study was to assess the relationship between sUA levels and the long-term prognosis of patients with NSTEMI.

Material and methods

The study was conducted at the Clinical Hospital of the Medical University of Bialystok (Poland). Based on the medical records, 9328 patients were hospitalized (1594 with ACS) between 2011 and 2013, of which 726 were NSTEMI cases.

From the group of patients with NSTEMI, our analysis excluded 177 patients with diagnosed neoplasms, with estimated glomerular filtration rate (eGFR) <15, those lost in follow-up and those with missing data, leaving 549 patients in the final analysis.

The norm for UA concentration was defined as 6 mg/dL for women and 7 mg/dL for men, as is standard in most studies.[13] The norm was exceeded by 52 women (30.6%) and 85 men (22.4%). The study population was divided into quartiles on the basis of their sUA levels, and for each of them, a comparative analysis and long-term observation was conducted.

Long-term observation

We conducted a two-stage follow-up examination. In the 1st stage, the general type of planned revascularization treatment was evaluated, and in the 2nd stage, we investigated total mortality. All-cause mortality was collected from the PESEL registry of the Polish Ministry of Digital Affairs on November 14, 2018.

The average time from inclusion in the study to death or the end of observation was 1866 days (standard deviation (SD) = 840); the median was 2092 days. In the group of living patients, the average observation time was 2324 days (SD = 327); the median was 2335 days. In the whole study group, 178 people died (32.4%). In the group of deceased patients, the average follow-up time was 913 days (SD = 791); the median was 660 days.

Statistical analysis

In the statistical analysis, the distribution of variables was evaluated using the Kolmogorov–Smirnov test. The two-tailed T-test and analysis of variance (ANOVA) test were used for comparative analysis. Non-normally distributed data was compared using the Mann–Whitney test. The results obtained were presented as mean values with SD or as percentage values corresponding to relative frequency.

Pearson's rank correlation test was applied for evaluating relationships among the biochemical parameters. A forward stepwise (Wald) logistic regression was used to determine mortality risk factors. The results were presented as risk ratios (RR) from the 5th to the 95th. A two-sided p-value ≤0.05 was considered significant. All analyses were performed using MS Excel v. 16.40 (Microsoft Corp., Redmond, USA) and SPSS IBM software v. 26 (IBM Corp., Armonk, USA).

The study was approved by the Bioethics Committee of the Medical University of Bialystok (approval No. R-1-002/18/2019).

Results

A total of 549 patients were qualified for the analysis, with men in the majority (n = 379, 69.03%). The mean age of the entire group was 68.42 years (SD = 11.66). The majority of the patients (n = 422, 76.87%) were burdened with

Table 1. Characteristics of the studied population

Parameter	Studied population (n = 549)
Age [years], mean (SD)	68.42 (11.66)
Male, % (n)	69.03 (379)
BMI [kg/m^2], mean (SD)	27.81 (4.92)
SBP on admission [mm Hg], mean (SD)	139.7 (23.46)
DBP on admission [mm Hg], mean (SD)	79.81 (13.71)
Heart rate on admission [mm Hg], mean (SD)	77.42 (17.61)
EF [%], mean (SD)	44.36 (10.68)
Gout, % (n)	4.19 (23)
Arterial hypertension, % (n)	76.87 (422)
DM2, % (n)	25.50 (140)
Previous myocardial infarction, % (n)	22.40 (123)
CKD, % (n)	28.78 (158)
sUA concentration [mg/dL], mean (SD)	5.78 (1.89)
Exceeded sUA norm, % (n)	24.95 (137)
Serum creatinine concentration [mg/dL], mean (SD)	1.00 (0.35)
eGFR [mL/min/1.73 m^2], mean (SD)	75.67 (21.99)
Hemoglobin concentration [g/dL], mean (SD)	13.69 (1.79)
Platelet count [×10^3/mm^3], mean (SD)	221.08 (88.25)
Leukocytes count [×10^6/mm^3], mean (SD)	9.23 (5.08)
Total serum cholesterol concentration [mg/dL], mean (SD)	198.04 (51.79)
Serum LDL cholesterol concentration [mg/dL], mean (SD)	130.49 (47.65)
Serum HDL cholesterol concentration [mg/dL], mean (SD)	47.67 (12.53)
Serum triglyceride concentration [mg/dL], mean (SD)	120.32 (84.88)
Serum glucose concentration on admission [mg/dL], mean (SD)	128.71 (45.84)
Potassium concentration [mEq/L], mean (SD)	4.28 (0.43)
Sodium concentration [mEq/L], mean (SD)	138.92 (3.52)
Fibrinogen concentration [mg/dL], mean (SD)	432.50 (107.86)
Patients with eGFR >90 mL/min/73 m^2, % (n)	31.33 (172)
Patients with eGFR 60–90 mL/min/1.73 m^2, % (n)	44.26 (243)
Patients with eGFR 45–60 mL/min/1.73 m^2, % (n)	12.75 (70)
Patients with eGFR 30–45 mL/min/1.73 m^2, % (n)	8.38 (46)
Patients with eGFR 15–30 mL/min/1.73 m^2, % (n)	3.28 (18)
Multi vessel disease	37.83 (199)
PCI LM, % (n)	4.19 (23)
PCI LAD, % (n)	28.42 (156)
PCI RCA, % (n)	24.77 (136)
PCI Diag, % (n)	4.74 (26)
PCI Cx, % (n)	25.14 (138)
PCI IM, % (n)	2.01 (11)
PCI M, % (n)	11.11 (61)
CABG, % (n)	6.19 (34)
In-hospital mortality, % (n)	2.55 (14)
Conservative treatment during follow-up, % (n)	51.55 (283)
CABG during follow-up, % (n)	9.11 (50)
PCI during follow-up, % (n)	30.6 (168)
Deaths during follow-up, % (n)	32.42 (178)

BMI – body mass index; SBP – systolic blood pressure; sUA – serum uric acid; DBP – diastolic blood pressure; DM2 – diabetes mellitus type 2; CABG – coronary artery bypass grafting; Cx – circumflex artery; EF – ejection fraction; CKD – chronic kidney disease; eGFR – estimated glomerular filtration rate; HDL – high density lipoprotein; IM – intermediate; LDL – low density lipoprotein; LMCA – left main coronary artery; LAD – left anterior descending artery; M – marginal; PCI – percutaneous coronary intervention; PDA – posterior descending artery; RCA – right coronary artery; SD – standard deviation.

arterial hypertension; 158 (28.78%) had CKD; 140 (25.5%) had DM2; 123 (22.4%) had a history of previous myocardial infarction; and 23 (4.19%) suffered from gout. All the patients had undergone invasive treatments. Nearly 1 in 3 patients had a narrowing of more than 1 coronary artery. The most common procedure they had undergone was a percutaneous coronary intervention (PCI) on the left anterior descending coronary artery (LAD; n = 156, 28.42%;). Coronary artery bypass surgery (CABG) had been performed on 34 (6.19%) of the patients. During the follow-up period, 168 (30.06%) of the patients had a PCI and 50 (9.11%) underwent a CABG procedure (Table 1).

The mean concentration of sUA in the study group was 5.78 mg/dL (SD = 1.89 mg/dL). The lowest observed value was 1.92 mg/dL. In 133 (25%) of the patients, the sUA concentration was below 4.42 mg/dL, and in 149 (25%) of the group the level was above 6.69 mg/dL. The highest observed value was 14.12 mg/dL. The median sUA value was 5.42 mg/dL (interquartile range (IQR) = 2.27) (Table 2, Fig. 1).

Serum UA concentration correlates inversely with total serum cholesterol concentration (R = –0.10) and serum high-density-lipoprotein (HDL) cholesterol concentration (R = –0.26). However, there is a positive correlation between sUA and creatinine concentration (R = 0.50), and between sUA and triglyceride (R = 0.14) concentration (Table 3).

The group with elevated sUA values (over 6.69 mg/dL) was significantly older than the one with sUA values under 4.42 mg/dL: 72.30 (SD = 10.38) compared to 67.13 (SD = 11.78); $p < 0.001$. The elevated group also had a significantly higher heart rate on admission (81.9 (SD = 18.09) compared to 75.93 (SD = 17.21)); $p < 0.001$) and a lower ejection fraction (EF) (41.11 (SD = 12.16) compared to 45.44 (SD = 9.93); $p < 0.001$) than the group with sUA values under 4.42 mg/dL. Additionally, gout was diagnosed more

Table 2. Serum uric acid concentration in the study population

Parameter	UA [mg/dL]
Minimum	1.92
Maximum	14.12
Mean	5.78
SD	1.89
Median	5.42
1Q	4.42
3Q	6.69
IQR	2.27
Sum	549

UA – uric acid; IQR – interquartile range; SD – standard deviation; 1Q – 1st quartile; 3Q – 3rd quartile.

Table 3. Pearson's correlations between biochemical parameters (significant results were underlined, p < 0.05)

Parameter	R
Creatinine concentration	0.50
Fibrinogen concentration	0.02
Hemoglobin concentration	0.02
Platelet count	–0.08
Leukocytes	0.04
Total serum cholesterol concentration	–0.10
Serum LDL cholesterol concentration	–0.07
Serum HDL cholesterol concentration	–0.26
Serum triglyceride concentration	0.14
Serum glucose concentration	0.09
Potassium concentration	0.10
Sodium concentration	–0.07

LDL – low-density lipoprotein; HDL – high-density lipoprotein.

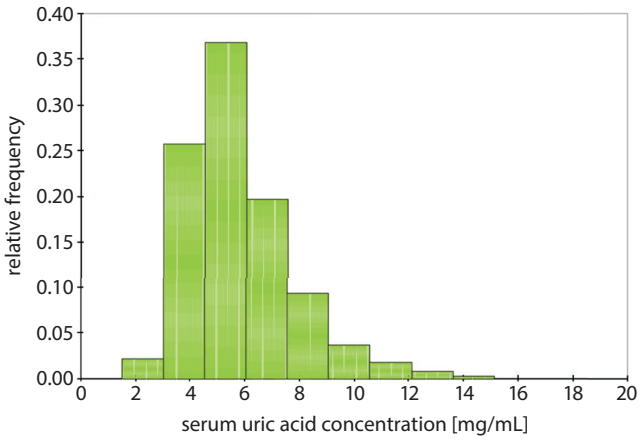

Fig. 1. Histogram of sUA concentration

frequently in this group (16 patients (11.67%) compared to 7 patients (1.70%); p < 0.001)), as well as CKD (84 patients (61.31%) compared to 74 patients (17.96%); p < 0.001), which was associated with differences in the frequency of different ranges of eGFR values. We also observed that the group with elevated sUA values had a significantly higher average

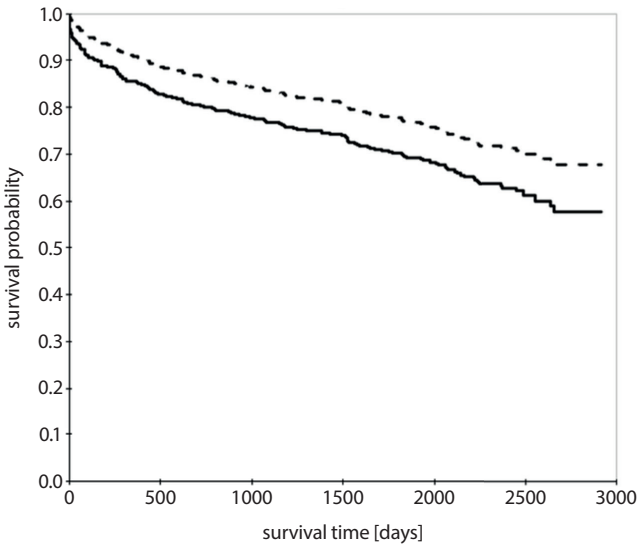

Fig. 2. Kaplan–Meier survival curve. Survival curves for normal serum uric acid values (continuous line) vs exceeded serum uric acid values (dashed line).

serum creatinine concentration (1.25 mg/dL (SD = 0.46) compared to 0.91 mg/dL (SD = 0.26); p < 0.001); a lower average eGFR (57.92 mL/min/1.73 m^2 (SD = 22.65) compared to 81.58 mL/min/1.73 m^2 (SD = 18.31); p < 0.001); and a lower average serum HDL cholesterol concentration (43.68 mg/dL (SD = 13.43) compared to 48.98 mg/dL (SD = 11.95); p < 0.001). Additionally, patients with hyperuricemia died more often during the study (60/137 patients (43.8%)) compared to patients with normal sUA values (118/412 values (28.64%)); p = 0.01) and had a higher in-hospital death rate (8/137 patients (5.84%) compared to 6/412 patients (1.46%); p = 0.04) (Table 4, Fig. 2).

A multivariable regression analysis showed that hyperuricemia was more likely to occur in women (RR = 1.52, 95% confidence interval (95% CI) = 1.016–2.288, p = 0.042) and in patients with CKD (RR = 3.452, 95% CI = 2.432–4.854, p < 0.001). People with higher body mass index (BMI) (RR = 1.048, 95% CI = 1.008–1.090, p = 0.018) were more likely to have increased sUA levels, but this likelihood decreased with an increase in EF (RR = 0.964, 95% CI = 0.946–0.981, p < 0.001) or in HDL concentration (RR = 0.963, 95% CI = 0.946–0.980, p < 0.001) (Table 5).

The study population was divided into quartiles based on their sUA level. Patients in the 4th quartile (4Q) were the oldest (p < 0.001) and showed the lowest EF (p < 0.001). The 2nd quartile (2Q) was associated with the rarest occurrence of DM2 and hypertension (p < 0.001). With increasing concentrations of sUA, the occurrence of CKD and death increased (p < 0.001), especially in the 4Q (Table 6, Fig. 3).

The patients who died during the observation period were statistically older than those who survived (74.76 years (SD = 9.86) compared to 65.37 years (SD = 11.23); p < 0.001); had higher heart rates on admission (82.53 bpm (SD = 18.61) compared to 74.97 bpm (SD = 16.59, p < 0.001); had lower EF (38.84% (SD = 12.21)

Table 4. Comparison of patients with exceeded sUA value and normal

Parameter	Exceeded value (n = 137)	Normal value (n = 412)	p-value
Age [years], mean (SD)	72.30 (10.38)	67.13 (11.78)	<0.001
Male, % (n)	62.04 (85)	71.36 (294)	0.045
BMI [kg/m^2], mean (SD)	28.68 (5.33)	27.52 (4.75)	0.03
SBP on admission [mm Hg], mean (SD)	137.56 (23.37)	140.42 (23.47)	0.22
DBP on admission [mm Hg], mean (SD)	78.86 (14.82)	80.13 (13.32)	0.37
Heart rate on admission [mm Hg], mean (SD)	81.9 (18.09)	75.93 (17.21)	<0.001
EF [%], mean (SD)	41.11 (12.16)	45.44 (9.93)	<0.001
Arterial hypertension, % (n)	81.02 (111)	75.49 (311)	0.16
DM2, % (n)	35.77 (49)	22.09 (91)	0.003
Gout, % (n)	11.67 (16)	1.7 (7)	<0.001
Previous myocardial infarction, % (n)	32.12 (44)	19.17 (79)	0.004
CKD, % (n)	61.31 (84)	17.96 (74)	<0.001
Patients with eGFR ≥90 mL/min/1.73 m^2, % (n)	8.76 (12)	38.83 (160)	<0.001
Patients with eGFR 60–89 mL/min/1.73 m^2, % (n)	35.04 (48)	47.33 (195)	0.01
Patients with eGFR 45–59 mL/min/1.73 m^2, % (n)	23.36 (32)	9.22 (38)	<0.001
Patients with eGFR 30–44 mL/min/1.73 m^2,% (n)	23.36 (32)	3.4 (14)	<0.001
Patients with eGFR 15–29 mL/min/1.73 m^2, % (n)	9.49 (13)	1.21 (5)	0.002
PCI LM [%] (n)	3.65 (5)	4.37 (18)	0.71
PCI LAD [%] (n)	32.85 (45)	26.94 (111)	0.20
PCI RCA [%] (n)	27.01 (37)	24.03 (99)	0.49
PCI Diag [%] (n)	2.19 (3)	5.58 (23)	0.045
PCI Cx [%] (n)	22.63 (31)	25.97 (107)	0.43
PCI IM [%] (n)	0.73 (1)	2.43 (10)	0.11
PCI M [%] (n)	10.95 (15)	11.17 (46)	0.94
Further conservative treatment, % (n)	46.72 (64)	53.16 (219)	0.19
CABG during admission, % (n)	6.57 (9)	6.07 (25)	0.84
Elective CABG, % (n)	12.41 (17)	8.01 (33)	0.16
Elective PCI, % (n)	28.47 (39)	31.31 (129)	0.53
In-hospital mortality, % (n)	5.84 (8)	1.46 (6)	0.04
Deaths, % (n)	43.8 (60)	28.64 (118)	<0.001
Serum creatinine concentration [mg/dL], mean (SD)	1.25 (0.46)	0.91 (0.26)	<0.001
eGFR, CKD-EPI (mL/min/1.73 m^2, % (n)), mean (SD)	57.92 (22.65)	81.58 (18.31)	<0.001
Hemoglobin concentration [g/dL], mean (SD)	13.37 (2.05)	13.79 (1.68)	0.03
Platelet count [×10^3/mm^3], mean (SD)	219.08 (110.74)	221.75 (79.53)	0.80
Leukocytes [×10^6/mm^3], mean (SD)	9.44 (1.29)	9.16 (3.78)	0.42
Total serum cholesterol concentration [mg/dL], mean (SD)	186.41 (55.9)	201.92 (49.82)	0.005
Serum LDL cholesterol concentration [mg/dL], mean (SD)	119.73 (48.8)	134.08 (46.78)	0.003
Serum HDL cholesterol concentration [mg/dL], mean (SD)	43.68 (13.43)	48.98 (11.95)	<0.001
Serum triglyceride concentration [mg/dL], mean (SD)	141.27 (107.59)	113.34 (74.68)	0.006
Serum glucose concentration on admission [mg/dL], mean (SD)	139.43 (49.36)	125.14 (44.1)	0.003
Potassium concentration [mEq/L], mean (SD)	4.36 (0.52)	4.25 (0.4)	0.03
Sodium concentration [mEq/L], mean (SD)	138.41 (4.5)	139.09 (3.11)	0.10
Fibrinogen concentration [mg/dL], mean (SD)	445.56 (110.77)	13.79 (1.68)	0.11

BMI – body mass index; SBP – systolic blood pressure; sUA – serum uric acid; DBP – diastolic blood pressure; DM2 – diabetes mellitus type 2; CABG – coronary artery bypass grafting; Cx – circumflex artery; EF – ejection fraction; CKD – chronic kidney disease; eGFR – estimated glomerular filtration rate; CKD-EPI – chronic kidney disease-epidemiology collaboration formula; HDL – high density lipoprotein; IM – intermediate; LDL – low density lipoprotein; LMCA – left main coronary artery; LAD – left anterior descending artery; M – marginal; PCI – percutaneous coronary intervention; PDA – posterior descending artery; RCA – right coronary artery; SD – standard deviation.

Table 5. Multivariable logistic regression forward stepwise Wald method – OR for exceeding the norm of UA concentration

Parameter	p-value	RR	95% CI for RR
Male	0.042	0.656	0.437–0.984
Age (for every 1 year)	<0.001	1.042	1.023–1.060
CKD	<0.001	3.452	2.432–4.854
EF (for each 1% increase)	<0.001	0.964	0.946–0.981
BMI (for each 1 kg/m^2 increase)	0.018	1.048	1.008–1.090
HDL (for each 1 mg/dL increase)	<0.001	0.963	0.946–0.980

R^2 Nagelkerke – 0.89; BMI – body mass index; CI – confidence interval; EF – ejection fraction; HDL – high density lipoprotein; RR – risk ratio; OR – odds ratio; UA – uric acid; CKD – chronic kidney disease.

Table 6. Quartiles of sUA in the study population

Parameters \ Quartiles	1Q (<4.42) (n = 133)	2Q (4.42–5.42) (n = 132)	3Q (5.36–6.69) (n = 135)	4Q (>6.69) (n = 149)	p-value
Male, % (n)	57.14 (76)	68.18 (90)	72.59 (98)	77.18 (115)	p < 0.001
Age [years], mean, (SD)	67.56 (11.46)	66.71 (11.89)	68.15 (12.7)	70.93 (10.24)	p < 0.001
EF (%), mean, (SD)	45.32 (9.29)	46.09 (10.26)	45.96 (9.05)	40.53 (12.57)	p < 0.001
Hypertension, %, (n)	77.44 (103)	69.7 (92)	79.26 (107)	80.54 (120)	p < 0.001
DM2, %, (n)	26.32 (35)	18.94 (25)	23.7 (32)	32.21 (48)	p < 0.001
CKD, %, (n)	12.78 (17)	18.18 (24)	25.19 (34)	55.7 (83)	p < 0.001
Deaths, %, (n)	27.82 (37)	28.03 (37)	27.41 (37)	44.97 (67)	p < 0.001

CKD – chronic kidney disease; EF – ejection fraction; DM2 – type 2 diabetes mellitus; SD – standard deviation; 1Q – 1st quartile; 2Q – 2nd quartile; 3Q – 3rd quartile; 4Q – 4th quartile.

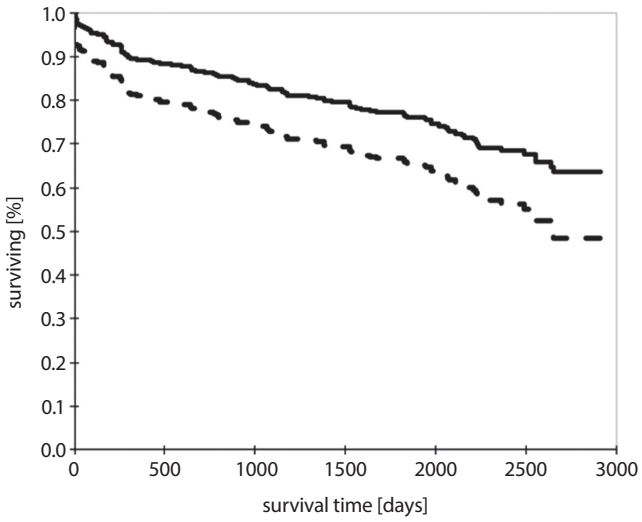

Fig. 3. Kaplan–Meier survival curve. Survival curves for 1 quartile of serum uric acid concentration (continuous line) vs 4 quartile (dashed line)

compared to 46.96% (SD = 8.77); p < 0.001); and more frequently had a history of DM2 (59 (33.15%) compared to 81 (21.83%); p = 0.007) and myocardial infarction (54 (30.34%) compared to 69 (18.6%); p = 0.004). They were diagnosed more frequently with CKD (83 patients (46.63%) compared to 75 (20.22%); p < 0.001); therefore, they were predominantly in the eGFR ranges of 45–59 mL/min and 30–44 mL/min. Regarding invasive artery treatment, the only difference between the group who died and the survivors was that PCIs for the left main coronary artery (PCI LM) had been performed more often on the patients who died (14 (7.87%) compared to 9 (2.43%); p = 0.013). The patients who died also had higher concentrations of sUA and creatinine, along with lower eGFR and hemoglobin concentration. On admission, they had lower concentrations of total cholesterol (185.3 mg/dL (SD = 52.76) compared to 204.1 mg/dL (SD = 50.28); p < 0.001) and its fractions than the survivors; they also had higher concentrations of glucose (138.81 mg/dL (SD = 52.49) compared to 123.85 mg/dL (SD = 41.5); p < 0.001) and fibrinogen (466 mg/mL (SD = 115.52) compared to 416.43 mg/mL (SD = 100.24); p < 0.001) (Table 7).

The multivariable regression analysis showed that the risk of death increased significantly with age (RR = 1.086, 95% CI = 1.065–1.108, p < 0.001) and increases in sUA concentration (RR = 1.245, 95% CI = 1.131–1.370, p = 0.041), but also decreased with increases in EF (RR = 0.928, 95% CI = 0.910–0.946, p < 0.001) and hemoglobin concentrations (RR = 0.685, 95% CI = 0.611–0.768, p < 0.001) (Table 8).

Discussion

In this long-term observational study, we assessed the influence of sUA levels among patients with NSTEMI. We found that a high sUA level was a factor that increased mortality. The study also showed that high levels

Table 7. Comparison of dead and surviving patients

Parameter	Alive patients (n = 371)	Dead patients (n = 178)	p-value
Age [years], mean (SD)	65.37 (11.23)	74.76 (9.86)	<0.001
Male, % (n)	71.16 (264)	64.61 (115)	0.128
BMI [kg/m^2], mean (SD)	28.05 (4.76)	27.32 (5.23)	0.115
SBP on admission [mm Hg], mean (SD)	141.15 (22.22)	136.7 (25.64)	0.048
DBP on admission [mm Hg], mean (SD)	80.83 (13.04)	77.7 (14.82)	0.017
Heart rate on admission [mm Hg], mean (SD)	74.97 (16.59)	82.53 (18.61)	<0.001
EF [%], mean (SD)	46.96 (8.77)	38.84 (12.21)	<0.001
Arterial hypertension, % (n)	76.01 (282)	78.65 (140)	0.487
DM2, % (n)	21.83 (81)	33.15 (59)	0.007
Gout, % (n)	3.5 (13)	5.62 (10)	0.286
Previous myocardial infarction, % (n)	18.6 (69)	30.34 (54)	0.004
CKD, % (n)	20.22 (75)	46.63 (83)	<0.001
eGFR ≥90 mL/min/1.73 m^2, % (n)	40.16 (149)	12.92 (23)	<0.001
eGFR 60–90 mL/min/1.73 m^2, % (n)	43.94 (163)	44.94 (80)	0.824
eGFR 45–60 mL/min/1.73 m^2, % (n)	8.63 (32)	21.35 (38)	<0.001
eGFR 30–45 mL/min/1.73 m^2, % (n)	5.39 (20)	14.61 (26)	0.002
eGFR 15–30 mL/min/1.73 m^2, % (n)	1.89 (7)	6.18 (11)	0.028
PCI LM, % (n)	2.43 (9)	7.87 (14)	0.013
PCI LAD, % (n)	30.19 (112)	24.72 (44)	0.175
PCI RCA, % (n)	25.07 (93)	24.16 (43)	0.817
PCI Diag, % (n)	4.31 (16)	5.62 (10)	0.52
PCI Cx, % (n)	25.07 (93)	25.28 (45)	0.957
PCI IM, % (n)	2.16 (8)	1.69 (3)	0.701
PCI M, % (n)	11.05 (41)	11.24 (20)	0.949
CABG, % (n)	53.37 (198)	47.75 (85)	0.219
Conservative treatment during follow-up, % (n)	6.2 (23)	6.18 (11)	0.993
CABG treatment during follow-up, % (n)	7.82 (29)	11.8 (21)	0.156
PCI treatment during follow-up, % (n)	32.61 (121)	26.4 (47)	0.132
sUA concentration [mg/dL], mean (SD)	5.52 (1.6)	6.32 (2.31)	<0.001
Exceeded sUA norm, % (n)	20.75 (77)	33.71 (60)	0.002
Serum creatinine concentration [mg/dL], mean (SD)	0.94 (0.32)	1.11 (0.4)	<0.001
eGFR [mL/min*1.73 m^2], mean (SD)	80.85 (20.1)	64.88 (21.9)	<0.001
Hemoglobin concentration [g/dL], mean (SD)	14.05 (1.7)	12.93 (1.74)	<0.001
Platelet count [×10^3/mm^3], mean (SD)	217.32 (72.17)	228.93 (114.6)	0.217
Leukocytes [×10^6/mm^3], mean (SD)	9.09 (3.37)	9.53 (1.69)	0.188
Total serum cholesterol concentration [mg/dL], mean (SD)	204.1 (50.28)	185.3 (52.76)	<0.001
Serum LDL cholesterol concentration [mg/dL], mean (SD)	136.22 (46.81)	118.45 (47.29)	<0.001
Serum HDL cholesterol concentration [mg/dL], mean, (SD)	48.86 (12.01)	45.2 (13.22)	0.002
Serum triglyceride concentration [mg/dL], mean (SD)	122.57 (89.76)	115.6 (73.58)	0.34
Serum glucose concentration on admission [mg/dL], mean (SD)	123.85 (41.5)	138.81 (52.49)	<0.001
Potassium concentration [mEq/L], mean (SD)	4.28 (0.41)	4.29 (0.49)	0.808
Sodium concentration [mEq/L], mean (SD)	139.14 (2.92)	138.48 (4.49)	0.075
Fibrinogen concentration [mg/dL], mean (SD)	416.43 (100.24)	466 (115.52)	<0.001

BMI – body mass index; SBP – systolic blood pressure; sUA – serum uric acid; DBP – diastolic blood pressure; DM2 – diabetes mellitus type 2; CABG – coronary artery bypass grafting; Cx – circumflex artery; EF – ejection fraction; CKD – chronic kidney disease; eGFR – estimated glomerular filtration rate; HDL – high density lipoprotein; IM – intermediate; LDL – low density lipoprotein; LMCA – left main coronary artery; LAD – left anterior descending artery; M – marginal; PCI – percutaneous coronary intervention; PDA – posterior descending artery; RCA – right coronary artery; SD – standard deviation.

Table 8. Multivariable logistic regression forward stepwise Wald method – risk of death

Parameter	p-value	RR	95% CI for RR
Age (for every 1 year)	<0.001	1.086	1.065–1.108
EF (for each 1% increase)	<0.001	0.928	0.910–0.946
sUA concentration (for each 1 mg/dL increase)	0.041	1.245	1.131–1.370
Hemoglobin concentration (for each 1 mg/dL increase)	<0.001	0.685	0.611–0.768

R^2 Nagelkerke – 0.72; sUA – serum uric acid; EF – ejection fraction; RR – risk ratio; 95% CI – 95% confidence interval.

of creatinine and triglycerides as well as a high BMI coexisted with high sUA, as did low HDL cholesterol and EF.

Uric acid is the end result of purine metabolism, which mainly occurs in the liver. Its serum levels depend on many factors, such as purine intake from the diet, liver metabolism, excretion by the kidneys, and intestinal degeneration.[14] There are several theories about possible pathophysiological mechanisms that are triggered by hyperuricemia. An increased concentration of UA may cause deposits of sodium urate crystals not only in the periarticular tissues but also within the walls of blood vessels. The consequence of the presence of these deposits within the walls of blood vessels is damage to the endothelium, which promotes atherosclerotic changes. The deposits also cause chronic inflammation and damage to the vessel structure, which may all play a role in the occurrence of ACS.[15,16] An additional mechanism is the influence of high sUA levels on the HMGB1/RAGE signaling pathway. This induces oxidative stress and an inflammatory response, which consequently causes endothelial dysfunction.[17]

Many previous studies have tried to establish the role of sUA in the occurrence of CVD, with contradictory results. In a recent study, researchers from Pakistan reported that in a group of acute myocardial infarction (AMI) patients, sUA levels were higher than in the control group, as was the number of patients with hyperuricemia.[18]

Hyperuricemia has already been linked to the occurrence of other diseases that are known risk factors for ACS, such as hypertension, dyslipidemia, obesity, metabolic syndrome, and CKD.[4,5] The significance of UA in hypertension is reflected in the guidelines of the European Society of Hypertension, which recommend testing sUA levels as a routine laboratory test in hypertensive patients.[19] The use of sUA as a marker for cardiac ischemia, which occurs in ACS, might be supported by the fact that adenosine, which is released during ischemia and tissue hypoxia, is degraded by the endothelium to UA, resulting in elevated sUA concentrations.[20,21]

In our study, we observed a positive correlation between the high sUA levels and elevated levels of creatinine and triglycerides. These results overlap with findings from Hajizadeh et al., Tuomilehto et al. and Nagahama et al.[8,22,23] A positive correlation was also found for lower EF and lower rates of CKS, as other researchers have also noted.[8,24,25]

Most studies have confirmed the impact of high sUA levels on increased mortality in patients with AMI, especially the STEMI subtype.[26,27] On the other hand, we can also find contradictory results,[8] including a study that denies any link between sUA and mortality from all causes, including CVD.[28]

A meta-analysis conducted in 2019 by He et al. noted that ACS patients with hyperuricemia had a higher risk of all-cause and cardiovascular mortality.[29] It was also suggested that further studies taking into account the specific subtype of ACS patients are needed. In the present study, almost every third patient with NSTEMI died during the observation. In the group of patients with elevated UA levels, the death rate was 1.5 times higher. A graded increase was demonstrated in the incidence of mortality by increasing quartiles of hyperuricemia.

In addition, Mora-Ramírez et al. showed that high levels of sUA on admission have an impact on short-term mortality among patients admitted due to STEMI with a high prevalence of cardiovascular risk factors.[30] In 2019, Wei et al. confirmed the influence of UA on long-term mortality in a group of patients with ACS who had undergone PCI.[31] In our long-term observation, hyperuricemia is associated with higher long-term mortality in patients following NSTEMI. Additional adverse prognostic factors were age, EF and hemoglobin concentration.

These findings encourage consideration of proceeding earlier with UA-lowering treatment in order to reduce cardiovascular risks and potential mortality if they occur, especially since hyperuricemia can be effectively controlled with pharmacological treatment. Prospective studies are necessary to show whether this treatment strategy will bring about the desired results

Limitations

Our study had several limitations. First, it was a single-center-based study that may not have general application, but the large study group and long follow-up period were certainly strengths. Second, survival data was obtained using personal identification numbers (PESEL) and causes of death were not taken into account – only when death occurred.

Conclusions

One in 4 patients had sUA levels above the norm. Factors predisposing patients to elevated UA levels were high BMI, CKD, female sex, low HDL, and low left ventricular

ejection fraction (LVEF). Nearly every 3rd patient with a diagnosis of ACS died during the observation. In the group of patients with elevated UA concentrations, the death rate was 1.5 times higher. Serum UA concentration is an independent risk factor of long-term mortality in patients who have undergone NSTEMI, and is associated with higher in-hospital death rates. Additional adverse prognostic factors were age, low EF and low hemoglobin concentration. Secondary prevention after NSTEMI should entail management of the patients" sUA levels.

ORCID iDs

Łukasz Kuźma https://orcid.org/0000-0002-4156-5695
Agata Kulikowska https://orcid.org/0000-0003-1038-4418
Anna Kurasz https://orcid.org/0000-0003-0526-3339
Marta Maria Niwińska https://orcid.org/0000-0002-9831-917X
Małgorzata Zalewska-Adamiec https://orcid.org/0000-0002-2466-4093
Sławomir Dobrzycki https://orcid.org/0000-0003-0599-7017
Hanna Bachórzewska-Gajewska https://orcid.org/0000-0002-0233-6996

References

1. Roth GA, Johnson C, Abajobir A, et al. Global, regional, and national burden of cardiovascular diseases for 10 causes, 1990 to 2015. *J Am Coll Cardiol*. 2017;70(1):1–25. doi:10.1016/j.jacc.2017.04.052
2. Anand SS, Islam S, Rosengren A, et al; INTERHEART Investigators. Risk factors for myocardial infarction in women and men: Insights from the INTERHEART study. *Eur Heart J*. 2008;29(7):932–940. doi:10.1093/eurheartj/ehn018
3. Li J, Muraki I, Imano H, et al; CIRCS Investigators. Serum uric acid and risk of stroke and its types: The Circulatory Risk in Communities Study (CIRCS). *Hypertens Res*. 2020;43(4):313–321. doi:10.1038/s41440-019-0385-5
4. Yokokawa H, Fukuda H, Suzuki A, et al. Association between serum uric acid levels/hyperuricemia and hypertension among 85,286 Japanese workers. *J Clin Hypertens (Greenwich)*. 2016;18(1):53–59. doi:10.1111/jch.12627
5. Coutinho TA, Turner ST, Peyser PA, Bielak LF, Sheedy 2nd PF, Kullo IJ. Associations of serum uric acid with markers of inflammation, metabolic syndrome and subclinical coronary atherosclerosis. *Am J Hypertens*. 2007;20(1):83–89. doi:10.1016/j.amjhyper.2006.06.015
6. Rahimi-Sakak F, Maroofi M, Rahmani J, Bellissimo N, Hekmatdoost A. Serum uric acid and risk of cardiovascular mortality: A systematic review and dose-response meta-analysis of cohort studies of over a million participants. *BMC Cardiovasc Disord*. 2019;19(1):218. doi:10.1186/s12872-019-1215-z DOI: 10.1186/s12872-019-1215-z
7. Kim SY, Guevara JP, Kim KM, Choi HK, Heitjan DF, Albert DA. Hyperuricemia and coronary heart disease: A systematic review and meta-analysis. *Arthritis Care Res (Hoboken)*. 2010;62(2):170–180. doi:10.1002/acr.20065
8. Hajizadeh R, Ghaffari S, Salehi R, Mazani S, Aghavali S. Association of serum uric acid level with mortality and morbidity of patients with acute ST-elevation myocardial infarction. *J Cardiovasc Thorac Res*. 2016;8(2):56–60. doi:10.15171/jcvtr.2016.11
9. Roger VL, Weston SA, Gerber Y, et al. Trends in incidence, severity, and outcome of hospitalized myocardial infarction. *Circulation*. 2010;121(7):863–869. doi:10.1161/CIRCULATIONAHA.109.897249
10. Car S, Trkulja V. Higher serum uric acid on admission is associated with higher short-term mortality and poorer long-term survival after myocardial infarction: Retrospective prognostic study. *Croat Med J*. 2009;50(6):559–566. doi:10.3325/cmj.2009.50.559
11. Trkulja V, Car S. On-admission serum uric acid predicts outcomes after acute myocardial infarction: Systematic review and meta-analysis of prognostic studies. *Croat Med J*. 2012;53(2):162–172. doi:10.3325/cmj.2012.53.162
12. Çanga Y, Emre A, Karataş MB, et al. Prognostic value of serum uric acid levels in patients with non-STEMI undergoing percutaneous coronary intervention. *Herz*. 2020;45(4):389–396. doi:10.1007/s00059-019-04849-3
13. Kuwabara M, Niwa K, Hisatome I, et al. Asymptomatic hyperuricemia without comorbidities predicts cardiometabolic diseases: Five-year Japanese cohort study. *Hypertension*. 2017;69(6):1036–1044. doi:10.1161/HYPERTENSIONAHA.116.08998
14. Basseville A, Bates SE. Gout, genetics and ABC transporters. *F1000 Biol Rep*. 2011;3:23. doi:10.3410/B3-23
15. Dalbeth N, House ME, Aati O, et al. Urate crystal deposition in asymptomatic hyperuricaemia and symptomatic gout: A dual energy CT study. *Ann Rheum Dis*. 2015;74(5):908–911. doi:10.1136/annrheumdis 2014-206397
16. Kato M, Histome I, Tomikura Y, et al. Status of endothelial dependent vasodilation in patients with hyperuricemia. *Am J Cardiol*. 2005;96(11):1576–1578. doi:10.1016/j.amjcard.2005.07.068
17. Cai W, Duan XM, Liu Y, et al Uric acid induces endothelial dysfunction by activating the HMGB1/RAGE signaling pathway. *Biomed Res Int*. 2017;2017:4391920. doi:10.1155/2017/4391920
18. Mal K, Jabar AJ, Fatima K, Rizwan A. Incidence of hyperuricemia in patients with acute myocardial infarction: A case-control study. *Cureus*. 2020;12(1):e6722. doi:10.7759/cureus.6722
19. European Society of Hypertension-European Society of Cardiology Guidelines Committee. 2003 European Society of Hypertension-European Society of Cardiology guidelines for the management of arterial hypertension. *J Hypertens*. 2003;21(6):1011–1053. doi:10.1097/00004872-200306000-00001
20. Raatikainen MJ, Peuhkurinen KJ, Hassinen IE. Contribution of endothelium and cardiomyocytes to hypoxia-induced adenosine release. *J Mol Cell Cardiol*. 1994;26(8):1069–1080. doi:10.1006/jmcc.1994.1127
21. Kroll K, Bukowski TR, Schwartz LM, Knoepfler D, Bassingthwaighte JB. Capillary endothelial transport of uric acid in guinea pig heart. *Am J Physiol*. 1992;262(2 Pt 2):H420–H431. doi:10.1152/ajpheart.1992.262.2.H420
22. Tuomilehto J, Zimmet P, Wolf E, Taylor R, Ram P, King H. Plasma uric acid level and its association with diabetes mellitus and some biologic parameters in a biracial population of Fiji. *Am J Epidemiol*. 1988;127(2):321–336. doi:10.1093/oxfordjournals.aje.a114807
23. Nagahama K, Iseki K, Inoue T, Touma T, Ikemiya Y, Takishita S. Hyperuricemia and cardiovascular risk factor clustering in a screened cohort in Okinawa, Japan. *Hypertens Res*. 2004;27(4):227–233. doi:10.1291/hypres.27.227
24. Ranjith N, Myeni NN, Sartorius B, Mayise C. Association between hyperuricemia and major adverse cardiac events in patients with acute myocardial infarction. *Metab Syndr Relat Disord*. 2017;15(1):18–25. doi:10.1089/met.2016.0032
25. Eleftheriadis T, Golphinopoulos S, Pissas G, Stefanidis I. Asymptomatic hyperuricemia and chronic kidney disease: Narrative review of a treatment controversial. *J Adv Res*. 2017;8(5):555–560. doi:10.1016/j.jare.2017.05.001
26. Xu Q, Zhang M, Abeysekera IR, Wang X. High serum uric acid levels may increase mortality and major adverse cardiovascular events in patients with acute myocardial infarction. *Saudi Med J*. 2017;38(6):577–585. doi:10.15537/smj.2017.6.17190
27. Celik T, Iyisoy A. Uric acid levels for the prediction of prognosis in patients with acute ST elevation myocardial infarction: A new potential biomarker. *Int J Cardiol*. 2010;145(1):e21–e22. doi:10.1016/j.ijcard.2008.12.073
28. Sakata K, Hashimoto T, Ueshima H, Okayama A; NIPPON DATA 80 Research Group. Absence of an association between serum uric acid and mortality from cardiovascular disease: NIPPON DATA 80, 1980–1994. National Integrated Projects for Prospective Observation of Non-communicable Diseases and its Trend in the Aged. *Eur J Epidemiol*. 2001;17(5):461–468. doi:10.1023/a:1013735717961
29. He C, Lin P, Liu W, Fang K. Prognostic value of hyperuricemia in patients with acute coronary syndrome: A meta-analysis. *Eur J Clin Invest*. 2019;49(4):e13074. doi:10.1111/eci.13074
30. Mora-Ramírez M, Estevez-Garcia IO, Irigoyen-Camacho ME, Bojalil R, Gonzalez-Pacheco H, Amezcua-Guerra LM. Hyperuricemia on admission predicts short-term mortality due to myocardial infarction in a population with high prevalence of cardiovascular risk factors. *Rev Invest Clin*. 2017;69(5):247–253. doi:10.24875/ric.17002167
31. Wei G, Dahao Y, Dengxuan W, et al. Hyperuricemia and long-term mortality in patients with acute myocardial infarction undergoing percutaneous coronary intervention. *Ann Transl Med*. 2019;7(22):636. doi:10.21037/atm.2019.10.110

Effects of efavirenz and tenofovir on bone tissue in Wistar rats

Agnieszka Matuszewska[1,A–F], Beata Nowak[1,A–F], Anna Nikodem[2,B,C,E,F], Diana Jędrzejuk[3,C,F], Danuta Szkudlarek[4,C,F], Krzysztof Zduniak[4,C,F], Jarosław Filipiak[2,C,E,F], Marta Sznadruk-Bender[1,C,E,F], Tomasz Tomkalski[5,C,E,F], Ireneusz Ceremuga[6,B,C,E,F], Marek Bolanowski[3,E,F], Adam Szeląg[1,E,F]

[1] Department of Pharmacology, Wroclaw Medical University, Poland
[2] Division of Biomedical Engineering and Experimental Mechanics, Wroclaw University of Technology, Poland
[3] Department of Endocrinology, Diabetes and Isotope Therapy, Wroclaw Medical University, Poland
[4] Department of Pathology, Wroclaw Medical University, Poland
[5] Department of Endocrinology, T. Marciniak Lower Silesian Specialist Hospital, Poland
[6] Department of Medical Biochemistry, Wroclaw Medical University, Poland

A – research concept and design; B – collection and/or assembly of data; C – data analysis and interpretation; D – writing the article; E – critical revision of the article; F – final approval of the article

Advances in Clinical and Experimental Medicine, ISSN 1899–5276 (print), ISSN 2451–2680 (online) *Adv Clin Exp Med*. 2020;29(11):1265–1275

Address for correspondence
Beata Nowak
E-mail: beata.nowak@umed.wroc.pl

Funding sources
This study was supported by Wroclaw Medical University (grant No. ST A080.17.035).

Conflict of interest
None declared

Received on March 27, 2020
Reviewed on June 14, 2020
Accepted on September 20, 2020

Abstract

Background. Clinical trials indicate an increased risk of osteoporosis and bone fractures in people infected with human immunodeficiency virus (HIV). The pathogenesis of bone disturbances in HIV-positive patients is unknown, but it is suggested that antiretroviral drugs may be involved.

Objectives. To assess the effects of efavirenz (EF) and tenofovir (T) on bone remodeling in rats.

Material and methods. The study involved 36 male Wistar rats divided into 3 groups, receiving normal saline (control group – group C), efavirenz (group EF) or tenofovir disoproxil (group T).

Results. After 24 weeks of the study, the following observations were made: In blood serum of the EF group compared to group C, there were increased levels of tartrate-resistant acid phosphatase form 5b (TRAP) and inorganic phosphorus. In the densitometric examination, group T showed a lower total body (TB) bone mineral density (BMD) than group C. In the immunohistochemical assessment, group EF showed a higher intensity and extension of anti-tartrate resistant acid phosphatase antibodies (abTRAP) compared to group C. In the histopathological examination of the second lumbar vertebra (L2), group EF showed a lower bone surface/volume ratio (BS/BV) and higher trabecular thickness (Tb.Th) than the control group. In the histopathological examination of the femur, a lower bone surface/tissue volume (BS/TV) and lower trabecular number (Tb.N) were found in group T compared to in group C. A lower value of the Young's modulus was observed in the four-point bending trial in groups EF and T compared to group C.

Conclusions. The results of this study indicate that EF affects bone microarchitecture and leads to impaired biomechanical properties of bones in rats. Additionally, the negative effect of T on bone tissue was confirmed.

Key words: bone, rat model, efavirenz, tenofovir, antiretroviral drug

Cite as
Matuszewska A, Nowak B, Nikodem A, et al. Effects of efavirenz and tenofovir on bone tissue in Wistar rats. *Adv Clin Exp Med*. 2020;29(11):1265–1275. doi:10.17219/acem/127684

DOI
10.17219/acem/127684

Introduction

Human immunodeficiency virus (HIV) and acquired immunodeficiency syndrome (AIDS) constitute an increasing epidemiological problem. It is estimated that about 36.9 million people in the world are HIV-positive, including 1.8 million children below 15 years of age.[1] Highly active antiretroviral therapy (HAART) is the only method of treatment of HIV infections. It is currently administered to neonates, infants and young children infected with HIV.

Effective antiretroviral treatment reduces HIV RNA viremia and the incidence of opportunistic infections and tumors in HIV-positive patients, thus extending their survival and reducing the mortality rate. The necessity of chronic antiretroviral therapy is associated with increasing challenges in the form of chronic drug-related adverse effects, including osteoporosis. A detailed knowledge of possible adverse effects of a drug allows medical teams to optimize the benefits of antiretroviral therapy while minimizing the risks associated with long-term treatment. The necessity of treating children requires assessments of the effects of the drugs administered on the processes of growth, development and maturation of individual organs.

Reduced bone mineral density (BMD), decreases in bone mass and changes in bone microarchitecture are reported in HIV-positive children and adolescents.[2,3] Lower BMD in HIV-positive children is associated with decreases in vitamin D levels and elevated parathyroid hormones (PTH).[4,5] T-cell activation with HIV infection decreases the number of osteogenic precursors, leading to lower peak bone mass and bone strength.[6] As a consequence, HIV-infected children do not reach the same peak bone mass as found in HIV-negative children, and experience an increased frequency of fractures.[7] In animal models of HIV-1, transgenic rats bone loss is a consequence of enhanced osteoclastic bone resorption expressed by an elevated RANKL/OPG ratio.[8] In addition, Ofotokun et al. reported that HIV directly infects circulating osteoclast precursors, enhancing their differentiation and migration to bones, which leads to enhanced bone resorption.[9] On the one hand, bone loss is a direct consequence of HIV infection and AIDS-associated diseases such as muscle wasting, kidney disease and hypogonadism. An effective antiretroviral treatment, causing viral suppression, should reduce the bone mass loss associated with chronic inflammation.[10] On the other hand, studies of adult patients demonstrate that some antiretroviral treatment schemes result in intensified bone mass loss, rather than reduced.[11–15] Low BMD is diagnosed in HAART-treated people 2.5 times more often than those receiving no HAART. Moreover, BMD is reduced by as much as 2–6% during the initial 2 years of antiretroviral therapy.[16] Overall, the fracture rate with HIV infection is 2–6 times higher than in the general population.[9] Shiau et al. reported that BMD decreases persist in HIV-infected children even in the immunologically stable phase of HIV infection.[2] Various antiretroviral drugs seem to have different effects on bone metabolism.

The results of previous studies on the effects of antiretroviral medication, including efavirenz (EF) and tenofovir (T), on bones in children are inconclusive. Some authors have reported reduced BMD in children treated with EF and T. [17] On the other hand, it has been reported that changing the HAART scheme from lopinavir/ritonavir to EF is associated with higher whole-body BMD.[18] However, Dave et al.[19] reported an unfavorable effect of EF on bones, demonstrating that exposure to EF as a part of the HAART scheme in young HIV-positive patients (aged 30–40 years) is independently correlated with lower total hip BMD compared to HAART-naive participants.

Gafni et al. reported reduced BMD in children treated with tenofovir as a part of the HAART scheme.[20] However, other authors have observed no BMD reduction in children treated with the tenofovir-containing HAART scheme.[3,21,22]

Bone mass acquired in childhood and adolescence in a main factor influencing peak adult bone mass, which is a crucial determinant of future osteoporosis and fracture. A 10% increase in peak bone mass delays the onset of osteoporosis by 13 years.[23] Therefore it is extremely important to identify strategies that will allow bone mass deterioration to be minimized in children with HIV.

Discrepancies in the results of the aforementioned studies may stem from non-homogeneous study groups, various stages of HIV infection and the use of polytherapy (which precludes monotherapy studies). For that reason, studies on an animal model are reasonable, as they may allow assessment of the effect of individual drugs on bone metabolism. A rat skeleton grows throughout the lifetime of the animal.[8]

The purpose of this study was to assess the effects of monotherapy with EF (non-nucleoside reverse transcriptase inhibitor – NNRTI) and T (nucleozide reverse transcriptase inhibitor – NRTI) on bone remodeling in rats. As the significance of bone loss associated with HAART in HIV-patients for fracture risk is unclear,[24] we planned to examine bone mechanical properties with a four-point-bending test.

Material and methods

Ethics, the animal model and the experimental design

The study protocol was approved by the Local Ethics Commission for animal experiments (approval No. LKE 41/2017). All the procedures involving animals performed during the study were in accordance with the ethical standards and practices of the institution where the study was conducted.

The study was conducted on 36 male albino Wistar rats, aged 8 weeks, weighing 240–290 g (Animal Research

Center, Wroclaw Medical University, Poland). Throughout the experiment, the rats were kept in pairs in cages with free access to water and standard feed, a diurnal 12:12 light-to-dark cycle and at a constant ambient temperature (21–23°C). The feed (Labofeed; Morawski Feed Company, Kcynia, Poland) contained 0.95% calcium, 0.75% phosphorus and 800 IU/kg of vitamin D.

After a one-week adaptation period, the animals were randomly divided into 3 groups (12 animals in each group): a control group (group C), receiving saline solution (4 mL/kg) (0.9% sodium chloride from B. Braun Melsungen AG, Melsungen, Germany), group EF, receiving 25 mg/kg of efavirenz[25] (Stocrin; Merck Sharp Dohme Ltd., Hoddesdon, UK) and group T, receiving 15 mg/kg of tenofovir disoproxil[26] (Teva Operations Poland sp. z o.o., Kraków, Poland). The saline solution and study drugs were administered daily for 24 weeks using gastric tubes.

Body weights were checked once daily throughout the 24-week experimental period. In weeks 12 and 24, blood samples for serum isolation were collected. The serum was separated with centrifugation (at 1500 × g) and then stored at –70°C until required for laboratory tests. In weeks 12 and 24 the rats were anesthetized intraperitoneally (i.p.) with ketamine (50 mg/kg) and diazepam (3 mg/kg). Their BMD was measured with dual-energy X-ray absorptiometry (DXA).

In week 24, the animals were euthanized under general anesthesia with ketamine (60 mg/kg i.p.) and xylazine (10 mg/kg i.p.). Tibial and femoral bones and second lumbar vertebrae (L2) were removed for further tests. The right tibial and femoral bones were stored at –70°C; the left tibial and femoral bones, as well as the L2 were fixed in buffered formaldehyde for further histological examination.

Macrometric bone measurements

The carefully cleaned right femurs and tibias were weighed on electronic scales (Radwag AS 60/220/C/; Radwag, Radom, Poland). The length and diameter of both bones were measured using electronic calipers (Pro sp. z o.o., Bielsko-Biała, Poland) with 0.01 mm resolution.

The femoral index was calculated from the formula (eq. 1):

$$\text{femoral index} = \frac{\text{femur mass [g]}}{\text{body weight [g]}} \times 100\% \quad (1)$$

The tibial index was calculated from the formula (eq. 2):

$$\text{tibial index} = \frac{\text{tibia mass [g]}}{\text{body weight [g]}} \times 100\% \quad (2)$$

Dual-energy X-ray absorptiometry

The BMD of the total body (TB), femurs and tibias was measured in vivo by trained examiners using DXA (Hologic Discovery DXA System; Hologic Inc., Marlborough, USA) with software for small animals. The BMD of the lumbar vertebrae (L1–L4) was measured ex vivo after the spine was isolated along with the ligaments and spinal muscles. The results were obtained as grams of mineral content per square centimeter of bone area [g/cm^2]. The scanner was calibrated daily using a phantom provided by the manufacturer.

Bone histological and immunohistochemical examination

Rat second lumbar vertebrae, left femurs and left tibias were cleaned, and then bones were fixed in 10% neutral buffered formalin and decalcified in 10% neutral buffered EDTA solution. The EDTA solution was changed once after 24 h. Second lumbar vertebrae, the metaphyseal and epiphyseal of the distal femur, and proximal tibia were harvested, embedded in paraffin and cut into 5-µm-thick slides. The slides were stained using the standard hematoxylin and eosin (H&E) method and scanned using the Hamamatsu NanoZoomer v. 2.0 histological slide scanner with NDP.scan SQ v. 1.0 software (Hamamatsu Photonics K.K., Iwata, Japan). A scanned area of at least 1.5 mm^2 (range: 1.5–4 mm^2) from each sample was exported to a TIFF file. The TIFF files were analyzed with ImageJ v. 1.52 software (National Institutes of Health, Bethesda, USA). The histopathological examination was consistent with the standardized nomenclature, symbols and units for bone histomorphometry as updated in 2012.[27]

The immunohistochemical examination was completed using paraffin-embedded 4-µm-thick sections of the L2 and anti-tartrate resistant acid phosphatase antibody (abTRAP) and recombinant anti-alkaline phosphatase antibody (abAP) (both from Abcam, Cambridge, UK). The specimens were stained according to the instructions provided by the manufacturer, using Autostainer Link 48 equipment (Dako GmbH, Glostrup, Denmark). abTRAP was used in a dilution of 0.5 µg/mL and abAP in a dilution of 1:500. Bound antibodies were assayed using the Dako EnVision™ FLEX detection system. Additional abTRAP and abAP staining was assessed quantitatively using 1–3 point scoring:

Intensity: score 1 – poor; score 2 – medium; score 3 – strong;

Extension: score 1 – from 0.5 to 10%; score 2 – from 11 to 50%; score 3 – over 51%.

According to the recommendation from the International Ad Hoc Expert Panel,[28] a negative reagent control (NRC) was used, and the primary antibody was replaced with unspecific immunoglobulins at the same concentration.

Laboratory determinations

The serum obtained through centrifuging the blood was stored at –80°C until the tests. The levels of beta C-terminated telopeptide of type I collagen (CTX),

osteoclast-derived tartrate-resistant acid phosphatase form 5b (TRAP) and osteocalcin were determined with commercially available enzyme-linked immunosorbent assay (ELISA) kits, following the manufacturer's instructions (all from Immunodiagnostic Systems Limited, Boldon, UK). The level of insulin-like growth factor 1 (IGF-1) was likewise determined using a commercially available kit in accordance with the manufacturer's instructions (Cloud-Clone Corp., Houston, USA).

A certified laboratory, using Architect plus ci4100 equipment (Abbott Laboratories, Chicago, USA) with commercial tests (also from Abbott), determined the levels of total calcium, inorganic phosphorus and creatinine in the serum samples.

Biomechanical testing

The right-side femurs were cleaned off, then the epiphysis of each femur was placed in aluminum alloy tubes with a diameter of 11 mm, and then fixed with self-polymerizing glue Duracryl® Plus (Spofa Dental Inc., Jičín, Czechy) (Fig. 1). We measured the mechanical properties of the right-side femurs by performing a four-point bending Samples were loaded at the rate of 1 mm/min. The loading points and the dimensions are shown in Fig. 2. For the test reported in this paper, a = 24 mm test on 858 MTS Mini-Bionix® equipment (MTS Systems Corporation, Eden Prairie, USA) (Fig. 2) and b = 20 mm. Based on the strength-deflection arrow characteristics, the following parameters were determined for each sample: the longitudinal elasticity modulus (Young's modulus, E), flexural strength (Rz) and rigidity (k).

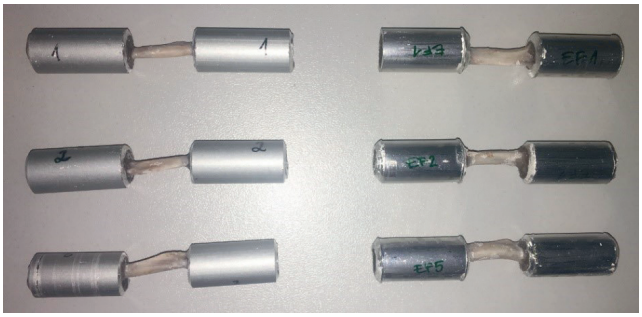

Fig. 1. Samples prepared for the four-point bending test

Young's modulus (E) was calculated from Formula 1:

$$E = \frac{P \times b^2}{6 \times f^1 \times b} (3a + 2b) \quad (1)$$

where E is Young's modulus [GPa]; a and b are the distances between supports [m]; P is maximum strength [N]; f_1 is the deflection arrow [m] and is the moment of inertia [m^4]. Flexural strength (Rz) was determined according to Formula 2.

$$Rz = \frac{Mg}{Wz} \quad (2)$$

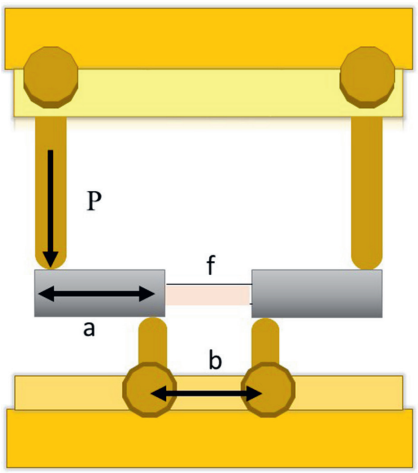

Fig. 2. The measuring system for the four-point bending test of femurs

where flexural strength [MPa]; M_g is the bending moment [Nm]; and W_Z is the flexural strength index [m^3].

The rigidity (k) of a sample was calculated from Formula 3:

$$K = E \times I \quad (3)$$

where k is the rigidity to bending [Nm^2]; E is Young's modulus [GPa]; and I is the moment of inertia of the sample cross-section [m^4].

Statistical analysis

The parameters studied were expressed as means ± standard deviation (SD). The statistical analysis was completed using STATISTICA software v. 12 (StatSoft, Inc., Tulsa, USA). A one-way analysis of variance (ANOVA) with a post hoc least significant difference (LSD) test was used to determine significant differences between the 3 study groups. The level of significance was set at $p < 0.05$.

Results

Body weight

The results are presented in Table 1. No differences in body weight were observed on day 1 between group C and the groups EF and T. The groups were compared in terms of body weight throughout the entire experiment, and on the last day of the experiment we found no significant differences among the groups.

Macrometric measurements of bones

The results are presented in Table 1. The femoral indices were lower in groups EF and T than in group C ($p = 0.006$ and $p = 0.001$, respectively); the weights of the femurs were likewise lower in groups EF and T than in group C (both $p = 0.001$). The tibial indices, the weight and length

of the tibias were lower in group EF compare to group C (p = 0.04, p = 0.003, p = 0.03, respectively). Mid-femoral diameters were lower in groups EF and T than in group C (p = 0.025 and, p = 0.004, respectively). The mid-tibial diameter was lower in group T compared to group C (p = 0.003).

Dual-energy X-ray absorptiometry (DXA)

The results are presented in Table 2. After 12 weeks, no differences were found between the study groups in terms of BM of the TB, femurs or tibias. After 24 weeks, we detected a lower TB BMD in group T compared to group C (p = 0.0043). The BMD of the lumbar spine L1–L4 was not different between the study groups at the end of the experiment.

Histopathological and immunohistochemical examinations

The results are presented in Table 3 and Fig. 3 and 4. In the histopathological assessment of the L2, the bone surface/volume ratio (BS/BV) was lower in group EF compared to group C (p = 0.014). A higher trabecular thickness (Tb.Th) was also observed in group EF compared to group C (p = 0.025). The immunohistochemical examination of the L2 demonstrated a higher intensity and extension of abTRAP in group EF than in group C (p = 0.04, p = 0.02, respectively). In group T, increased extension of recombinant abAP compared to group C was at the border of statistical significance (p = 0.054).

The histopathological examination of the femurs demonstrated a lower bone surface/tissue volume (BS/TV) and a lower number of trabeculae (Tb.N) in group T compared with group C (p = 0.014, p = 0.04, respectively). Moreover, trabecular separation (Tb.Sp) was higher in group T compared to C (p = 0.009).

Serum parameters

The results are presented in Table 4. After 12 weeks, no statistically significant differences were found in CTX and osteocalcin levels between group C and groups EF and T. After 24 weeks, higher serum levels of TRAP, calcium and inorganic phosphorus, and a lower osteocalcin level were observed in group EF compared to C (p = 0.002, p = 0.013, p = 0.0003 and p = 0.008, respectively).

Table 1. The effect of long-term administration of efavirenz and tenofovir on body weight and macrometric parameters of bones (one-way ANOVA with post hoc LSD test)

Parameter		Group C	Group EF	Group T
Body weight [g]	week 1	270.0 ±13.5	266.2 ±11.0	257.8 ±12.8
	week 24	468.7 ±30.5	440.7 ±27.3	450.2 ±33.9
Femur	femoral index	0.3353 ±0.0328	0.3068 ±0.0161*	0.3013 ±0.0171*
	femur weight [g]	1.558 ±0.157	1.349 ±0.060*	1.358 ±0.141*
	femur length [mm]	38.061 ±1.626	39.093 ±1.676	38.428 ±1.584
	mid-femoral diameter [mm]	3.963 ±0.171	3.762 ±0.151*	3.702 ±0.256*
Tibia	tibial index	0.2367 ±0.0204	0.2201 ±0.0129*	0.2271 ±0.02023
	tibial weight [g]	1.108 ±0.106	0.968 ±0.047*	1.023 ±0.121
	tibia length [mm]	43.611 ±0.856	42.583 ±1.090*	43.603 ±1.186
	mid-tibial diameter [mm]	2.813 ±0.150	2.833 ±0.151	2.627 ±0.116*

Results are presented as mean ±standard deviation (SD); * p < 0.05 compared to the control group; ANOVA – analysis of variance; LSD – least significant difference.

Table 2. The effect of long-term administration of efavirenz and tenofovir on bone mineral density (one-way ANOVA with post hoc LSD test)

Parameter		Group C (n = 12)	Group EF (n = 12)	Group T (n = 12)
Week 12	total body BMD [g/cm^2]	0.2122 ±0.0040	0.2101 ±0.0046	0.2067 ±0.0122
	femoral BMD [g/cm^2]	0.3155 ±0.0320	0.3077 ±0.0191	0.3088 ±0.0281
	tibial BMD [g/cm^2]	0.2425 ±0.0174	0.2316 ±0.0264	0.2332 ±0.0290
Week 24	total body BMD [g/cm^2]	0.2272 ±0.0096	0.22 ±0.0078	0.2146 ±0.0066*
	femoral BMD [g/cm^2]	0.3836 ±0.0167	0.3785 ±0.0194	0.371 ±0.022
	tibial BMD [g/cm^2]	0.2606 ±0.0116	0.2518 ±0.0112	0.2516 ±0.0152
	L1–L4 spine BMD [g/cm^2]	0.3565 ±0.0283	0.3548 ±0.0235	0.3382 ±0.0280

Results are presented as mean ±standard deviation (SD); * p < 0.05 compared to the control group; BMD – bone mineral density; ANOVA – analysis of variance; LSD – least significant difference.

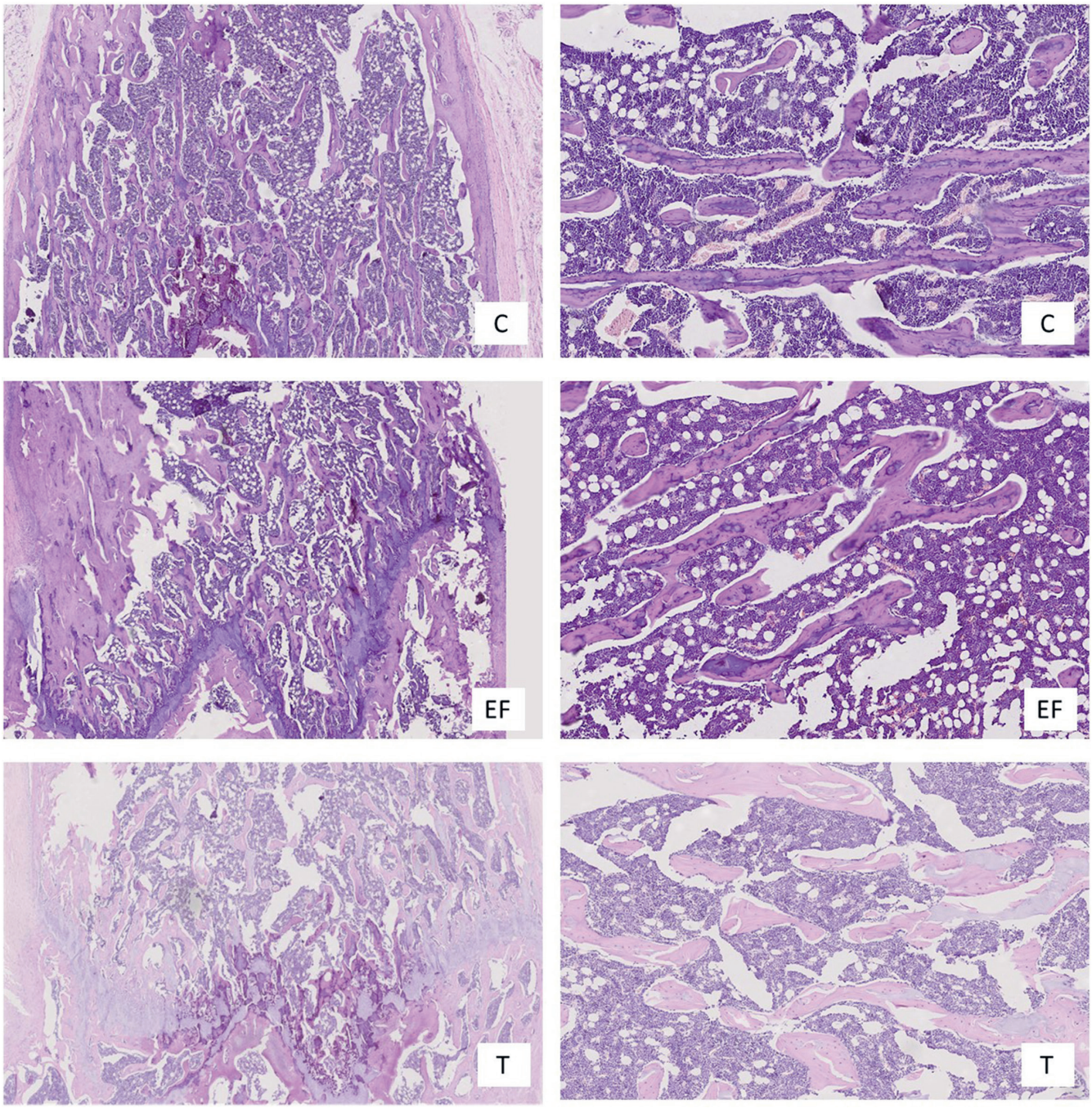

Fig. 3. Sample images of the histopathological examination (H&E staining) of the distal metaphysis of the femur in groups C, EF and T (magnification ×15 and ×50)

Bone biomechanical properties

The results are presented in Table 5. The four-point bending test demonstrated a lower value of Young's modulus in groups EF and T than in group C ($p = 0.037$, $p = 0.006$, respectively).

Discussion

The aim of this study was to assess the effect of 2 antiretroviral medications – EF and T – on growing skeletons. Abnormal increases in bone mass during the critical period of development of the skeleton may lead to disorders in bone growth and/or lower adult peak bone mass. Lower peak bone mass increases the risk of osteoporosis and fractures occurring later in life.[29]

Insulin-like growth factor 1 participates in the regulation of the growing process, as well in increasing and maintaining bone mass. It constitutes the main mediator in the action of the growth hormone on target cells, mainly on chondrocytes, osteoblasts and endocrine cells.[30] This study failed to demonstrate the effect of the substances studied (EF and T) on the level of IGF-1, which suggests

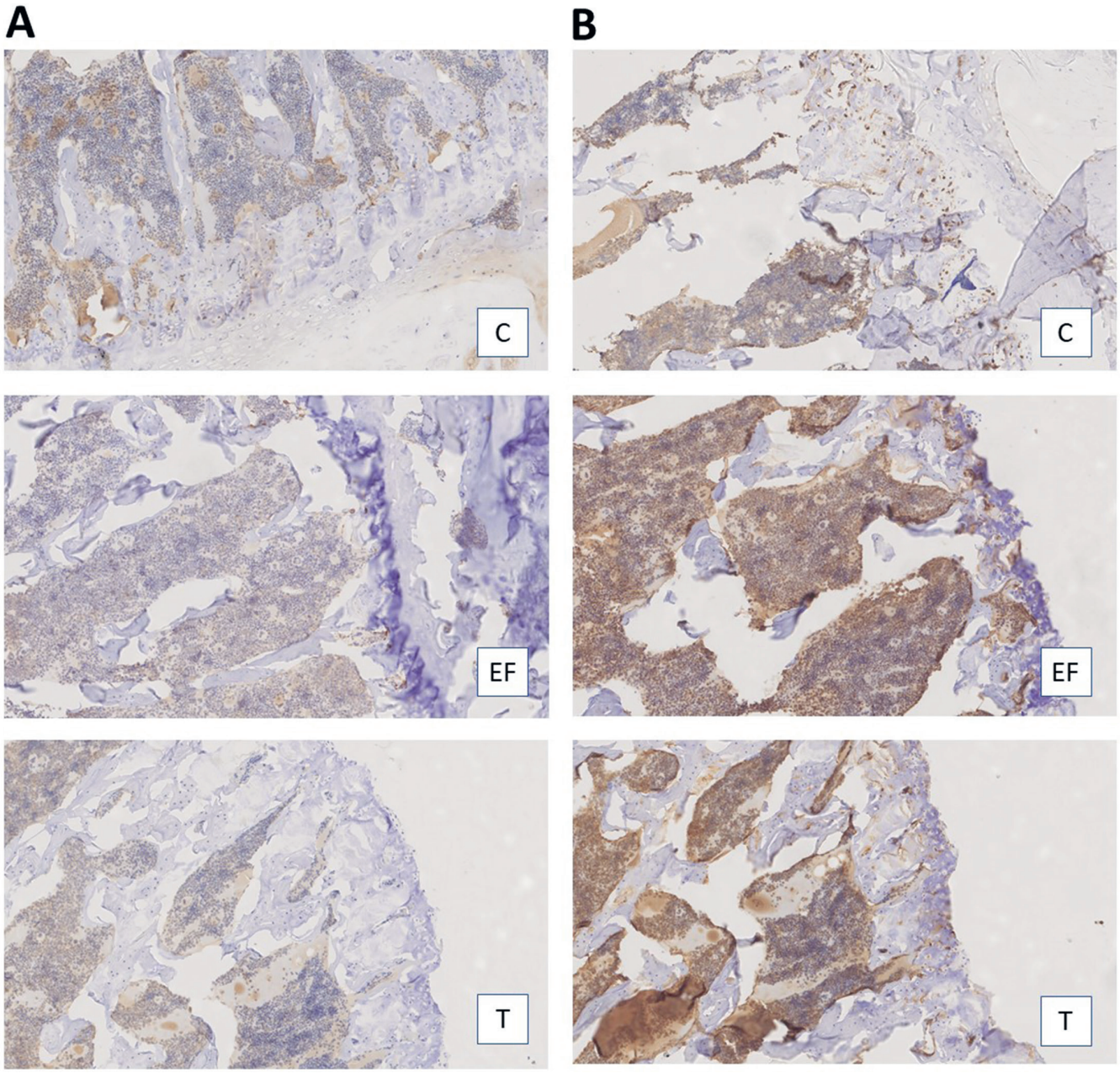

Fig. 4. Sample images of the immunohistochemical examination (A – abTRACP staining; B – abAP staining) of the L2 in groups C, EF and T (magnification ×10)

that the effect of those substances on bone does not depend on IGF-1.

In this study, we observed lower femoral and tibial indices in group EF, which indicates lower relative dimensions of the examined bones in this group. However, we did not observe reduced BMD of the bones analyzed, which is consistent with the results from Arpadi et al.[18] Our histopathological examination of the L2 demonstrated a reduction in BS/BV. A 36% reduction in the number of trabeculae accompanied by a higher trabecular thickness (Tb.Th) was observed at the same time. The absence of significant changes in the histopathological examination of femurs and tibias in the group EF could be attributed to a more rapid remodeling of osseous tissue in the spine as compared to long bones.[31]

An increased serum level of TRAP and increased abTRAP expression in our immunohistochemical examination of L2 were observed in the group EF, indicating an increased number and increased activity of osteoclasts[32] in this group. The influence of the high SD of abTRAP (in both intensity and extension) on the obtained results cannot be excluded. However, as the serum concentration of TRAP corresponds to the immunohistochemical results, it does not affect our overall conclusion on the influence of T on bone turnover. At the same time, EF decreased levels of osteocalcin, a marker of bone formation. This suggests that the changes observed in bone microarchitecture in the group EF could result from increased activity of resorption and decreased bone formation. In the animals receiving EF, phosphorus

Table 3. The effects of long-term administration of efavirenz and tenofovir on histopathological and immunohistochemical parameters of bone (one-way ANOVA with post hoc LSD test)

Parameter		Group C (n = 12)	Group EF (n = 12)	Group T (n = 12)
L2 vertebra	abTRAP – intensity	0.625 ±1.188	1.778 ±1.394*	0.1818 ±0.603
	abTRAP – extension	0.375 ±0.744	1.111 ±0.928 *	0.0909 ±0.3015
	abAP – intensity	3.0 ±0.0	3.0 ±0.0	3.0 ±0.0
	abAP – extension	1.875 ±0.991	2.0 ±0.8165	2.545 ±0.5222
	BV/TV [%]	0.1391 ±0.0088	0.2157 ±0.2386	0.1345 ±0.0058
	BS/BV [mm^2/mm^3]	68.57 ±41.93	36.727 ±24.659*	52.14 ±4.913
	BS/TV [mm^2/mm^3]	9.616 ±5.859	6.145 ±3.785	7.006 ±0.656
	Tb.Th [mm]	0.0455 ±0.0365	0.0752 ±0.0391*	0.0387 ±0.0034
	Tb.N [1/mm]	4.808 ±2.929	3.072 ±1.892	3.503 ±0.3279
	Tb.Sp [mm]	0.2832 ±0.2617	0.3777 ±0.2649	0.2518 ±0.02944
Femur	BV/TV [%]	0.2512 ±0.0473	0.2621 ±0.1519	0.1899 ±0.0763
	BS/BV [mm^2/mm^3]	46.724 ±17.336	40.395 ±12.937	44.11 ±7.858
	BS/TV [mm^2/mm^3]	11.811 ±5.083	9.035 ±1.551	7.962 ±1.906
	Tb.Th [mm]	0.0471 ±0.0134	0.0582 ±0.0333	0.0468 ±0.0092
	Tb.N [1/mm]	5.906 ±2.542	4.517 ±0.7757	3.981 ±0.9531*
	Tb.Sp [mm]	0.1471 ±0.05531	0.1687 ±0.05228	0.2174 ±0.06817*
Tibia	BV/TV [%]	0.2398 ±0.0491	0.2007 ±0.0332	0.2044 ±0.04270
	BS/BV [mm^2/mm^3]	44.661 ±17.357	44.223 ±6.283	43.96 ±6.231
	BS/TV [mm^2/mm^3]	10.339 ±3.375	8.778 ±1.252	8.812 ±1.165
	Tb.Th [mm]	0.0496 ±0.0149	0.0460 ±0.0059	0.0463 ±0.0065
	Tb.N [1/mm]	5.17 ±1.688	4.389 ±0.6261	4.406 ±0.5827
	Tb.Sp [mm]	0.1580 ±0.04195	0.1856 ±0.02811	0.1842 ±0.03210

Results are presented as mean ±standard deviation (SD); * $p < 0.05$ compared to the control group; L2 – second lumbar vertebra; abTRAP – anti-tartrate resistant acid phosphatase antibody; abAP – recombinant anti-alkaline phosphatase antibody; BV – bone volume; TV – tissue volume; BV/TV – tissue volume ratio; BS – bone surface; Tb.Th – trabecular thickness; Tb.N – trabecular number; Tb.Sp – trabecular separation; ANOVA – analysis of variance; LSD – least significant difference.

Table 4. The effects of long-term administration of efavirenz and tenofovir on serum parameters (one-way ANOVA with post hoc LSD test)

Parameter	Group C (n = 12)	Group EF (n = 12)	Group T (n = 12)
IGF-1 [ng/mL]	3.0183 ±0.8979	4.5537 ±3.5369	2.5656 ±1.2765
Osteocalcin [pg/mL]	193.865 ±46.260	138.022 ±45.965*	223.857 ±45.200
CTX [ng/mL]	17.759 ±4.337	19.299 ±9.259	17.883 ±4.662
TRAP [U/L]	0.776 ±0.265	1.088 ±0.264*	0.843 ±0.165
1,25-hydoxy-vitamin D3 [nmol/L]	1.52 ±0.16	1.40 ±0.32	1.46 ±0.22
Total calcium [mg/dL]	6.427 ±1.769	8.192 ±1.358*	6.250 ±1.731
Inorganic phosphorus [mg/dL]	3.618 ±1.018	5.683 ±1.210*	3.608 ±1.453
Alkaline phosphatase [U/L]	56.363 ±19.185	64.333 ±16.041	60.300 ±24.891
Creatinine [mg/dL]	0.303 ±0.051	0.324 ±0.075	0.358 ±0.105

Results are presented as mean ±standard deviation (SD); * $p < 0.05$ compared to the control group CTX – beta C-terminated telopeptide of type I collagen; TRAP – osteoclast-derived tartrate-resistant acid phosphatase form 5b; IGF-1 – insulin-like growth factor 1; ANOVA – analysis of variance; LSD – least significant difference.

and calcium levels were higher compared to group C. The observed changes may be a consequence of increased osteoclast activity and increased bone resorption. Several studies have demonstrated decreases in vitamin D levels in patients treated with NNRTIs.[33–35] However, we did not detect decreases in vitamin D levels in our study. It is hypothesized that decreases in vitamin D levels in patients treated with efavirenz may stem from induction of the cytochrome P450 (CYP24A), which is responsible for the breakdown of active vitamin D in humans,[36] but not in rats.[37]

Table 5. The effects of long-term administration of efavirenz and tenofovir on biomechanical parameters of the right femur (one-way ANOVA with post hoc LSD test)

Parameter	Group C	Group EF	Group T
Young's modulus [GPa]	16.216 ±3.014	12.989 ±2.391*	13.872 ±1.927*
Flexural strength [MPa]	98.881 ±30.608	85.633 ±25.961	105.285 ±19.296
Rigidity [Nm]	0.2823 ±0.0441	0.2406 ±0.0665	0.2438 ±0.0664

Results are presented as mean ±standard deviation (SD); * $p < 0.05$ compared to the control group; ANOVA – analysis of variance; LSD – least significant difference.

In group EF, besides the reductions in femoral indices and disturbances of bone microarchitecture demonstrated in the histological examination, a 20% reduction of Young's modulus was found in the four-point bending test, which is a sign of deterioration of bone biomechanical properties that may lead to increased risk of fractures.

Reduced femoral indices and mid-femoral diameters were also found in group T, as in group EF. However, no effect of T on tibial indices was observed. Moreover, a reduction in TB BMD was found in group T. These results are consistent with the observations of Gafni et al. and Purdy et al., who found reduced BMD in T-treated patients.[20,38] In their studies of growing rhesus monkeys, Castillo et al. demonstrated a mineralization defect in newly-formed cortical bones in monkeys receiving T, leading to the formation of completely non-mineralized osteons.[39] This is consistent with the observation of a lower percentage of mineralizing surfaces in inflammation-free rats receiving T in a study by Conradie et al.[40] The results of our study also suggest bone mineralization disorders during treatment with T. Clinical studies also report greater decreases in BMD associated with T therapy.[41–45] Besides the reduction in TB BMD, expression of recombinant anti-alkaline phosphatase (anti-AP) was extended by 36% in L2 in group T. Moreover, reductions in femoral BS/TV and in the number of trabeculae (Tb.N) with simultaneous increases in Tb.Sp were observed in group T. Changes like this in bone histomorphometry were not reported by Ramalho et al.[44] Some authors have suggested that T-associated decreases in BMD may be a consequence of renal failure and subsequent decreases in vitamin D activation, but in our study we detected neither an increase in creatinine level nor a decrease in vitamin D level. Our results are consistent with the report by Bagger et al. suggesting that T-associated decreases in BMD cannot be explained by decreased renal function.[46]

The pathogenesis of bone lesions occurring during treatment with T is poorly understood and needs to be further elucidated. A direct effect of the drug on osteoclasts and/or osteoblasts is considered, as well as an indirect effect resulting from injury to the proximal renal tubules, hypophosphatemia and an increased release of parathyroid hormones.[47] Serum phosphate levels may not reflect TB phosphate depletion, nor even re-absorption of phosphates into the renal tubules.[48] Despite the significant reductions in BMD and changes in bone microarchitecture observed in group T, our study did not demonstrate the effect of T on serum inorganic phosphorus levels, nor on any other recognized markers of bone turnover. Therefore, the pathomechanism of the observed phenomenon needs to be studied further.

Decreased biomechanical properties of bones expressed by the 14% reduction in Young's modulus were observed in group T in the four-point bending test. Conradie et al. reported that biomechanical properties of femurs from non-HIV infected rats were not statistically different between group T and group C.[40] This could be a consequence of the fact that in their study a three-point bending test was performed. The four-point bending test may be more sensitive, but further biomechanical experiments are required to verify this hypothesis. The four-point bending method differs from three-point bending due to the way the measurements are carried out. The three-point bending test, compared to four-point bending, underestimates the modulus of elasticity due to the fact that the shear effect and the indentation effect of the loading head and the supports are neglected. A four-point test tends to be the best choice, especially if the examined material is (like bones) not homogeneous. The stress of a three-point test is concentrated under the center of the loading point, whereas the stress concentration of a four-point test is over a larger region. We have already introduced this method in several other studies,[49,50] and it gives very good results, especially since it does not cause permanent bone deformation in the places of where force is directly applied. The bending energy is therefore directly related only to the fracture site. Thus, the results obtained are characterized by higher values of the mechanical parameters and a smaller range of results in comparison to the three-point test.

Conclusions

In a controlled environment where HIV-associated factors were absent, the long-term monotherapy with EF and tenofovir disoproxil had an adverse effect on the bones of growing male rats. The results of this study indicate that EF affects bone microarchitecture and leads to impaired bone biomechanical properties – an effect that seems to be associated with increased activity of osteoclasts and decreased new bone formation.

ORCID iDs

Agnieszka Matuszewska https://orcid.org/0000-0003-1082-0793
Beata Nowak https://orcid.org/0000-0003-0014-6344
Anna Nikodem https://orcid.org/0000-0002-1418-247X
Diana Jędrzejuk https://orcid.org/0000-0001-7053-142X
Danuta Szkudlarek https://orcid.org/0000-0001-5736-310X
Krzysztof Zduniak https://orcid.org/0000-0003-4652-4478
Jarosław Filipiak https://orcid.org/0000-0002-9380-0642
Marta Sznadruk-Bender https://orcid.org/0000-0002-4571-9452
Tomasz Tomkalski https://orcid.org/0000-0003-2850-7316
Ireneusz Ceremuga https://orcid.org/0000-0001-5744-2860
Marek Bolanowski https://orcid.org/0000-0002-2360-6596
Adam Szeląg https://orcid.org/0000-0001-8104-5267

References

1. UNAIDS. 2017 Global HIV Statistics. Fact sheet. Geneva, Switzerland: The Joint United Nations Programme on HIV and AIDS; 2017.
2. Shiau S, Yin MT, Strehlau R, et al. Decreased bone turnover in HIV-infected children on antiretroviral therapy. *Arch Osteoporos*. 2018; 13(1):40. doi:10.1007/s11657-018-0452-6
3. Zuccotti G, Viganò A, Gabiano C, et al. Antiretroviral therapy and bone mineral measurements in HIV-infected youths. *Bone*. 2010; 46(6):1633–1638. doi:10.1016/j.bone.2010.02.029
4. Margossian R, Williams PL, Yu W, et al; Pediatric HIV/AIDS Cohort Study (PHACS). Markers of bone mineral metabolism and cardiac structure and function in perinatally HIV-infected and HIV-exposed but uninfected children and adolescents. *J Acquir Immune Defic Syndr*. 2019;81(2):238–246. doi:10.1097/QAI.0000000000002007
5. Jacobson DL, Stephensen CB, Miller TL, et al; Pediatric HIV/AIDS Cohort Study. Associations of low vitamin D and elevated parathyroid hormone concentrations with bone mineral density in perinatally HIV-infected children. *J Acquir Immune Defic Syndr*. 2017;76(1): 33–42. doi:10.1097/QAI.0000000000001467
6. Manavalan JS, Arpadi S, Tharmarajah S, et al. Abnormal bone acquisition with early-life HIV infection: Role of immune activation and senescent osteogenic precursors. *J Bone Miner Res*. 2016;31(11):1988–1996. doi:10.1002/jbmr.2883
7. Eckard AR, Mora S. Bone health in HIV-infected children and adolescents. *Curr Opin HIV AIDS*. 2016;11(3):294–300. doi:10.1097/COH.0000000000000270
8. Vikulina T, Fan X, Yamaguchi M, et al. Alterations in the immunoskeletal interface drive bone destruction in HIV-1 transgenic rats. *Proc Natl Acad Sci U S A*. 2010;107(31):13848–13853. doi:10.1073/pnas.1003020107
9. Ofotokun I. Deciphering how HIV-1 weakens and cracks the bone. *Proc Natl Acad Sci U S A*. 2018;115(11):2551–2553. doi:10.1073/pnas.1801555115
10. Biver E, Calmy A, Rizzoli R. Bone health in HIV and hepatitis B or C infections. *Ther Adv Musculoskelet Dis*. 2016;9(1):22–34. doi:10.1177/1759720X16671927
11. Brown TT, Qaqish RB. Antiretroviral therapy and the prevalence of osteopenia and osteoporosis: A meta-analytic review. *AIDS*. 2006; 20(17):2165–2174. doi:10.1097/QAD.0b013e32801022eb
12. Madeddu G, Spanu A, Solinas P, et al. Different impact of NNRTI and PI-including HAART on bone mineral density loss in HIV-infected patients. *Eur Rev Med Pharmacol Sci*. 2015;19(23):4576–4589.
13. Tebas P, Kumar P, Hicks C, et al. Greater change in bone turnover markers for efavirenz/emtricitabine/tenofovir disoproxil fumarate versus dolutegravir + abacavir/lamivudine in antiretroviral therapy-naive adults over 144 weeks. *AIDS*. 2015;29(18):2459–2464. doi:10.1097/QAD.0000000000000863
14. Ofotokun I, Titanji K, Vunnava A, et al. Antiretroviral therapy induces a rapid increase in bone resorption that is positively associated with the magnitude of immune reconstitution in HIV infection. *AIDS*. 2016;30(3):405–414. doi:10.1097/QAD.0000000000000918
15. Yin MT, Chan ES, Brown TT, et al. Vitamin D does not modulate immune-mediated bone loss during ART initiation. *Antivir Ther*. 2019; 24(5):355–362. doi:10.3851/IMP3316
16. McComsey GA, Kitch D, Daar ES, et al. Bone mineral density and fractures in antiretroviral-naive persons randomized to receive abacavir-lamivudine or tenofovir disoproxil fumarate-emtricitabine along with efavirenz or atazanavir-ritonavir: AIDS Clinical Trials Group A5224s, a substudy of ACTG. *J Infect Dis*. 2011;203(12):1791–1801. doi:10.1093/infdis/jir188
17. Aurpibul L, Puthanakit T. Review of tenofovir use in HIV-infected children. *Pediatr Infect Dis J*. 2015;34(4):383–391. doi:10.1097/INF.0000000000000571
18. Arpadi SM, Shiau S, Strehlau R, et al. Efavirenz is associated with higher bone mass in South African children with HIV. *AIDS*. 2016;30(16): 2459–2467. doi:10.1097/QAD.0000000000001204
19. Dave JA, Cohen K, Micklesfield LK, Maartens G, Levitt NS. Antiretroviral therapy, especially efavirenz, is associated with low bone mineral density in HIV-infected South Africans. *PLoS One*. 2015;10(12): e0144286. doi:10.1371/journal.pone.0144286
20. Gafni RI, Hazra R, Reynolds JC, et al. Tenofovir disoproxil fumarate and an optimized background regimen of antiretroviral agents as salvage therapy: Impact on bone mineral density in HIV-infected children. *Pediatrics*. 2006;118(3):e711–e718. doi:10.1542/peds.2005-2525
21. Viganò A, Zuccotti GV, Puzzovio M, et al. Tenofovir disoproxil fumarate and bone mineral density: A 60-month longitudinal study in a cohort of HIV-infected youths. *Antivir Ther*. 2010;15(7):1053–1058. doi:10.3851/IMP1650
22. Unsal AB, Mattingly AS, Jones SE, et al. Effect of antiretroviral therapy on bone and renal health in young adults infected with HIV in early life. *J Clin Endocrinol Metab*. 2017;102(8):2896–2904. doi:10.1210/jc.2017-00197
23. Hernandez CJ, Beaupré GS, Carter DR. A theoretical analysis of the changes in basic multicellular unit activity at menopause. *Bone*. 2003; 32(4):357–363. doi:10.1016/s8756-3282(03)00037-1
24. Compston J. HIV infection and bone disease. *J Intern Med*. 2016; 280(4):350–358. doi:10.1111/joim.12520
25. Goffinet C, Allespach I, Keppler OT. HIV-susceptible transgenic rats allow rapid preclinical testing of antiviral compounds targeting virus entry or reverse transcription. *Proc Natl Acad Sci*. 2007;104(3):1015–1020. doi:10.1073/pnas.0607414104
26. Watkins ME, Wring S, Randolph R, et al. Development of a novel formulation that improves preclinical bioavailability of tenofovir disoproxil fumarate. *J Pharm Sci*. 2017;106(3):906–919. doi:10.1016/j.xphs.2016.12.003
27. Dempster DW, Compston JE, Drezner MK, et al. Standardized nomenclature, symbols, and units for bone histomorphometry: A 2012 update of the report of the ASBMR Histomorphometry Nomenclature Committee. *J Bone Miner Res*. 2013;28(1):2–17. doi:10.1002/jbmr.1805
28. Torlakovic EE, Francis G, Garratt J, et al; International Ad Hoc Expert Panel. Standardization of negative controls in diagnostic immunohistochemistry: Recommendations from the international ad hoc expert panel. *Appl Immunohistochem Mol Morphol*. 2014;22(4):241–252. doi:10.1097/PAI.0000000000000069
29. Tandon N, Fall CHD, Osmond C, et al. Growth from birth to adulthood and peak bone mass and density data from the New Delhi Birth Cohort. *Osteoporos Int*. 2012;23(10):2447–2459. doi:10.1007/s00198-011-1857-x
30. Filus A, Zdrojewicz Z. Insulin-like growth factor-1 (IGF-1) – structure and the role in the human body [in Polish]. *Pediatr Endocrinol Diabetes Metab*. 2014;20(4):161–169. doi:10.18544/PEDM-20.04.0016
31. Datta HK, Ng WF, Walker JA, Tuck SP, Varanasi SS. The cell biology of bone metabolism. *J Clin Pathol*. 2008;61(5):577–587. doi:10.1136/JCP.2007.048868
32. Hlaing TT, Compston JE. Biochemical markers of bone turnover: Uses and limitations. *Ann Clin Biochem*. 2014;51(Pt 2):189–202. doi:10.1177/0004563213515190
33. Vescini F, Cozzi-Lepri A, Borderi M, et al; Icona Foundation Study Group. Prevalence of hypovitaminosis D and factors associated with vitamin D deficiency and morbidity among HIV-infected patients enrolled in a large Italian cohort. *J Acquir Immune Defic Syndr*. 2011; 58(2):163–172. doi:10.1097/QAI.0b013e31822e57e9
34. Conesa-Botella A, Florence E, Lynen L, Colebunders R, Menten J, Moreno-Reyes R. Decrease of vitamin D concentration in patients with HIV infection on a non-nucleoside reverse transcriptase inhibitor-containing regimen. *AIDS Res Ther*. 2010;7:40. doi:10.1186/1742-6405-7-40
35. Welz T, Childs K, Ibrahim F, et al. Efavirenz is associated with severe vitamin D deficiency and increased alkaline phosphatase. *AIDS*. 2010; 24(12):1923–1928. doi:10.1097/QAD.0b013e32833c3281

36. Guryev O, Carvalho RA, Usanov S, Gilep A, Estabrook RW. A pathway for the metabolism of vitamin D3: Unique hydroxylated metabolites formed during catalysis with cytochrome P450scc (CYP11A1). *Proc Natl Acad Sci U S A*. 2003;100(25):14754–14759. doi:10.1073/pnas.2336107100
37. Horst RL, Omdahl JA, Reddy S. Rat cytochrome P450C24 (CYP24) does not metabolize 1,25-dihydroxyvitamin D 2 to calcitroic acid. *J Cell Biochem*. 2003;88(2):282–285. doi:10.1002/jcb.10359
38. Purdy JB, Gafni RI, Reynolds JC, Zeichner S, Hazra R. Decreased bone mineral density with off-label use of tenofovir in children and adolescents infected with human immunodeficiency virus. *J Pediatr*. 2008;152(4):582–584. doi:10.1016/j.jpeds.2007.12.020
39. Castillo AB, Tarantal AF, Watnik MR, Bruce Martin R. Tenofovir treatment at 30 mg/kg/day can inhibit cortical bone mineralization in growing rhesus monkeys (*Macaca mulatta*). *J Orthop Res*. 2002;20(6):1185–1189. doi:10.1016/S0736-0266(02)00074-8
40. Conradie MM, van de Vyver M, Andrag E, Conradie M, Ferris WF. A direct comparison of the effects of the antiretroviral drugs stavudine, tenofovir and the combination lopinavir/ritonavir on bone metabolism in a rat model. *Calcif Tissue Int*. 2017;101(4):422–432. doi:10.1007/s00223-017-0290-3
41. Gallant JE, Staszewski S, Pozniak AL, et al. Efficacy and safety of tenofovir DF vs stavudine in combination therapy in antiretroviral-naive patients: A 3-year randomized trial. *JAMA*. 2004;292(2):191–201. doi:10.1001/jama.292.2.191
42. Stellbrink H, Orkin C, Arribas JR, et al; ASSERT Study Group. Comparison of changes in bone density and turnover with abacavir-lamivudine versus tenofovir-emtricitabine in HIV-infected adults: 48-week results from the ASSERT study. *Clin Infect Dis*. 2010;51(8):963–972. doi:10.1086/656417
43. Hamzah L, Tiraboschi JM, Iveson H, et al. Effects on vitamin D, bone and the kidney of switching from fixed-dose tenofovir disoproxil fumarate/emtricitabine/efavirenz to darunavir/ritonavir monotherapy: A randomized, controlled trial (MIDAS). *Antivir Ther*. 2016;21(4):287–296. doi:10.3851/IMP3000
44. Ramalho J, Martins CSW, Galvão J, et al. Treatment of human immunodeficiency virus infection with tenofovir disoproxil fumarate-containing antiretrovirals maintains low bone formation rate, but increases osteoid volume on bone histomorphometry. *J Bone Miner Res*. 2019;34(9):1574–1584. doi:10.1002/jbmr.3751
45. Venter WDF, Kambugu A, Chersich MF, et al. Efficacy and safety of tenofovir disoproxil fumarate versus low-dose stavudine over 96 weeks: A multicountry randomized, noninferiority trial. *J Acquir Immune Defic Syndr*. 2019;80(2):224–233. doi:10.1097/QAI.0000000000001908
46. Bagger YZ, Rasmussen HB, Alexandersen P, Werge T,Christiansen C, Tankó LB; PERF study group. Links between cardiovascular disease and osteoporosis in postmenopausal women: Serum lipids or atherosclerosis per se? *Osteoporos Int*. 2007;18(4):505–512. doi:10.1007/s00198-006-0255-2
47. Grigsby IF, Pham L, Mansky LM, Gopalakrishnan R, Mansky KC. Tenofovir-associated bone density loss. *Ther Clin Risk Manag*. 2010;6(1):41–47. doi:10.2147/TCRM.S8836
48. Casado JL. Renal and bone toxicity with the use of tenofovir: Understanding at the end. *AIDS Rev*. 2016;18(2):59–68.
49. Nowak B, Matuszewska A, Filipiak J, et al. The influence of bexarotene, a selective agonist of the retinoid receptor X (RXR), and tazarotene, a selective agonist of the retinoid acid receptor (RAR), on bone metabolism in rats. *Adv Med Sci*. 2016;61(1):85–89. doi:10.1016/j.advms.2015.09.001
50. Markiewicz-Górka I, Kuropka P, Januszewska L, et al. Influence of physical training on markers of bone turnover, mechanical properties, morphological alterations, density and mineral contents in the femur of rats exposed to cadmium and/or alcohol. *Toxicol Ind Health*. 2019;35(4):277–293. doi:10.1177/0748233719831534

Exosome EpCAM promotes the metastasis of glioma by targeting the CD44 signaling molecule on the surface of glioma cells

Quan Gu[A–C,F], Xuelin Chen[B,C,F], Lin Zhou[B,C,F], Xianglu Liu[A,D–F]

Department of Neurosurgery, Fudan University Affiliated Zhongshan Hospital Qingpu Branch, Shanghai, China

A – research concept and design; B – collection and/or assembly of data; C – data analysis and interpretation;
D – writing the article; E – critical revision of the article; F – final approval of the article

Advances in Clinical and Experimental Medicine, ISSN 1899–5276 (print), ISSN 2451–2680 (online) *Adv Clin Exp Med*. 2020;29(11):1277–1282

Address for correspondence
Xianglu Liu
E-mail: lxl191218@yeah.net

Funding sources
None declared

Conflict of interest
None declared

Received on May 9, 2020
Reviewed on May 14, 2020
Accepted on August 5, 2020

Abstract

Background. Glioma, the most common primary tumor in the central nervous system, originates from glial cells and has a poor prognosis.

Objectives. This experimental laboratory study was designed to explore the role of epithelial cell adhesion molecule (EpCAM) in the metastasis of glioma.

Material and methods. Serum samples were collected from patients with non-metastatic or metastatic glioma (n = 20 per group), and healthy volunteers (n = 8). Exosomes were isolated from the serum and the morphological characteristics were observed under a scanning electron microscope (SEM). The expression of CD81 and CD63 was measured to identify exosomes. Glioma tissue and the adjacent normal tissue samples were obtained from patients with non-metastatic or metastatic glioma (n = 12 per group). Meanwhile, 4 normal brain tissue samples were collected. The expression of CD44, hyaluronan-mediated motility receptor (HMMR), and matrix metalloproteinase-9 (MMP-9) was determined in each group using immunohistochemistry. The protein expression of CD44, HMMR, matrix metalloproteinase-2 (MMP-2), MMP-9, and selectin E (SELE) was measured with western blotting.

Results. Exosomes were present in the serum, and the proteins CD81 and CD63 were expressed in all 3 groups. CD44 was highly expressed in the non-metastasis and metastasis groups. The expression of HMMR and MMP-9 in the Adj-metastasis and Adj-non-metastasis groups was high, while in the other groups, the levels were low. The expression of CD44 in the metastasis and non-metastasis groups was significantly higher than that of the negative control (NC) group, and the expression in the metastasis group was higher than that of the non-metastasis group. The MMP-2 and MMP-9 were not found in either the metastasis or non-metastasis group. The protein expression of HMMR and SELE was high in all groups.

Conclusions. Exosome EpCAM promoted the metastasis of glioma by targeting CD44.

Key words: metastasis, CD44, glioma, exosome, epithelial cell adhesion molecule

Cite as
Gu Q, Chen X, Zhou L, Liu X. Exosome EpCAM promotes the metastasis of glioma by targeting the CD44 signaling molecule on the surface of glioma cells. *Adv Clin Exp Med*. 2020;29(11):1277–1282. doi:10.17219/acem/126051

DOI
10.17219/acem/126051

Introduction

Glioma is the most common primary tumor in the central nervous system; it originates from glial cells and has a poor prognosis.[1] Glioma is classified into 4 grades according to the latest classification of the World Health Organization (WHO).[2,3] Although glioma can be treated with advanced chemotherapy drugs, surgery, new generations of gamma rays, and other interventions, the invasiveness of glioma and the protective effect of the blood–brain barrier remain obstacles in glioma treatment. Normal brain tissue is more prone to radiation brain damage, resulting in a five-year mortality rate for glioma patients that remains at over 95%.[4] In recent years, some researchers have come to believe that the occurrence of tumors is closely related to the interaction between external environmental factors and the host's internal genetic factors. The discovery of a proto-oncogene and tumor suppressor gene have led to a more profound understanding of the mechanism of tumor occurrence and development.[5] The research on the occurrence and development mechanism of brain glioma has been raised to the molecular level. Studies have found that many cytokines and genes participate in the occurrence and development of brain glioma, and that these cytokines and genes have broad application prospects in clinical practice.

Epithelial cell adhesion molecule (EpCAM) is a single transmembrane protein which is encoded by the tumor-associated calcium signal transduction gene 1 (TACSTD1) and which belongs to the family of adhesion molecules.[6] It participates in the regulation of intercellular adhesion, signal transduction, and cell migration, proliferation and differentiation.[7] The EpCam is expressed in the epithelium of different organs and tumors in different sites.[8] In carcinomatous cells, EpCAM is overexpressed.[9] Cimino et al. found that EpCAM was upregulated in breast cancer metastasis.[10] It was also found that the expression of EpCAM in metastatic gastric cancer (GC) was higher than in primary GC. The downregulation of EpCAM by siRNA led to the inhibition of GC cell invasion and migration.[11] The EpCAM expression is related to tumor prognosis and may be used for tumor-targeted therapy. Stoecklein et al. showed that the mean recurrence interval for patients with strongly EpCAM-positive esophageal squamous cell carcinoma was 9 months, while the mean recurrence interval of EpCAM-negative, weakly EpCAM-positive or -positive patients was 43 months, indicating the poor prognosis of patients with overexpressed EpCAM.[12]

In this study, we explored the role of EpCAM in glioma and its relationship with CD44 on the surface of glioma cells.

Material and methods

Tissue and serum samples

In this experimental laboratory study, 20 patients with non-metastatic glioma and 20 patients with metastatic glioma admitted to Chifeng College Affiliated Hospital, China, from May 2016 to April 2018 were enrolled. Eight healthy volunteers were also recruited as the negative control group (NC). This study was approved by the ethics committee of Chifeng College Affiliated Hospital and all patients signed informed consent forms. Fasting peripheral venous blood (3 mL) was drawn from all participants, placed into EDTA anticoagulant test tubes (Sigma-Aldrich, St. Louis, USA), and centrifuged at 1000 × g for 10 min. The supernatant was transferred into an RNA-enzyme-free centrifuge tube (Sigma-Aldrich) and stored at –20°C for later use.

Samples of glioma tissue and adjacent normal tissue were collected from 12 non-metastatic patients and 12 metastatic patients. Meanwhile, normal brain tissue samples were collected from 4 healthy subjects. All tissues were frozen immediately after resection and stored at –80°C for further experiments.

Exosome extraction and identification

Exosomes were isolated from human serum using an exosome separation reagent (Invitrogen, Carlsbad, USA). In order to remove impurities, 500 µL of serum was centrifuged at 2000 × g for 30 min. Then, 300-µL samples were mixed with 60 µL of separation reagent and incubated at 4°C for 30 min. After centrifugation at 10,000 × g for 10 min, the supernatant was discarded. Next, 150 µL of phosphate-buffered saline (PBS) was added to the suspended sediment and placed in storage at 4°C for later use. The exosomes were fixed with paraformaldehyde (Sigma-Aldrich), added to the copper mesh, and negatively stained with uranium dioxide-acetate (Invitrogen). The morphology was observed using a transmission electron microscope (Nikon, Tokyo, Japan).

Immunohistochemistry

The paraffin-embedded sections were routinely dewaxed to water, soaked in 3% hydrogen peroxide (Sigma-Aldrich) at room temperature for 5 min to inactivate endogenous enzymes, and washed thrice in distilled water for 3 min each time. The antigen was thermally remediated, cooled and washed twice with PBS. The sections were then treated with 5% bovine serum albumin (BSA) sealant and placed at room temperature for 20 min, incubated with primary antibody (rabbit IgG, l:50 dilution; Abcam, Cambridge, UK) at 37°C for 60 min, and washed 3 times with PBS. Then, the sections were incubated with secondary antibody (Abcam) at 37°C for 1 h, colored with 3,3'-diaminobenzidine (Sigma-Aldrich), rinsed, and counter-stained with hematoxylin.

Western blotting

The tissue samples were lysed with radioimmunoprecipitation assay (RIPA) lysate (Bio-Rad, Hercules, USA) on ice, and the supernatant was collected after centrifugation at 12,000 × g for 20 min at 4°C. The protein concentration was determined with a BCA kit (Shanghai Biyuntian, Shanghai, China). SDS-PAGE electrophoresis (Merck Millipore, Burlington, USA) was performed to isolate the protein after mixing it with the buffer solution. Then, it was transferred to polyvinylidene fluoride (PVDF) membrane, sealed with a sealant, incubated overnight with CD44, matrix metalloproteinase-2 (MMP2), MMP9, selectin E (SELE), and ERBB2 primary antibodies (Abcam) at 4°C, and incubated with horseradish peroxidase (HRP)-labeled secondary antibody (Abcam) at room temperature for 2 h. After treating the samples with chemiluminescent substrate working fluid (Merck Millipore), the membrane was developed in a Tanon 5200 chemiluminescence analysis system (Thermo Fisher Scientific, Waltham, USA).

Statistical analysis

The statistical analysis was done in SPSS v. 19.0 software (IBM Corp., Armonk, USA). The t-test was used to identify any differences between the 2 groups. A p-level <0.05 was considered statistically significant.

Results

Morphology of exosomes

The exosomes were extracted from the blood of the patients and the healthy volunteers. The findings of transmission electron microscopy (Fig. 1) revealed that the exosomes in the non-metastasis and metastasis groups were round or nearly round, with a double-layer lipid molecular structure, uneven size and distribution, and a diameter of 20–200 nm. These findings confirmed that exosomes existed in the serum of the glioma patients.

Exosome identification

Western blotting was applied to determine the protein expression of CD81 and CD63, the specific surface markers of exosomes. As shown in Fig. 2, the proteins CD81 and CD63 were expressed in all 3 groups, which further confirmed that exosomes were abundant in the serum of patients with glioma.

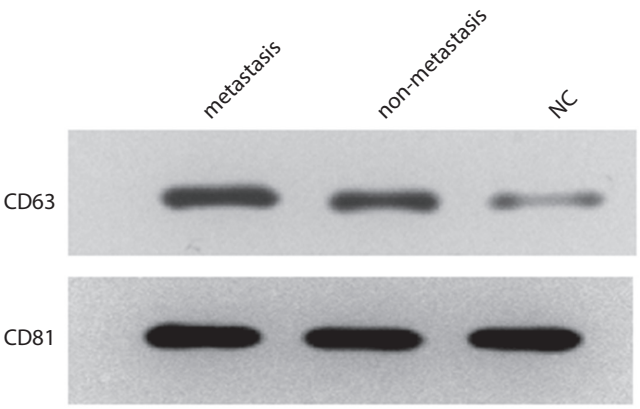

Fig. 2. The protein expression of 2 specific surface markers, exosomes CD81 and CD63, was measured with western blotting

CD44, HMMR, and MMP9 expression in non-metastatic and metastatic gliomas

Immunohistochemistry was performed to measure the expression of CD44, hyaluronan-mediated motility receptor (HMMR) and MMP-9 in the metastasis, adjacent(Adj)metastasis, non-metastasis, Adj-non-metastasis, and NC groups. As shown in Fig. 3, CD44 was highly expressed in the non-metastasis and metastasis groups, though it was expressed very little in the other groups. The expression of HMMR and MMP-9 in the Adj-metastasis group was the highest, followed by the Adj-non-metastasis group. Other groups demonstrated a low expression of HMMR and MMP-9.

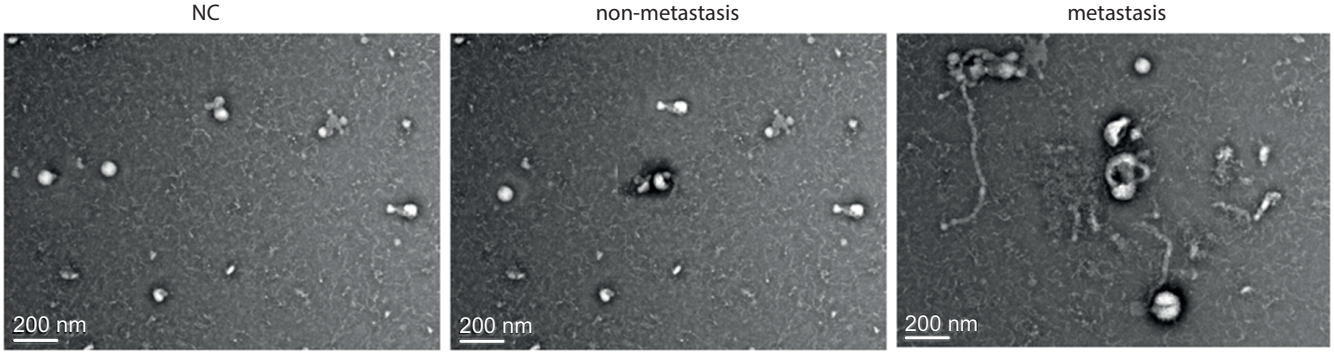

Fig. 1. The morphology of exosomes was examined using a transmission electron microscope

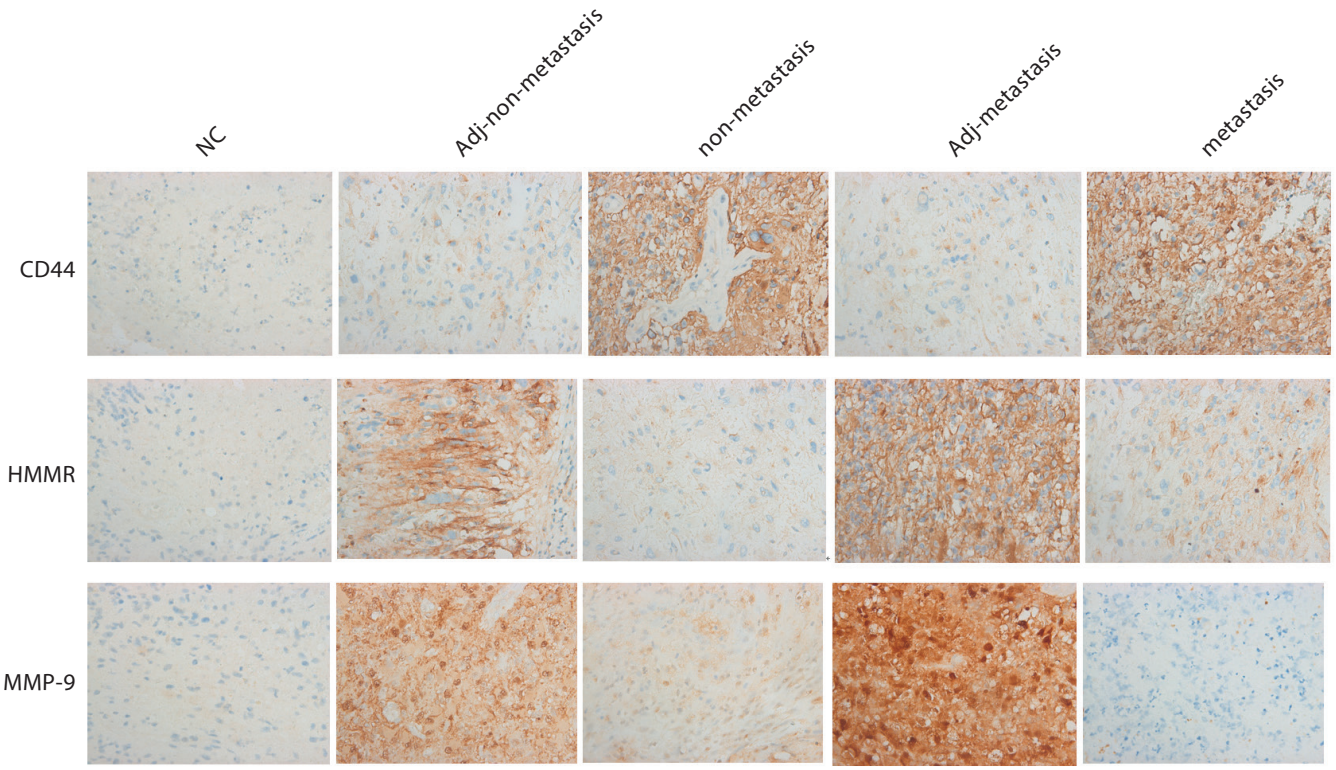

Fig. 3. The expression of CD44, HMMR and MMP-9 in the metastasis, Adj-metastasis, non-metastasis, Adj-non-metastasis, and NC groups was determined using immunohistochemistry assay

Metastasis influences gene expression

The protein expression of CD44, HMMR, MMP-2, MMP-9, and SELE in the metastasis, Adj-metastasis, non-metastasis, Adj-non-metastasis, and NC groups were measured. As shown in Fig. 4, CD44 expression in the metastasis and non-metastasis groups was significantly higher than in the NC group, while it was not expressed in the Adj-metastasis or Adj-non-metastasis groups. Moreover, the expression of CD44 in the metastasis group was higher than in the non-metastasis group. The MMP-2 and MMP-9 were not expressed in the metastasis or non-metastasis groups, and they were expressed to a much higher degree in the Adj-metastasis and Adj-non-metastasis groups than in the NC group. The expression of HMMR and SELE in the metastasis, Adj-metastasis, non-metastasis, and Adj-non-metastasis groups were all higher than the expression in the NC group. In addition, HMMR and SELE showed a much higher expression in the Adj-metastasis and Adj-non-metastasis groups in comparison to the metastasis and non-metastasis groups.

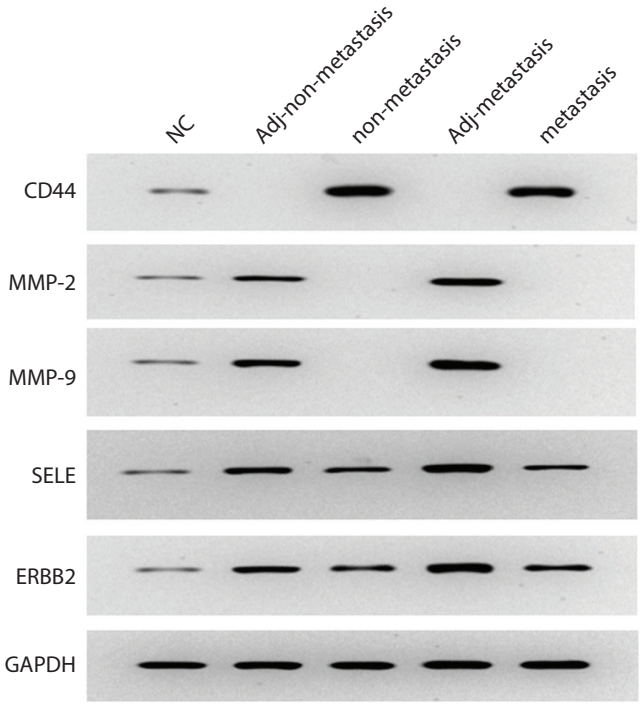

Fig. 4. The protein expression of CD44, HMMR, MMP-2, MMP-9, and SELE in the metastasis, Adj-metastasis, non-metastasis, Adj-non-metastasis, and NC groups was measured with western blotting

Discussion

Glioma is often invasive and the boundaries between the tumor and surrounding tissue are blurred, making it difficult to remove completely during surgery.[13] At present, the clinical treatment of glioma remains unsatisfactory, so recent studies have focused on the development of gene therapy, immunotherapy, targeted therapy, and other emerging therapeutic technologies for glioma patients. The mechanisms underlying these therapies need to be elucidated through molecular and pathological experimental

studies on glioma cells. Therefore, research on the molecular processes of glioma is important. Exosomes have become an area of interest in research over the past few years, and studies have proven that exosomes are a key factor in the occurrence and development of tumors.[14] Exosomes secreted by tumor cells carry specific small molecules or RNA that can affect the biological functions of other cells and thus regulate the progression of cancer.[15]

Exosomes are cup-shaped vesicles with a double-layer membrane structure, with a diameter of 40~100 nm and a density of 1.13~1.21 g/mL. Most of them are located in intercellular spaces or extracellular fluid, or they circulate in the peripheral blood.[16] Both tumor and non-tumor cells can release a range of cytokines, growth factors, adhesion molecules, and extracellular matrix proteins that mediate cell–cell communication in the tumor microenvironment.[17] Exosomes are involved in the tumor microenvironment and participate in the signal transduction between cells.[18] Compared with normal cells, cancer cells secrete larger exosomes, which may be an effective diagnostic marker.[19] In our study, we isolated and identified exosomes and found that exosomes were abundant in the serum samples of patients with glioma.

The EpCAM is a protein marker of exosomes. To study the mechanism underlying the role of EpCAM in glioma, we determined the expression of CD44, HMMR and MMP-9 with immunohistochemistry in the study groups: metastasis, Adj-metastasis, non-metastasis, Adj-non-metastasis, and NC. The results revealed that CD44 was highly expressed in the non-metastasis and metastasis groups and that the expression of CD44 in the metastasis group was higher than in the non-metastasis group. The levels of HMMR and MMP-9 expression were the highest in the Adj-metastasis and metastasis groups. CD44 is a key receptor of MT1-MMP, which degrades the extracellular matrix.[20] Expression of CD44 is upregulated in many types of cancer. Moreover, it mediates metastasis by recruiting CD44 to the cell surface.[21] In colorectal cancer, specific CD44 isoforms are expressed according to the progression of the disease.[22] CD44 is a molecular marker associated with cancer stem cell population and treatment resistance in glioma.[23] The HMMR is found in many cancers, such as colorectal cancer.[24] It is an oncogene that is highly expressed in glioblastomas and supports the growth of GBM.[25] Taking this into consideration, we speculated that CD44 was involved in the metastasis of glioma. Our results from western blotting demonstrated significantly higher expression of CD44 in the metastasis and non-metastasis groups in comparison to the NC group, and higher CD44 expression in the metastasis group than in the non-metastasis group.

There are some limitations of the current study. Firstly, the sample size was relatively small. Secondly, the regulatory effect of EpCAM in the metastasis of glioma needs to be evaluated in animal studies. The recruitment of CD44 to the surface of glioma cells also needs to be confirmed in vivo.

Conclusions

We found that the exosome EpCAM promoted the metastasis of glioma by increasing the expression of CD44.

ORCID iDs

Quan Gu https://orcid.org/0000-0002-5316-4151
Xuelin Chen https://orcid.org/0000-0002-8572-9989
Lin Zhou https://orcid.org/0000-0003-0265-9776
Xianglu Liu https://orcid.org/0000-0001-5276-1467

References

1. Eckel-Passow JE, Lachance DH, Molinaro AM, et al. Glioma groups based on 1p/19q, IDH, and TERT promoter mutations in tumors. *N Eng J Med*. 2015;372(26):2499–2508.
2. Iwadate Y, Matsutani T, Hirono S, Shinozaki N, Saeki N. Transforming growth factor-β and stem cell markers are highly expressed around necrotic areas in glioblastoma. *J Neurooncol*. 2016;129(1):101–107.
3. Louis DN, Perry A, Reifenberger G, et al. The 2016 World Health Organization classification of tumors of the central nervous system: A summary. *Acta Neuropathol*. 2016;131(6):803–820.
4. Zeng T, Cui D, Gao L. Glioma: An overview of current classifications, characteristics, molecular biology and target therapies. *Front Biosci (Landmark Ed)*. 2015;20:1104–1115.
5. Jeon BN, Yoo JY, Choi WI, Lee CE, Yoon HG, Hur MW. Proto-oncogene FBI-1 (Pokemon/ZBTB7A) represses transcription of the tumor suppressor Rb gene via binding competition with Sp1 and recruitment of co-repressors. *J Biol Chem*. 2008;283(48):33199–33210.
6. Kurtz JE, Dufour P. Adecatumumab: An anti-EpCAM monoclonal antibody, from the bench to the bedside. *Exp Opin Biol Ther*. 2010;10(6):951–958.
7. Trzpis M, McLaughlin PMJ, de Leij LMFH, Harmsen MC. Epithelial cell adhesion molecule: More than a carcinoma marker and adhesion molecule. *Am J Pathol*. 2007;171(2):386–395.
8. Went PTH, Lugli A, Meier S, et al. Frequent EpCam protein expression in human carcinomas. *Hum Pathol*. 2004;35(1):122–128.
9. Maetzel D, Denzel S, Mack B, et al. Nuclear signalling by tumour-associated antigen EpCAM. *Nat Cell Biol*. 2009;11(2):162–171.
10. Cimino A, Halushka M, Illei P, Wu X, Sukumar S, Argani P. Epithelial cell adhesion molecule (EpCAM) is overexpressed in breast cancer metastases. *Breast Cancer Res Treat*. 2010;123(3):701–708.
11. Du W, Ji H, Cao S, et al. EpCAM: A potential antimetastatic target for gastric cancer (Retraction of vol 55, pg 2165, 2010). *Digest Dis Sci*. 2013;58(6):1811.
12. Stoecklein NH, Siegmund A, Scheunemann P, et al. Ep-CAM expression in squamous cell carcinoma of the esophagus: A potential therapeutic target and prognostic marker. *BMC Cancer*. 2006;6:165.
13. Hu B, Wang Q, Wang YA, et al. Epigenetic activation of WNT5A drives glioblastoma stem cell differentiation and invasive growth. *Cell*. 2016;167(5):1281–1295.e18.
14. Kalluri R. The biology and function of exosomes in cancer. *J Clin Invest*. 2016;126(4):1208–1215.
15. Zhao R, Zhang Y, Zhang X, et al. Exosomal long noncoding RNA HOTTIP as potential novel diagnostic and prognostic biomarker test for gastric cancer. *Mol Cancer*. 2018;17:68.
16. Bang C, Thum T. Exosomes: New players in cell–cell communication. *Int J Biochem Cell Biol*. 2012;44(11):2060–2064.
17. Sivori S, Falco M, Della Chiesa M, et al. CpG and double-stranded RNA trigger human NK cells by Toll-like receptors: Induction of cytokine release and cytotoxicity against tumors and dendritic cells. *Proc Natl Acad Sci U S A*. 2004;101(27):10116–10121.
18. Ji H, Greening DW, Barnes TW, et al. Proteome profiling of exosomes derived from human primary and metastatic colorectal cancer cells reveal differential expression of key metastatic factors and signal transduction components. *Proteomics*. 2013;13(10–11):1672–1686.
19. Rabinowits G, Gerçel-Taylor C, Day JM, Taylor DD, Kloecker GH. Exosomal microRNA: A diagnostic marker for lung cancer. *Clin Lung Cancer*. 2009;10(1):42–46.
20. Kajita M, Itoh Y, Chiba T, et al. Membrane-type 1 matrix metalloproteinase cleaves CD44 and promotes cell migration. *J Cell Biol*. 2001;153(5):893–904.

21. Senbanjo LT, Chellaiah MA. CD44: A multifunctional cell surface adhesion receptor is a regulator of progression and metastasis of cancer cells. *Front Cell Dev Biol*. 2017;5:18.
22. Wielenga VJM, Heider KH, Johan G, et al. Expression of CD44 variant proteins in human colorectal cancer is related to tumor progression. *Cancer Res*. 1993;53(20):4754–4756.
23. Fu J, Yang Q, Sai K, et al. TGM2 inhibition attenuates ID1 expression in CD44-high glioma-initiating cells. *Neuro Oncol*. 2013;15(10):1353–1365.
24. Liu W, Ma J, Cheng Y, et al. HMMR antisense RNA 1, a novel long noncoding RNA, regulates the progression of basal-like breast cancer cells. *Breast Cancer (Dove Med Press)*. 2016;8:223–229.
25. Li J, Ji X, Wang H. Targeting long noncoding RNA HMMR-AS1 suppresses and radiosensitizes glioblastoma. *Neoplasia*. 2018;20(5):456–466.

In vitro SEM analysis of desensitizing agents and experimental hydroxyapatite-based composition effectiveness in occluding dentin tubules

Łukasz Rafał Pałka[1,A–F], Zbigniew Rybak[1,A,C,E,F], Piotr Kuropka[2,C,F], Maria Krystyna Szymonowicz[1,B,C], Jan Kiryk[3,B,C], Krzysztof Marycz[4,B,C], Maciej Dobrzyński[5,A–D]

[1] Department of Experimental Surgery and Biomaterials Research, Wroclaw Medical University, Poland
[2] Department of Animal Physiology and Biostructure, Wrocław University of Environmental and Life Sciences, Poland
[3] Department of Dental Surgery, Wroclaw Medical University, Poland
[4] Department of Experimental Biology, Wrocław University of Environmental and Life Sciences, Poland
[5] Department of Conservative Dentistry and Pedodontics, Wroclaw Medical University, Poland

A – research concept and design; B – collection and/or assembly of data; C – data analysis and interpretation; D – writing the article; E – critical revision of the article; F – final approval of the article

Advances in Clinical and Experimental Medicine, ISSN 1899–5276 (print), ISSN 2451–2680 (online) *Adv Clin Exp Med*. 2020;29(11):1283–1297

Address for correspondence
Łukasz Rafał Pałka
E-mail: regmed.klinika@gmail.com

Funding sources
This study was supported by a "Grant PLUS" provided by the Marshall's Office of the Lower Silesian Region in Wrocław, directed by Łukasz Pałka.

Conflict of interest
None declared

Received on April 16, 2020
Reviewed on August 22, 2020
Accepted on October 7, 2020

Cite as
Pałka ŁR, Rybak Z, Kuropka P, et al. In vitro SEM analysis of desensitizing agents and experimental hydroxyapatite-based composition effectiveness in occluding dentin tubules. *Adv Clin Exp Med*. 2020;29(11):1283–1297. doi:10.17219/acem/128197

DOI
10.17219/acem/128197

Abstract

Background. Novel materials used for dentin hypersensitivity (DH) treatment, including hydroxyapatite-based desensitizers, are not only effective in occluding dentinal tubules, but are also biocompatible and non-toxic. A newly formulated desensitizer containing hydroxyapatite was evaluated in comparison to commercially available desensitizers.

Objectives. To compare the occluding efficacy and durability of 3 commercially available desensitizing agents with a pharmaceutical composition developed by the authors based on hydroxyapatite (HAp).

Material and methods. For the experiment, 40 disc-shaped dentin specimens (5 mm thick) were obtained from extracted human teeth. Each disc was divided into 4 sections, so that each desensitizing agent could be applied to each specimen and prepared for further evaluation in most homogenous conditions. The chemical composition of the dentin surfaces was analyzed using scanning electron microscopy (SEM) equipped with an energy-dispersive X-ray spectroscope (EDS), Fourier-transform infrared (FTIR) and Raman spectra techniques. The specimens were immersed in an artificial saliva solution for 24 h, 48 h and 7 days to assess the durability of the layers and the tubule-obliteration effectiveness. Data analysis was performed using Student's t-test with an average value of normal distribution at an unknown variance with a standard deviation (SD) of σ–0.4.

Results. All the test groups showed some degree of dentinal tubule occlusion or a covering layer, but the HAp-based composition proved to be the longest-lasting. It was concluded that the developed pharmaceutical composition creates a coating on the dentin surface built of hydroxyapatite crystals sized 10–20 μm, which are likely to constitute a reservoir of calcium and phosphate ions, as well as smaller crystals (0.2–0.3 μm) that occlude dentinal tubules.

Conclusions. The composition containing biocompatible hydroxyapatite effectively occluded dentinal tubules and therefore exhibits a potential for reducing the pain and discomfort caused by dentin hypersensitivity.

Key words: scanning electron microscopy, dental material, dentin hypersensitivity, dentin tubules, hydroxyapatite

Introduction

One of the many sensations accompanying us throughout our lifetime is pain. This physical sensation warns us against any violation of physiological barriers or events exceeding the adaptive possibilities of our bodies and body structures, including teeth. A healthy tooth consists of a well innervated and vascularized pulp, dentin, enamel, and cement. If physical, chemical or iatrogenic factors damage this structure, it causes pain, which may become unbearable and force patients to seek specialized help. Tooth hypersensitivity, or more appropriately dentin (or dentinal) hypersensitivity (DH), is defined as an excessive response to harmless external stimuli,[1] which, according to researchers, affects as many as 74–80% of the adult population, depending on the geographical region.[2,3]

According to hydrodynamic theories, any restriction of tubular fluid movement contributes to the reduction of DH.[4] There are 2 main chairside approaches for treating DH: the obliteration of dentin tubules to reduce tubular fluid movement, and desensitization of nerves to reduce their sensitivity to stimuli.[5,6] Nerves can be desensitized with the use of potassium nitrate, and dentin tubules can be occluded with, e.g., glutaraldehyde, silver nitrate or zinc chloride, sealed by dentinal adhesives, or by laser (Nd:YAG, GaAlAs, Er:YAG).[7–14]

To date, numerous studies have been conducted with different active ingredients such as strontium chloride, potassium nitrate, potassium, iron and aluminum oxalates, bioactive glass, sodium citrate, potassium citrate, calcium hydroxyapatite, glutaraldehyde, potassium bicarbonate, cyanoacrylates, strontium chloride, calcium hydroxide, and silver nitrate in search of a perfect solution for DH.[15–18] Among these materials, nanohydroxyapatite (nHAp) is believed to be one of the most effective treatment options. Its biocompatibility and bioactive nature have been widely used in medicine and dentistry.[19,20] Hydroxyapatite is a crystallized nonorganic calcium compound that is biocompatible and a natural constituent of bones and teeth, and it has gained acceptance in treating DH in recent years. There are many in vitro and clinical studies that have reported the effective dentin occlusion capabilities of nHAp.[19–25]

The aim of this in vitro study was to develop a novel biocompatible, non-toxic hydroxyapatite-based agent that could be used in restorative dentistry.

Material and methods

This study was based on chemical and radiographic examinations. The experiment protocol was approved by the Bioethics Committee at Wroclaw Medical University (Poland), approval No. KB 230/2014, and has been conducted in full accordance with the World Medical Association Declaration of Helsinki. The experimental part of this study included selected desensitizing agents that are known for their obliterating features (Isodan®, Bifluorid®, Cervitec®) and are commonly used in dentistry, as well as a hydroxyapatite-based composition developed by the authors.

Preparation of the HAp-based composition

The present study aimed to create a composition obliterating dentinal tubules with the use of substances that may be metabolized by the cells present in the proximity and inside the tooth. The newly formulated desensitizer consisted of hydroxyapatite (Nanosynhap, Poznań, Poland), citric acid and glycerol in a self-developed molar ratio. It was prepared by mixing citric acid with glycerol and then incubating it at 100°C for 24 h. After this time, the pH of the mixture was measured; it ranged from 1.5 to 3.0. In the next step, calcium hydroxyapatite was added in the amount of 5–10% of the mixture weight. Tubes with the mixture were mounted on an IKA MS 3 basic mixer (IKA-Werke GmbH, Staufen im Breisgau, Germany) and mixed for 20 s. Then it was reheated at 100°C for 10 h. The pH of the mixture ranged from 2.45 to 4.19.

Infrared spectra

Infrared spectra in the 4000–400 cm^{-1} range were measured using a Vertex 70V Fourier-transform infrared spectroscopy (FTIR) vacuum spectrometer (Brüker Corp., Billerica, USA) for the self-developed composition at different concentrations. The measurements were made with the attenuated internal reflection technique, using a single-reflection ATR with a diamond crystal in vacuum conditions.

Raman spectra

After analyzing the infrared spectra and literature reports, we decided to perform additional Raman spectra measurements on the same samples. Raman spectra were measured on a Multi-RAM FT-Raman spectrometer (Brüker Corp.) equipped with a germanium detector. The samples were induced with a 1064 nm wavelength laser (Nd:YAG). The measurements were made in the 3600–50 cm^{-1} spectral range, with a resolution of 4 cm^{-1}; the number of scans was 256, with laser power on a 500 mW sample.

Desensitizing agents and artificial saliva

The commercially-available desensitizing agents included in the study were Isodan®, Bifluorid® and Cervitec®. Isodan® (Septodont Corp., Saint-Maur-des-Fossés, France) is a multi-compound product in the form of a gel that consists of 2-hydroxyethyl methacrylate, potassium nitrate and sodium fluoride. Bifluorid 10® (Voco GmbH, Cuxhaven, Germany) is a fluoride varnish that contains 5% sodium fluoride and 5% calcium fluoride. Cervitec® (Ivoclar

Vivadent AG, Schaan, Liechtenstein) is a varnish consisting of chlorhexidine and thymol.

We used a buffered solution of artificial saliva commonly used for experiments, with pH 6.7, in g/dm^3, consisting of K2HPO$_4$ (0.20); Na$_2$HPO$_4$ (0.26); KSCN (0.33); NaHCO$_3$ (1.5); NaCl (0.70); CO(NH$_2$)2 (0.13); KCl (1.2).

Preparation of the teeth

Forty human teeth extracted due to orthodontic indications were used to assess the tubule occluding effectiveness of the desensitizers. Under macroscopic evaluation, the teeth appeared fully developed, without caries or enamel damage, and free of dental fillings. They were cleaned of any tissue residue, blood and saliva, and rinsed in NaCl. After drying at room temperature, each tooth was sectioned using a diamond separator (ST-DD 22×0; Falcon Medical, Lucca, Italy) under constant water cooling to obtain 2 mm-thick enamel-dentin discs. The external layer of the enamel was removed to expose the dentin using turbine diamond drills and Sof-Lex polishing discs (3M ESPE, Saint Paul, USA) to obtain homogeneous, flat and smooth surfaces. Selected discs were polished and rinsed in demineralized water for 5 min, and then etched in 40% citric acid for 1 min to remove the smear layer and open dentinal tubules to simulate DH. Afterward, they were washed in demineralized water and rinsed in an ultrasound washer for 10 min to remove any contaminations. Each of the discs was sectioned horizontally and vertically, as described in earlier studies,[26–29] and divided in 4 equal parts (Fig. 1) to compare the tested desensitizers on each tooth in similar conditions. The substances under investigation were then applied to the surfaces of the open tubules, as in the description shown in Fig. 1.

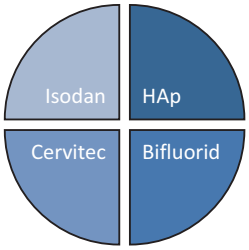

Fig. 1. Dentin disc with desensitizing agents

SEM surface examination

The samples were observed at ×500, ×1000, ×2000, and ×5000 magnification using an EVO® LS 15 scanning electron microscope (SEM) (Carl Zeiss, Oberkochen, Germany). Before the images were taken, a gold layer was sprayed onto the test specimens using the EDWARDS SCANCOAT Six device (BOC Edwards, West Sussex, UK).

The SEM examination was performed before applying the desensitizing materials, immediately after applying them, and after 24 h and 48 h of immersion in the artificial saliva solution. After 7 days of immersion in the artificial saliva, a SEM examination of the sample with the HAp-based formulation was carried out. Each of the images representing the tooth surface was investigated in terms of the agent used (B-Bifluorid®, C-Cervitec®, H-Hydroxyapatite, I-Isodan®) and the elapsed time (0 h, 24 h, 48 h, 168 h) to analyze the dynamics of the changes.

Examination of the dentin disc surface

The extent of tubule occlusion was assessed by a trained examiner grading the SEM images. Each of the discs was divided into 4 sections, as shown in Fig. 1, to conduct a comparative assessment of the obliterating ability of the 3 commercial desensitizers and our own composition. Specific regions of each specimen were covered with the desensitizing agents according to the manufacturer's instructions, while our own composition was rubbed into the disc surface using a micro brush for 10 s and left to dry. After the treatment, the specimens were prepared for analysis with SEM.

Statistical analysis of the diameter of the dentinal tubules

In the study, 8 tooth surface sets with 6 samples in sets 1–7 and 3 samples in set 8 were randomly selected from among the tubules visible on 8 representative SEM photographs. The t-test was used to test the null hypothesis, which assumed a mean value ≥3 and standard deviation (SD) σ–0.4.

Results

FTIR spectra

When analyzing the FTIR spectra of the individual components, we observed that the calcium phosphate (V) vibration bands were obscured by the bands derived from citric acid and glycerol. In particular, the range of $Ca_3(PO_4)^2$ bands is in the area in which we observed glycerol vibration bands. This method did not give us information on the qualitative composition of the self-developed mixture, and we could not determine the change in the calcium phosphate (V) form in the analyses.

Raman spectra

After analyzing infrared spectra, we decided to measure Raman spectra on a Multi-RAM FT-Raman spectrometer (Brüker Corp.) equipped with a germanium detector. The samples were excited with a 1064 nm wavelength laser (Nd:YAG). The measurements were performed in the 3600–50 cm^{-1} spectral range, with a resolution of 4 cm^{-1}, 256 scans per sample, and a laser power of 500 mW/sample.

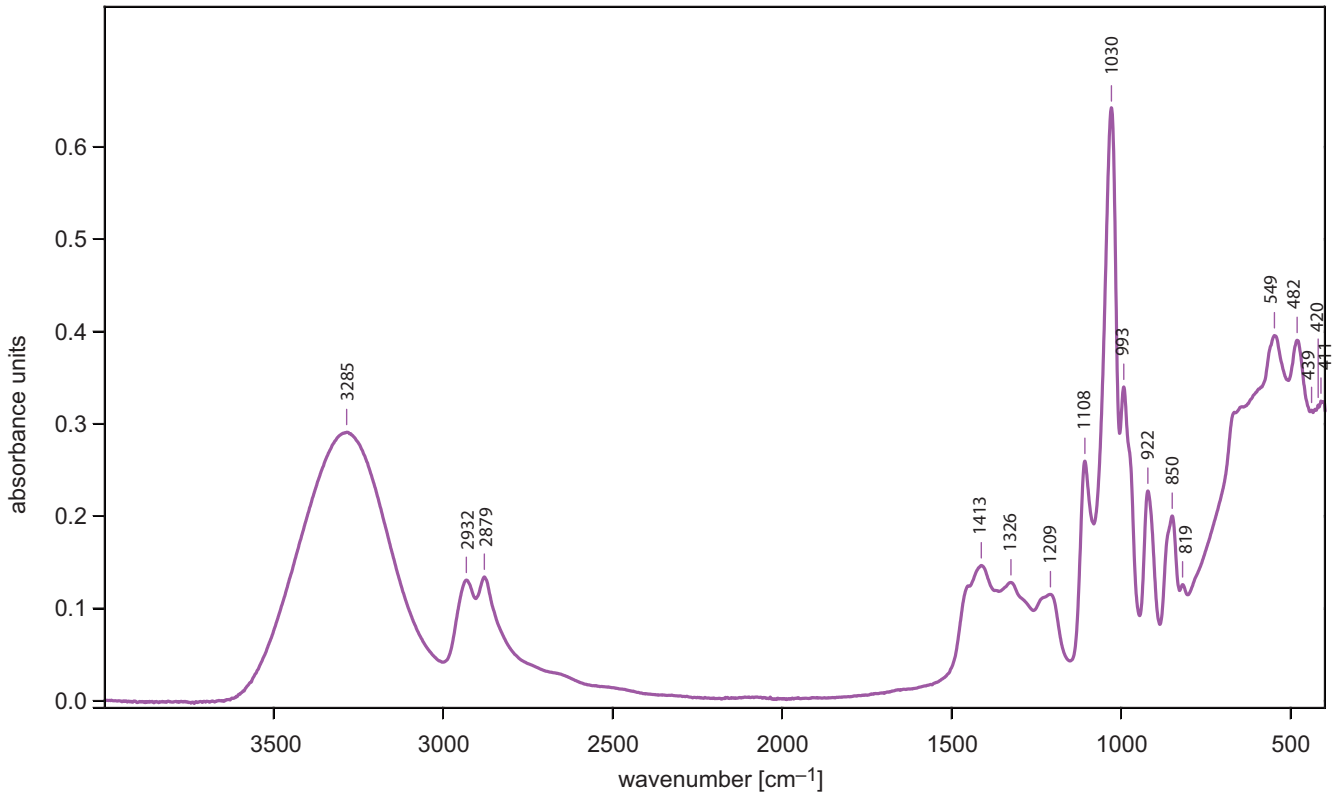

Fig. 2. A representative oscillation spectrum for a selected sample of the self-developed mixture

We compared all the samples looking for differences in the oscillatory spectra (Fig. 2). Such differences would indicate the formation of a new compound, but we did not notice any changes. The bands present in the reference sample, which contained only calcium phosphate, were also present in the samples under analysis. The marker band, which is very intense in the spectrum of $(PO_4)_2$, at 963 cm^{-1}, was present in each sample, which may indicate that no new compound had been formed. If a new form of phosphate had been formed, the marker band would have been absent. According to the literature, in Raman spectra of pure calcium phosphate (V), 4 bands (for different types of vibration symmetry) should be present: 2 bands of anion stretching vibrations $[PO_4]^{3-}$ ($\nu[PO_4]^{3-}$) and 2 bands that correspond to bending vibrations, i.e., $\delta[PO_4]^{3-}$.[30] Theoretically, these bands occur at appropriate frequencies:

- $\nu_1[PO_4]^{3-} \rightarrow 938$ cm^{-1} (type A symmetry),
- $\nu_3[PO_4]^{3-} \rightarrow 1017$ cm^{-1} (type T symmetry),
- $\delta_2[PO_4]^{3-} \rightarrow 420$ cm^{-1} (type E symmetry), and
- $\delta_4[PO_4]^{3-} \rightarrow 567$ cm^{-1} (type T symmetry).

They correspond to the wave numbers on the infrared calcium phosphate (V) spectra (FTIR):

- $\nu_1 = 962$ cm^{-1},
- $\nu_3 = 1024$ cm^{-1},
- $\delta_2 = 472$ cm^{-1}, and
- $\delta_4 = 600 + 561$ cm^{-1}.

The same bands are observed in Raman spectra:

- $\nu_1 = 963$ cm^{-1} (the most important characteristic band, the very intense marker band),
- $\nu_3 = 1017 + 1048 + 1030$ cm^{-1} (mean of 3 bands, fission caused by the solid effect),
- $\delta_2 = 470 + 432$ cm^{-1} (mean of 2 bands), and
- $\delta_4 = 609 + 592 + 581$ cm^{-1} (mean of 3 bands).

Based on the above, the most promising mixture was selected for further study; it showed a similar amount of glycerol and calcium phosphate (V). The intensity of the bands was similar (e.g., the intensity of the band at 1055 cm^{-1} from glycerol vibrations was similar to the intensity of the band at 963 cm^{-1}). A small addition of citric acid was also observed in this sample (band at 1626 cm^{-1}, vibrations in the dilution of -COOH citric acid groups).

SEM analysis

The SEM examinations did not show any pathological changes in the discs we evaluated. Their surfaces with open tubules, after removing the smear layer, are shown in Fig. 3. The image of the surface has been magnified ×1000, ×2000 and ×5000. The dentinal tubule diameters were measured at ×5000 magnification, and they ranged from 2.714 µm to 3.729 µm (Fig. 3D).

After application of the desensitizers

Isodan® was evenly spread across the surface of the dentin. Irregularly shaped particles (sized 4–10 µm) were found, which were probably crystallized potassium salts,

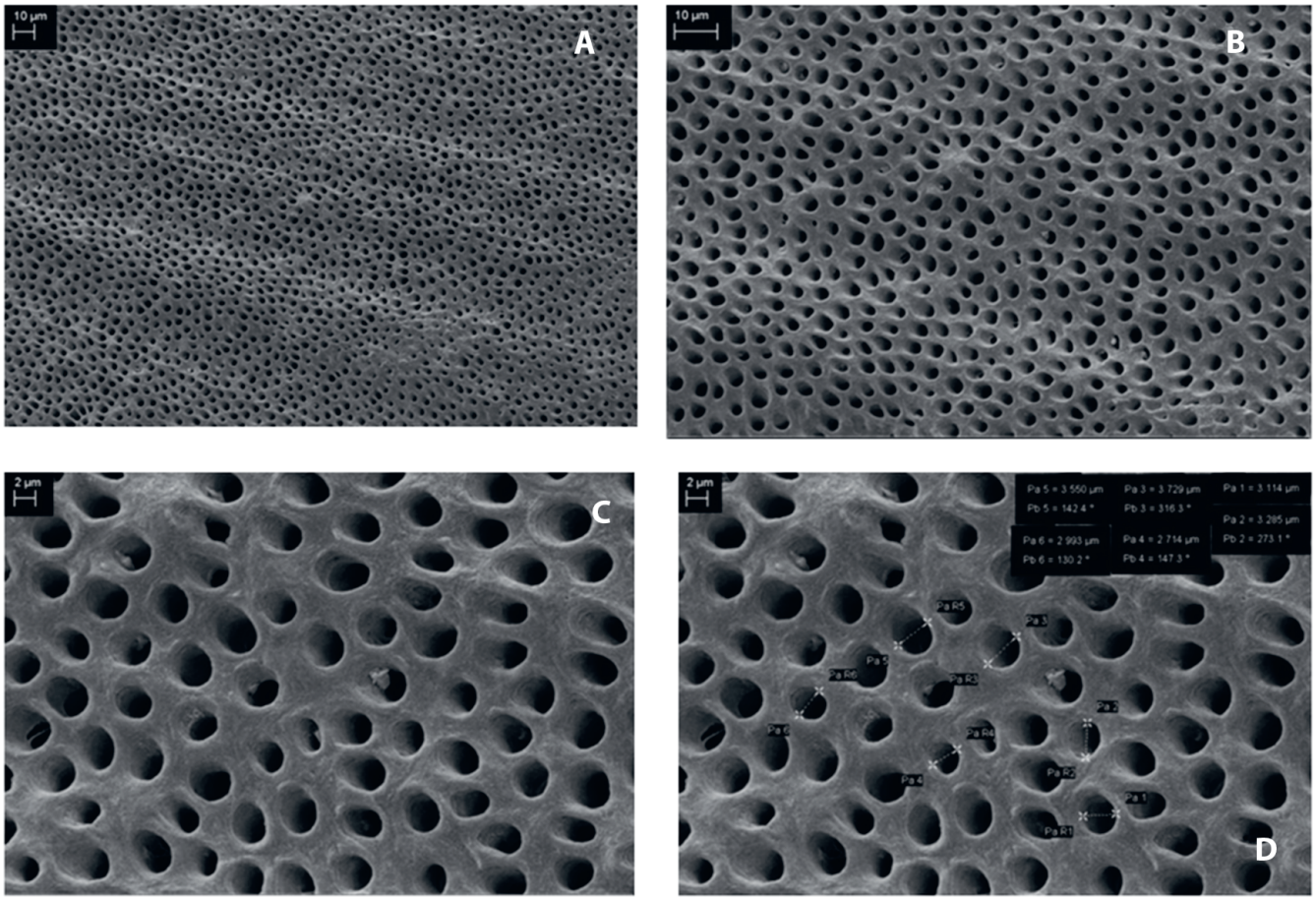

Fig. 3. SEM images of the dentin surface. A – Isodan®, SEM magnification ×1000; B – HAp, SEM magnification ×2000; C – Bifluorid®, SEM magnification ×5000; D – Cervitec®, SEM magnification ×5000, showing the sizes of the tubules obtained with morphometric analysis

one of the ingredients of the material (Fig. 4A). The HAp-based composition developed by the authors tightly covered the dentin tubules with particles of unconnected hydroxyapatite with a maximum size of 30 µm (Fig. 4B) and small crystals (sized 200 nm) obliterating the tubules. Bifluorid® created a tight, undulating layer on the dentin surface (Fig. 4C), whereas Cervitec® formed a tight varnish-like layer (Fig. 4D).

After 24 hours

On the dentin surface covered with Isodan® and incubated for 24 h in artificial saliva (Fig. 4), crystals of the ingredients of the desensitizer were visible. Still, they showed indications of solvency, such as blurred edges and melting. The layer covering the tubules was still present, and in comparison with the image taken just after its application (in which single tubules were open), much larger areas with still-open tubules could be seen. After examining the surface covered with HAp after a 24-hour incubation in artificial saliva (Fig. 4F), larger hydroxyapatite crystals had become smaller, and the number of smaller crystals directly blocking the tubules increased. No layer covering the dentin was observed in contrast with the previous examination, presented in Fig. 4B. After 24 h, Bifluorid® still covered only some areas of the surface, revealing a number of dentinal tubules (Fig. 4G). It could not be ascertained unequivocally whether the cracks present resulted from the solubility of the layer or from procedures connected with imaging. Since Bifluorid® is a varnish, the ingredients probably cracked after covering the surface and in contact with saliva, and a layer of the product probably peeled off the dentin surface. The surface covered with Cervitec® (Fig. 4H) was comparable to the image taken just after its application. The crater-like artifacts present in the image probably resulted from the process of preparing the sample for the SEM examination.

After these images were taken, the specimens were again immersed in the artificial saliva solution.

After 48 hours

After a 48-hour incubation in the artificial saliva solution, there was no trace of Isodan® on the surface (Fig. 4I). Probably, the layer dissolved and desorbed from the surface, causing the dentinal tubules to open. Also, single crystal-like formations appeared, but they may have been contaminants of the saliva solution. After 48 h in the artificial saliva solution, the surface covered with hydroxyapatite

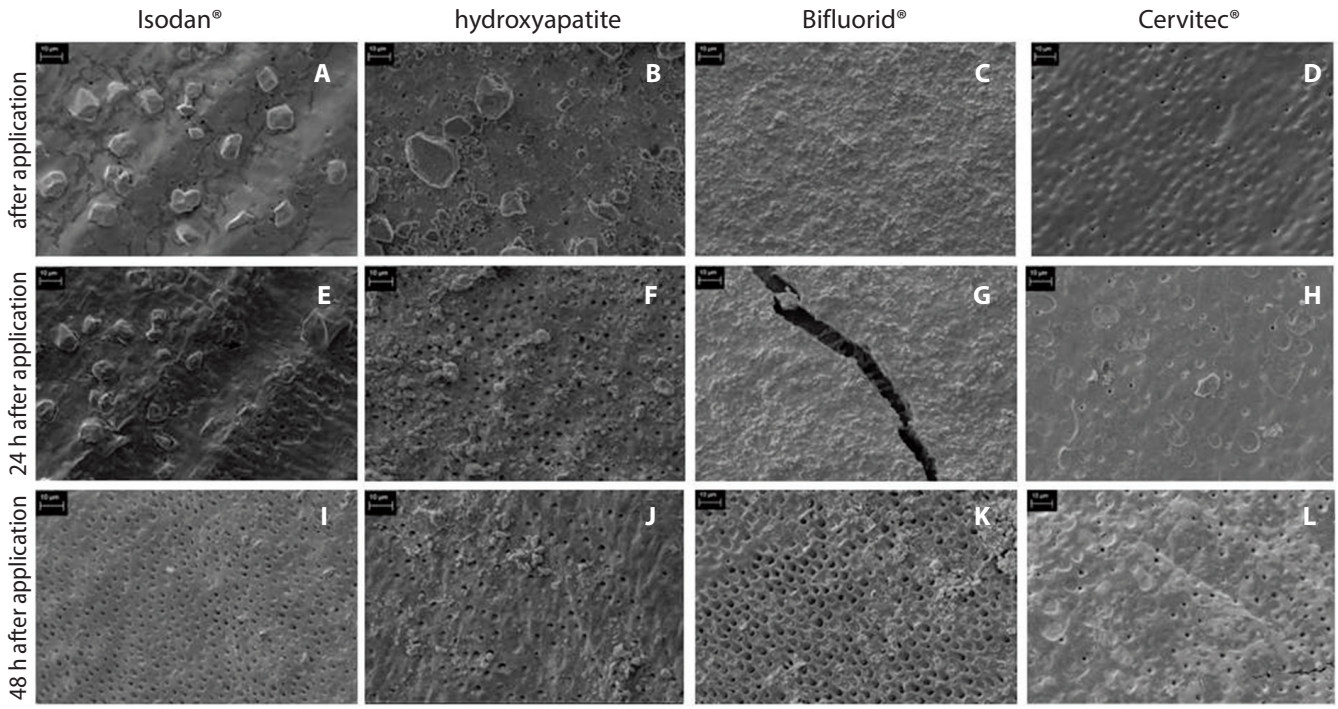

Fig. 4. Surface morphology of dentin specimens after treatment with commercial desensitizing agents (Isodan, Bifluorid, Cervitec: A/C/D) and nano-hydroxyapatite (B); after 24 h (E–H) and 48 h (I–L) of immersion in artificial saliva. Dental specimens covered with the examined substances after drying (A–D); the different textures and sizes of crystallized compounds predominant in each desensitizer are visible. The surfaces of the discs covered with the desensitizing agents after 24 h of incubation in artificial saliva (E,H). The rinse-off process from the tooth surfaces; opening of the dentinal tubules can be seen. The SEM images of the dentin surfaces 48 h after the application of the desensitizing agents (I–L)

(Fig. 4J) still showed hydroxyapatite crystals (sized approx. 1 μm), creating conglomerates with uneven distribution. Also, dentinal tubules obliterated with small crystals were seen, as well as the layer covering the dentin. Examination of the surface covered with Bifluorid® after 48 h (Fig. 4K) revealed evident disintegration of the coating, covering the dentin with cracks, and areas with open dentinal tubules were visible. Under microscopic evaluation, dentinal tubules obliterated with particles or crystals formed from the disintegrating layer were seen. The surface covered with Cervitec® (Fig. 4L) showed single cracks and a larger number of open dentinal tubules in comparison with the previous images (Fig. 4D,H).

After 7 days

After a seven-day incubation in artificial saliva, we performed an SEM examination only for the HAp-based composition. It was impossible to do the same with the remaining desensitizers, as the layers were completely dissolved. In the sample we examined, both large and small hydroxyapatite crystals and a coating covering the dentinal surface with many cracks were observed. There were many open dentinal tubules, but also quite a large number of obliterated ones. A SEM image magnified ×15,000 was taken, in which hydroxyapatite crystals obliterating dentinal tubules could be seen, as well as the layer covering the dentin around the tubules (Fig. 5).

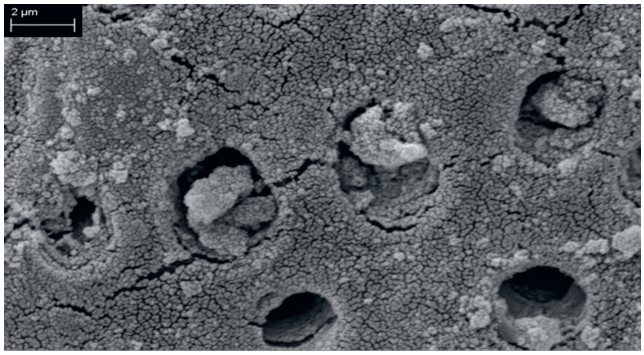

Fig. 5. The image of the dentinal disc after applying self-developed HAp-based composition and incubation in artificial saliva for 7 days. The nanoparticles constituting the composition filled dentinal tubules and effectively blocked tubular fluid flow (SEM, magnification ×15,000)

Analysis of the dynamics of changes in the desensitizers

The analysis of the dynamics of changes aimed to determine the effectiveness of closing the open dentin tubules depending on the type of desensitizer used over time (Table 1). We observed that Bifluorid®, despite achieving the best results immediately after application, was characterized by very dynamic degradation at subsequent stages of observation, indicating its average durability. Cervitec® showed good results immediately after application and

Table 1. The dynamics of changes in the number of open dentin tubules over time

Tested agent	After application	24 h after application	48 h after application	168 h after application	Initial	Dynamics
Bifluorid®	0.00	∞%↑	362%↑	no data	++	−−
Cervitec®	45.00	20%↓	64%↑	no data	+/−	+/−
HAp	4.00	1050%↑	67%↓	7%↓	+	+
Isodan®	0.00	17.00%↓	no data	no data	+	−−

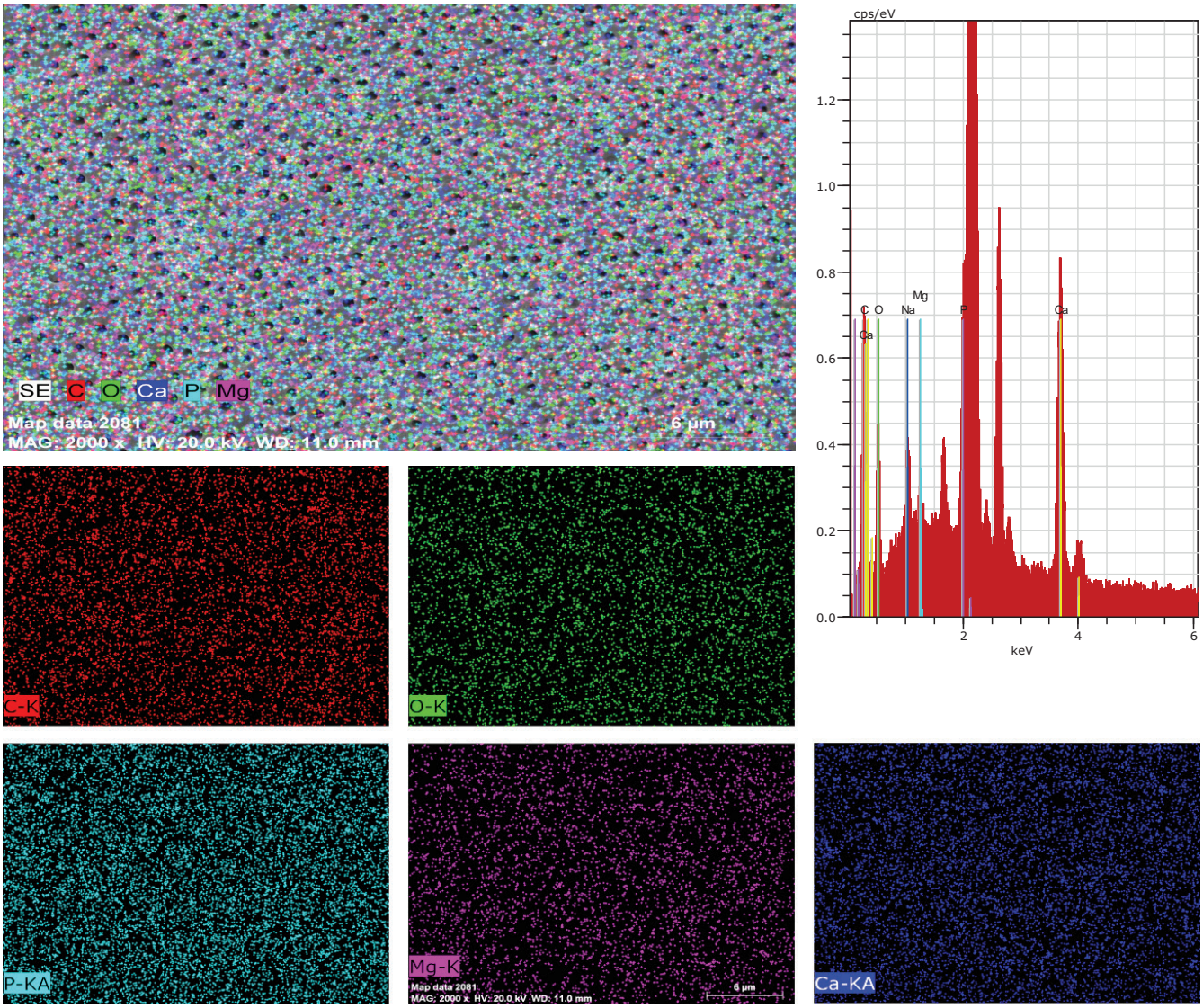

Fig. 6. Surface mapping of the reference sample with a chemical composition graph. Chemical analyses of the 4 surfaces after application of the tested preparations showed the presence of characteristic elements for the given agent. For Isodan®, it was potassium and fluorine; for the self-developed desensitizer, calcium and phosphorus; for Bifluorid® it was fluorine; and for Cervitec®, chlorine. Also see Fig. 7 and 8

a very slow degradation rate at subsequent stages of observation, which indicated its relatively higher effectiveness. Our hydroxyapatite-based agent, despite its initially limited effectiveness, was the only substance showing gradation at successive time stages. In other words, its effectiveness only appeared some time after the compound was deposited on the surface of the tooth. This shows its superiority over the other agents, in which the quality of tooth protection weakened with time. Isodan® exhibited moderate efficacy when the first measurement was performed and significant (almost total) degradation with subsequent analyses. These results allowed us to draw very cautious conclusion that, in terms of the stability of the effects of the applied tubular obliteration technique, the best results can be obtained with the use of a hydroxyapatite-based formulation with apatite crystals sized ≤300 nm.

Results of the chemical analyses of the tested surfaces

After performing the chemical analyses and surface mapping of the reference sample, the presence of elements such as carbon, oxygen, calcium, phosphorus, and magnesium characteristic of the dentin surface imaged using the SEM technique was revealed (Fig. 6).

Figure 7 presents the dynamics of the changes in the concentration of elements over time (0 h, 24 h, 48 h, 168 h) for all the tested agents. Since the protective layer created by Isodan® dissolved completely within 48 h, it was excluded from further analysis. At hour 168, only the self-developed pharmaceutical composition was analyzed because it was the only agent still present on the dentin surface. The cumulative chart presents 4 samples (B, C, H, I) with selected elements. The bars on the graph do not represent the entire chemical composition, but only quantitative contents of the selected compounds (Fig. 8).

The chemical analysis of Isodan® performed immediately after its application showed the presence of elements such as potassium and sodium, as well as fluorine and nitrogen, most likely derived from the potassium nitrate and calcium fluoride present in the formulation (Fig. 7A). The hydroxyapatite-based desensitizer showed the presence of 2.26% phosphorus and 1.17% calcium in a molar ratio similar to the reference sample (Fig. 7B). The surface covered with the 3rd desensitizer (Bifluorid®) showed significant amounts of fluorine, representing 47.52% of the chemical composition of the whole surface (Fig. 7C). The percentage increase in calcium content and the significant amounts of fluoride are most likely derived from calcium fluoride, which is the main component of Bifluorid®. In the chemical analysis of Cervitec® (Fig. 7D), the presence of chlorine was observed, most likely derived from chlorhexidine acetate, the main active ingredient of the product.

After 24 h of immersion in the artificial saliva solution, another chemical analysis of the surfaces was performed. In the case of Isodan®, an absence of fluorine and potassium (present in the first image) and unchanged levels of nitrogen and sodium were observed (Fig. 7E). The chemical composition of the HAp-based substance had not changed, but the ratio of phosphate ions to calcium ions was different (Fig. 7F) with an increase in phosphate ions. The chemical analysis of Bifluorid® revealed 1.5 times greater concentrations of calcium and phosphorus, and a ten-fold increase in fluorine (Fig. 7G) compared to the analysis immediately after application. This may indicate the release of these ions under the influence of saliva. The analysis of Cervitec® (Fig. 7H) showed that chlorine ions were still present (3 times fewer of them compared to the sample analyzed immediately after application).

After 48 h of immersion (Fig. 7J), the quantity of calcium and phosphorus ions in the HAp-based product was 4 times higher than in the earlier samples. This may indicate that artificial saliva influenced the dissolution of hydroxyapatite crystals and caused a steady release of calcium and phosphorus. Fluorine ions were still present on the Bifluorid®-treated surface (Fig. 7K); however, compared to the 1st measurements, their quantity had decreased by 1/3. A significant decrease in the concentration of phosphorus and calcium ions was also observed. For Cervitec® (Fig. 7L), minimal levels of calcium, phosphate and chloride ions were found. Chemical analysis of the HA-p-based desensitizer made 7 days after immersion in the artificial saliva solution showed the presence of calcium and phosphate ions in a molar ratio of about 1: 1, similarly to the test performed after 24 h (Fig. 9).

Statistical analysis

The study showed an empirical average of observed tubular diameters of 3.01 μm, with a minimum of 2.18 μm and a maximum of 4.30 μm. We tested the null hypothesis that the size of dentin tubules was ≥3 μm, with $p > 0.9$ (Table 2). Thus, the results of the statistical analysis confirm that as objects with diameters not exceeding 2.00 μm, hydroxyapatite crystals used as the active substance can penetrate defects occurring in the tooth surface and block tubular light.

Table 2. Sizes of the dentin tubules (where σ is standard deviation, andH is the null hypothesis)

N	45
min [μm]	2.18
median [μm]	3.01
max [μm]	4.30
σ [μm]	0.40
T (H_0:μ_0 ≥ 3 μm)	0.16
H_0:μ_0 ≥ 3 μm	true
p-value (H_0:μ_0 ≥ 3 μm)	> 0.9

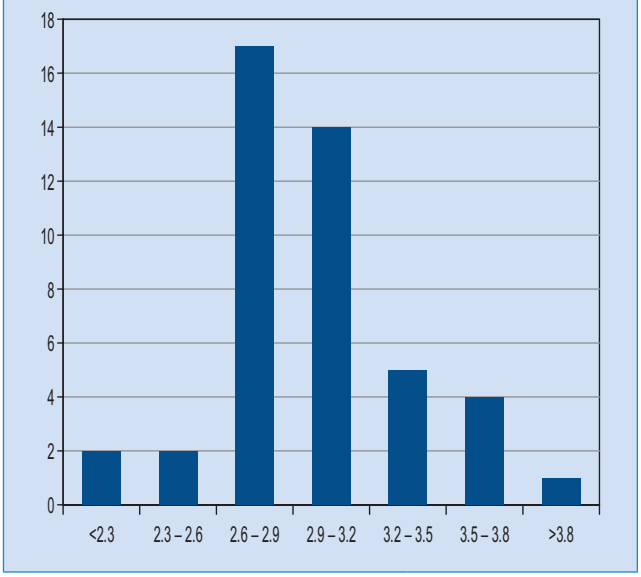

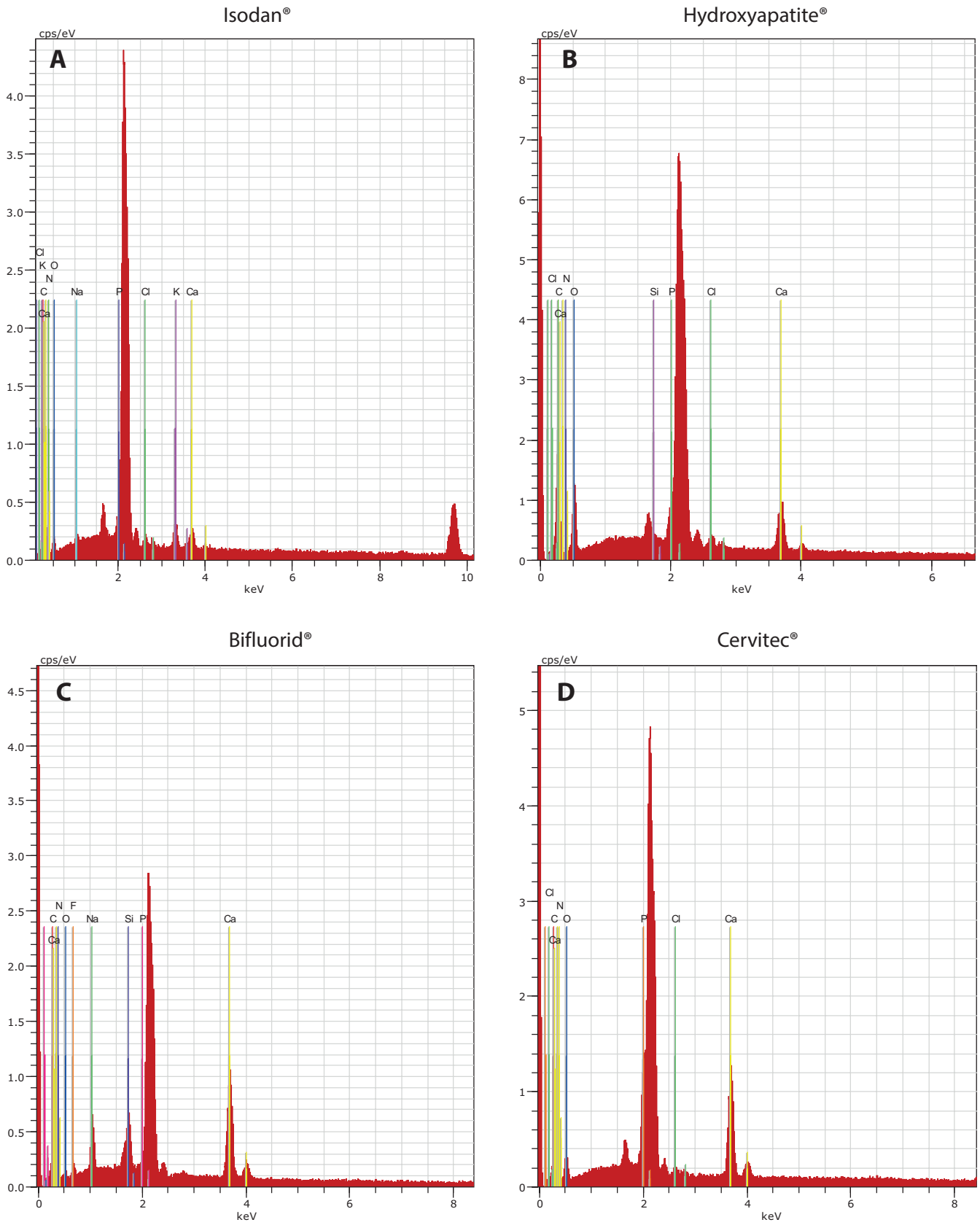

Fig. 7A–D. Chemical analysis of the surfaces with the agents applied. Chemical structure of the specimens just after application

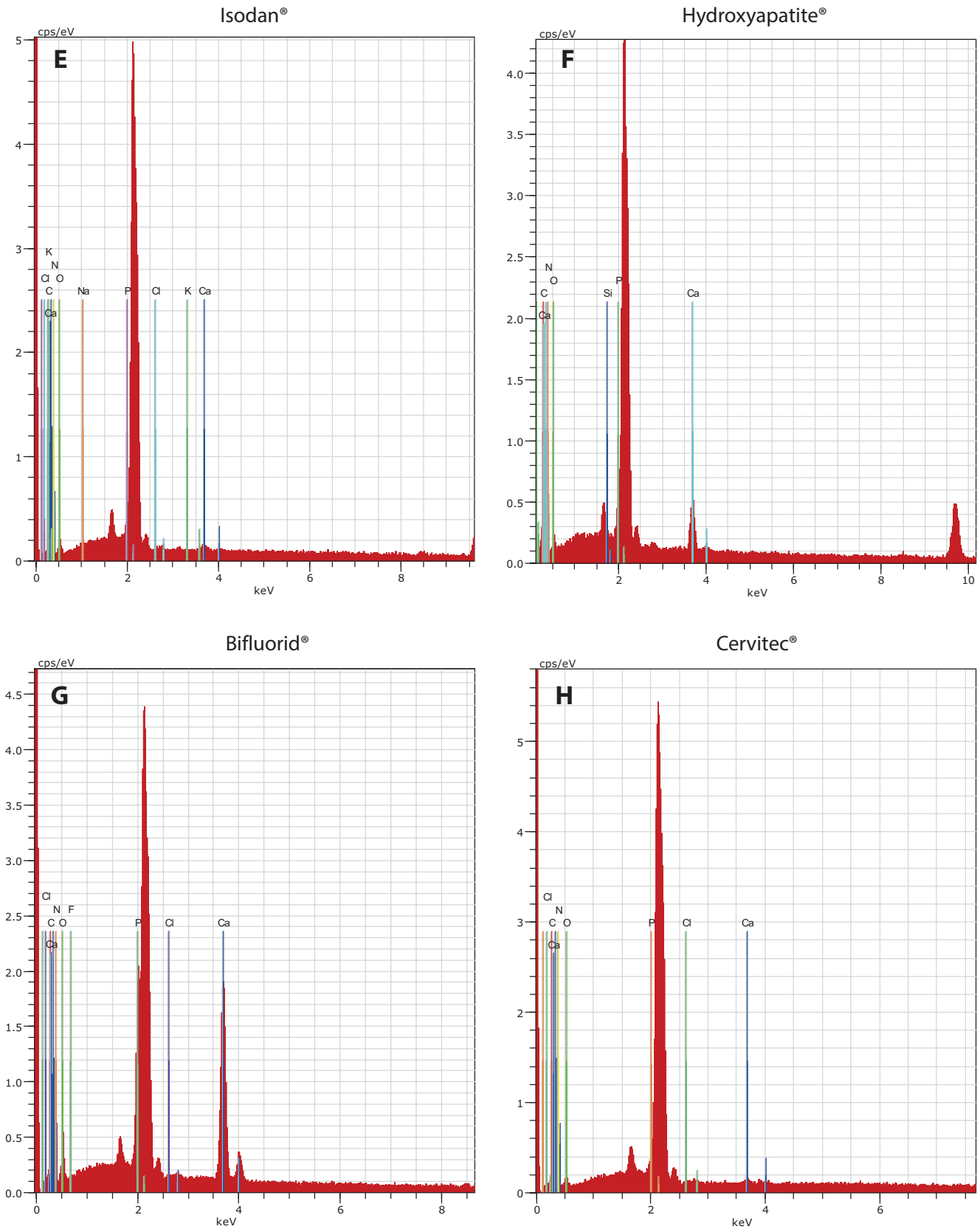

Fig. 7E–H. Chemical analysis of the surfaces with the agents applied. After a 24 h of immersion in artificial saliva

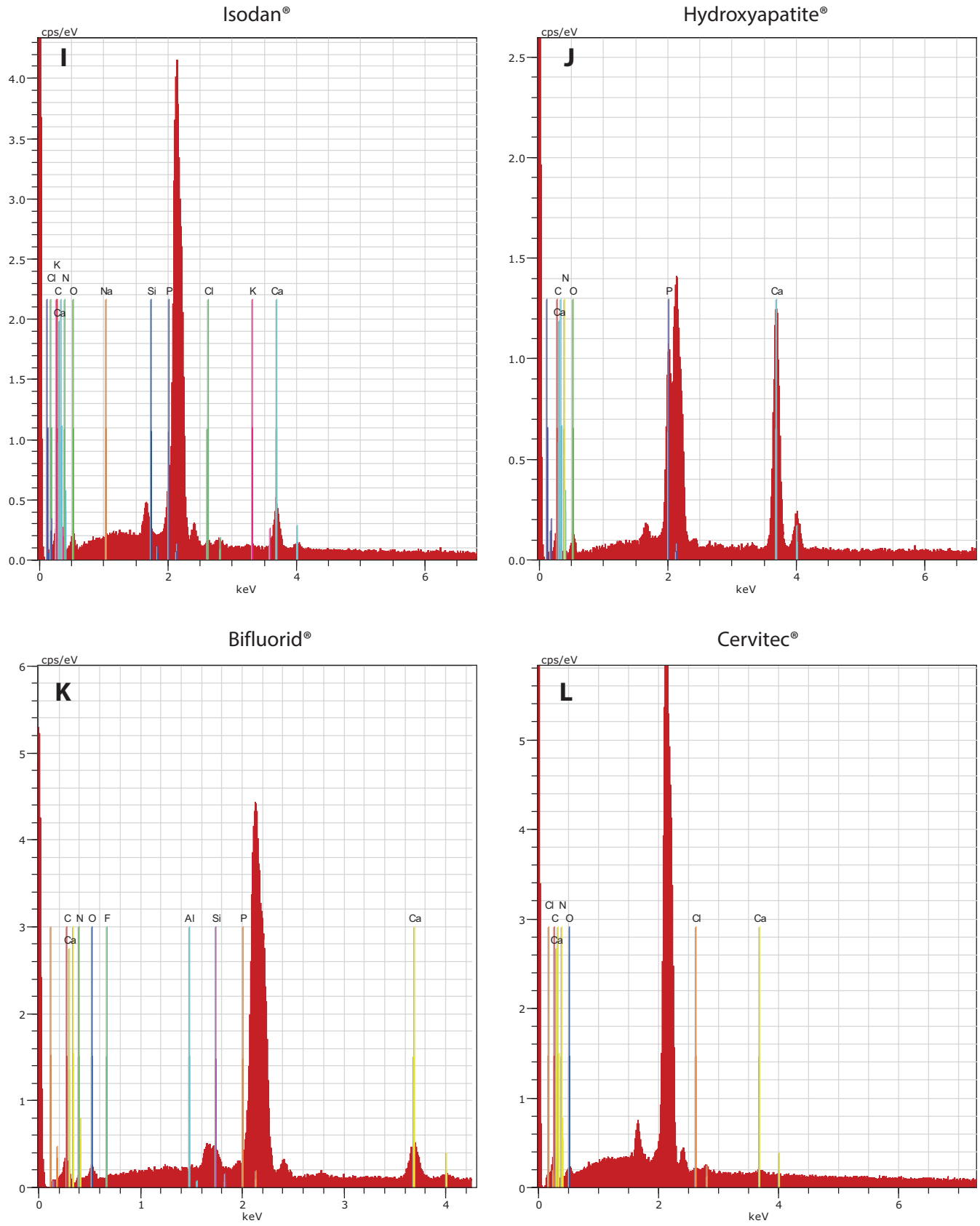

Fig. 7I–L. Chemical analysis of the surfaces with the agents applied. After 48 h of immersed in artificial saliva

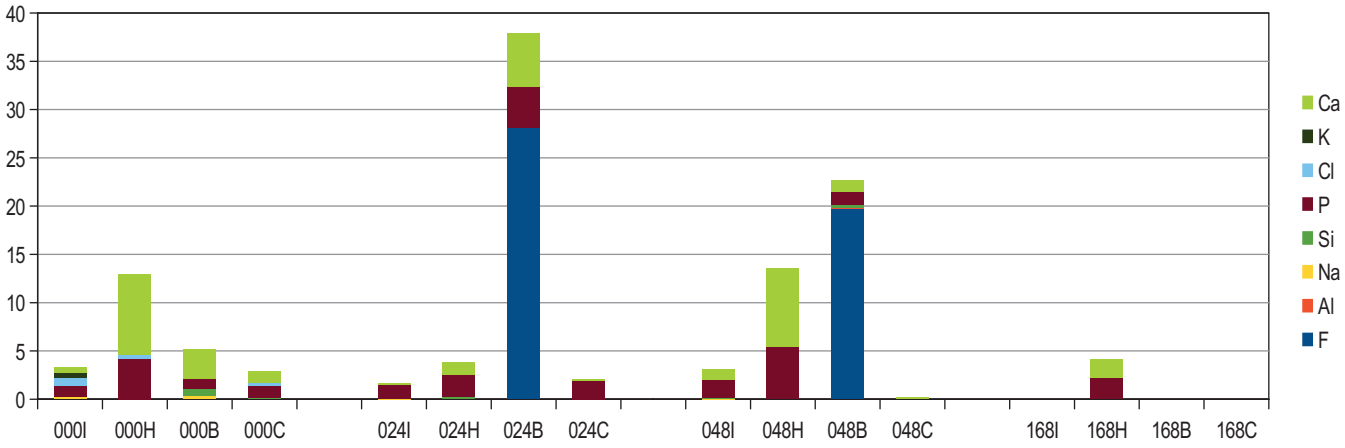

Fig. 8. Dynamics of change in the concentration of chemical elements over time (B – Bifluorid®; C – Cervitec®; I – Isodan®; H – hydroxyapatite)

Discussion

Tubule occlusion can be brought about by the deposition of mineral crystals either on the surface and/or within the dentinal tubules. Superficial occlusion of tubules can provide only short-term relief as the precipitate can either be removed by daily tooth brushing or dissolved by saliva and/or consumption of acidic beverages. Effective treatment with long-term results has been related to intratubular deposition of mineral crystals.[31,32]

Treatment of DH focuses on using substances that limit dentin permeability by obliterating dentinal tubules, making the dentin insensitive to stimuli like airflow or probing, which, in normal conditions, cause dentinal fluid flow, and as a consequence activate the nerve endings present, inflicting pain.[33] Studies have shown that dentinal fluid flow is proportional to the 4th power of the tubule radius. This means that when we reduce the radius by half anywhere along its length, the fluid flow will not decrease by half but to the 4th power, i.e., to 1/16 of its primary flow.[34] On the basis of the above, it may be concluded that to reduce or eliminate DH, it is not necessary to occlude tubules completely; but at the same time, the question arises what extent of obliteration is sufficient and what percentage of exposed tubules should be obliterated to reduce DH so that the patient feels relief. Different active ingredients have been studied to assess their ability to treat DH. The commercially available desensitizing agents used in the present study consisted of such active ingredients as potassium nitrate, sodium fluoride, calcium fluoride, and chlorhexidine. McCornack and Davies suggested that potassium nitrate stimulates odontoblasts to synthesize and secrete nitric oxide (NO), which may act as a nerve blocker.[34] Moreover, it has been observed that in the right concentration, potassium salts (e.g., potassium chloride) are able to block the activity of the tubular nerve endings.[33] Calcium salts and phosphate-containing substances are supposed to generate the deposition of amorphous calcium phosphate crystals in the openings, while acidic calcium phosphate forms precipitates inside the dentinal tubules.[35] Fluorine ions may react with free calcium ions and form calcium fluoride aggregates by occluding dentinal tubules.[36] Ten Cate observed that a very low concentration of fluorine in liquid form at a low pH could almost completely block the dissolution of apatite crystals and reduce the degree of demineralization.[37] Bizhang et al. reported that chlorhexidine (which inhibits the growth of bacteria permanently present on the tooth surface) protects teeth against demineralization.[38] Also, satisfactory effects were obtained by combining chlorhexidine with fluoride.[39] Madruga et al. compared the desensitizing efficacy of the resin-modified glass ionomer cement (GIC) Clinpro™ XT (3M ESPE) and the conventional GIC Vidrion R (SS White Group, Gloucester, UK). Their findings suggest that conventional and resin-modified glass ionomer cements are also successful in managing DH.[40]

Dentin adhesion is not as easily achieved as enamel adhesion, since dentin is living tissue and enamel is not. The undisturbed permeability of the dentinal fluid from the chamber to the outside while preparing dentin causes its surface to undergo constant changes. In addition, all the agents applied to dentin and enamel surfaces are dissolved by tubular fluid. The smear layer on a prepared tooth consists of particles of dentin, collagen fibers, odontoblast residue, and bacteria. Its thickness ranges from 0.5 μm to 5.0 μm. It also prevents contact and chemical reactions with an active agent bonding with the dentin or with a desensitizing agent.[41,42] This is why in order to expose the tubules and collagen fibers, it is necessary to achieve bonding of the desensitizers with the dentin, which has to undergo chemo-mechanical preparations. The HAp-based composition seems to create a layer made of larger hydroxyapatite crystals (10–20 μm in size), which may constitute a reservoir of phosphorus and calcium ions as precursors of calcium phosphate – a substrate necessary for the next stage in the dentin remineralization process.[43–46] Our chemical analysis and SEM examinations demonstrated that the HAp-based composition also consists of smaller

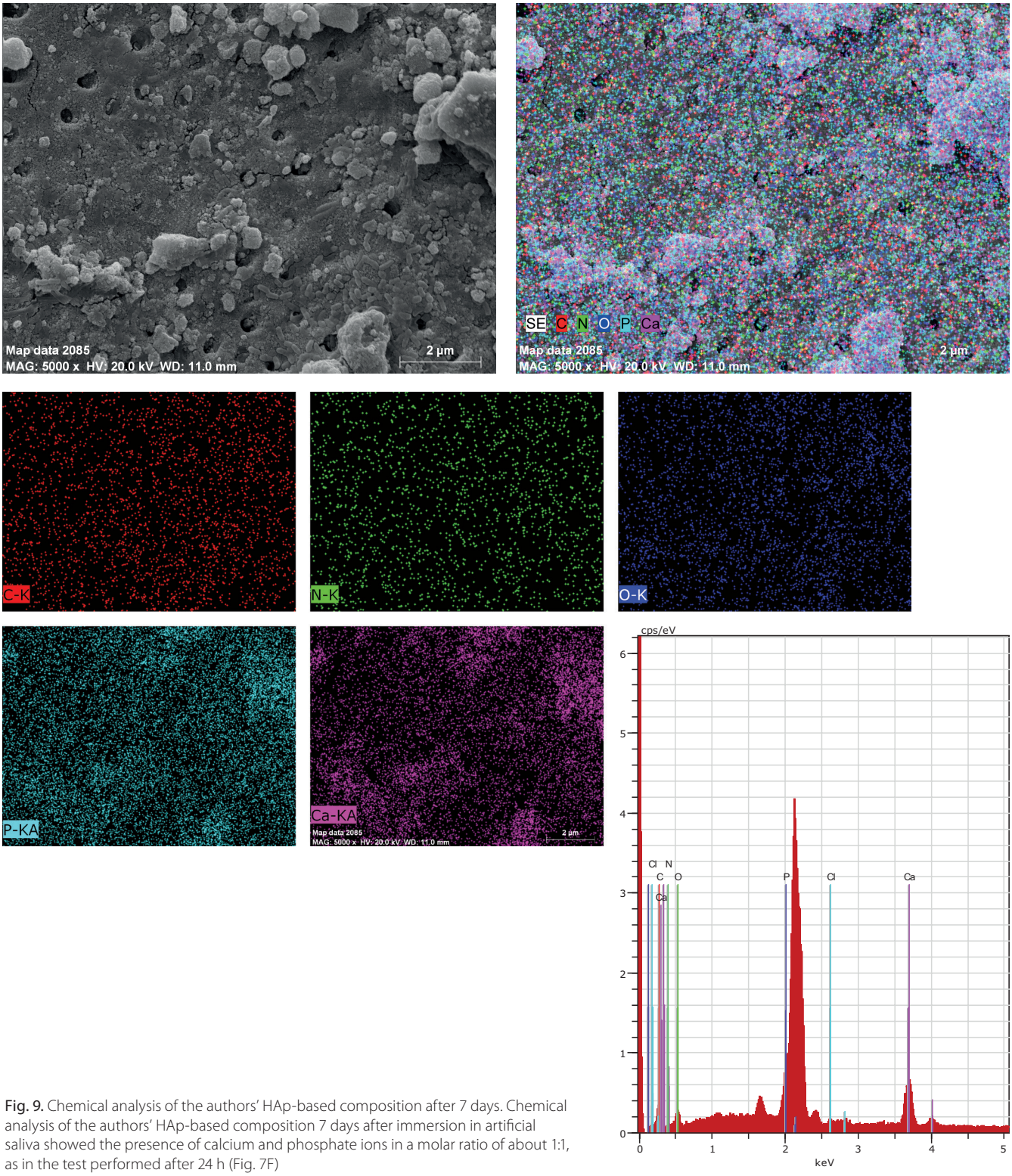

Fig. 9. Chemical analysis of the authors' HAp-based composition after 7 days. Chemical analysis of the authors' HAp-based composition 7 days after immersion in artificial saliva showed the presence of calcium and phosphate ions in a molar ratio of about 1:1, as in the test performed after 24 h (Fig. 7F)

crystals (0.2–0.3 µm) that successfully occlude dentinal tubules. Moreover, the layer formed seems to be durable, which has been proven by showing that both larger and smaller crystals were still present after rinsing for 24 h, 48 h and 7 days in the artificial saliva solution.

The aim of the analysis was to determine the ability to close open dentin tubules depending on the type of the desensitizer used and time elapsed since its application (Table 1). The analysis of the dynamics of the number of exposed dentinal tubules showed that Bifluorid®, in spite of achieving the best results immediately after application, is characterized by very dynamic degradation at subsequent stages of observation, indicating its moderate durability; Cervitec® showed good results immediately

after application and a very slow degradation rate at subsequent stages of observation, which indicates its good quality; the HAp-based composition, despite its initially limited effectiveness, was the only substance showing a gradation at successive time stages. In other words, its effectiveness only appeared after some time, when compounds were deposited on the surface of the tooth closing the tubules. Isodan® exhibited moderate efficacy when the 1st measurement was performed and significant (almost total) degradation with subsequent analyses. The HAp-based pharmaceutical composition consists of biocompatible and biodegradable chemical compounds that can be found in our bodies. Hence any products of its dissolution should be removed through natural metabolic processes. This composition did not change its properties during storage. These results allow us to draw very cautious conclusions that, in terms of the stability of the effects of the applied tubular obliteration technique, the best results can be obtained with the use of a hydroxyapatite-based formulation with apatite crystals sized ≤300 nm.

Conclusions

This in vitro study has shown that the use of hydroxyapatite particles <300 nm suspended in glycerol allows effective obliteration of dentinal tubules, which was shown in SEM images. It has been demonstrated that the use of a HAp-based agent with crystals smaller than 300 nm may occlude dentinal tubules, making it useful in the treatment and prevention of DH. In the given experimental conditions, the durability of the protective coating after applying the authors' own pharmaceutical composition was greater than all the other tested desensitizers.[47] This makes it an excellent alternative to pharmaceutical products based on fluoride, potassium nitrate or multi-component products, but further studies are required to confirm these findings.

ORCID iDs

Łukasz Rafał Pałka https://orcid.org/0000-0002-9365-7882
Zbigniew Rybak https://orcid.org/0000-0002-1906-6435
Piotr Kuropka https://orcid.org/0000-0002-0682-4743
Maria Krystyna Szymonowicz https://orcid.org/0000-0003-4251-6841
Jan Kiryk https://orcid.org/0000-0002-5442-1412
Krzysztof Marycz https://orcid.org/0000-0003-3676-796X
Maciej Dobrzyński https://orcid.org/0000-0003-2368-1534

References

1. Farooq I, Moheet IA, Al-Shwaimi E. In vitro dentin tubule occlusion and remineralization competence of various toothpastes. *Arch Oral Biol*. 2015;60(9):1246–1253. https://doi.org/10.1016/j.archoralbio.2015.05.012
2. Gillam DG. Current diagnosis of dentin hypersensitivity in the dental office: An overview. *Clin Oral Investig*. 2013;17(Suppl 1):S21–S29. https://doi.org/10.1007/s00784-012-0911-1
3. Saeki K, Marshall GW, Gansky SA, Parkinson CR, Marshall SJ. Strontium effects on root dentin tubule occlusion and nanomechanical properties. *Dent Mater*. 2016;32(2):240–251. https://doi.org/10.1016/j.dental.2015.11.020
4. Brännström M. Sensitivity of dentin. *Oral Surg Oral Med Oral Pathol*. 1966;21(4):517–526. https://doi.org/10.1016/0030-4220(66)90411-7
5. Brännström M, Garberoglio R. The dentinal tubules and the odontoblast processes: A scanning electron microscopic study. *Acta Odontol Scand*. 1972;30(3):291–311. https://doi.org/10.3109/00016357209004598
6. Cakar G, Kuru B, Ipci SD, Aksoy ZM, Okar I, Yilmaz S. Effect of Er:YAG and CO_2 lasers with and without sodium fluoride gel on dentinal tubules: A scanning electron microscope examination. *Photomed Laser Surg*. 2008;26(6):565–571. https://doi.org/10.1089/pho.2007.2211
7. Miglani S, Aggarwal V, Ahuja B. Dentin hypersensitivity: Recent trends in management. *J Conserv Dent*. 2010; 13(4):218–224. https://doi.org/10.4103/0972-0707.73385
8. Poulsen S, Errboe M, Lescay Mevil Y, Glenny AM. Potassium containing toothpastes for dentin hypersensitivity. *Cochrane Database Syst Rev*. 2006;2006(3):CD001476. https://doi.org/10.1002/14651858.CD001476.pub2
9. Pereira J, Sales-Peres S, Francisconi L, et al. Current and novel clinical approaches for the treatment of dentin hypersensitivity. In: Gilligan D, ed. *Dentin Hypersensitivity: Advances in Diagnosis, Management, and Treatment*. Cham, Switzerland: Springer International Publishing Switzerland; 2015:101–132.
10. Birang R, Poursamimi J, Gutknecht N, Lampert F, Mir M. Comparative evaluation of the effects of Nd:YAG and Er:YAG laser in dentin hypersensitivity treatment. *Lasers Med Sci*. 2007;22(1):21–24. https://doi.org/10.1007/s10103-006-0412-z
11. Shetty S, Kohad R, Yeltiwar R, Shetty K. Comparative evaluation of hydroxyapatite, potassium nitrate and sodium monofluorophosphate as in office desensitising agents: A double blinded randomized controlled clinical trial. *J Oral Hyg Health*. 2013;1:104. doi:10.4172/2332-0702.1000104
12. Low B, Allen EP, Kontogiorgos ED. Reduction in dental hypersensitivity with nano-hydroxyapatite, potassium nitrate, sodium monofluorophosphate and antioxidants. *Open Dent*. 2015;(9):92–97. doi:10.2174/1874364101509010092
13. Orchardson R, Gillam DG. The efficacy of potassium salts as agents for treating dentin hypersensitivity. *J Orofac Pain*. 2000;14(1):9–19.
14. Orchardson R, Gillam DG. Managing dentin hypersensitivity. *J Am Dent Assoc*. 2006;137(7):990–998, quiz 1028–1029. doi:10.14219/jada.archive.2006.0321
15. Peacock JM, Orchardson R. Effects of potassium ions on action potential conduction in A- and C-fibers of rat spinal nerves. *J Dent Res*. 1995;74(2):634–641. doi:10.1177/00220345950740020301
16. James JM, Puranik MP, Sowmya KR. Dentinal tubule occluding effect of potassium nitrate in varied forms, frequencies and duration: An in vitro SEM analysis. *J Clin Diagn Res*. 2017;11(8):ZC06–ZC08. doi:10.7860/JCDR/2017/26442.10340
17. Mahmoodi B, Wood RJK, Cook RB. Nanomechanical properties of hydroxyapatite like coatings formed by bioactive glasses, arginine and calcium silicate for dentin protection. *J Mech Behav Biomed Mater*. 2020;105:103702. doi:10.1016/j.jmbbm.2020.103702
18. Rosenthal MW. Historic review of the management of tooth hypersensitivity. *Dent Clin North Am*. 1990;34(3):403–427.
19. Yu J, Yang H, Li K, Lei J, Zhou L, Huang C. A novel application of nano-hydroxyapatite/mesoporous silica biocomposite on treating dentin hypersensitivity: An in vitro study. *J Dent*. 2016;50:21–29. doi:10.1016/j.jdent.2016.04.005
20. Hanni M, Hannig C. Nanomaterials in preventive dentistry. *Nat Nanotechnol*. 2010;5(8):565–569. doi:10.1038/nnano.2010.83
21. Ohta K, Kawamata H, Ishizaki T, Hayman R. Occlusion of dentinal tubules by nano-hydroxyapatite. *J Dent Res*. 2007;86(Spec Iss A): New Orleans Abstracts No. 1759.
22. Tschoppe P, Zandim DL, Martus P, Kielbassa AM. Enamel and dentin remineralization by nano-hydroxyapatite toothpastes. *J Dent*. 2011;39(6):430–437. doi:10.1016/j.jdent.2011.03.008
23. Al-Maliky MA, Mahmood AS, Al-Karadaghi TS, et al. The effects of CO_2 laser with or without nanohydroxyapatite paste in the occlusion of dentinal tubules. *ScientificWorldJournal*. 2014;2014:798732. https://doi.org/10.1155/2014/798732
24. Onwubu SC, Mhlungu S, Mdluli PS. In vitro evaluation of nanohydroxyapatite synthesized from eggshell waste in occluding dentin tubules. *J Appl Biomater Funct Mater*. 2019;17(2):2280800019851764. doi:10.1177/2280800019851764

25. Pajor K, Pajchel L, Kolmas J. Hydroxyapatite and fluorapatite in conservative dentistry and oral implantology: A review. *Materials (Basel)*. 2019;12(17):2683. doi:10.3390/ma12172683
26. Mordan NJ, Barber PM, Gillam DG. The dentine disc. A review of its applicability as a model for the in vitro testing of dentine hypersensitivity. *J Oral Rehabil*. 1997;24(2):148–156. doi:10.1046/j.1365-2842.1997.d01-260.x
27. Mordan NJ, Barber PM, Gillam DG. The dentin disc: A review of its applicability as a model for the in vitro testing of dentin hypersensitivity. *J Oral Rehabil*. 1997;24(2):148–156. https://doi.org/10.1046/j.1365-2842.1997.d01-260.x
28. Gillam DG, Mordan NJ, Newman HN. The dentin disc surface: A plausible model for dentin physiology and dentin sensitivity evaluation. *Adv Dent Res*. 1997;11(4):487–501. https://doi.org/10.1177/08959374970110041701
29. Ling TY, Gillam DG, Barber PM, Mordan NJ, Critchell J. An investigation of potential desensitizing agents in the dentin disc model: A scanning electron microscopy study. *J Oral Rehabil*. 1997;24(3):191–203. https://doi.org/10.1111/j.1365-2842.1997.tb00313.x
30. Nakamoto K. Infrared and Raman spectra of inorganic and coordination compounds. In: Chalmers JM, Griffiths PR, eds. *Handbook of Vibrational Spectroscopy*. Hoboken NJ: John Wiley & Sons; 2006. doi:10.1002/0470027320.s4104
31. Lodish HF, Berk A, Kaiser C, et al, eds. *Molecular Cell Biology*. London, UK: Palgrave Macmillan; 2008.
32. Suge T, Ishikawa K, Kawasaki A, Yoshiyama M, Asaoka K, Ebisu S. Effects of fluoride on the calcium phosphate precipitation method for dentinal tubule occlusion. *J Dent Res*. 1995;74(4):1079–1085. https://doi.org/10.1177/00220345950740040801
33. Markowitz K, Kim S. Hypersensitive teeth: Experimental studies of dentinal desensitizing agents. *Dent Clin North Am*. 1990;34(3):491–501.
34. McCormack K, Davies, R. The enigma of potassium ion in the management of dentin hypersensitivity: Is nitric oxide the elusive second messenger? *Pain*. 1998;68(1):5–11.
35. Suge T, Ishikawa K, Kawasaki A, et al. Calcium phosphate precipitation method for the treatment of dentin hypersensitivity. *Am J Dent*. 2002;15(4):220–226.
36. Thrash WJ, Jones DL, Dodds WJ. Effect of a fluoride solution on dentinal hypersensitivity. *Am J Dent*. 1992;5(6):299–302.
37. Ten Cate JM. In vitro studies on the effects of fluoride on de- and remineralization. *J Dent Res*. 1990;69(Spec No):614–619, discussion 634–636.
38. Bizhang M, Seemann R, Römhild G, et al. Effect of a 40% chlorhexidine varnish on demineralization of dentin surfaces in situ. *Am J Dent*. 2007;20(3):193–197.
39. Brailsford SR, Fiske J, Gilbert S, Clark D, Beighton D. The effects of the combination of chlorhexidine/thymol- and fluoride-containing varnishes on the severity of root caries lesions in frail institutionalised elderly people. *J Dent*. 2002;30(7–8):319–324.
40. Madruga MM, Silva AF, Rosa WL, Piva E, Lund RG. Evaluation of dentin hypersensitivity treatment with glass ionomer cements: A randomized clinical trial. *Braz Oral Res*. 2017;31:e3. doi:10.1590/1807-3107bor-2017.vol31.0003
41. Markowitz K. A new treatment alternative for sensitive teeth: A desensitizing oral rinse. *J Dent*. 2013;41(Suppl 1):S1–11. https://doi.org/10.1016/j.jdent.2012.09.007
42. Mader CL, Baumgartner JC, Peters DD. Scanning electron microscopic investigation of the smeared layer on root canal walls. *J Endod*. 1984;10(10):477–483. https://doi.org/10.1016/S0099-2399(84)80204-6
43. Kokkas AB, Boutsioukis ACh, Vassiliadis LP, Stavrianos CK. The influence of the smear layer on dentinal tubule penetration depth by three different root canal sealers: An in vitro study. *J Endod*. 2004;30(2):100–102. https://doi.org/10.1097/00004770-200402000-00009
44. Tay FR, Pashley DH. Guided tissue remineralisation of partially demineralised human dentin. *Biomaterials*. 2008;29(8):1127–1137. https://doi.org/10.1016/j.biomaterials.2007.11.001
45. Besinis A, van Noort R, Martin N. Infiltration of demineralized dentin with silica and hydroxyapatite nanoparticles. *Dent Mater*. 2012;28(9):1012–1023. https://doi.org/10.1016/j.dental.2012.05.007
46. Zhang X, Neoh KG, Lin CC, Kishen A. Remineralization of partially demineralized dentin substrate based on a biomimetic strategy. *J Mater Sci Mater Med*. 2012;23(3):733–742. https://doi.org/10.1007/s10856-012-4550-5
47. Pałka Ł. *Ocena porównawcza obliteracji kanalików zębinowych po zastosowaniu własnej kompozycji farmaceutycznej – badania in vitro* [doctoral dissertation]. Wroclaw Medical University, Poland; 2015.

New methods of differentiation between primary and secondary hypertension in a pediatric population: A single-center experience

Julia Rasała[1,B–D], Paweł Marschollek[1,B–D], Karol Marschollek[1,B–D], Anna Ciszewska[1,B–D], Danuta Zwolińska[2,E,F], Kinga Musiał[2,A,C–F]

[1] Student Scientific Association, Department of Pediatric Nephrology, Wroclaw Medical University, Poland
[2] Department of Pediatric Nephrology, Wroclaw Medical University, Poland

A – research concept and design; B – collection and/or assembly of data; C – data analysis and interpretation; D – writing the article; E – critical revision of the article; F – final approval of the article

Advances in Clinical and Experimental Medicine, ISSN 1899–5276 (print), ISSN 2451–2680 (online) *Adv Clin Exp Med*. 2020;29(11):1299–1304

Address for correspondence
Kinga Musiał
E-mail: kinga_musial@hotmail.com

Funding sources
None declared

Conflict of interest
None declared

Received on June 2, 2020
Reviewed on June 23, 2020
Accepted on September 9, 2020

Abstract

Background. Kidney diseases are the main causative factors of secondary hypertension (HTN) in children. Although primary HTN is less common in the pediatric population, its increasing prevalence, especially among teenagers, makes early diagnosis an emerging issue.

Objectives. To analyze the potential differences between primary HTN and HTN secondary to renal diseases, in order to tailor diagnostic procedures to pediatric patients with suspicion of HTN.

Material and methods. A retrospective evaluation was performed of medical records of 168 children (aged from 1 month to 18 years) diagnosed with arterial HTN in the Pediatric Nephrology Department of Wroclaw Medical University (Poland). The comparative analysis concerned demographics, causes of HTN, clinical picture, laboratory tests, and parameters of ambulatory blood pressure monitoring (ABPM).

Results. Out of 168 children, 47% were diagnosed with primary HTN and 53% with secondary renal HTN. The patients with primary HTN were significantly older than those with HTN secondary to renal disease. Among the children with primary HTN, 26% were overweight and 42% were obese; among those with renal HTN, the proportions were 16% and 19%, respectively. The patients with primary HTN had significantly higher body mass index (BMI) percentiles and z-scores, and tended toward higher pulse pressure (PP) values. In the group with secondary HTN, ABPM parameters of diastolic blood pressure (DBP) and total cholesterol were significantly elevated. The BMI z-scores correlated positively with PP in the whole group.

Conclusions. As expected, HTN secondary to renal disease prevails in younger children, but primary HTN has become an emerging issue in teenagers. The diagnostics of HTN secondary to kidney disease have revealed risk factors worsening the prognosis, including higher values of cholesterol or of parameters connected with DBP. Primary HTN risk factors include obesity and a tendency towards higher PP values.

Key words: obesity, teenagers, ambulatory blood pressure monitoring, mean arterial pressure, pulse pressure

Cite as
Rasała J, Marschollek P, Marschollek K, Ciszewska A, Zwolińska D, Musiał K. New methods of differentiation between primary and secondary hypertension in a pediatric population: A single-center experience. *Adv Clin Exp Med*. 2020;29(11):1299–1304. doi:10.17219/acem/127425

DOI
10.17219/acem/127425

Introduction

Hypertension (HTN) affects 3–5% of children.[1,2] Despite the increasing prevalence of primary HTN in teenagers, HTN secondary to other underlying disorders still prevails in the pediatric population.[3] Among causes of secondary HTN, renal diseases are predominant and responsible for faster disease progression, as well as clinically apparent complications appearing before adulthood.[4] Moreover, the occurrence of HTN in childhood is associated with high blood pressure (BP) in later life and early development of cardiovascular disease (CVD).[5,6] Thus, early diagnosis is of utmost importance in this age group.

In addition to routine procedures including demographic, laboratory and imaging data, new tools are being used to increase the efficiency of diagnostics and to establish a prognosis.

In particular, ambulatory blood pressure monitoring (ABPM) is recommended in children, as it ensures comprehensive observation during normal patient activity in both day- and nighttime periods.[7,8] This method ensures direct measurement of mean arterial pressure (MAP), which is reported to increase the sensitivity of mild HTN diagnoses in patients with borderline BP values.[9] Mean arterial pressure is also a predictor of hyperkinetic circulation, which can already be observed at the early stages of primary HTN.[10] Current guidelines emphasize the role of MAP in the monitoring of treatment effectiveness.[2] Another new tool, pulse pressure (PP), is an established predictor of target-organ damage in the course of HTN, especially in primary HTN.[11]

The aim of the study was to analyze the potential differences between primary HTN and HTN secondary to kidney disease, revealed in the course of diagnostic procedures including the clinical picture, laboratory test results and selected parameters assessed by ABPM.

Material and methods

We carried out a retrospective analysis of the medical records of 168 children, aged from 1 month to 18 years, diagnosed for arterial HTN in the Department of Pediatric Nephrology at Wroclaw Medical University (Poland). Basic demographic data are presented in Table 1.

Hypertension was diagnosed in children <16 years whose diastolic and/or systolic blood pressure (DBP and SBP) values, obtained during 3 independent measurements, were over the 95th percentile for their age, sex and height. In teenagers aged 16–18 years, the threshold value was ≥140/90 mm Hg.[12] In each child, the diagnosis of HTN was established by 3 independent oscillometric office BP measurements. Additionally, in children aged >5 years, ABPM was performed as a part of the diagnostic process.

The patients were diagnosed with primary HTN or HTN secondary to kidney disease according to the European Society of Hypertension guidelines.[13]

The patients were divided into 2 groups according to HTN etiology. The group diagnosed with primary HTN included 79 children, and the group with HTN secondary to renal disease comprised 89 patients. The data collected throughout the diagnostic process involved demographics, the type and cause of HTN, clinical manifestations, laboratory tests, and the results of selected ABPM measurements.

Body mass index (BMI) was assessed in both percentiles and z-scores established using the WHO AnthroPlus software (World Health Organization, Geneva, Switzerland). Patients with BMI equal to or lower than the 3rd percentile were qualified as underweight, those with BMI between the 85th and 95th as overweight, and those with BMI equal or greater than the 95th percentile were qualified as obese.

The ABPM was performed in 118 children >5 years (67 with primary and 51 with secondary HTN) using the Oscar 2 ambulatory blood pressure monitor (SunTech Medical Inc., Morrisville, USA) and interpreted in accordance with recommendations concerning ABPM in children and adolescents.[12,13] Each of the measurements was also divided into daytime (7:00–23:00) and nighttime (23:00–7:00) periods. When the number of measurements was insufficient (<14 in a daytime session and <7 at night), or less than 70% of the measures were interpretable, the results were excluded from the analysis. The median values of SBP and DBP, as well as their loads (percentage of measurements above the threshold) MAP and PP were assessed. If there was more than 1 ABPM examination for a single patient, the results from the time of diagnosis, before treatment introduction, was included in the analysis.

All procedures involving human treatment were performed in accordance with the Declaration of Helsinki and its further amendments. According to the rules and regulations of Wroclaw Medical University, the study did not require Ethics Committee approval. However, informed consent regarding the data collection and analysis was obtained from the parents and the patients over 16 years of age.

Statistical analysis

The results are presented as median values and interquartile ranges (IQRs) or percentages. The χ^2 test, Student's t-test and Pearson's correlation coefficient were used for normally distributed data, and non-parametric tests (Mann–Whitney U test and Spearman's correlation coefficient) were used for other variables. The p-values <0.05 were considered significant. The statistical analysis was performed with STATISTICA v. 13.0 software (StatSoft Inc., Tulsa, USA).

Results

Out of 168 patients, 79 were diagnosed with primary HTN (47%) and 89 (53%) with HTN secondary to renal disease. Basic clinical data concerning the study groups

are shown in Table 1. The patients with primary HTN were significantly older than the children with secondary renal HTN (Table 1). However, there was no age difference between patients with primary and renal secondary HTN when only children who had undergone ABPM were analyzed. Teenagers prevailed in the primary HTN group, whereas the secondary HTN group included comparable numbers of children below and above 11 years old (Table 1). There was no gender domination in either group, and boys' and girls' age was comparable in both groups. In children under 11 years old, secondary renal HTN was diagnosed in 86.5% of the cases; in teenagers primary HTN was the main diagnosis (62%). In the group with secondary renal HTN, congenital anomalies tended to prevail in older children and glomerulopathies in younger patients, but these differences did not reach statistical significance (Table 2).

Headache, the most frequent symptom related to HTN, was present in almost 1/3 of the children, significantly more often in the primary HTN group (Table 1) and in adolescents ($p < 0.001$).

Median values of BMI, BMI percentiles and BMI z-scores were significantly higher in patients with primary HTN. These patients were also more often obese (Table 1).

Serum lipid disorders showed a preponderance toward secondary HTN (Table 3), whereas serum sodium and total protein concentrations were higher in the primary HTN group than in the secondary HTN group.

The ABPM results revealed significantly higher DBP values and loads in the secondary HTN group in the 24-hour and nighttime periods, with a similar trend observed for the daytime period (Table 4).

In the whole study group, there was a relationship between BMI z-scores and median DBP values ($R = -0.3$; $p = 0.002$), as well as DBP loads ($R = -0.22$; $p = 0.03$). There was also a significant correlation between high-density lipoprotein (HDL) level and DBP values ($R = 0.24$, $p = 0.036$). However, in the subgroups (primary and secondary HTN), these correlations failed to reach statistical significance.

Among the children who had ABPM performed, MAP values in boys were significantly higher than in girls (60 mm Hg compared to 53 mm Hg; $p < 0.001$). There was a tendency towards higher PP values in children with primary HTN, but the difference did not reach statistical significance. We also observed a significant positive correlation between BMI z-scores and PP ($R = 0.21$; $p = 0.037$) in the whole study group.

Table 1. Basic patient characteristics

Parameter	Primary HTN (n = 79)		Secondary HTN (n = 89)		p-value
Median age [years]	15.7		10.7		<0.001*
Age distribution	<11 years	≥11 years	<11 years	≥11 years	<0.001**
	7 (8.9%)	72 (91.1%)	45 (50.6%)	44 (49.4%)	
Gender	boys	girls	boys	girls	0.93**
	44 (55.7%)	35 (44.3%)	49 (55.1%)	40 (44.9%)	
Height [cm]	165.3		137		<0.001*
Median BMI percentile	92.3		67.3		<0.001*
Median BMI z-score	1.43		0.45		<0.001*
Overweight	25%		16%		0.19**
Obesity	43%		19%		0.002**
Headaches	43%		18%		<0.001**

HTN – hypertension; BMI – body mass index; *Mann–Whitney U test; **χ^2 test.

Table 2. Specific causes of HTN secondary to renal disease (differences established with χ^2 test and optional Yates's correction)

Etiology of HTN secondary to renal disease	All patients with secondary renal HTN	Patients < 11 years	Patients ≥11 years	p-value
Congenital anomalies of kidneys and urinary tract (CAKUT)	37 (41.57%)	16 (35.56%)	21 (47.73%)	0.24
Glomerulopathies	32 (35.96%)	21 (46.67%)	13 (29.55%)	0.09
Polycystic kidney disease	11 (12.36%)	6 (13.33%)	5 (11.36%)	0.78
Hemolytic-uremic syndrome	4 (4.49%)	2 (4.44%)	2 (4.55%)	0.98
Renovascular HTN	3 (3.37%)	0 (0%)	3 (6.82%)	0.07
In total	89 (100%)	45 (100%)	44 (100%)	

HTN – hypertension.

Table 3. Basic laboratory test results (statistical significance assessed with Mann–Whitney U test)

Serum parameters (median value; interquartile range)	Primary HTN	Secondary HTN	p-value
Total cholesterol [mg/dL]	163.5 (143–190)	184.5 (158.5–219)	0.002
LDL cholesterol [mg/dL]	93.0 (73–113)	105.0 (84–131)	0.08
HDL cholesterol [mg/dL]	46.0 (40–54)	49.0 (44–66)	0.01
Triglycerides [mg/dL]	101.5 (76–133)	117.0 (80–195)	0.052
Creatinine [mg/dL]	0.86 (0.72–0.97)	0.83 (0.59–1.1)	0.55
Uric acid [mg/dL]	5.6 (4.5–6.5)	5.5 (4.2–6.6)	0.4
Potassium [mmol/L]	4.36 (4.1–4.6)	4.38 (4.2–4.7)	0.51
Sodium [mmol/L]	139.5 (138–141)	138.5 (136.5–140)	0.009
Total protein [g/dL]	7.4 (7.0–7.7)	6.9 (6.3–7.4)	<0.001

HTN – hypertension; LDL – low-density lipoprotein; HDL – high-density lipoprotein.

Table 4. Selected ABPM measurements in the 2 groups

ABPM parameter, median (IQR)	Primary HTN (n = 67)	Secondary HTN (n = 51)	p-value
24 h SBP [mm Hg]	132 (127–143)	137 (125–142)	0.57*
Daytime SBP [mm Hg]	134 (129–146)	138 (128–146)	0.62**
Nighttime SBP [mm Hg]	122 (115–132)	123 (118–131)	0.41*
24 h DBP [mm Hg]	74 (70–78)	77 (69–84)	0.02**
Daytime DBP [mm Hg]	76 (72–81)	79 (73–86)	0.06**
Nighttime DBP [mm Hg]	65 (59–70)	67.5 (64–74)	0.02**
24 h SBP load [%]	58 (35–82)	67 (42–85)	0.29**
Daytime SBP load [%]	57 (29–80)	64 (40–88)	0.23**
Nighttime SBP load [%]	63 (30–88)	67 (44.5–93.5)	0.13*
24 h DBP load [%]	32 (17–49)	48 (23–68)	0.028**
Daytime DBP load [%]	29 (13–45)	40 (16–67)	0.067**
Nighttime DBP load [%]	40 (22–63)	56 (33–82)	0.03**
24 h PP [mm Hg]	59 (53–65)	56 (50–62)	0.08**
24 h MAP [mm Hg]	94 (88–99)	96 (90–102)	0.07**

ABPM – ambulatory blood pressure monitoring; HTN – hypertension; BMI – body mass index; SBP – systolic blood pressure; DBP – diastolic blood pressure; PP – pulse pressure; MAP – mean arterial pressure; *independent t-test; **Mann–Whitney U test; IQR – interquartile range.

Discussion

In our study, the majority of adolescents (11 years or older) were diagnosed with primary HTN, whereas 86.5% of the children <11 years had secondary renal HTN, which is consistent with other observations.[14,15] These data suggest that a renal background should be suspected first in young children with elevated BP, whereas primary HTN is the more probable diagnosis in adolescents. However, almost 38% of the adolescents in our study were diagnosed with secondary HTN. Thus, as Litwin stressed,[4] the role of routine screening for secondary HTN in asymptomatic teenagers should not be underestimated.

The guidelines of the Polish Society of Pediatric Nephrology also emphasize the need for differentiation between primary and secondary HTN as soon as the diagnosis is made.[7] These recommendations indicate that younger age, higher BP and more intense clinical symptoms are factors suggesting secondary HTN.

The age discrepancy between primary and secondary renal HTN in our study group was most probably a consequence of the fact that 69% of the patients were teenagers. However, when the age distribution in the secondary HTN group was taken into account, teenagers still constituted a half of this group. This observation suggests that the diagnosis of HTN due to renal diseases was made rather late. Such a conclusion should evoke deep concern, especially in light of the fact that inborn anomalies are the major cause of renal HTN. Therefore, the issue of early wide screening of the pediatric population with abdominal ultrasound should be revisited. Likewise, the necessity (emphasized in the Polish Society of Pediatric Nephrology guidelines) of taking blood pressure measurements during every outpatient visit in every child over 3 years old should be kept firmly in mind.[7]

Headache was the only clinical symptom reported more often in patients with primary HTN than in those with secondary renal HTN. However, it was also more frequent in teenagers (38% compared to 9%), who constituted more than 90% of the patients with primary HTN. Thus, it should always be treated as an alarming sign, irrespective of the child's age.

In the study group, 68% of the children with primary HTN were overweight or obese. For secondary HTN, that percentage was significantly smaller, but still meaningful (35%). Our observation confirms the data reported by Skrzypczyk et al.[16] Thus, obesity may be among the most important features indicating HTN etiology. Indeed, the prevalence of obesity and its relationship with the increasing number of children diagnosed with HTN is now one of the biggest challenges in pediatrics.[17–19] To deal with this issue, new American BP percentile tables excluding children with overweight and obesity were introduced in 2017.[20]

Our analysis revealed that children with secondary HTN had higher rates of lipid profile elements, although no correlation to BP values was found. However, Garí-Llanes et al. showed a significant positive correlation between serum lipid profiles and BP values that was already present at the pre-HTN stage.[21] Future analyses involving a more representative group may show similar relationships.

Ambulatory blood pressure monitoring has recently emerged as a method of choice in diagnosing and monitoring HTN in the pediatric population.[22] The Clinical Practice Guidelines developed by the American Academy of Pediatrics emphasize the role of ABPM in confirming diagnoses, detecting and excluding masked and white-coat HTN, and assessing therapeutic results in children.[23] The ABPM has also been reported to be a useful tool to differentiate between primary and secondary HTN.[24]

In our study, among the children who underwent ABPM, DBP values and loads were significantly higher in children with secondary HTN during the 24-hour and nighttime periods. A similar trend was noticed for the daytime, but it did not reach statistical significance. These results were confirmatory of our previous analysis involving a smaller group of patients.[25] Flynn et al. reported similar results, although in secondary HTN greater loads were also observed in nocturnal SBP measurements.[24] Another study on a cohort of untreated HTN patients showed higher nighttime loads.[26] Undoubtedly, differences in nighttime loads may make ABPM an important tool in early suspicion of secondary HTN, as this is the reference method of monitoring BP at night.

Our patients' BMI z-scores were negatively correlated with mean DBP values and loads. Although this correlation disappeared when the subgroups of primary and secondary HTN were analyzed separately, high BMI remains an important marker suggesting primary HTN.

In our research, based on APBM results, PP values did not differ significantly between patients with primary and secondary HTN. When PP values from office BP records were analyzed for the whole study group, those in the primary HTN subgroup were significantly higher than in the secondary HTN subgroup ($p < 0.02$). However, some patients showed significant differences between PP values calculated from office and ABPM measurements, so this method-related bias requires further verification. Pulse pressure and MAP are non-invasive BP parameters obtained from ABPM. The significance of PP has increased in recent years, as it has turned out to be a prognostic factor of HTN in currently normotensive patients, and of a target-organ damage in the course of HTN, both in children and adults.[27–29] Our observation is convergent with the reported role of PP as a marker of arterial stiffness in essential HTN.[30] Moreover, the values of PP in boys were significantly higher than those in girls, which requires confirmation on a larger group of patients. The positive correlation between BMI z-scores and PP values found in our entire HTN group was similar to results of Chandramohan et al., who revealed a statistically significant association between wide PP and high waist circumference in a large cohort of children ($n = 4667$).[31]

The potential strength of MAP values gained from ABPM comes from the fact that the oscillometric technique measures MAP directly. MAP has been shown to be a predictor of cardiovascular mortality in adults.[32] In our group of patients, MAP revealed no differences in terms of the type of HTN, age or gender. However, the usefulness of this parameter in diagnosing and differentiating the type of HTN in the pediatric population remains unknown and requires further investigation.

This study confirms the worldwide tendency toward the increasing occurrence of primary HTN among teenagers, as well as its close connection with the obesity epidemic. We have also upheld the growing importance of ABPM, both due to the efficient diagnostics of nighttime BP elevation and the potential prognostic value of PP. The need for earlier diagnostics of renal HTN should be given high priority.

Our study has limitations. Apart from age-related bias, it did not take into account all the possible reasons for secondary HTN. However, it did analyze renal causes in detail. This research should be continued in order to draw more reliable conclusions, especially in the promising area of ABPM measurements.

Conclusions

According to previous international observations, primary HTN has become an emerging issue in teenagers, whereas in younger children HTN secondary to renal disease still prevails. Primary HTN has shown a higher occurrence of obesity and a tendency towards higher values of PP, both of which may potentially facilitate diagnosis. Risk factors worsening the prognosis in HTN secondary to kidney disease include higher values of cholesterol or parameters connected with DBP.

ORCID iDs

Julia Rasała https://orcid.org/0000-0002-0856-448X
Paweł Marschollek https://orcid.org/0000-0003-4588-309X
Karol Marschollek https://orcid.org/0000-0001-9093-180X
Anna Ciszewska https://orcid.org/0000-0001-9039-8638
Danuta Zwolińska https://orcid.org/0000-0002-6714-3992
Kinga Musiał https://orcid.org/0000-0002-9000-7585

References

1. McNiece KL, Poffenbarger TS, Turner JL, Franco KD, Sorof JM, Portman RJ. Prevalence of hypertension and pre-hypertension among adolescents. *J Pediatr*. 2007;150(6):640–644.
2. Litwin M, Niemirska A, Obrycki Ł, et al. Guidelines of the Pediatric Section of the Polish Society of Hypertension on diagnosis and treatment of arterial hypertension in children and adolescents. *Arterial Hypertens*. 2018;22(2):45–73. doi:10.5603/AH.2018.0007
3. Muntner P, He J, Cutler JA, Wildman RP, Whelton PK. Trends in blood pressure among children and adolescents. *JAMA*. 2004;291(17): 2107–2113.
4. Litwin M. Why should we screen for arterial hypertension in children and adolescents? *Pediatr Nephrol*. 2018;33(1):83–92. doi:10.1007/s00467-017-3739-8
5. MacMahon S, Peto R, Cutler J, et al. Blood pressure, stroke, and coronary heart disease. Part 1: Prolonged differences in blood pressure: Prospective observational studies corrected for the regression dilution bias. *Lancet*. 1990;335(8692):765–774.
6. Bao W, Threefoot SA, Srinivasan SR, Berenson GS. Essential hypertension predicted by tracking of elevated blood pressure from childhood to adulthood: The Bogalusa Heart Study. *Am J Hypertens*. 1995; 8(7):657–665.
7. Żurowska A, Zwolińska D, Roszkowska-Blaim M, et al. Rekomendacje Polskiego Towarzystwa Nefrologii Dziecięcej (PTNFD) dotyczące postępowania z dzieckiem z podwyższonym ciśnieniem tętniczym. *Forum Med Rodz*. 2015;9(5):349–375.
8. Flynn JT, Daniels SR, Hayman LL, et al; on behalf of the American Heart Association Atherosclerosis, Hypertension and Obesity in Youth Committee of the Council on Cardiovascular Disease in the Young. Update: Ambulatory blood pressure monitoring in children and adolescents. A scientific statement from the American Heart Association. *Hypertension*. 2014;63(5):1116–1135.
9. Suláková T, Feber J. Should mean arterial pressure be included in the definition of ambulatory hypertension in children? *Pediatr Nephrol*. 2013;28(7):1105–1112.
10. Niemirska A, Obrycki Ł, Wojciechowska E, Litwin M. Haemodynamic patterns in children with primary hypertension: Preliminary brief report. *Arterial Hypertens*. 2014;18(4):204–210.
11. Litwin M, Niemirska A, Sladowska J, et al. Left ventricular hypertrophy and arterial wall thickening in children with essential hypertension. *Pediatr Nephrol*. 2006;21(6):811–819.
12. Tykarski A, Filipiak KJ, Januszewicz A, et al. 2019 Guidelines for the management of hypertension: Part 8–9. *Arterial Hypertens*. 2019;23(4): 203–239. doi:10.5603/AH.a2019.0021
13. Lurbe E, Agabiti-Rosei E, Cruickshank JK, et al. 2016 European Society of Hypertension guidelines for the management of high blood pressure in children and adolescents. *J Hypertension*. 2016;34(10): 1887–1920. doi:10.1097/HJH.0000000000001039
14. Gupta-Malhotra M, Banker A, Shete S, et al. Essential hypertension vs secondary hypertension among children. *Am J Hypertens*. 2015;28(1): 73–80. doi:10.1093/AJH/HPU083
15. Chrysaidou K, Chainoglou A, Karava V, Dotis J, Printza N, Stabouli S. Secondary hypertension in children and adolescents: Novel insights. *Curr Hypertens Rev*. 2020;16(1):37–44. doi:10.2174/1573402115666190416152820
16. Skrzypczyk P, Pańczyk-Tomaszewska M, Roszkowska-Blaim M. 24-godzinny pomiar ciśnienia tętniczego u dzieci z nadciśnieniem tętniczym pierwotnym i wtórnym do miąższowych chorób nerek. *Med Og Nauk Zdr*. 2013;19(1):49–54.
17. Savino A, Pelliccia P, Giannini C, et al. Implications for kidney disease in obese children and adolescents. *Pediatr Nephrol*. 2011;26(5):749–758. doi:10.1007/S00467-010-1659-Y
18. Natsis M, Antza C, Doundoulakis I, Stabouli S, Kotsis V. Hypertension in obesity: Novel insights. *Curr Hypertens Rev*. 2020;16(1):30–36. doi:10.2174/1573402115666190415154603
19. Wühl E. Hypertension in childhood obesity. *Acta Paediatr*. 2019;108(1): 37–43. doi:10.1111/APA.14551
20. Flynn JT, Falkner BE. New clinical practice guideline for the management of high blood pressure in children and adolescents. *Hypertension*. 2017;70(4):683–686.
21. Garí-Llanes M, García-Nóbrega Y, Chávez-González E, González-Rodríguez E, García-Sáez J, Del Carmen Llanes-Camacho M. Biochemical markers and hypertension in children. *MEDICC Rev*. 2019;21(2–3): 10–15.
22. Andrade H, Pires A, Noronha N, et al. Importance of ambulatory blood pressure monitoring in the diagnosis and prognosis of pediatric hypertension. *Rev Port Cardiol*. 2018;37(9):783–789. doi:10.1016/J.REPCE.2018.08.005
23. Khoury M, Madsen N. Screening and management of high blood pressure in children and adolescents. *JAMA Pediatr*. 2018;172(11): 1087–1088. doi:10.1001/JAMAPEDIATRICS.2018.2882
24. Flynn JT. Differentiation between primary and secondary hypertension in children using ambulatory blood pressure monitoring. *Pediatrics*. 2002;110(1 Pt 1):89–93. doi:10.1542/PEDS.110.1.89
25. Marschollek P, Marschollek K, Rasała J, Ciszewska A, Zwolińska D, Musiał K. Differences between primary and secondary hypertension in children based on ambulatory blood pressure monitoring. *Przegl Lek*. 2019;76(5):232–236.
26. Seeman T, Palyzová D, Dušek J, Janda J. Reduced nocturnal blood pressure dip and sustained nighttime hypertension are specific markers of secondary hypertension. *J Pediatr*. 2005;147(3):366–371. doi:10.1016/J.JPEDS.2005.04.042
27. Zachariah JP, Graham DA, de Ferranti SD, Vasan RS, Newburger JW, Mitchell GF. Temporal trends in pulse pressure and mean arterial pressure during the rise of pediatric obesity in US children. *J Am Heart Assoc*. 2014;3(3):1–10.
28. Eguchi K, Matsui Y, Shibasaki S, et al; Japan Morning Surge-1 (JMS-1) Study Group. Age-specific impact of self-monitored pulse pressure on hypertensive target organ damage in treated hypertensive patients. *J Clin Hypertens (Greenwich)*. 2007;9(7):522–529. doi:10.1111/j.1524-6175.2007.06672.x
29. Olesen TB, Stidsen JV, Blicher MK, et al. Impact of age and target-organ damage on prognostic value of 24-hour ambulatory blood pressure. *Hypertension*. 2017;70(5):1034–1041. doi:10.1161/HYPERTENSIONAHA.117.09173
30. Litwin M, Obrycki Ł, Niemirska A, Sarnecki J, Kułaga Z. Central systolic blood pressure and central pulse pressure predict left ventricular hypertrophy in hypertensive children. *Pediatr Nephrol*. 2019;34(4): 703–712.
31. Chandramohan G, Kalantar-Zadeh K, Kermah D, Go SCM, Vaziri ND, Norris KC. Relationship between obesity and pulse pressure in children: Results of the National Health and Nutrition Survey (NHANES) 1988–1994. *J Am Soc Hypertens*. 2012;6(4):277–283. doi:10.1016/J.JASH.2012.05.002
32. Strandberg TE, Salomaa VV, Vanhanen HT, Pitkälä K, Miettinen TA. Isolated diastolic hypertension, pulse pressure, and mean arterial pressure as predictors of mortality during a follow-up of up to 32 years. *J Hypertens*. 2002;20(3):399–404. doi:10.1097/00004872-200203000-00014

Multicenter experiences with levosimendan therapy and its safety in patients with decompensated advanced heart failure

Małgorzata Lelonek[1,A–F], Iwona Stopczyńska[2,B,F], Ewa Korościk[3,B,D,F], Ewa Straburzyńska-Migaj[3,A–C,E,F], Marcin Gruchała[2,A,C,E,F]

[1] Department of Noninvasive Cardiology, Medical University of Lodz, Poland
[2] 1st Department of Cardiology, Medical University of Gdańsk, Poland
[3] 1st Department of Cardiology, Poznan University of Medical Sciences, Poland

A – research concept and design; B – collection and/or assembly of data; C – data analysis and interpretation;
D – writing the article; E – critical revision of the article; F – final approval of the article

Advances in Clinical and Experimental Medicine, ISSN 1899–5276 (print), ISSN 2451–2680 (online) *Adv Clin Exp Med*. 2020;29(11):1305–1312

Address for correspondence
Malgorzata Lelonek
E-mail: malgorzata.lelonek@umed.lodz.pl

Funding sources
None declared

Conflict of interest
I. Stopczyńska – Orion Pharma Poland travel grants
M. Gruchała – Orion Pharma Poland research and travel grants
E. Straburzyńska-Migaj – Orion Pharma Poland travel grants and lecture honoraria
M. Lelonek – no conflict of interest

Acknowledgements
Authors would like to thank Andrzej Bissinger for his assistance in preparing the draft of this article.

Received on April 14, 2020
Reviewed on July 1, 2020
Accepted on August 11, 2020

Cite as
Lelonek M, Stopczyńska I, Korościk E, Straburzyńska-Migaj E, Gruchała M. Multicenter experiences with levosimendan therapy and its safety in patients with decompensated advanced heart failure. *Adv Clin Exp Med*. 2020;29(11):1305–1312. doi:10.17219/acem/126301

DOI
10.17219/acem/126301

Abstract

Background. Advanced heart failure (AdvHF) is associated with high morbidity and mortality. Patients with this clinical condition are potential candidates for heart transplantation or mechanical circulatory support. Initially, however, they are usually supported with inotropic drugs. Recent studies have suggested that levosimendan, independently of hemodynamic improvements, may lead to outcome benefits.

Objectives. To present clinical experiences concerning the indications, effectiveness, tolerance, and safety of levosimendan in the real-life therapy of patients with decompensated AdvHF in 3 cardiac centers in Poland.

Material and methods. This is a prospective, observational, three-center study. Forty-nine patients with AdvHF admitted with decompensation were included (88% men, mean age 58 years, 65% ischemic etiology, left ventricular ejection fraction (LVEF) in median 20%) and followed up for an early (3 months) and prolonged period (1 year) after infusion of levosimendan. Patients were analyzed in relation to death.

Results. Levosimendan therapy was associated with reduced HF symptoms and signs, New York Heart Association (NYHA) class and level of B-type natriuretic peptide (BNP) at discharge. Five patients died during hospitalization, a further 10 during the three-month follow-up and 3 died during the next nine-month follow-up. During the three-month follow-up, 22 patients were re-hospitalized due to HF and in the next nine-month follow-up 8 were re-hospitalized. A multivariate analysis indicated the QRS duration at discharge (hazard ratio (HR) = 1.02; 95% confidence interval (95% CI) = 1.003–1.03; p = 0.018), high-sensitivity C-reactive protein (hsCRP) (HR = 1.01; 95% CI = 1.004–1.02; p = 0.002), and simultaneous dobutamine infusion (HR = 6.54; 95% CI = 1.4–30.5; p = 0.017) were independent risk factors for death in the one-year follow-up. There were no side effects leading to the interruption of the levosimendan infusion.

Conclusions. The use of levosimendan was safe and associated with clinical improvement and reduction in BNP level in AdvHF patients hospitalized due to HF decompensation, although the mortality and re-hospitalization rate during the one-year follow-up remains high.

Key words: prognosis, levosimendan, advanced heart failure

Introduction

Patients with advanced heart failure (AdvHF), which is associated with poor prognosis, comprise an estimated 1% to 10% of the overall heart failure (HF) population and this number is still increasing.[1,2] In acute HF, the estimated in-hospital mortality is 2–17%, a high 30-day mortality of 6.5%, and one-year mortality of up to 45%.[3] On the other hand, the implementation of evidence-based therapies in chronic HF, which improved outcomes,[2] showed improvement in the advanced stage of the disease. Therefore, a growing proportion of patients with AdvHF often need mechanical circulatory support, heart transplantation or palliative care.[1–4] The pharmacotherapy in AdvHF is insignificant. Recent innovative drugs in acute HF reported no evidence of benefit on outcomes.[5] Therapy with classical inotropes, such as dobutamine and milrinone, is able to temporary improve hemodynamic and reduce symptoms, but long-term prognosis of patients with AdvHF remains unfavorable.[1,2,4,6] In the last (2016) HF guidelines, infusion of classical inotropic agents is limited to patients with signs of hypotension and/or hypoperfusion despite adequate filling status to increase cardiac output, vital organ perfusion and blood pressure (Class IIb).[2] Additional pharmacological options that improve prognosis are still desirable. One such option is levosimendan, a calcium sensitizer. Its inotropic effect is dependent on changes in troponin C conformation during systole, leading to sensitization of the contractile apparatus to calcium ions. Levosimendan also has vasodilator effect related to the activation of ATP-dependent potassium channels.[7,8] There are data and meta-analyses indicating significant benefits from levosimendan therapy in acute HF and AdvHF.[9–16] However, due to high costs and limited access to the therapy, clinical experience with levosimendan is still limited in many countries including Poland. The real-life use of levosimendan remains restricted to high-expertise AdvHF centers in Poland.

Therefore, the aim of this study is to present the clinical experiences concerning the real-life clinical indications, effectiveness, tolerance, and safety of levosimendan in the therapy of patients with AdvHF.

Material and methods

This prospective, observational multicenter study was conducted between August 2015 and December 2018 at 3 clinical centers in Poland (Gdańsk, Łódź and Poznań) specializing in HF management. Eligible patients were admitted to hospital with decompensation of AdvHF (New Yotk Heart Association (NYHA) class IV and/or signs of congestion) with reduced left ventricular ejection fraction (LVEF) diagnosed at least 3 months before admission and receiving individually optimized HF therapy in accordance with treatment guidelines,[2] which constituted the inclusion criteria. Advanced HF was recognized according to the updated definition published in 2018.[1]

All 49 included patients received infusion of levosimendan. Mean cumulative drug dose per patient was 12.5 ±4.7 mg. Twenty-two patients (45%) were treated with simultaneous dobutamine infusion. Median hospitalization duration was 22 days (interquartile range (IQR)) 10–32).

All patients had routinely measured laboratory tests and echocardiograms.

The follow-up after infusion was in early (3 months) and prolonged (1 year) period. The study was approved by the local Ethics Committees (approval No. RNN/231/19/KE, KE/335/20). The paper includes an analysis of the levosimendan safety and tolerability profile and the prognosis (death, hospitalization due to HF).

Statistical analysis

Quantitative variables are described with mean and standard deviation (SD), or for non-normally distributed variables the median and IQR. Normality of the variables was verified using the Shapiro–Wilk normality test. For categorical variables, the number of observations (N) with the corresponding percentage (%) is given. To compare 2 independent groups, Student's t-test for continuous variables with normal distribution or the non-parametric Mann–Whitney U test for non-normally distributed variables was used.

For qualitative variables, Pearson's χ^2 test, ML χ^2 test or χ^2 test with Yates's correction was applied (regarding the expected counts in the contingency tables). Variables significant in univariate comparisons at $p < 0.10$ were included in the multivariate stepwise Cox proportional hazards model to determine the independent risk factors of death. The Kaplan–Meier survival curve was also determined.

Missing data were imputed using the missForest algorithm (a multiple imputation procedure). In multivariate analysis, the results were considered statistically significant at $p < 0.05$.

To compare 2 dependent groups (i.e., before and after the treatment), the nonparametric Wilcoxon signed-rank test (for quantitative variables) and the McNemar–Bowker test with correction for continuity (for categorical variables) were used.

All the calculations were performed using the statistical packages STATISTICA PL v. 13.3 (StatSoft Inc., Tulsa, USA) and the R environment (the "missForest" package; www.r-project.org).

Results

Data of 49 patients (43 men, 88%) with median age 58 (IQR = 43–63) years were analyzed. In the majority of patients, ischemic cardiomyopathy was the cause of HF

Table 1. Baseline demographic, clinical presentation and laboratory parameters

Variable	Mean ±SD or median (IQR)
Age [years]	58 (43–63)
BMI [kg/m^2]	28.1 ±5.4
Number of HF hospitalizations within the last 12 months, N	2 (1–3)
HR [bpm]	82 (76–95)
QRS [ms]	132 (106–159)
BNP [pg/mL]	1838 (823–3271)
Hs-TnT [µg/L]	0.03 (0.02–0.07)
RDW [%]	16 (14.6–17.0)
Ferritin [g/L]	125 (68–254)
Transferrin saturation [%]	11.8 (8.8–20.0)
Serum sodium [mmol/L]	137 (134–139)
Serum potassium [mmol/L]	4.20 (3.7–4.5)
Creatinine [mmol/L]	115 (90–139)
eGFR (MDRD) [mL/min/1.73 m^2]	58.5 (40.1–83.0)
hsCRP [mg/L]	9.1 (4.2–13.4)
Total cholesterol [mmol/L]	3.46 ±1.18
LDL cholesterol [mmol/L]	2.09 ±0.94
HDL cholesterol [mmol/L]	0.85 (0.59–1.14)
Triglycerides [mmol/L]	0.93 (0.74–1.39)
Total bilirubin [µmol/L]	26.93 (18.5–44.5)
AST [IU/L]	39 (29–55)
ALT [IU/L]	30 (22–49)
6MWT [m]	235 ±48.9

Data is presented as mean (standard deviation – SD) or median and interquartile range (IQR) related to normal or non-normal distribution. BMI – body mass index; DBP – diastolic blood pressure; eGFR – estimated glomerular filtration rate; hsCRP – high-sensitivity C-reactive protein; hs-TnT – high-sensitivity troponin-T; HR – heart rate; MDRD – modification of diet in renal disease; BNP – B-type natriuretic peptide; NT-pro-BNP – N-terminal-pro B-type natriuretic peptide; RDW – red blood cell distribution width; SBP – systolic blood pressure; LDL – low-density lipoprotein; HDL – high-density lipoprotein; AST – aspartate transaminase; ALT – alanine transaminase; 6MWT – 6-minute walk test

Table 2. Etiology, history of HF at admission, concomitant diseases and treatment

Parameter	N (%)
Etiology	
Ischemic	32 (65)
Non-ischemic	17 (35)
Duration of HF	
<1 year	7 (14)
1–5 years	12 (24)
>5 years	30 (62)
Atrial fibrillation at admission	30 (67)
LBBB	10 (20)
RBBB	5 (10)
ICD	8 (16)
CRT-D	4 (8)
Concomitant diseases	
Hypertension	21 (43)
Renal failure	18 (37)
Diabetes mellitus	17 (35)
History of stroke/TIA	7 (14)
History of pulmonary embolism	3 (6)
Chronic obstructive lung disease	1 (2)
Pharmacotherapy	
ACEI/ARB	25 (51)
β-blocker	47 (96)
MRA	48 (98)
Diuretic	47 (96)
Ivabradine	7 (14)
ARNI	10 (20)
Digoxin	6 (12)

ACEI – angiotensin-converting-enzyme inhibitors; ARB – angiotensin II receptor blockers; ARNI – angiotensin receptor-neprilysin inhibitors; CRT-D – cardiac resynchronization therapy defibrillator; ICD – implantable cardioverter defibrillator; LBBB – left bundle branch block; MRA – mineralocorticoid receptor antagonists; RBBB – right bundle branch block; TIA – transient ischemic attack; HF – heart failure.

(Table 2) and left ventricular ejection fraction (LVEF) was in median 20% (Table 3) with enlargement of left ventricle, dysfunction of right ventricle (measured by tricuspid annular plane systolic excursion – TAPSE) with high probability of pulmonary hypertension (SPAP – systolic pulmonary arterial pressure – estimated from tricuspid regurgitation flow – Table 3) and concomitant functional mitral regurgitation (FMR; 44 patients, 90%). At admission, systolic blood pressure (SBP) was 107 mm Hg (IQR = 97–115 mm Hg), while diastolic blood pressure (DBP) was 70 mm Hg (IQR = 60–77 mm Hg). The level of B-type natriuretic peptide (BNP) was 1838 pg/mL (IQR = 823–3271 pg/mL).

Baseline demographics, laboratory parameters and clinical presentation are shown in Tables 1 and 2, echocardiographic data in Table 3.

At discharge, a significant reduction in HF symptoms and signs was observed (Fig. 1). At admission, 24 (49%) patients had NYHA class IV, while at discharge only 5/44 (11%) patients had class IV. Also, BNP concentration was significantly reduced from 1838 pg/mL (IQR = 823–3271 pg/mL) at admission to 1654 pg/mL (IQR = 1001–2706 pg/mL) at discharge (p = 0.018).

Five (10%) patients died during hospitalization due to worsening HF, but not during the infusion of levosimendan. During the three-month follow-up, 22 of 44 patients (50%) were re-hospitalized for decompensation of HF, and 10 (23%) patients died. The next 3 patients died during the following nine-month observation period and 8 were hospitalized due to HF. During the hospitalization with levosimendan, 5 patients received left ventricular assist device (LVAD) implantation at 18.2 ±18.9 days, and 2 patients

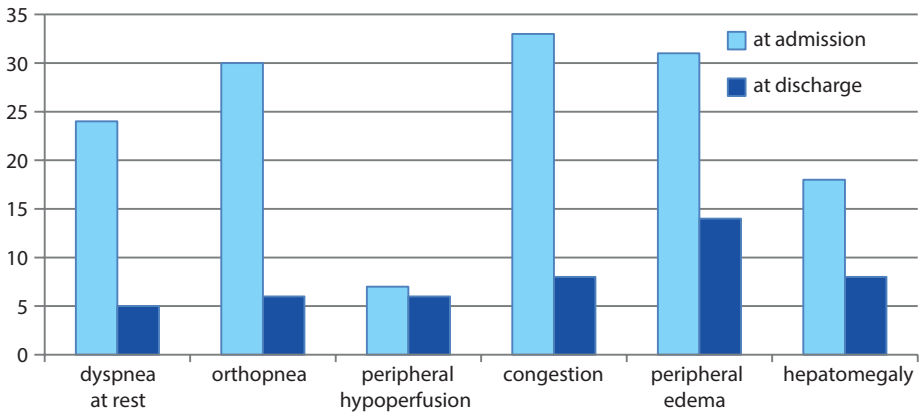

Fig. 1. Clinical improvement in N patients – all $p < 0.05$ apart from peripheral hypoperfusion and hepatomegaly

Table 3. Echocardiographic data at admission

Parameter	Mean ±SD or median (IQR)
LVEF [%]	20 (15–26)
TAPSE [mm]	13 (11–15)
LVEDd [mm]	71 ±9.9
LVESd [mm]	61.5 (56.0–67.5)
LVEDV [mL]	252 (205–286)
LVESV [mL]	188 (170–240)
VCI [mm]	24.44 ±6.08
SPAP [mm Hg]	51.74 ±16.10
FMR-VC [mm]	5.94 ±1.88
LAVi [mL/m^2]	42 (31.0–61.5)

Data is presented as mean (standard deviation – SD) or median and interquartile range (IQR) related to normal or non-normal distribution. FMR-VC – functional mitral regurgitation – vena contracta; LVEDd – left ventricular end-diastolic diameter; LAVi – left atrial volume index; LVEDV – left ventricular end-diastolic volume; LVEF – left ventricular ejection fraction; LVESV – left ventricular end-systolic volume; LVESd – left ventricular end-systolic diameter; SPAP – systolic pulmonary artery pressure; TAPSE – tricuspid annulus peak systolic excursion; VCI – vena cava inferior.

had heart transplantation at 45 and 97 days after being treated with levosimendan use, respectively.

From univariate analysis, longer levosimendan infusion ($p = 0.045$), lower minimum systolic ($p = 0.027$) and diastolic ($p = 0.05$) BP during infusion, QRS duration at discharge ($p = 0.06$), and higher high-sensitivity C-reactive protein (hsCRP) ($p = 0.0001$) were associated with death. The differences between analyzed groups related to death from all collected data are presented in Table 4.

Finally, Cox proportional hazards model revealed independent variables for death: QRS duration at discharge (hazard ratio (HR) = 1.02; 95% confidence interval (95% CI) = 1.003–1.03; $p = 0.018$), hsCRP (HR = 1.01; 95% CI = 1.004–1.02; $p = 0.002$) and simultaneous dobutamine infusion (HR = 6.54; 95% CI = 1.4–30.5; $p = 0.017$).

The Kaplan–Meier survival curve is presented in Fig. 2. The probability of survival during the 1st year was at 69%.

Safety and tolerability

Levosimendan infusions were associated with a mean reduction of SBP by –13.31 mm Hg and DBP by –9.64 mm Hg. Due to hypotension, 22 (45%) patients received simultaneous dobutamine infusion and/or a slower levosimendan infusion rate without interruption. There were no episodes of symptomatic hypotension. The other observed potential side effects were ventricular extrasystoles (31%), atrial fibrillation (7%), supraventricular tachycardia (3%), and non-sustained ventricular tachycardia (12%).

Table 4. From all analyzed variables statistical important differences between the studied groups

Parameter	Died (n = 18)	Survived (n = 31)	p-value
	mean ±SD or median (IQR)	mean ±SD or median (IQR)	
QRS duration at discharge [ms]	150 ±50	128 ±22.3	0.0595
hsCRP [mg/L]	34.3 (17–157)	7.6 (3.7–15.5)	0.0001
RDW [%]	17.8 (16.1–22.8)	16.1 (14.6–17)	0.0071
Total bilirubin [µmol/L]	76.95 (39.3–90.6)	22.91 (15.6–33.3)	0.0047
Minimum SBP during infusion [mm Hg]	86.07 ±11.95	95.24 ±12.43	0.0269
Minimum DBP during infusion [mm Hg]	52.93 ±9.4	58.41 ±9.03	0.0495
Duration of infusion [h]	30 (25–30)	25 (23–27)	0.0451
Dobutamine infusion [%]	16 (87)	10 (31)	0.0015

DBP – diastolic blood pressure; hsCRP – high-sensitivity C-reactive protein; SBP – systolic blood pressure; SD – standard deviation; IQR – interquartile range.

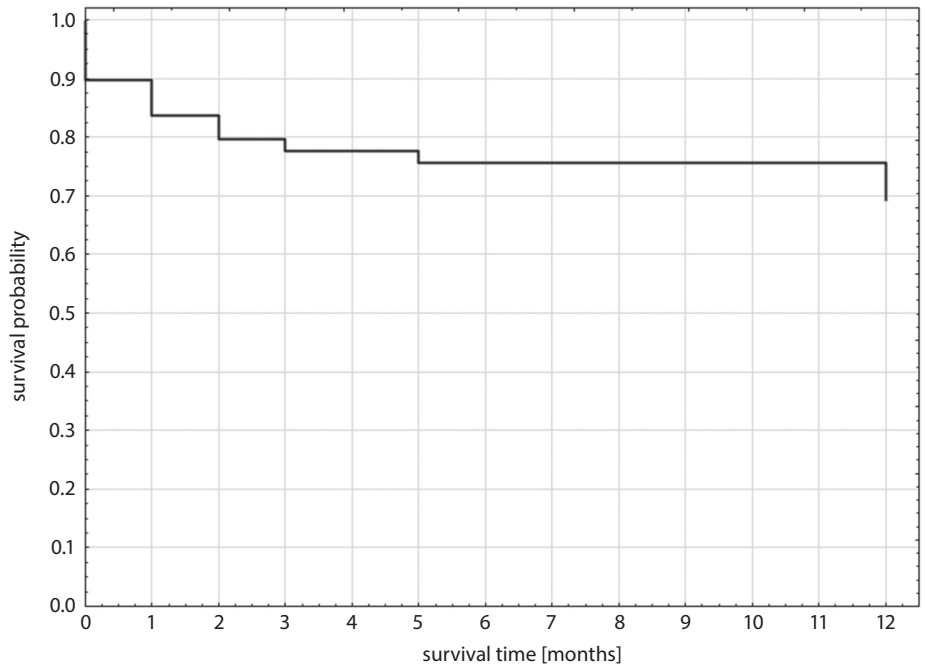

Fig. 2. The Kaplan–Meier survival curve

Discussion

The paper presents Polish real-life multicenter experiences with levosimendan in the treatment of patients with decompensated AdvHF. According to 2018 updates of the Heart Failure Association, classical inotropic drugs are not recommended as a routine treatment in AdvHF, but may be used in selected patients as short-term therapy, especially as a bridge to mechanical circulatory support or transplantation.[1] Intermittent use of levosimendan may also be useful in such cases to improve clinical outcome and reduction in hospitalizations.[1,17] Despite this recommendation, levosimendan is rarely used in Poland. This limitation is not only due to relatively high cost of the therapy, but also due to concerns about its safety and is related to its little experience in the treatment of AdvHF.

Our study reported high re-hospitalizations rates in short- and long-term period with survival at 69% in a one-year follow-up in a population with AdHF hospitalized due to HF decompensation. The studied population was in advanced stage of HF with significant dysfunction of LVEF (median 20%), enlargement of LV 71/61.5 mm (left ventricle end-diastolic volume (LVEDV)/left ventricle end-systolic volume (LVESV) 252/188 mL) and dysfunction of the right ventricle (TAPSE in median 13 mm). Among analyzed variables, longer levosimendan infusion, lower minimum SBP and DBP during infusion, and simultaneous dobutamine infusion were associated with mortality. These factors confirm that patients with hypotension and hypoperfusion have a serious prognosis and high mortality rates. Patients requiring simultaneous inotropic support with dobutamine infusion had a very serious clinical status, which is why they died frequently. It is worth noting that low use of angiotensin-converting-enzyme inhibitors (ACEI), angiotensin II receptor blockers (ARB) and angiotensin receptor-neprilysin inhibitors (ARNI) in the studied group (73%) was related to hypotension and/or worsening renal function.

However, on discharge patients showed improvement in the clinical status, NYHA class and BNP levels after levosimendan therapy. So far, levosimendan has been studied in different clinical situations of acute HF, also showing the reduction of HF clinical signs and symptoms, and improved hemodynamics in patients with acute HF. REVIVE I trial was a pilot study of 100 patients, which showed that acute decompensated HF (ADHF) patients treated with levosimendan saw a significant improvement of clinical signs and symptoms of HF.[15] A 600-patient trial (REVIVE II) comprising of patients with acute decompensated HF with LVEF < 35% revealed that fewer levosimendan patients experienced worsening HF (15% of patients in the levosimendan group and 26% of patients in the control group). In patients with ADHF, levosimendan infusion provided rapid and long-lasting symptomatic relief.[15]

In the double-blind study, levosimendan infusion versus dobutamine (LIDO) in 203 patients with severe low-output acute HF, the hemodynamic improvement defined as an increase of 30% or more in cardiac output and a decrease of 25% or more in pulmonary capillary wedge pressure (PCWP) after 24 h was achieved in 28% of the levosimendan group and 15% in the dobutamine group (HR = 1.9; 95% CI = 1.1–3.3; p = 0.022). The defined primary endpoint as the hemodynamic improvement was associated with clinical benefit for mortality in 180 days in levosimendan population (HR = 0.57; 95% CI = 0.34–0.95; p = 0.029).[12] Moreover, a post hoc analysis of the LIDO trial showed that hemodynamic effect of levosimendan compared to dobutamine was better in the presence of beta-blockers.[12]

On the other hand, the SURVIVE trial was the first randomized multicenter double-blind, prospective trial to monitor long-term survival in patients with ADHF evaluating 2 inotropic agents, levosimendan and dobutamine. In 1,327 patients with LVEF < 30% not responding to standard therapy, in all-cause mortality, there was no significant difference between the studied groups (levosimendan 26% compared to dobutamine 28%, HR = 0.91 (95% CI = 0.74–1.13); p = 0.401).[14] However, the retrospective analysis of the SURVIVE trial revealed that in the presence of β-blockers, mortality was lower for levosimendan than for dobutamine.[18] In another multinational, randomized, double-blind, phase IV study among HF patients in NYHA class III and IV, despite optimal treatment for HF including β-blocker therapy, improvement in hemodynamic parameters like PCWP and cardiac index (CI) with levosimendan was significantly greater compared with dobutamine at 24 h after the start of the infusion, and the effects lasting at 48 h though levosimendan was only administered for 24 h and dobutamine for 48 h.[19] Therefore, levosimendan is perceived as an therapeutic option in ADHF population on optimal medical treatment, requiring inotropic agents.[19] This observation is clinically important, because the majority of patients with HF are receiving β-blockers. In our study at admission with HF decompensation, 96% of patients were treated with β-blockers (in 4% there were side effects as hypotension and/or bradycardia). In contrast to dobutamine, hemodynamic effects of levosimendan are not reduced by a β-blocker use.[20] According to the 2016 European Society of Cardiology (ESC) HF guidelines, levosimendan should be the preferred inotropic agent for a HF decompensated patient with concomitant β-blocker treatment.[1,2]

Important concerns limiting the use of levosimendan in AdvHF are its possible side effects, especially hypotension. Levosimendan should be used with caution in patients with low baseline SBP (<100 mm Hg) or DBP (<60 mm Hg), or those at risk of a hypotensive episode; also, hypovolemia should be corrected prior to levosimendan infusion.[20] Current use of an initial bolus of levosimendan is not recommended in order to minimize the risk of hypotension.[20] Infusion should be started at a dose of 0.1 mg/kg/min or even 0.05 mg/kg/min when SBP is below 100 mm Hg and titrated to 0.2 mg/kg/min if BP remains stable after the first 2–3 h.[20] If patients develop hypotension, one should reduce the infusion rate or co-administer dobutamine or norepinephrine. In our group, the infusion was not initiated with a loading bolus. Due to hypotension, 22 (45%) of our patients received simultaneous dobutamine infusion. However, dobutamine infusion was one of the independent variable for risk of death (HR = 6.54, p < 0.01) in our study. Levosimendan infusions were associated with a mean reduction in SBP of –13.31 mm Hg and DBP of –9.64 mm Hg. No serious hypotonic episodes or consequent discontinuation of levosimendan infusion were observed. However, the reduction of BP during infusion recorded in the meta-analysis by Gong at al.[21] was lower than in our group – in SBP –7.08 mm Hg and DBP –4.75 mm Hg – which is probably related to the studied population.

Other frequent side effects of levosimendan infusion are supra- and ventricular arrhythmias. Also, hypokalemia is mentioned. In the SURVIVE study,[18] patients treated with levosimendan were more likely to experience atrial fibrillation (AF) episodes, but no differences were observed with respect to frequency of ventricular arrhythmias comparing to dobutamine. Similarly, the REVIVE II study also showed that patients treated with levosimendan more frequently had atrial arrhythmias (levosimendan 9% compared to placebo 2%; p < 0.001) and also episodes of ventricular tachycardia (25% compared to 17%, respectively, p = 0.031).[15,20] In the studied population, there is no data about AF episodes during infusion, because over 2/3 of patients had AF at admission. However, in our opinion, AF episodes in levosimendan patients could also be the sign of advanced stage of HF, not only the side effect of the therapy, similar as for non-sustained ventricular tachycardia (in our population 4 (12%) cases). Although no patient in our group had hypokalemia, it is worth mentioning that the potassium level should be checked before and monitored during infusion of levosimendan, and corrected if low. Because infusion of levosimendan may cause a decrease in the potassium level, increasing it should be considered before infusion even with borderline low potassium. Hypokalemia may also be a trigger of arrhythmia. No episodes of sudden cardiac arrest were observed in our study.

Side effects of levosimendan may be related to more advanced state of HF. Nevertheless, AdvHF patients have a high mortality rate and some of the observed side effects might not be as relevant.

In our study, as seen in multivariate analysis, QRS duration and hsCRP were also independent risk factors for death. A wide QRS complex on the electrocardiography (ECG), especially left bundle branch block (LBBB), indicates interventricular dyssynchrony, and is a well-known marker of poor prognosis in HF.[22–24] C-reactive protein is a biomarker of local and systemic inflammation and its correlation with the severity and prognosis of HF is also well documented.[25,26] Although there are many risk markers (clinical, laboratory, imaging, etc.) and numerous risk scores in patients with AdvHF, clinical history, number of recurrent HF hospitalizations and the physician's experience are still critical.[1]

It is worth noting that LVADs were implanted in 5 described patients and heart transplantations were performed in the other 2 patients during the follow-up. This suggests that infusion of levosimendan may be of value especially in patients waiting for advanced treatment in HF. There was the low rate of device usage at baseline – implantable cardioverter defibrillator and cardiac resynchronization therapy in only 24%. In one-year follow-up the subsequent 20 patients received ICDs and 6 CTRs.

Only 1 patient underwent a Mitraclip procedure 3 years before. These data indicate that there is still a large need for invasive procedures in this population in our country.

Despite the successful treatments for chronic HF in AdvHF, it is still impossible to demonstrate the survival benefit and find the effective pharmacotherapy. The last (2019) expert consensus proposed levosimendan as a safer inodilator option than traditional agents in AdvHF, with prolonged action and pleiotropic properties, including anti-inflammatory and anti-oxidative effects, and as protection not only of myocardial cells, but also of hepatic, renal and neural cells from ischemia/reperfusion injury.[27]

In our study, the patients benefited from levosimendan therapy, as their symptoms, signs of HF and the level of BNP were reduced. Clinical improvement with levosimendan creates an opportunity in AdvHF to bridge therapy to invasive procedures, including LVAD or heart transplantation. Therefore, levosimendan therapy should be used more frequently and earlier in HF journey of patients with HFrEF. The cost of 1 ampulla of levosimendan is about 3,400 PLN, which in the hospitalization rate of E52 group for AdvHF (5,813 PLN) might be well settled. Our results indicate the relative safety of this drug, which may contribute to its greater popularity.

On the other hand, AdvHF represents a severe form of the syndrome, usually worsening over time and, therefore, requiring the frequent administration of inotropes.[30] Levosimendan with its long-lasting effect of active metabolite is the only inodilator in this setting and there is evidence from some studies indicating the benefits of repetitive use of levosimendan in AdvHF.[28] Finally, we still need further clinical experiences with levosimendan therapy in multicenter, prospective trials to establish the impact of levosimendan on mortality in AdvHF.

Limitations of the study

This was an observational study without a control group and the size of the analyzed group was limited. The observed side effects of levosimendan might be related to more advanced state of HF; however, without a control group, side effects can only potentially be associated with the drug.

Conclusions

The use of levosimendan in patients with decompensated AdvHF is safe and is associated with clinical benefits, reflected by reduced HF symptoms and signs, NYHA class and BNP level, although mortality and re-hospitalization rates were high during the one-year follow-up. In AdvHF, levosimendan might be used more often as bridge therapy to invasive advanced procedures, such as LVAD or transplantation.

ORCID iDs

Małgorzata Lelonek https://orcid.org/0000-0003-0756-5541
Iwona Stopczynska https://orcid.org/0000-0003-0860-475X
Ewa Korościk https://orcid.org/0000-0003-2481-9777
Ewa Straburzynska-Migaj https://orcid.org/0000-0002-0545-3370
Marcin Gruchala https://orcid.org/0000-0003-4901-2291

References

1. Crespo-Leiro MG, Metra M, Lund LH, et al. Advanced heart failure: A position statement of the Heart Failure Association of the European Society of Cardiology. *Eur J Heart Fail*. 2018;20(11):1505–1535.
2. Ponikowski P, Voors AA, Anker SD, et al; ESC Scientific Document Group. 2016 ESC Guidelines for the diagnosis and treatment of acute and chronic heart failure: The Task Force for the diagnosis and treatment of acute and chronic heart failure of the European Society of Cardiology (ESC). Developed with the special contribution of the Heart Failure Association (HFA) of the ESC. *Eur Heart J*. 2016; 37(27):2129–2200.
3. Seferovic PM, Jankowska E, Coats AJS, et al; Task Force of the HFA Atlas, and the ESC Atlas of Cardiology leadership, developed in collaboration with the National Heart Failure Societies of the ESC member and ESC affiliated member countries. The Heart Failure Association Atlas: Rationale, objectives, and methods. *Eur J Heart Fail*. 2020;22(4):638–645.
4. Rame JE. Introduction to topical collection on updates in advanced heart failure. *Curr Heart Fail Rep*. 2019;16(5):117–118.
5. Machaj F, Dembowska E, Rosik J, Szostak B, Mazurek-Mochol M, Pawlik A. New therapies for the treatment of heart failure: A summary of recent accomplishments. *Clin Risk Manag*. 2019;15:147–155.
6. Pollesello P, Gal TB, Bettex B, et al. Short-term therapies for treatment of acute and advanced heart failure: Why so few drugs available in clinical use, why even fewer in the pipeline? *J Clin Med*. 2019; 8(11):1834–1853.
7. Pollesello P, Ovaska M, Kaivola J, et al. Binding of a new Ca2+ sensitizer, levosimendan, to recombinant human cardiac troponin C: A molecular modeling, fluorescence probe, and proton nuclear magnetic resonance study. *J Biol Chem*. 1994;269(46):28584–28590.
8. Papp Z, Édes I, Fruhwald S, et al. Levosimendan: Molecular mechanisms and clinical implications. Consensus of experts on the mechanisms of action of levosimendan. *Int J Cardiol*. 2012;159(2):82–87.
9. Nieminen MS, Akkila J, Hasenfuss G, et al. Hemodynamic and neurohumoral effects of continuous infusion of levosimendan in patients with congestive heart failure. *J Am Coll Cardiol*. 2000;36(6):1903–1912.
10. Bouchez S, Fedele F, Giannakoulas, et al. Levosimendan in acute and advanced heart failure: An expert perspective on posology and therapeutic application. *Cardiovasc Drugs Ther*. 2018;32(6):617–624.
11. Lunghetti S, Palmerini E, Urselli R, et al. Effects of levosimendan without loading dose on systolic and diastolic function in patients with end-stage heart failure. *Cardiol J*. 2011;18(5):532–537.
12. Follath F, Cleland JG, Just H, et al; Steering Committee and Investigators of the Levosimendan Infusion versus Dobutamine (LIDO) Study. Efficacy and safety of intravenous levosimendan compared with dobutamine in severe low-output heart failure (the LIDO study): A randomised double-blind trial. *Lancet*. 2002;360(9328): 196–202.
13. Landoni G, Biondi-Zoccai G, Greco M, et al. Effects of levosimendan on mortality and hospitalization: A meta-analysis of randomized controlled studies. *Crit Care Med*. 2012;40(2):634–646.
14. Mebazaa A, Nieminen MS, Packer M, et al; SURVIVE Investigators. Levosimendan vs dobutamine for patients with acute decompensated heart failure: The SURVIVE Randomized Trial. *JAMA*. 2007;297(17): 1883–1891.
15. Packer M, Colucci W, Fisher L, et al; REVIVE Heart Failure Study Group; Effect of levosimendan on the short-term clinical course of patients with acutely decompensated heart failure. *JACC Heart Fail*. 2013;1(2): 103–111.
16. Polleselo P, Parissis J, Kivikko M, Harjola VP. Levosimendan meta-analyses: Is there a pattern in the effect on mortality. *Int J Cardiol*. 2016;209:77–83.
17. Silvetti S, Nieminen MS. Repeated or intermittent levosimendan treatment in advanced heart failure: An updated meta-analysis. *Int J Cardiol*. 2016;202:138–143.

18. Mebazaa A, Nieminen MS, Filippatos GS, et al. Levosimendan vs dobutamine: Outcomes for acute heart failure patients on beta-blockers in SURVIVE. *Eur J Heart Fail*. 2009;11(3):304–311.
19. Bergh CH, Andersson B, Dahlström U, et al. Intravenous levosimendan vs dobutamine in acute decompensated heart failure patients on beta-blockers. *Eur J Heart Fail*. 2010;12(4):404–410.
20. Harjola VP, Giannakoulas G, von Lewinski D, et al. Use of levosimendan in acute heart failure. *Eur Heart J Suppl*. 2018;20(Suppl I):I2–I10.
21. Gong B, Li Z, Yat Wong PC. Levosimendan treatment for heart failure: A systematic review and meta-analysis. *J Cardiothorac Vasc Anesth*. 2015;29(6):1415–1425.
22. Lund LH, Jurga J, Edner M, et al. Prevalence, correlates, and prognostic significance of QRS prolongation in heart failure with reduced and preserved ejection fraction. *Eur Heart J*. 2013;34(7):529–539.
23. Kashani A, Barold SS. Significance of QRS complex duration in patients with heart failure. *J Am Coll Cardiol*. 2005;46(12):2183–2192.
24. Braunschweig F, Linde C, Benson L, Ståhlberg M, Dahlström U, Lund LH. New York Heart Association functional class, QRS duration, and survival in heart failure with reduced ejection fraction: Implications for cardiac resynchronization therapy. *Eur J Heart Fail*. 2017;19(3):366–376.
25. Minami Y, Kajimoto K, Sato N, Hagiwara N; ATTEND Study Investigators. Effect of elevated C-reactive protein level at discharge on long-term outcome in patients hospitalized for acute heart failure. *Am J Cardiol*. 2018;121(8):961–968.
26. Matsumoto H, Kasai T, Sato A, et al. Association between C-reactive protein levels at hospital admission and long-term mortality in patients with acute decompensated heart failure. *Heart Vessels*. 2019;34(12):1961–1968.
27. Agostoni P, Farmakis DT, Garcia-Pinilla JM, et al. Haemodynamic balance in acute and advanced heart failure: An expert perspective on the role of Levosimendan. *Card Fail Rev*. 2019;5(3):155–161.
28. Farmakis D, Agastoni P, Baholli L, et al. A pragmatic approach to the use of inotropes for the management of acute and advanced heart failure: An expert panel consensus. *Int J Cardiol*. 2019;297:83–90.

Neutrophil to lymphocyte ratio as noninvasive predictor of pulmonary vascular resistance increase in congestive heart failure patients: Single-center preliminary report

Tomasz Kamil Urbanowicz[1,A–F], Anna Olasińska-Wiśniewska[2,C–F], Michał Michalak[3,C,E], Ewa Straburzyńska-Migaj[4,A,B,D–F], Marek Jemielity[2,A,E,F]

[1] Cardiac Surgery and Transplantology Department, University Hospital of Lord's Transfiguration, Poznan University of Medical Sciences, Poland
[2] Department of Cardiac Surgery and Transplantology, Poznan University of Medical Sciences, Poland
[3] Department of Computer Science and Statistics, Poznan University of Medical Sciences, Poland
[4] Department of Cardiology, Poznan University of Medical Sciences, Poland

A – research concept and design; B – collection and/or assembly of data; C – data analysis and interpretation; D – writing the article; E – critical revision of the article; F – final approval of the article

Advances in Clinical and Experimental Medicine, ISSN 1899–5276 (print), ISSN 2451–2680 (online) *Adv Clin Exp Med*. 2020;29(11):1313–1317

Address for correspondence
Tomasz Urbanowicz
E-mail: tk.urbanowicz@gmail.com

Funding sources
None declared

Conflict of interest
None declared

Received on April 30, 2020
Reviewed on July 3, 2020
Accepted on August 11, 2020

Abstract

Background. Nowadays, heart failure (HF) is a significant health problem due to steady increase in diagnosis, unpredictable acute decompensations and high mortality rate. Early risk stratifications of clinical deterioration are essential in preventing life-threatening events and ensuring proper patients management. Increased neutrophil to lymphocytes ratio (NTLR) above 6 is associated with the risk of re-hospitalizations and increased mortality.

Objectives. To compare NTLR and clinical, laboratory and hemodynamic results obtained from patients re-hospitalized within six-month intervals due to HF decompensation.

Material and methods. We evaluated 41 patients (n = 36 males (87%) and n = 5 females (13%), mean age 50 ±10 years) admitted to our hospital at least twice within six-month interval due to decompensation of chronic heart failure (CHF) between 2017 and 2019. All patients were divided into 2 groups depending on the NTLR values.

Results. There was no death in presented group during the observational time. We observed a significant difference in cardiac index (CI) – 2.4 ±0.5 compared to 2.6 ±0.6 L/m^2/min – between the 1st and 2nd admission (p = 0.0356). The right ventricle systolic pressure (RVSP) results related to NTLR level revealed significant difference (43 ±14 mm Hg compared to 59 ±21 mm Hg, p = 0.0438). We observed a significant increase of pulmonary vascular resistance (PVR) values (175 ±106 compared to 438 ±300 dyn*s*cm^{-5}, p = 0.0386) in patients with NTLR above 6.

Conclusions. Neutrophil to lymphocyte ratio may be an easy and suitable tool for monitoring of the HF progression. According to our study, the ratio correlates with PVR and RVSP increase.

Key words: neutrophils, heart failure, pulmonary hypertension, pulmonary vascular resistance

Cite as
Urbanowicz TK, Olasińska-Wlśniewska A, Michalak M, Straburzyńska-Migaj E, Jemielity M. Neutrophil to lymphocyte ratio (NTLR) as noninvasive predictor of pulmonary vascular resistance increase in congestive heart failure patients. Single center preliminary report. *Adv Clin Exp Med*. 2020;29(11):1313–1317. doi:10.17219/acem/126292

DOI
10.17219/acem/126292

Background

Nowadays, heart failure (HF) is a significant health problem due to steady increase in diagnosis, unpredictable acute decompensations and high mortality rate.[1] Early risk stratifications of clinical deterioration are essential in preventing life-threatening events and ensuring proper patient management.[2] Pulmonary hypertension secondary to HF is a factor of poor prognosis and has a significant influence on the severity of the disease.[3]

Increased neutrophil to lymphocytes ratio (NTLR) above 6 is associated with the risk of re-hospitalizations and increased mortality.[4] In response to a variety of signals, neutrophils produce several cytokines and other inflammatory factors, including neutrophil serine proteases, peroxidases, proteinases, gelatinases, NADPH oxidase, and pentraxin 3.[5,6] Cytokine hypothesis involving serum elevation levels of interleukin 1 (IL-1), tumor necrosis factor α (TNF-α), transmembrane suppression of tumorigenicity-2 receptor (ST2), IL-6, and galectin-3 in HF patients support inflammatory contribution of disease progression.[7]

We analyzed the clinical status, laboratory results and hemodynamic parameters in patients suffering from chronic heart failure (CHF), re-hospitalized within 6 months in our hospital.

Material and methods

We evaluated 41 patients (n = 36 men (87%) and n = 5 women (13%), mean age 50 ± 10 years) admitted to our hospital at least twice within a six-month interval due to decompensation of CHF due to HF with reduced ejection fraction (HFrEF) between 2017 and 2019. Twenty of them were diagnosed with dilated cardiomyopathy (DCM) and 21 with ischemic cardiomyopathy (ICM). Mean body mass was 85 ±15 kg compared to 87 ±16 kg on 1st and 2nd admission, respectively, and the mean height was 176 ±8 cm. Concomitant diseases included diabetes mellitus (DM; 3 patients), chronic obstructive pulmonary disease (COPD; 2 patients), kidney dysfunction (2 patients), and a history of stroke (1 patient).

On admission and during hospitalization, laboratory tests, echocardiography, right catheterization, and 6-minute walking test (6MWT) were performed (Table 1). We analyzed baseline patients' demographics, change in functional class according to World Health Organization

Table 1. Differences in laboratory, echocardiographic and RHC parameters between 1st and 2nd hospitalization

Parameters	1st admission	2nd admission	p-value
Whole blood count			
Leukocyte count [10e/L = 10^9/L]	7.3 [6.3–8.4]	7 [5.8–8.3]	0.0593
Neutrophil count [10e/L = 10^9/L]	4.9 [4.1–5.9]	4.8 [3.9–5.8]	0.1561
Lymphocyte count [10e/L = 10^9/L]	1.4 [1.2–1.8]	1.5 [1–2]	0.2461
NTLR	3.5 [2.5–4.7]	3.3 [2.2–4.4]	0.7216
Hemoglobin [mmol/L]	9.2 [8.7–9.6]	8.9 [8.5–9.5]	0.3724
Albumin [mg/dL]	40.3 [38.5–42.8]	40.5 [38.5–41.9]	0.4476
AST [IU/L]	136 [31–140]	136 [34–139]	0.8174
Creatinine [mg/dL]	101.4 [85.9–128.2]	94 [83.3–122.9]	0.8055
CRP [mg/L]	2 [1.0–6.2]	2.8 [1.1–8.8]	0.2256
BNP [pg/mL]	310 [133.4–645.1]	360 [131.9–567.0]	0.2158
proBNP [pg/mL]	1652 [743–2618]	1467 [831–2627]	0.4661
Echocardiographic parameters			
LVD [mm]	75 [67–80]	73 [65–82]	0.8561
RVD [mm]	35 [32–39]	35 [31–37]	0.4461
RVSP [mm Hg]	40 [34–55]	45 [35–50]	0.9652
LVEF [%]	20 [15–25]	20 [15–25]	0.5888
Right heart catheterization			
PAPm [mm Hg]	32.5 [23–44]	29.5 [21.5–40.0]	0.3626
CO [L/min]	4.7 [3.9–5.5]	5.3 [4.6–6.0]	0.0534
CI [L/m^2/min]	2.3 [2–2.7]	2.6 [2.4–2.9]	0.0356
PVR [dyn*s*cm^{-5}]	151.5 [113–270]	150 [106.0–218.5]	0.1401

Data presented as median [LQ–UQ]; LQ – lower quartile; UQ – upper quartile; AST – aspartate aminotransferase; BNP – natriuretic brain peptide; CI – cardiac index; CO – cardiac output; CRP – C-reactive protein; EF – ejection fraction; LVD – left ventricle diameter; LVEF – left ventricle ejection fraction; NTLR – neutrophil to lymphocyte ratio; NT-proBNP – N-terminal prohormone natriuretic brain peptide; PAPm – mean pulmonary artery pressure; PVR – pulmonary vascular resistance; RHC – right heart catheterization; RSVP – right ventricle systolic pressure.

(WHO) classification, results of 6MWT, and vital signs on admission (including heart rate, blood pressure). Laboratory data included brain natriuretic peptide (BNP), N-terminal prohormone of brain natriuretic peptide (NT-pro-BNP), blood morphology, C-reactive protein (CRP), creatinine, alanine aminotransaminase (ALT), aspartate transaminase (AST), and NTLR. Echocardiography was performed in each patient at the admission, including left and right ventricle and atrial diameters, left ventricle ejection fraction (LVEF), presence of pericardial effusion, right atrial pressure (RAP) estimated by evaluating the inferior cava (IVC) size and change with respiration, and right ventricle systolic pressure (RVSP). The estimation of RVSP was based on the peak tricuspid regurgitation velocity (TRV) taking into account RAP as described by the simplified Bernoulli equation.

Right heart catheterization was performed in the catheterization lab. Pressure measurements were obtained, including mean RAP, right ventricle pressure (systolic, diastolic and end-diastolic), pulmonary artery pressure (systolic, diastolic and mean), and wedge pressure. Cardiac output (CO) was measured with thermodilution with cold saline. The cardiac index (CI), pulmonary vascular resistance (PVR), systemic vascular resistance (SVR), and transpulmonary gradient (TPG) were estimated.

All patients were divided into 2 groups depending on the NTLR values obtained from blood samples taken on admission. The values above or below 6 determined the division according to previous reports.[7]

Statistical analysis

Mean body mass, weight, 6MWT results and drugs daily dosages were presented as mean values and standard deviations (SD). The analyzed parameters were presented as medians and interquartile range (IQR), since data did not follow according to normal distribution (Shapiro–Wilk test); therefore, non-parametric tests were used. The comparison between data obtained during the 1st and 2nd admission was performed with Wilcoxon matched pairs test. Parameters between patients with NTLR value lower or greater than 6 were compared with Mann–Whitney test. Statistical analysis was performed using STATISTICA v. 13.3 (StatSoft Inc., Tulsa, USA). All tests were considered significant at $p < 0.05$.

Results

There was no death in the presented group during the observational time (2017–2019). The clinical evaluation of severity of HF decompensation was based on the New York Heart Association (NYHA) classification with mean NYHA functional class on the 1st and 2nd admissions 2.5 ±0.5 and 3.2 ±0.5, respectively. The indications for 2nd admission were based on worsening in clinical symptoms regarding shortness of breath in 41 (100%), easy fatigue in 35 (85%) and lower extremities swellings in 38 (93%) patients. Five (12%) patients reported persistent cough.

There was neither a statistically significant difference in NYHA stage nor a correlation between NYHA stage and NTLR between both admissions. Moreover, the differences in BNP and NT-pro-BNP serum levels between both admissions were non-significant. The BNP serum levels were 435 ±409 pg/mL compared to 485 ±537 pg/mL on the 1st and 2nd admission, respectively. The NT-pro-BNP serum levels were 2103 ±1942 pg/mL compared to 2171 ±2239 pg/mL on the 1st and 2nd admission, respectively. The results of BNP serum levels related to NTLR were still insignificant (413 ±418 pg/mL compared to 566 ±263 pg/mL, respectively, $p = 0.0736$). The results of NT-pro-BNP serum levels related to NTLR were not significant (1961 ±1982 pg compared to 2938 ±1979 pg/mL, respectively, $p = 0.0933$). Detailed data is presented in Table 1.

There was no significant difference in echocardiographic parameters between both admissions including RSVP results (45 ±16 mm Hg compared to 45 ±13 mm Hg, respectively). The RVSP results related to NTLR subgroups revealed a significant difference (43 ±14 mm Hg compared to 59 ±21 mm Hg, $p = 0.0438$). Detailed data is presented in Table 2.

The clinical evaluation was also performed with 6MWT before discharge. The mean values of achieved distances on 1st and 2nd hospitalization were 356 ±41 m compared to 361 ±52 m, respectively. The results of 6MWT during the 2nd hospitalization in 2 NTLR subgroups were significantly different: 331 ±42 compared to 378 ±39 m, in patients with NTLR ratio above and below 6, respectively.

We observed a significant difference in CI (2.4 ±0.5 compared to 2.6 ±0.6 L/m^2/min) between the 1st and 2nd admission ($p = 0.0356$). However, there was no relationship between NTLR level and CI.

There was no statistical difference in PVR values between admissions in studied group (212 ±170 compared to 190 ±117 dyn*s*cm^{-5}). However, we observed a significant increase in PVR values (175 ±106 compared to 438 ±300 dyn*s*cm^{-5}), $p = 0.0386$ in patients with NTLR above 6.

Pharmacotherapy on 1st admission included β-blockers, diuretics, eplerenone, and angiotensin-converting-enzyme inhibitors (ACE-I). The doses of diuretics and ACE-I were optimized increased during 1st hospitalization. Pharmacotherapy regimes between both admissions are compared in Table 3.

Discussion

To the best of our knowledge, this is the first study presenting the correlation between NTLR and PVR and RVSP increase in patients with CHF. Heart failure is a challenging clinical problem with high mortality risk, exceeding 50% within 5 years.[8] Therapy is focused on clinical improvement

Table 2. Differences in laboratory, echocardiographic and RHC parameters between NTLR subgroups

Parameter	NTLR ≤ 6	NTLR > 6	p-value
Laboratory results			
Leukocyte count [10e/L = 10^9/L]	7.1 [6.2–8]	9.9 [8.4–10.6]	0.0036
Hemoglobin [mmol/L]	9.2 [8.7–9.6]	9.1 [8.5–9.4]	0.5922
Albumin [mg/dL]	40.7 [38.4–43.0]	39.4 [38.6–40.4]	0.5444
AST [IU/L]	136 [30–140]	137 [31–140]	0.9410
Creatinine [mg/dL]	93.9 [81.8–125.3]	125.4 [111.9–134.4]	0.0797
CRP [mg/L]	1.8 [1.0–5.2]	8.9 [6.2–10.2]	0.0676
BNP [pg/mL]	240 [122.1–574.4]	519.4 [356.1–650.4]	0.0736
NT-proBNP [pg/mL]	1293 [674–2590]	2775.5 [1763–4626]	0.0933
Echocardiography			
LV [mm]	73 [64–80]	80 [75–84]	0.0930
RV [mm]	34 [31–39]	35 [35–37]	0.3952
EF [%]	20 [15–25]	20 [15–23]	0.7930
RVSP [mm Hg]	40 [32–49]	60 [40–65]	0.0438
Right catheterization			
PAPm [mm Hg]	28.5 [21.5–42.5]	44 [33.0–57.5]	0.1005
CO [L/min]	4.9 [4.2–5.5]	3.7 [3.6–4.6]	0.2244
CI [L/m^2/min]	2.4 [2.1–2.7]	2 [1.8–2.4]	0.1227
PVR [dyn*s*cm^{-5}]	142 [99.5–244.3]	407 [186–690]	0.0386

Data presented as median [LQ–UQ]; LQ – lower quartile; UQ – upper quartile; AST – aspartate aminotransferase; BNP – natriuretic brain peptide; CI – cardiac index; CO – cardiac output; CRP – C-reactive protein; EF – ejection fraction; LVD – left ventricle diameter; LVEF – left ventricle ejection fraction; NTLR – neutrophil to lymphocyte ratio; NT-proBNP – N-terminal pro hormone natriuretic brain peptide; PAPm – mean pulmonary artery pressure; PVR – pulmonary vascular resistance; RHC – right heart catheterization; RSVP – right ventricle systolic pressure.

Table 3. Pharmacology during both hospitalizations

Pharmacotherapy	1st admission (n = 41 patients)	2nd admission (n = 41 patients)
β-blockers:		
Metoprolol [mg/daily]	100 ±37.5	100 ±25
number of patients	4 (10%)	4 (10%)
Bisoprolol [mg/daily]	10 ±2.5	10 ±2.5
number of patients	2 (5%)	2 (5%)
Carvedilol [mg/daily]	25 ±12.5	25 ±6.25
number of patients	35 (85%)	35 (85%)
Diuretics:		
Furosemide [mg/daily]	120 ±80	180 ±40
number of patients	41 (100%)	41 (100%)
Eplenorone [mg/daily]	50 ±1.25	50 ±0.25
number of patients	41 (100%)	41 (100%)
Torasemide [mg/daily]	10 ±3	20 ±4
number of patients	4 (10%)	6 (15%)
ACE-I:		
Ramipril [mg/daily]	3.3 ±1.6	4.8 ±1.2
number of patients	41 (100%)	41 (100%)

ACE-I – angiotensin-converting-enzyme inhibitors.

by blocking neurohormonal and sympathetic systems activation.[9] In different types of cardiomyopathies, the trigger insult may be of inflammatory etiology with secondary immune system activation in response. The blood-recruited monocytes infiltrate the myocardium, causing further deterioration of the heart function.[10,11] The persistence of inflammation after acute phases promotes adverse heart remodeling.[12] In our study, we focused on a possible risk prognosis for future clinical deterioration assessed with NTLR. Neutrophils are known to be important effector cells in the immune system responding to multiple signals by producing inflammatory factors.[13,14] They are involved in cell activation at the inflammatory sites.[15] The link between HF development and clinical progression is strong and complementary to neurohormonal activation.[16] Neutrophil to lymphocyte ratio above 6 is a known predictor for in-hospital mortality among patients with acute decompensations.[17]

In our study, there was a correlation noticed between NTLR and PVR values. Hence, the NTLR could be a possible prognostic factor for future clinical status deterioration among patients requiring readmission within a six-month time interval. Right heart catheterization (RHC) is a definitive tool for accurate hemodynamic monitoring.[18] We found the PVR increased from 175 ±105 dyn*s*cm^{-5} to 438 ±300 dyn*s*cm^{-5} in the subgroup of patients with elevated NTLR. Although the BNP and NT-pro-BNP values were insignificant, the progression of the failing heart was noticed by hemodynamic results of heart function. In our study, we present the results confirming NTLR as a significant marker for future heart function deterioration. There was no statistically significant difference in RVSP between admissions, but an increase was noted (42 ±14 mm Hg compared to 59 ±21 mm Hg) regarding NTLR.

Although the population did not differ in NYHA stage between both admissions, the clinical symptoms requiring hospitalizations may be related to increase in pulmonary hypertension evaluated easily using RSVP results in echocardiographic imaging. Among predictors in patients with left ventricular dysfunction, impaired function of right ventricle is believed to be an independent predictor of less than 30% survival within 5 years.[19] Echocardiography of right ventricle hemodynamics is focused on its function and on risk estimation of pulmonary hypertension. Both parameters are significant for patients' prognosis including disease severity and survival.[20] We present the results of the study, indicating NTLR as an easy laboratory tool of parallel significance related to RHC results.

We noticed that despite clinical deterioration, heart catheterization revealed an increase in CI. The initial results were 2.4 ±0.5 2.6 ±0.6 L/m^2/min and changed to 2.6 ±0.6 L/m^2/min (p = 0.0356). The differences may be explained by pharmacotherapy optimization including diuretics and ACE-I doses increase. However, there was no relationship between NTLR level and CI.

The most significant result of the study is connected to the NTLR to PVR estimation with RHC. Pulmonary vascular resistance is a lone predictor of poor outcomes according to previous studies in patients suffering from HF.[21] Moreover, the PVR increase indicates ominous disease progression.[22,23] The results of our study suggest that NTLR can be a suitable, quick and easy tool for assessing the risk of PVR progression stratification in patients suffering from circulatory insufficiency.

Conclusions

Neutrophil to lymphocyte ratio may be an easy and suitable tool for monitoring HF progression. According to our study, the ratio correlates with PVR and RVSP increase.

ORCID iDs

Tomasz Kamil Urbanowicz https://orcid.org/0000-0001-8080-2764
Anna Olasińska-Wiśniewska https://orcid.org/0000-0002-4213-8708
Michał Michalak https://orcid.org/0000-0002-2852-3984
Ewa Straburzyńska-Migaj https://orcid.org/0000-0002-0545-3370
Marek Jemielity https://orcid.org/0000-0003-2442-4644

References

1. Ponikowski P, Voors AA, Anker SD, et al; Authors/Task Force Members; Document Reviewers. 2016 ESC Guidelines for diagnosis and treatment of acute and chronic heart failure: The Task Force for the diagnosis and treatment of acute and chronic heart failure of European Society of Cardiology (ESC). Developed with the special contribution of the Heart Failure Association (HFA) of ESC. *Eur J Heart Fail*. 2016;18(8):891–975.
2. Wang X, Fan X, Ji S, Ma A, Wang T. Prognostic value of neutrophil to lymphocyte ratio in heart failure patients. *Clin Chim Acta*. 2018;485:44–49.
3. Berthelot E, Bailly MT, Hatimi SE, et al. Pulmonary hypertension due to left heart disease: Pulmonary hypertension due to left heart disease. *Arch Cardiovasc Dis*. 2017;110(6–7):420–431.
4. Ni J, Wang H, Li Y, Shu Y, Liu Y. Neutrophil to lymphocyte ratio (NLR) as a prognostic marker for in-hospital mortality of patients with sepsis: A secondary analysis based on a single-center, retrospective, cohort study. *Medicine (Baltimore)*. 2019;98(46):1–5.
5. Rosales C. Neutrophil: A cell with many roles in inflammation or several cell types? *Front Physio*. 2018;9:113–129.
6. Selders GS, Fetz AE, Radic MZ, Bowlin GR. An overview of the role of neutrophils in innate immunity, inflammation and host-biomaterial integration. *Regen Biomater*. 2017;4(1):55–68.
7. Zhang Y, Bauersachs J, Langer HF. Immune mechanisms in heart failure. *Eur J Heart Fail*. 2017;19(11):1379–1389.
8. Dick SA, Epelman S. Chronic heart failure and inflammation: What do we really know? *Circ Res*. 2016;119(1):159–176.
9. Drazner MH. The progression of hypertensive heart disease. *Circulation*. 2011;123(3):327–334.
10. Bajpai G, Bredemeyer A, Li W, et al. Tissue resident CCR2- and CCR2+ cardiac macrophages differentially orchestrate monocyte recruitment and fate specification following myocardial injury. *Circ Res*. 2019;124(2):263–278.
11. Gentek R, Hoeffel G. The innate immune response in myocardial infarction, repair, and regeneration. *Adv Exp Med Biol*. 2017;1003:251–272.
12. Mortensen RM. Immune cell modulation of cardiac remodeling. *Circulation*. 2012;125(13):1597–1600.
13. Mayadas, TN, Cullere X, Lowell CA. The multifaceted functions of neutrophils. *Annu Rev Pathol*. 2014;9:181–218.
14. Nauseef, WM, Borregaard N. Neutrophils at work. *Nat Immunol*. 2014;15(7):602–61.
15. Casanova-Acebes M, Pitaval C, Weiss LA, et al. Rhythmic modulation of the hematopoietic niche through neutrophil clearance. *Cell*. 2013;153(5):1025–1035.
16. Van Linthout 1, Tschöpe C. Inflammation: Cause or consequence of heart failure or both? *Curr Heart Fail Rep*. 2017;14(4):251–265.
17. Cho JH, Cho HJ, Lee HY, et al. Neutrophil-lymphocyte ratio in patients with acute heart failure predicts in-hospital and long-term mortality. *J Clin Med*. 2020;9(2):557.
18. Kałużna-Oleksy M, Araszkiewicz A, Migaj J, Lesiak M, Straburzyńska-Migaj E. "From right to left": The role of right heart catheterization in the diagnosis and management of left heart diseases. *Adv Clin Exp Med*. 2017;26(1):135–141.
19. Zelt JGE, Chaudhary KR, Cadete VJ, Mielniczuk LM, Stewart DJ. Medical therapy for heart failure associated with pulmonary hypertension. *Circ Res*. 2019;124(11):1551–1567.
20. Annone U, Bocchino PP, Marra WG, et al. Echocardiographic estimation of right ventricular wall tension: Haemodynamic comparison and long-term follow-up. *Pulm Circ*. 2019;9(4):2045894019895420.
21. Naeije R, Gerges M, Vachiery JL, Caravita S, Gerges C, Lang IM. Hemodynamic phenotyping of pulmonary hypertension in left heart failure. *Circ Heart Fail*. 2017;10(9):e004082.
22. Dragu R, Rispler S, Habib M, et al. Pulmonary arterial capacitance in patients with heart failure and reactive pulmonary hypertension. *Eur J Heart Fail*. 2015;17(1):74–80.
23. Urbanowicz T, Straburzyńska-Migaj E, Katyńska I, et al. Sustained improvement of clinical status and pulmonary hypertension in patients with severe heart failure treated with sildenafil. *Ann Transplant*. 2014;19:325–330.

Chromogranin A assessment in patients with neuroendocrine neoplasm of the small bowel and carcinoid syndrome treated with somatostatin analogues

Paweł Gut[1,A–D], Agata Czarnywojtek[2,C,E,F], Marek Ruchała[1,E,F]

[1] Department of Endocrinology, Metabolism and Internal Medicine, Poznan University of Medical Sciences, Poland
[2] Department of Pharmacology, Poznan University of Medical Sciences, Poland

A – research concept and design; B – collection and/or assembly of data; C – data analysis and interpretation; D – writing the article; E – critical revision of the article; F – final approval of the article

Advances in Clinical and Experimental Medicine, ISSN 1899–5276 (print), ISSN 2451–2680 (online) *Adv Clin Exp Med*. 2020;29(11):1319–1324

Address for correspondence
Paweł Gut
E-mail: gutpj@poczta.onet.pl

Funding sources
None declared

Conflict of interest
None declared

Received on January 25, 2020
Reviewed on June 2, 2020
Accepted on August 11, 2020

Abstract

Background. Chromogranin A (CgA) is one of the non-specific markers measured in the biochemical diagnostics of neuroendocrine neoplasms (NENs).

Objectives. To analyze the CgA levels of patients with carcinoid syndrome who are being treated with somatostatin analogues (SSAs), depending on the histologic maturity of the neoplasm, the degree of liver involvement and the stage of the disease.

Material and methods. The study group comprised of 41 patients, including 29 women (70.7%) and 12 men (29.3%). All of the patients had undergone surgical removal of the primary site. Hepatic metastases were found in all patients and they all were treated with SSAs. Chromogranin A concentration was determined using the enzyme-linked immunosorbent assay (ELISA).

Results. Among the patients with grade 1 tumors, the mean CgA value was 298.83 ng/mL, whereas in the group with grade 2 tumors, the CgA value was 1498.44 ng/mL, which was a statistically significant difference ($p < 0.001$). In the group of patients with 10% liver involvement, the mean CgA value was 394.44 ng/mL, whereas in the group of patients with 25% liver involvement, this value was 1770.63 ng/mL, demonstrating significantly higher values ($p < 0.001$). Among the patients with a progressing disease, the mean CgA concentration value was 1620.78 ng/mL, whereas in the group of patients with a stable disease, these were considerably lower, amounting to 230.36 ng/mL ($p < 0.001$).

Conclusions. Assessing CgA level in patients with carcinoid syndrome is helpful in the diagnostics and monitoring of treatment because CgA values depend on the tumor grade and the severity of the disease.

Key words: chromogranin A, carcinoid syndrome, somatostatin analogues

Cite as
Gut P, Czarnywojtek A, Ruchała M. Chromogranin A assessment in patients with neuroendocrine neoplasm of the small bowel and carcinoid syndrome treated with somatostatin analogues. *Adv Clin Exp Med*. 2020;29(11):1319–1324. doi:10.17219/acem/126290

DOI
10.17219/acem/126290

Introduction

Neuroendocrine neoplasms (NENs) are characterized by hormonal activity, which is used in diagnosis and monitoring of the treatment. Biochemical markers measured in the blood serum may be specific or non-specific. Non-specific markers include chromogranin A (CgA) and neuron-specific enolase (NSE).[1] Chromogranin A is a highly stable molecule and no special precautions are needed to store the serum or plasma.[2–4] The highest CgA concentrations have been found in patients with carcinoid syndrome; thus, it is an important marker used in the monitoring and treatment of neuroendocrine cancers and an independent prognostic indicator of survival in patients with NENs. Based on research conducted on patients with carcinoid tumors, it has been determined that CgA concentration may reflect the severity of the disease and correlate with disease progression. Chromogranin A concentrations are considerably higher in the majority of NEN cases, but particularly high values are observed in the classic carcinoid tumor.[5] Chromogranin A may also be used as a marker in the estimation of a tumor's rate of growth. The time of CgA concentration doubling is of significant prognostic value, that is, the shorter the doubling time the worse the prognosis.[6,7] Treatment with somatostatin analogues (SSAs) considerably reduces CgA concentrations, particularly with carcinoid tumors, by inhibiting the synthesis and release of CgA from tumor cells. In the case of disease progression during treatment with SSAs, elevated CgA concentration may reflect a lack of control over the tumor secretion activity or its growth.[8–15] The aim of our study was to assess the concentration of CgA in patients with carcinoid syndrome who were continuously treated with SSAs. The study compared patients according to the degree of histological maturity and the degree of liver involvement by metastases, and depending on whether the disease was stable or progressing. The study had a purely clinical aspect – to assess the prognosis of treatment in patients with varying degrees of disease progression.

Material and methods

The study group comprised 41 patients – 29 women (70.7%) and 12 men (29.3%) – diagnosed with a NEN of the small bowel. The mean age of the men was 60.41 ±4.90 years, and for the women it was 64.20 ±10.39 years. All patients had undergone surgical removal of the primary site with histopathological assessment according to the World Health Organization (WHO) 2017 classification. Grade G1 was found in 19 tissue preparations (46.3%) and the remaining 22 preparations were classified as G2 (53.7%). All patients underwent detailed imaging diagnostics (abdominal cavity ultrasonography and computed tomography (CT) of the chest, abdominal cavity, and small pelvis) and supplementary biochemical monitoring (CgA, serotonin and 5-HIAA) in order to assess their clinical progress. In each case, cardiologic consultation was performed with echocardiography in order to identify any carcinoid heart disease (tricuspid and pulmonary valve lesions were found in 32 cases). All of the patients were found to have hepatic metastases (10% liver involvement in 23 cases and 25% liver involvement in 18 cases). All patients exhibited symptoms of carcinoid syndrome in the form of diarrhea, facial flush, telangiectasia, and myopathic symptoms.

In each case, to qualify the patients for SSA therapy, receptor scintigraphy was performed using ^{99m}Tc-EDDA/HYNIC-TOC. The degree of radiotracer uptake in liver metastases was assessed according to the qualitative scale developed by E. Krenning (degrees 0–4). In the study group, the radiotracer uptake in the liver ranged between grades 3 and 4 on Krenning's scale. In patients with histological maturity (G1), the radiotracer uptake was grade 4, while in the G2 patients, it was grade 3. It is also worth adding that the degree of radiotracer uptake in patients with disease progression in most cases was grade 3. The study group was treated with SSAs from 2014 to 2018 and were administered octreotide LAR at a dose of 30 mg (intramuscularly) or lanreotide autogel at a dose of 120 mg (subcutaneously) every 4 weeks. The CgA levels were measured every 3 months. However, the abdominal CT imaging tests every 6 months in order to obtain an objective assessment of the response to treatment according to RECIST 1.1 criteria. Chromogranin A concentration was determined using enzyme-linked immunosorbent assay (ELISA), using the Cisbio-Bioassays sets (Perkin Elmer, Waltham, USA). The cut-off point for CgA was 100 ng/mL at an analytical sensitivity of 19 ng/mL, in line with the manufacturer's recommendations.

Statistical assessment

An analysis of the quantitative variables was performed by calculating the means, standard deviation (SD), medians, minimum quartiles, and maximum values. The Mann–Whitney test was used to compare the quantitative variables in the 2 groups. Correlation between 2 quantitative variables was analyzed using Pearson's and Spearman's coefficients. A significance level of 0.05 was adopted in the analysis. Thus, all values below 0.05 were interpreted as indicating statistically significant relationships. The analysis was performed in the software R v. 3.3.1 (www.r-project.org).

Results

Assessment of CgA concentration depending on histologic maturity

In the group of patients with G1 tumors (n = 19), the mean CgA value was 298.83 ±99.81 ng/mL, whereas in the G2 group (n = 22) the CgA value was 1498.44 ±459.64 ng/mL; this represents a significant difference between the groups

($p < 0.001$; Table 1). A similar relationship was observed in the analysis of the final CgA concentration values, that is, in the G1 group the mean of the final CgA values was 755.14 ±218.33 ng/mL, while in the G2 group it was 3486.88 ±1241.35 ng/mL ($p < 0.001$; Table 2). The CgA doubling time in the G1 group was 39.00 ±11.13 months, whereas in the G2 group it was considerably shorter, amounting to 18.81 ±11.64 months. It is worth emphasizing that in the G1 group, the increase in CgA concentration during SSA treatment was significantly lower and more prolonged in comparison to the patients from the G2 group ($p < 0.001$). This resulted in a significant increase in progression-free time.

Assessment of CgA concentration depending on liver involvement

Among the patients with 10% liver involvement (n = 23), the mean CgA value was 394.44 ±120.51 ng/mL, whereas in the group of patients with 25% liver involvement (n = 18), this value was 1770.63 ±404.11 ng/mL, representing a statistically significant difference ($p < 0.001$; Table 3). In the case of the final CgA values in the 1st group, the mean of the final CgA values was 566.86 ±285.44 ng/mL, whereas in the 2nd group the values were also higher, with a mean of 4123.44 ±1874.77 ng/mL ($p < 0.001$; Table 4). It should be also noted that among patients with 10% liver involvement, the CgA doubling time was 37.12 ±12.99 months, while in the group with 25% liver involvement, it was considerably shorter: 15.16 ±7.52 months. In the group of patients with 10% liver involvement, the increase in CgA value during SSA treatment was statistically lower than in the group of patients with 25% liver involvement ($p < 0.001$). This had a considerable impact on extending the progression-free time.

Assessment of CgA concentration depending the stage of the disease

Among the patients for whom the disease was found to be progressing during the SSA treatment (n = 21), the mean CgA concentration was 1620.78 ±385.55 ng/mL, whereas in the group of patients with stable disease (n = 20), they were considerably lower, amounting to 230.36 ±106.44 ng/mL ($p < 0.001$; Table 5). The analysis of the final CgA values revealed similar results: the group with a stable disease

Table 1. Mean chromogranin A (CgA) value [ng/mL] depending on grading

Grading	Mean CgA value [ng/mL]								p-value*
	n	mean	SD	median	min	max	Q1	Q3	
G1	19	298.83	99.81	220.80	144.71	836.85	190.81	253.04	p < 0.001
G2	22	1498.44	459.64	1452.07	127.86	3801.5	547.50	2243.63	

* Mann–Whitney test; SD – standard deviation.

Table 2. Final chromogranin A (CgA) value [ng/mL] depending on grading

Grading	Final CgA value [ng/mL]								p-value*
	n	mean	SD	median	min	max	Q1	Q3	
G1	19	755.14	218.33	321.34	200.76	2254.74	260.56	366.67	p < 0.001
G2	22	3486.88	1241.35	2514.14	65.43	9876.34	1230.38	5612.95	

* Mann–Whitney test; SD – standard deviation.

Table 3. Mean chromogranin A (CgA) value [ng/mL] depending on the degree of liver involvement

Liver involvement degree	Mean CgA value [ng/mL]								p-value*
	n	mean	SD	median	min	max	Q1	Q3	
10%	23	394.44	120.51	219.52	127.86	820.77	176.79	253.04	p < 0.001
25%	18	1770.63	404.11	1655.67	198.23	3801.5	745.87	2684.41	

* Mann–Whitney test; SD – standard deviation.

Table 4. Final chromogranin A (CgA) value [ng/mL] depending on the degree of liver involvement

Liver involvement degree	Final CgA value [ng/mL]								p-value*
	n	mean	SD	median	min	max	Q1	Q3	
10%	23	566.86	285.44	321.23	65.43	2793.61	240.43	366.67	p < 0.001
25%	18	4123.44	1874.7	3886.72	432.67	9876.34	1788.93	5673.98	

* Mann–Whitney test; SD – standard deviation.

Table 5. Mean chromogranin A (CgA) value [ng/mL] vs stage of disease

Stage of disease	Mean CgA value [ng/mL]								p-value*
	n	mean	SD	median	min	max	Q1	Q3	
PD	21	1620.78	385.55	1465.06	198.23	3801.5	688.82	2264.51	p < 0.001
StD	20	230.36	106.44	196.78	127.86	587.86	172.12	231.52	

* Mann–Whitney test; PD – progressing disease; StD – stable disease; SD – standard deviation.

Table 6. Final chromogranin A (CgA) value [ng/mL] compared to the stage of disease

Stage of disease	Final CgA value [ng/mL]								p-value*
	n	mean	SD	median	min	max	Q1	Q3	
PD	21	3841.95	750.79	2793.61	432.67	9876.34	1677.42	5673.23	p < 0.001
SD	20	328.91	99.33	293.2	65.43	1010.16	236.02	321.79	

* Mann–Whitney test; PD – progressing disease; StD – stable disease; SD – standard deviation.

had a mean level of 328.91 ±99.33 ng/mL, which was markedly lower than in the group with a progressing disease, where the values were 3841.95 ±750.79 ng/mL (p < 0.001; Table 6). Also, among the patients with disease progression, the CgA doubling time was 15.71 ±7.28 months, whereas in the group with a stable disease it was considerably shorter: 41.40 ±8.46 months.

Discussion

Advances in the diagnostics and treatment of NENs has led to increased interest in these rare tumors. Assessment of secretory activity in NENs constitutes an important element in the monitoring and assessment of treatment. Our study assessed CgA values in patients with carcinoid syndrome being treated with SSAs, according to the degree of neoplasm histological maturity, the stage of the disease and the degree of liver involvement from metastatic lesions. In the group of patients with G1 tumors (n = 19), both the mean and the final CgA values were significantly lower than in the G2 group (n = 22). According to the analysis, the patients with 25% liver involvement had significantly higher CgA concentration, for both mean and final values, than the patients with 10% liver involvement.

Chromogranin A is a major non-specific biochemical marker which can be tested for in the blood as a circulating tumor marker; its level depends on the type of cells and secretory granules. In their meta-analysis, Zatelli et al. presented the levels of CgA in a group of 123 patients diagnosed with a NEN as the major marker in the monitoring of treatment and prognosis. In their conclusions, the authors emphasized that CgA values are proportionate to the size of the primary site and the number of metastases in the liver. The specificity of CgA measurements is estimated to be 90%, while the sensitivity is 68% relative to the severity of the disease.[16] Donica et al., who examined the level of CgA in a group of 41 patients with highly differentiated midgut NENs, reported that the highest CgA concentrations were found in patients with carcinoid syndrome and numerous metastatic lesions in the liver.[17] Rossi et al., in a study on 91 patients with midgut NENs, demonstrated that a marked increase of CgA precedes by approx. 6 months a disease progression which is detectable with radiography.[18] These studies prove that monitoring biochemical markers constitutes an independent prognostic index of the possible disease progression. Similar observations have been documented by Cheng et al., where an increase in CgA level among 122 patients with NENs was associated with later progression in imaging tests.[19]

The observations of Ardill et al. are also noteworthy: they reported that neurokinin A is a more sensitive marker for the monitoring of carcinoid syndrome than CgA or 5-HIAA.[20] In a group of 523 patients with a NEN of the small bowel, elevated values of neurokinin A were found in as many as 72.6% of cases.

In the current study, we also performed an analysis of CgA measurements depending on the stage of the disease. Among the patients whose disease was found to be progressing during SSA treatment (n = 21), the mean CgA values were statistically significantly higher than in the group with a stable form of the disease. It should also be noted that among patients with disease progression, the CgA doubling time was 15.71 months, whereas in the group with stable disease, it was considerably shorter, amounting to 41.40 months. Similar observations were made by Tang et al., in a study determining the risk factors of disease progression: the doubling time of CgA concentration in patients with midgut NENs is an important prognostic element.[21] Similar relationships were observed in the assessment of serotonin and 5-HIAA concentrations.[22] Raoof et al. presented an assessment of CgA concentration in patients with non-secreting pancreatic NENs as the predictive factor for the decision of whether to treat surgically. Patients with lesions measuring less than 2 cm in the pancreas and with high CgA levels should be treated surgically.[23,24] Likewise, Rossi et al. reported that levels of CgA circulating in the blood are important in the assessment of disease recrudescence and progression, but considerably less so in differential diagnosis.[25]

It is currently known that the highest CgA values are found in NENs of the small bowel, large bowel and pancreas. The highest values have been recorded in carcinoid syndrome with numerous liver metastases. In these assays, the test sensitivity was 85.8% and the specificity 98.5%.[26–28] Oberg and Modlin presented completely new NEN biomarkers in the form of circulating gene transcriptors, micro-RNA or the neoplastic cells themselves originating from the tumor. The sensitivity and specificity of these measurements is significantly higher than CgA measurement.[29–33] Corsello et al. also presented in their study that the CgA 1-76 fragment, known as vasostatin 1 (VS-1), is a more sensitive marker independent of the use of proton pump inhibitors (PPIs).[34] Somatostatin analogue treatment reduces CgA concentrations considerably, particularly in patients with carcinoid syndrome, by inhibiting the synthesis and release of CgA from tumor cells and not by reducing tumor mass. In the case of progressing disease during SSA treatment, elevated CgA concentration may reflect a lack of control over the tumor secretion activity or growth.[35,36] Somatostatin analogues demonstrate an antiproliferative action (cytotoxic or cytostatic), which exerts a direct inhibiting influence on angiogenesis and the induction of apoptosis. Most patients had abnormal fasting blood glucose levels when using SSAs. In rare cases, patients developed non-insulin-dependent diabetes. Gallstones and dyspepsia associated with a suppression of pancreatic exocrine function are common.

The results of the CLARINET study, which concerned the use of lanreotide autogel in NENs, confirmed the antiproliferative effect of SSAs. The study involved 204 patients with NENs of grades 1 and 2 (Ki-67 < 10%), hormonally non-functioning, with the primary site in the pancreas (45%), midgut (36%), hindgut (7%), or unknown (13%); there was >25% liver involvement in 33% of the patients. The two-year treatment with 120 mg of lanreotide autogel every 4 weeks demonstrated no disease progression or death in 62% of the treated patients, compared with 22% of patients administered a placebo.[37]

Similar results were obtained in the PROMID study, which used octreotide LAR in patients with midgut G1 neoplasm. In the group of patients administered the drug, the median of progression-free survival time (PFS) was 14.3 months, whereas in the placebo group it was 6.2 months. This study found that the use of octreotide LAR at a dosage of 30 mg for 18 months led to a lack of disease progression in 67% of patients.[38] Treatment with long-acting SSAs is the treatment of choice in the case of carcinoid syndrome symptoms.

Conclusions

It should be mentioned that despite the fact that CgA is not a perfect biomarker, it remains an important element in the diagnostics and monitoring of treatment of NEN patients.

ORCID iDs

Paweł Gut https://orcid.org/0000-0002-1661-175X
Agata Czarnywojtek https://orcid.org/0000-0003-3595-8449
Marek Ruchała https://orcid.org/0000-0002-6296-7220

References

1. Nehar D, Lombard Bohas C, Olivieri S. Interest of chromogranin A for diagnosis and follow-up of endocrine tumors. *Clin Endocrinol (Oxf)*. 2004;60(5):644–652.
2. Glinicki P, Jeske W. Chromogranin A (CgA): Characteristics of available research methods and conditions that may affect the results obtained [in Polish]. *Endokrynol Pol*. 2009;60(5):415–419.
3. Glinicki P, Jeske W. Chromogranin A (CgA): The influence of various factors in vivo and in vitro and existing disorders on its concentration in blood. *Endokrynol Pol*. 2010;61(4):384–387.
4. Nobels FR, Kwekkeboom DJ, Coopmans W, et al. Chromogranin A as serum marker for neuroendocrine neoplasia: Comparison with neuron-specific enolase and the alpha subunit of glycoprotein hormones. *J Clin Endocrinol Metab*. 1997;82(8):2622–2628.
5. Bilek R, Safarik L, Ciprova V, Vlcek P, Lisá L. Chromogranin A, a member of neuroendocrine secretory proteins, as a selective marker for laboratory diagnosis of pheochromocytoma. *Physiol Res*. 2008;57(Suppl 1): S171–S179.
6. O'Connor DT, Pandian MR, Carlton E, Cervenka JH, Hslao RJ. Rapid radioimmunoassay of circulating chromogranin A: In vitro stability, exploration of the neuroendocrine character of neoplasia, and assessment of the effects of organ failure. *Clin Chem*. 1989;35(8): 1631–1637.
7. Waldum HL, Syversen U. Serum chromogranin A in the control of patients on long-term treatment with inhibitors of acid secretion. *Eur J Clin Invest*. 2001;31(9):741–743.
8. Gut P, Czarnywojtek A, Fischbach J, et al. Chromogranin A – unspecific neuroendocrine marker: Clinical utility and potential diagnostic pitfalls. *Arch Med Sci*. 2016;12(1):1–9.
9. Glinicki P, Kapuścińska R, Jeske W. The differences in chromogranin A concentrations measured in serum and in plasma by IRMA and ELISA methods. *Endokrynol Pol*. 2010;61(4):346–350.
10. Kos-Kudła B. Treatment of neuroendocrine tumors: New recommendations based on the CLARINET study. *Contemp Oncol (Pozn)*. 2015; 19(5):345–349.
11. Kunikowska J, Królicki L, Sowa-Staszczak A, Pawlak D, Hubalewska-Dydejczyk A, Mikołajczak R. Nephrotoxicity after PRRT: Still a serious clinical problem? Renal toxicity after peptide receptor radionuclide therapy with 90Y-DOTATATE and 90Y/177Lu-DOTATATE. *Endokrynol Pol*. 2013;64(1):13–20.
12. Kos-Kudła B, Bolanowski M, Handkiewicz-Junak D, Jarząb B. Diagnostic and therapeutic guidelines for gastrointestinal neuroendocrine tumors (recommended by the Polish Network of Neuroendocrine Tumors). *Endokrynol Pol*. 2008;59(1):41–56.
13. Foltyn W, Zajęcki W, Marek B, et al. The value of the Ki-67 proliferation marker as a prognostic factor in gastroenteropancreatic neuroendocrine tumours. *Endokrynol Pol*. 2012;63(5):362–366.
14. Fischbach J, Gut P, Matysiak-Grześ M, et al. Combined octreotide and peptide receptor radionuclide therapy ((90)Y-DOTA-TATE) in case of malignant insulinoma. *Neuro Endocrinol Lett*. 2012;33(3): 273–278.
15. Stridsberg M, Eriksson B, Oberg K, Janson ET. A comparison between three commercial kits for chromogranin A measurenents. *J Endocrinol*. 2003;177(2):337–341.
16. Zatelli MC, Torta M, Leon A, et al; Italian CromaNet Working Group. Chromogranin A as a marker of neuroendocrine neoplasia: An Italian Multicenter Study. *Endocr Relat Cancer*. 2007;14(2):473–482.
17. Donica H, Malecha-Jędraszek A, Strosławska E, Burska A, Szubstarski F. Significance of plasma chromogranin A determination in neuroendocrine tumour (NET) diagnosis. *Folia Histochem Cytobiol*. 2010; 48(4):603–610.
18. Rossi RE, Garcia-Hernandez J, Meyer T, et al. Chromogranin A as a predictor of radiological disease progression in neuroendocrine tumours. *Ann Transl Med*. 2015;3(9):118.
19. Cheng Y, Sun Z, Bai C, et al. Serum chromogranin A levels for the diagnosis and follow-up of well-differentiated non-functioning neuroendocrine tumors. *Tumour Biol*. 2016;37(3):2863–2869.

20. Ardill JE, Armstrong L, Smye M, Doherty R, McCance DR, Johnston BT. Neuroendocrine tumours of the small bowel: Interpretation of raised circulating chromogranin A, urinary 5 hydroxy indole acetic acid and circulating neurokinin A. *QJM*. 2016;109(2):111–115.
21. Tang C, Gong L, Zou W, et al. Multivariate analysis of metastasis-related risk factors for patients with gastroenteropancreatic neuroendocrine tumors based on clinicopathological and endoscopic features. *Oncol Rep*. 2016;36(6):3343–3352.
22. Allen KR, Degg TJ, Anthoney DA, Fitzroy-Smith D. Monitoring the treatment of carcinoid disease using blood serotonin and plasma 5-hydroxyindoleacetic acid: Three case examples. *Ann Clin Biochem*. 2007;44(Pt 3):300–307.
23. Raoof M, Jutric Z, Melstrom LG, et al. Prognostic significance of chromogranin A in small pancreatic neuroendocrine tumors. *Surgery*. 2018;165(4):760–766.
24. Jun E, Kim SC, Song KB, et al. Diagnostic value of chromogranin A in pancreatic neuroendocrine tumors depends on tumor size: A prospective observational study from a single institute. *Surgery*. 2017; 162(1):120–130.
25. Rossi RE, Ciafardini C, Sciola V, Conte D, Massironi S. Chromogranin A in the follow-up of gastroenteropancreatic neuroendocrine neoplasms: Is it really game over? A systematic review and meta-analysis. *Pancreas*. 2018;47(10):1249–1255.
26. Hofland J, Zandee WT, de Herder WW. Role of biomarker tests for diagnosis of neuroendocrine tumours. *Nat Rev Endocrinol*. 2018; 14(11):656–669.
27. Lyubimova NV, Churikova TK, Kushlinskii NE. Chromogranin as a biochemical marker of neuroendocrine tumors. *Bull Exp Biol Med*. 2016; 160(5):702–704.
28. Di Giacinto P, Rota F, Rizza L, et al. Chromogranin A: From laboratory to clinical aspects of patients with neuroendocrine tumors. *Int J Endocrinol*. 2018;2018:8126087.
29. Oberg K, Modlin IM, De Herder W, et al. Consensus on biomarkers for neuroendocrine tumour disease. *Lancet Oncol*. 2015;16(9):435–446.
30. Modlin IM, Oberg K, Taylor A, Drozdov I, Bodei L, Kidd M. Neuroendocrine tumor biomarkers: Current status and perspectives. *Neuroendocrinology*. 2014;100(4):265–277.
31. Genç CG, Jilesen APJ, Nieveen van Dijkum EJM, et al. Measurement of circulating transcript levels (NETest) to detect disease recurrence and improve follow-up after curative surgical resection of well-differentiated pancreatic neuroendocrine tumors. *J Surg Oncol*. 2018; 118(1):37–48.
32. Modlin IM, Kidd M, Malczewska A, et al. The NETest: The clinical utility of multigene blood analysis in the diagnosis and management of neuroendocrine tumors. *Endocrinol Metab Clin North Am*. 2018; 47(3):485–504.
33. Malczewska A, Bodei L, Kidd M, Modlin IM. Blood mRNA measurement (NETest) for neuroendocrine tumor diagnosis of image-negative liver metastatic disease. *J Clin Endocrinol Metab*. 2019;104(3): 867–872.
34. Corsello A, Di Filippo L, Massironi S, et al. Vasostatin-1: A novel circulating biomarker for ileal and pancreatic neuroendocrine neoplasms. *PLoS One*. 2018;13(5):e0196858. doi:10.1371/journal.pone.0196858
35. Kruljac I, Vurnek I, Maasberg S, et al. A score derived from routine biochemical parameters increases the diagnostic accuracy of chromogranin A in detecting patients with neuroendocrine neoplasms. *Endocrine*. 2018;60(3):395–406. doi:10.1007/s12020-018-1592-6
36. Tseng CM, Cheng TY, Chen TB, et al. Low accuracy of chromogranin A for diagnosing early-stage pancreatic neuroendocrine tumors. *Oncol Lett*. 2018;15(6):8951–8958. doi:10.3892/ol.2018.8472
37. Caplin ME, Pavel M, Ćwikła JB, et al. Anti-tumour effects of lanreotide for pancreatic and intestinal neuroendocrine tumours: The CLARINET open-label extension study. *Endocr Relat Cancer*. 2016;23(3):191–199.
38. Arnold R, Müller H, Schade-Brittinger C, et al; PROMID Study Group. Placebo-controlled, double-blind, prospective, randomized study of the effect of octreotide LAR in the control of tumor growth in patients with metastatic neuroendocrine midgut tumors: A report from the PROMID study group. *J Clin Oncol*. 2009; 27(28):4656–4663.

Cerebral oxygenation and circulatory parameters during pressure-controlled vs volume-targeted mechanical ventilation in extremely preterm infants

Michalina Bugiera[1,B–D,F], Tomasz Szczapa[1,A,D–F], Anna Sowińska[2,C,F], Charles Christoph Roehr[3,E,F], Marta Szymankiewicz-Bręborowicz[1,A,E,F]

[1] Department of Neonatology, Poznan University of Medical Sciences, Poland
[2] Department of Computer Science and Statistics, Poznan University of Medical Sciences, Poland
[3] Newborn Services, John Radcliffe Hospital, Oxford University Hospitals NHS Foundation Trust, United Kingdom

A – research concept and design; B – collection and/or assembly of data; C – data analysis and interpretation; D – writing the article; E – critical revision of the article; F – final approval of the article

Advances in Clinical and Experimental Medicine, ISSN 1899–5276 (print), ISSN 2451–2680 (online) *Adv Clin Exp Med*. 2020;29(11):1325–1329

Address for correspondence
Michalina Bugiera
E-mail: michalina.bugiera@gmail.com

Funding sources
None declared

Conflict of interest
None declared

Received on August 14, 2020
Reviewed on September 10, 2020
Accepted on October 7, 2020

Abstract

Background. Respiratory distress syndrome (RDS) is the most common cause of respiratory failure of infants born prematurely with very low birth weight (VLBW). Essential elements of RDS management include ventilatory support and endotracheal administration of a surfactant.

Objectives. To assess the effect of volume-targeted compared to pressure-controlled mechanical ventilation (MV) on circulatory parameters and cerebral oxygenation StO_2 in extremely preterm infants.

Material and methods. This prospective, cross-over trial enrolled neonates born before 28 weeks of gestation. The patients were ventilated for 3 h in pressure-controlled assist-control (PC-AC) mode, followed by 3 h of volume-guarantee assist-control ventilation (VG-AC). Pulse oximetry (saturation (SpO_2) and heart rate (HR)), near-infrared spectroscopy (NIRS), StO_2, and electrical cardiometry (EC) were used in monitoring of the patients.

Results. Twenty preterm infants with a mean gestational age of 26 weeks were studied. The patients' mean postnatal age was 7.7 days. The SpO_2 values and HR were comparable during PC-AC and VG-AC. The mean values of peak inspiratory pressure (PIP), mean airway pressure (MAP) and expiratory tidal volume (VT_E) were lower, while the respiratory rate (RR) was higher during PC-VG. There were no significant differences in the mean values of StO_2, but based on a comparison of the standard deviations (SD) the StO_2 variability was significantly lower during VG-AC. The circulatory parameters were comparable.

Conclusions. The StO_2 is more stable during VG than PC ventilation. These findings support the use of VG mode in premature infants.

Key words: respiratory distress syndrome, volume-targeted ventilation, preterm infant, cerebral oxygenation, electrical cardiometry

Cite as
Bugiera M, Szczapa T, Sowińska A, Roehr CC, Szymankiewicz-Bręborowicz M. Cerebral oxygenation and circulatory parameters during pressure-controlled vs volume-targeted mechanical ventilation in extremely preterm infants. *Adv Clin Exp Med*. 2020;29(11):1325–1329. doi:10.17219/acem/128198

DOI
10.17219/acem/128198

Introduction

Respiratory distress syndrome (RDS) is the most common cause of respiratory failure in infants born prematurely with a very low birth weight (VLBW).[1] Its course may also influence other important complications of prematurity, such as intraventricular hemorrhage (IVH) or periventricular leukomalacia.[2] Essential elements of RDS management include ventilatory support and endotracheal administration of a surfactant.[1] The aim of mechanical ventilation (MV) is to ensure adequate gas exchange while avoiding lung injury.[3] Neonatal MV can be provided using pressure-controlled (PC) or volume-targeted modes (VTV) such as volume-guarantee (VG), pressure-regulated volume control (PRVC) or volume-controlled ventilation (VCV). Historically, PC ventilation that directly controls inspiratory pressure used to be the standard mode for preterm infants until technology advanced enough to allow accurate delivery of small expiratory tidal volumes (VT_E) using VTV. A meta-analysis conducted in 2017 presented the advantages of VTV over PC ventilation in the treatment of acute respiratory failure of newborns. Its use is associated with a reduced risk of death or bronchopulmonary dysplasia (BPD) and a reduction in the occurrence of pneumothorax, IVH stage III or IV, and periventricular leukomalacia.[4] According to the European Consensus Guidelines on the Management of RDS 2019, VTV is the preferred mode of ventilation because it enables clinicians to ventilate with less variable VT_E and to lower the pressure in real time as lung compliance improves.[1] Despite the reported benefits and recommendations, VTV is not used routinely in every neonatal intensive care unit (NICU). One recent study conducted in Italy reported that VTV was chosen during the acute phase of RDS in only 27% of 113 tertiary NICUs, while in 45% of them this mode was only set during the weaning phase.[5] The knowledge of the physiological effects of VTV is incomplete; therefore, the aim of this study was to assess the effects of VG ventilation on circulation and cerebral oxygenation (StO_2) in extremely premature infants.

Material and methods

This prospective crossover study was conducted at the Department of Neonatology of Poznan University of Medical Sciences, Poland, after approval from the Bioethical Committee (decision No. 388/16). Premature infants born before 28 weeks of gestation were enrolled in the study with written parental consent when the following criteria were met: 1) respiratory failure in the course of RDS requiring MV, 2) stable condition with pH > 7.2 and pCO_2 < 60 mm Hg in the blood gas analysis, and 3) no identified genetic syndromes or serious congenital malformations.

The study was carried out after initial stabilization when no other interventions that could influence the ventilatory status had been performed (e.g., surfactant administration, rescue high-frequency ventilation, pneumothorax, or surgical treatment). In each newborn, pressure controlled assist-control (PC-AC) ventilation was carried out for 3 h followed by AC VG ventilation for 3 h using a Dräger Babylog VN500 ventilator (Drägerwerk AG, Lübeck, Germany). The VT_E was set in the range of 4–6 mL/kg, aiming for the values observed during PC ventilation. The FiO_2 was titrated manually to keep the peripheral oxygen saturation (SpO_2) in the range of 90–95%.

During the study, StO_2 was measured using a near-infrared spectroscopy (NIRS) monitor (NONIN SenSmart X-100; Nonin Medical Inc., Plymouth, USA) with the pediatric sensor (EQUANOX Advance; Nonin Medical Inc.) placed on the patient's forehead. A pulse oximetry module integrated with the NIRS oximeter was used simultaneously to assess heart rate (HR) and SpO_2 which allowed the fractional oxygen extraction to be calculated ($FOE = (SpO_2 - StO_2)/SpO_2$).[6]

Continuous, non-invasive monitoring of hemodynamic parameters, such as stroke volume (SV), cardiac output (CO), stroke index (SI), cardiac index (CI), stroke volume variation (SVV), and index of contractility (ICON), was performed using electrical cardiometry (EC) with 4 electrocardiography (ECG) electrodes placed on the left side of the infant's body (ICON; Osypka Medical, La Jolla, USA).

The Shapiro–Wilk test, Student's t-test, and the Wilcoxon test were used in the statistical analysis (STATISTICA v. 12; StatSoft, Inc., Tulsa, USA) with p-values <0.05 considered significant.

Results

Twenty-five neonates were included in the study. Four patients had to be excluded due to the poor quality of the records and 1 due to prenatal exposure to methamphetamine (confirmed in the urine test). All patients received surfactant replacement therapy after birth. Data from 20 newborns was included in the final analysis. The patients' demographic and clinical parameters are presented in Tables 1 and 2.

The expiratory minute volumes (MV_E) were comparable during PC and VG ventilation. With VG ventilation, mean airway pressure (MAP) and peak inspiratory pressure (PIP) were significantly reduced, whereas the standard deviation (SD) of MAP and PIP were higher in VG mode. A lower VT_E was delivered at higher respiratory rates (RRs) during VG ventilation (Table 3).

No significant differences in mean StO_2 values were found between PC and VG ventilation (Table 4), though the StO_2 SD was significantly higher during the PC mode, suggesting higher variability (Fig. 1).

The mean values and SD of hemodynamic parameters were not significantly different during PC and VG ventilation (Table 5). Mean values of HR were similar during both modes of ventilation, but there was a trend for lower variability of this parameter during the VG ventilation.

Table 1. Characteristics of the study group

Parameter	Mean	Median	Standard deviation	Minimum	Maximum
Gestational age [weeks]	25 4/7	25 3/7	1	24 4/7	27 6/7
Body weight [g]	848	803	138	620	1070
Postnatal age [days]	7.7	5.5	5.3	2	21
Surfactant doses	1.6	1	0.7	1	3
Starting FiO_2	0.27	0.24	0.08	0.21	0.5

Table 2. Selected perinatal data and complications in the study group

Parameter	Value
Age of the mother [years] [mean; range]	30; 19–41
Pregnancy-induced hypertension (n, %)	1; 5%
Prenatal steroids (n, %)	16; 80%
Cesarean section (n, %)	13; 65%
Premature rapture of membranes (n, %)	8; 40%
Early onset sepsis (n, %)	2; 10%
Pneumothorax (n, %)	1; 5%
Pulmonary interstitial emphysema (n, %)	3; 15%
Pulmonary hypertension (n, %)	1; 5%
Bronchopulmonary dysplasia (n, %)	19; 95%
Patent ductus arteriosus requiring treatment (n, %)	11; 55%
Severe intraventricular hemorrhage (grades III–IV) (n, %)	3; 15%
Retinopathy of prematurity requiring treatment (n, %)	9; 45%
Death before discharge (n, %)	2; 10%

Discussion

The purpose of the study was to investigate the effect of VG ventilation on StO_2 and cardiac function in extremely premature infants. We found that while cardiac parameters were similar with both modes of ventilation, StO_2 was more stable during VTV.

The challenging aspects of MV in premature infants include the high RR, the low and rapidly changing lung compliance, and the very short inspiratory time and small VT_E in combination with a relatively large gas leakage and dead space volume.[7] The prevailing influence of volutrauma over barotrauma on the risk of ventilator-induced lung injury (VILI) in neonates confirmed in animal models and in clinical trials make VTV the preferred "lung-protective" strategy of MV.[3]

The results confirm the beneficial respiratory effects of VTV. As in previous studies, VG ventilation provided

Table 3. Ventilation parameters during PC and VG ventilation

Parameter		PC	VG	p-value
RR [1/min]	mean	49	53	<0.02
	SD	7.6	10.7	ns
PIP [mbar]	mean	18.3	16.7	<0.0001
	SD	2.9	3.2	<0.00001
MAP [mbar]	mean	8.7	8.4	<0.01
	SD	1.1	1.3	<0.01
MV_E [L/min]	mean	0.25	0.25	ns
	SD	0.07	0.08	<0.001
VT_E [mL/kg]	mean	6.1	5.8	<0.04
	SD	1.2	1.1	<0.0001

RR – respiratory rate; PIP – peak inspiratory pressure; MAP – mean airway pressure; MV_E – expiratory minute volume; VT_E – expiratory tidal volume; SD – standard deviation; ns – not significant.

Table 4. Cerebral oxygenation, peripheral oxygen saturation and fractional oxygen extraction during PC and VG ventilation

Parameter		PC	VG	p-value
StO_2 (%)	mean	80.7	80.4	ns
	SD	2.7	2.2	p < 0.01
SpO_2 (%)	mean	93.7	93.3	ns
	SD	2.8	2.6	ns
FOE	mean	0.14	0.14	ns
	SD	0.04	0.04	ns

SD – standard deviation; ns – not significant; StO_2 – cerebral oxygenation; SpO_2 – peripheral oxygen saturation; FOE – fractional oxygen extraction.

Table 5. Hemodynamic parameters during PC and VG ventilation

Parameter		PC	VG	p-value
Heart rate [1/min]	mean	140	145	ns
	SD	5.1	4.6	ns
Stroke volume [mL]	mean	1.7	1.6	ns
	SD	0.14	0.13	ns
Cardiac output [L/min]	mean	0.24	0.23	ns
	SD	0.06	0.06	ns
Index of contractility	mean	115	115	ns
	SD	23	18	ns
Stroke index [mL/m^2]	mean	19	19.5	ns
	SD	1.6	1.7	ns
Cardiac index [L/min/m^2]	mean	2.8	2.9	ns
	SD	0.4	0.4	ns
Stroke volume variation (%)	mean	14	13	ns
	SD	3.8	5.4	ns

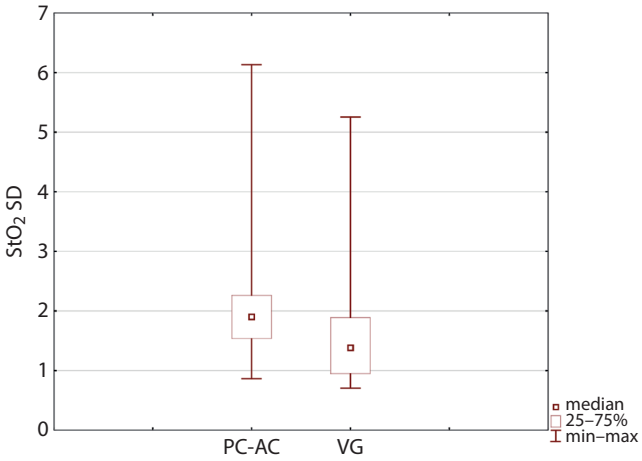

Fig. 1. Standard deviation of StO_2 during PC and VG ventilation

patients with more stable ventilation and lower airway pressures (PIP and MAP).[8] Lower V_T values during VG ventilation with an MV_E similar to the PC ventilation period may explain the increase in RR. The lower variability of MV_E during VG mode suggests a more balanced ventilation.

Continuous measurement of StO_2 has been used to identify newborns with a higher risk of brain damage.[9] The StO_2 levels that are either too high or too low have been identified as risk factors for cerebral injury.[10] Our results have shown no statistically significant differences between the mean values of StO_2 and FOE during PC when compared to VG ventilation, which is similar to the findings of a small pilot study that compared PC synchronized intermittent ventilation (SIMV) with VG SIMV.[11] In both groups, the mean StO_2 was about 80%, which is in the upper range of values considered to be normal in the neonate.[12] However, we found that the StO_2 variability was significantly lower during VG ventilation. The more stable StO_2 during the VTV mode could be attributed to more stable ventilation, as CO_2 is an important regulator of cerebral blood flow.[13,14] The association between CO_2 fluctuations and StO_2 is well-known in preterm neonates. An acute increase in CO_2 may result in increased StO_2 with decreased electrical activity, while hypocapnia has an opposite effect and increases FOE.[15,16] The significantly higher variability of StO_2 was previously reported in preterm infants with RDS when compared to without RDS.[2] Hence, VG ventilation in this group of patients would be expected to provide an important "brain-protective" effect by better stabilizing the cerebral brain fluid. Data from clinical trials and meta-analyses confirm this assumption, showing a significantly lower risk of IVH in patients ventilated using VTV modes.[17]

Mechanical ventilation with VG is thought to facilitate a more constant ventilation-to-perfusion ratio, which should translate into improved clinical stability, including StO_2 as well as hemodynamic parameters. The stable volume of breath administered with each inspiration causes less distension of the lungs, resulting in more constant venous return to the left atrium. To our knowledge, this is the first study that compared hemodynamic parameters between PC and VG modes of MV by the means of EC. It is a non-invasive method that evaluates cardiac function based on modified thoracic electrical bioimpedance. The measurement is based on the relationship between the change in tissue resistance and blood flow through the large arteries.[18] This method employs a very low current of 2–4 mA and a high frequency of 20–100 Hz, which makes it a completely painless and safe method. Numerous comparisons between EC and echocardiography have shown a close correlation of the results, even in very premature newborns.[19,20] The selected hemodynamic parameters were stable throughout the study and no statistically significant differences were found between PC and VG MV.

However, there was a trend for lower variability of HR during VG ventilation. This seems to indicate that VG mode does not have equally significant effects on ventilatory and circulatory status when PC ventilation is carefully monitored and adjusted.

These results should be interpreted with caution due to the limitations of the study, which include the relatively small size of the study group, the limited observation time and the lack of transcutaneous blood gas monitoring, which could provide additional information on the potential link between CO_2 and StO_2 variability.

Our results confirm the beneficial respiratory and cerebral effects of VTV in extremely premature infants. The findings add to the existing evidence supporting the use of VTV modes of ventilation in a neonatal intensive care setting.

ORCID iDs

Michalina Bugiera https://orcid.org/0000-0003-1787-1681
Tomasz Szczapa https://orcid.org/0000-0002-5214-2719
Anna Sowińska https://orcid.org/0000-0001-5319-5057
Charles Christoph Roehr https://orcid.org/0000-0001-7965-4637
Marta Szymankiewicz-Bręborowicz
https://orcid.org/0000-0002-7389-0708

References

1. Sweet DG, Carnielli V, Greisen,G, et al. European Consensus Guidelines on the Management of Respiratory Distress Syndrome – 2019 update. *Neonatology*. 2019;115(4):432–450.
2. Lemmers PM, Toet M, van Schelven LJ, van Bel F. Cerebral oxygenation and cerebral oxygen extraction in the preterm infant: The impact of respiratory distress syndrome. *Exp Brain Res*. 2006;173(3):458–467.
3. Reiterer F, Schaberger B, Freidl T, Schmölzer G, Pichler G, Urlesberger B. Lung-protective ventilatory strategies in intubated preterm neonates. *Paediatr Respir Rev*. 2017;23:89–96.
4. Klingenberg C, Wheeler KI, McCallion N, et al. Volume-targeted versus pressure-limited ventilation in neonates. *Cochrane Database Syst Rev*. 2017;10(10):CD003666.
5. Petrillo F, Gizzi C, Maffei G, et al; Neonatal Pneumology Study Group Italian Society of Neonatology. Neonatal respiratory support strategies for the management of extremely low gestational age infants: An Italian survey. *Ital J Pediatr*. 2019;45(1):44.
6. Pellicer A, Bravo Mdel C. Near-infrared spectroscopy: A methodology-focused review. *Semin Fetal Neonatal Med*. 2011;16(1):42–49.
7. Roumiantsev S. Invasive mechanical ventilation in premature infants: Where do we stand today? *J Pulmon Resp Med*. 2013;2013:S13.
8. Duman N, Tuzun F, Sutcuoglu S, Yesilirmak CD, Kumral A, Ozkan H. Impact of volume guarantee on synchronized ventilation in preterm infants: A randomized controlled trial. *Intensive Care Med*. 2012;38(8):1358–1364.
9. Hyttel-Sorensen S, Greisen G, Als-Nielsen B, Gluud C. Cerebral near-infrared spectroscopy monitoring for prevention of brain injury in very preterm infants. *Cochrane Database Sys Rev*. 2017;9(9):CD011506.
10. Greisen G, Leung T, Wolf M. Has the time come to use near-infrared spectroscopy as a routine clinical tool in preterm infants undergoing intensive care? *Philos Trans A Math Phys Eng Sci*. 2011;369(1955):4440–4451.
11. Dotta A, Crescenzi F, Campi F, et al. Cerebral haemodynamics and lung mechanics in preterm infants during synchronized intermittent mandatory ventilation (SIMV) and synchronized intermittent positive pressure ventilation (SIPPV), with and without volume guaranteed (VG). *Pediatr Res*. 2004;56(3):498.
12. McNeil S, Gatenby JC, McElroy S, Engelhardt B. Normal cerebral, renal and abdominal regional oxygen saturations using near-infrared spectroscopy in preterm infants. *J Perinatol*. 2011;31(1):51–57.
13. Greisen G. Autoregulation of cerebral blood flow in newborn babies. *Early Hum Dev*. 2005;81(5):423–428.
14. Noori S, Anderson M, Soleymani S, Seri I. Effect of carbon dioxide on cerebral blood flow velocity in preterm infants during postnatal transition. *Acta Paediatr*. 2014;103(8):e334–e339.
15. Dix LML, Weeke LC, de Vries LS, et al. Carbon dioxide fluctuations are associated with changes in cerebral oxygenation and electrical activity in infants born preterm. *J Pediatr*. 2017;187:66–72.e1.
16. Kissack CM, Garr R, Wardle SP, Weindling AM. Cerebral fractional oxygen extraction in very low birth weight infants is high when there is low left ventricular output and hypocarbia but is unaffected by hypotension. *Pediatr R*es. 2004;55(3);400–405.
17. van Kaam AH, Rimensberger PC. Lung-protective ventilation strategies in neonatology: What do we know – what do we need to know? *Crit Care Med*. 2007;35(3):925–931.
18. McGovern M, Miletin J. Cardiac output monitoring in preterm infants. *Front Pediatr*. 2018;6:84.
19. Song R, Rich W, Kim JH, Finer NN. The use of electrical cardiometry for continuous cardiac output monitoring in preterm neonates: A validation study. *Am J Perinatol*. 2014;31(12):1105–1110.
20. Grollmuss O, Gonzalez P. Non-invasive cardiac output measurement in low and very low birth weight infants: A method comparison. *Front Peadiatr*. 2014;2:16.

Assessment of orofacial dysfunction in a group of Polish children with unilateral cleft lip and palate: A preliminary report

Natalia Kaczorowska[1,A–E], Patrycja Markulak[2,B,D], Marcin Mikulewicz[1,F]

[1] Department of Dentofacial Orthopedics and Orthodontics, Division of Facial Abnormalities, Wroclaw Medical University, Poland
[2] Department of Dentofacial Orthopedics and Orthodontics, Division of Dentofacial Orthopedics and Orthodontics, Wroclaw Medical University, Poland

A – research concept and design; B – collection and/or assembly of data; C – data analysis and interpretation;
D – writing the article; E – critical revision of the article; F – final approval of the article

Advances in Clinical and Experimental Medicine, ISSN 1899–5276 (print), ISSN 2451–2680 (online) *Adv Clin Exp Med*. 2020;29(11):1331–1336

Address for correspondence
Natalia Kaczorowska
E-mail: nataliakaczorowskaa@gmail.com

Funding sources
None declared

Conflict of interest
None declared

Received on July 26, 2020
Reviewed on September 13, 2020
Accepted on October 6, 2020

Abstract

Background. Cleft lip and palate (CLP) is a genetic and environmental malformation of the face. The resulting interruption of the tissue in the mouth and nasal cavity undoubtedly impairs basic physiological functions, which impacts the quality of life (QoI) of such patients.

Objectives. To assess orofacial dysfunction using the Nordic Orofacial Test-Screening (NOT-S) in a group of Polish children with unilateral CLP (UCLP). The following hypotheses were presented: 1) orofacial dysfunction is more common in children with UCLP and 2) patients with UCLP have a worse QoL than the control group.

Material and methods. Seventy children at the age of 7–13 years took part in the study. The inclusion criterion was a diagnosis of UCLP. The control group (non-UCLP) was matched by gender and age to the cleft group. The research used the NOT-S questionnaire.

Results. In the cleft group, there were statistically significantly more disorders of functions, such as breathing, chewing and swallowing, and drooling; in the NOT-S examination, there were more disorders of the face at rest, facial expression and speech in the cleft group. Comparing the NOT-S total scores, it was found that in the cleft group, there a disorder of at least 1 function was statistically significantly more prevalent than in the control group. Likewise, the median results in the cleft group were 3 points higher than in the control group.

Conclusions. Using the NOT-S survey, it was possible to confirm both hypotheses. Orofacial dysfunction is more common in children with UCLP and this contributes to a worse QoL for them than for children without UCLP.

Key words: quality of life, orthodontics, cleft and lip palate, NOT-S questionnaire

Cite as
Kaczorowska N, Markulak P, Mikulewicz M. Assessment of orofacial dysfunction in a group of Polish children with unilateral cleft lip and palate: A preliminary report. *Adv Clin Exp Med*. 2020;29(11):1331–1336. doi:10.17219/acem/128187

DOI
10.17219/acem/128187

Introduction

Cleft lip and palate (CLP) is a genetic and environmental face malformation.[1] According to WHO data, it occurs once per approx. 1,100 births around the world.[2] Facial deformities include a disruption of soft and hard tissues, and asymmetry. Scientific studies have shown that asymmetry is present not only in the maxilla, but can also apply to the orbital, zygomatic and frontal bones.[3] Dental anomalies among these patients include hypodontia, supernumerary teeth, microdontia, taurodontism, and transposition of teeth,[4] while occlusal disorders are most often cross-bite and class III malocclusion.[5]

There is no doubt that the abovementioned abnormalities affect speech, articulation, chewing, nose function, and facial appearance.[6] In addition, patients with CLP significantly suffer from otitis media.[7] Speech disorders of people with CLP include delayed speech development, articulation disorders and dysphonia. Moreover, in some cases, fluid and food refluxes often occur and swallowing is difficult.[8] However, it should be noted that the negative impact of CLP mainly concerns psychosocial problems.[9]

The amount of research conducted around the world shows that there is an interest in the quality of life (QoL) of patients with CLP. Researchers from Brazil have proven that the effect of CLP on QoL increases with age.[10] Studies conducted in Iran showed that the biggest difference compared to the control group was in difficulty pronouncing words and that the impact on QoL also concerned the patients' families, emphasizing mainly the financial aspect and parental stress.[11] A survey of CLP patients in the Netherlands, on the other hand, showed that gender does not affect QoL among this group.[12] Furthermore, studies in Switzerland involving patients with unilateral CLP (UCLP) showed a worse sleep pattern than in patients without the disorder; it was emphasized, however, that this is not due to CLP, but to psychosocial loads.[13]

Despite the fact that the QoL of people with cleft lips and palates has been studied for many years, there is no standardized test for its assessment. As a result, researchers evaluate various aspects of life and activities in society and use a variety of questions. One such tool is the Nordic Orofacial Test-Screening (NOT-S) survey.[14] The NOT-S has been used to assess the QoL of people with cleft palates,[15] cerebral palsy[16] or ectodermal dysplasia[17] since 2007.

We conducted a survey among the Polish population to study the QoL of patients with UCLP in comparison with a control group. This is the first study to use the NOT-S questionnaire in Poland.

The following hypotheses were proposed:

1. Orofacial dysfunction is more common in children with UCLP.
2. Patients with UCLP have a worse QoL than the control group.

Material and methods

Material

This study was conducted in full accordance with the World Medical Association Declaration of Helsinki and was approved by the Ethics Committee of the Wroclaw Medical University, Poland.

The cleft group (n = 35) comprised of patients of the Department of Maxillofacial Orthopedics and Orthodontics of the Division of Facial Abnormalities at the Wroclaw Medical University. The inclusion criteria were a diagnosis of UCLP (diagnosis code Q37.1 of the ICD10) and an age of 7–13 years. The exclusion criteria were mental retardation, being under 7 or over 13 years of age, and missing teeth not related to tooth replacement. The age of the cleft group was between 7 and 13 years. Before conducting the study, legal guardians were informed about it and were assured about the confidentiality of the data of the children.

The control group, without a diagnosis of CLP (n = 35) and matched in terms of sex and age to the cleft group, were patients of the Division of Maxillofacial Orthopedics and Orthodontics at the Wroclaw Medical University.

Methods

The study used the NOT-S survey after it was translated into Polish by the researchers. The children were examined by the same trained examiner according to the same protocol. Each survey contained data on age, gender, diagnostic code (ICD-10), examination position, and position of the head when seated. The interview reflected 6 domains: I) sensory function, II) breathing, III) habits, IV) chewing and swallowing, V) drooling, and VI) dryness of the mouth. The examination contains sections: 1) the face at rest and tasks regarding 2) nose breathing, 3) facial expression, 4) masticatory muscle and jaw function, 5) oral motor function, and 6) speech. Each of these domains contains from 1 to 5 components for which the patients' responses or examination results were recorded: X = yes, 0 = no, or (–) = not assessed. If there was 1 or more X answers in a section, the researchers placed a score of 1 in the domain. The results were recorded at the time the survey was conducted on pre-printed NOT-S forms. The total possible NOT-S score ranges from 0 to 12 points. The higher the score, the more severe the orofacial dysfunction and the worse the QoL.

Statistical analysis

Statistical analysis was performed using STATISTICA v. 13 (StatSoft Inc., Tulsa, USA). For measurable variables, the mean, median (Me), upper and lower quartile, and range of variability (extreme values – minimum (Min) and maximum (Max)) were calculated. The frequency

of occurrence (percent) was calculated for qualitative variables. All quantitative variables were checked with the Shapiro–Wilk test to determine the type of distribution. The qualitative variables between groups (cleft compared to the control) were compared using the two-tailed Fisher's exact test. The quantitative variables between groups were compared using the Mann–Whitney U test. The level of $\alpha = 0.05$ was used for all comparisons.

Results

Table 1 presents a comparison of the frequency of a particular function based on the NOT-S between the cleft group (n = 35) and the control group (n = 35). The 1st part presents the results from the 6 sections assessed with NOT-S interviews: sensory functions, breathing, habits, chewing and swallowing, drooling, and dryness of the mouth. The 2nd part contains the results from the 6 NOT-S examination sections: face at rest, nose breathing, facial expression, masticatory muscle and jaw function, oral motor function, and speech. The 3rd part is the summary of the entire test (NOT-S total score).

In the NOT-S interview, it was observed that disorders of functions such as breathing, drooling, chewing, and swallowing were statistically significantly more prevalent in the cleft group. In the cleft group, breathing disorders were found in almost 46% (n = 16) of the study participants, while in the control group, this figure was 11.4 (n = 4; p = 0.003). Disorders of the next 2 functions were also more common in the cleft group: disorders of chewing and swallowing function were noted in 51.4% of patients (n = 18 compared to the control group: 8.6%; n = 3; p < 0.001), and drooling in 25.7% (n = 9 compared to the control group: 2.9%; n = 1; p = 0.013). In addition, the summaries of the interview part were compared. The number

Table 1. Comparison of the frequency of selected function disorders based on NOT-S between the cleft group and the control group

Nordic Orofacial Test		Cleft group (n = 35)		Control group (n = 35)		p-value*
		n	%	n	%	
I. NOT-S interview						
Sensory function	0 1	32 3	91.4 8.6	35 –	100 –	0.23
Breathing	0 1	19 16	54.3 45.7	31 4	88.6 11.4	0.003
Habits	0 1	17 18	48.6 51.4	25 10	71.4 28.6	0.087
Chewing and swallowing	0 1	17 18	48.6 51.4	32 3	91.4 8.6	<0.001
Drooling	0 1	26 9	74.3 25.7	34 1	97.1 2.9	0.013
Dryness of the mouth	0 1	25 10	71.4 28.6	32 3	91.4 8.6	0.062
NOT-S interview – total score	0 ≥1	2 33	5.7 94.3	16 19	45.7 54.3	<0.001
II. NOT-S examination						
Face at rest	0 1	12 23	34.3 65.7	31 4	88.6 11.4	<0.001
Nose breathing	0 1	32 3	91.4 8.6	35 –	100 –	0.24
Facial expression	0 1	5 30	14.3 85.7	34 1	97.1 2.9	<0.001
Masticatory muscle and jaw function	0 1	33 2	94.3 5.7	35 –	100 –	0.49
Oral motor function	0 1	33 2	94.3 5.7	35 –	100 –	0.49
Speech	0 1	10 25	28.6 71.4	32 3	91.4 8.6	<0.001
NOT-S examination – total score	0 ≥1	0 35	0 100	27 8	77.1 22.9	<0.001
III. NOT-S – Total score						
Total score	0 ≥1	0 35	0 100	11 24	31.4 68.6	<0.001

NOT-S – Nordic Orofacial Test-Screening; 0 – non-affected; 1 – affected; n – number of participants; *two-tailed Fisher's exact test.

Table 2. Comparison of the total results of NOT-S between the cleft group and the control group

Nordic Orofacial Test	Cleft group (n = 35)					Control group (n = 35)					p-value*
	Me	Q1	Q3	Min	Max	Me	Q1	Q3	Min	Max	
NOT-S interview – total score	2	1	3	0	5	1	0	1	0	2	<0.001
NOT-S examination – total score	2	2	3	1	4	0	0	0	0	1	<0.001
NOT-S – Total score	4	4	5	2	8	1	0	1	0	2	<0.001

NOT-S – Nordic Orofacial Test-Screening; Me – median; Q1 – lower quartile; Q3 – upper quartile; Min – minimum value; Max – maximum value; *Mann–Whitney U test.

of participants with a disorder of at least 1 function was also listed. There was a disorder of at least 1 function statistically significantly more often in the cleft group than in the control group (94.3% compared to 54.3%; $p < 0.001$).

In the NOT-S examination, it was observed that in the cleft group, there were statistically significantly more disorders of functions such as face at rest, facial expression and speech. In the cleft group, facial disorders at rest were found in almost 66% (n = 23) of the study participants, while in the control group, it was 11.4% (n = 4; $p < 0.001$). Disorders of the 2 other functions were also more common in participants from the cleft group. In the cleft group, facial expression disorders occurred in 85.7% (n = 30 compared to the control group: 2.9%; n = 1; $p < 0.001$) and speech disorders in 71.4% (n = 25 compared to the control group: 8.6%; n = 3; $p < 0.001$). In addition, the summary results of the NOT-S examination were also compared. In the cleft group, there were statistically significantly more disorders of at least 1 function than in the control group (100% compared to 22.9%; $p < 0.001$).Comparing the total score, it was also found that in the cleft group there were statistically significantly more disorders of at least 1 function than in the control group (100% compared to 68.6%; $p < 0.001$).

A comparison of the results of the NOT-S between the cleft group (n = 35) and the control group (n = 35) is presented in Table 2. The summary of the NOT-S interview results, the NOT-S examination and the NOT-S total score showed statistically significantly higher values in the cleft group than in the control group. In the cleft group, the Me of the NOT-S interview scores was 2 points, the Min was 0 points and the Max was 5 points (compared to the control group: Me = 1 point, Min = 0, Max = 2; $p < 0.001$). The Me in the NOT-S examination total score was 2 points, (Min = 1, Max = 4; compared to the control group: Me = 0; $p < 0.001$). Comparing the NOT-S total score, it was also found that Me values in the cleft group were 3 points higher than in the control group ($p < 0.001$).

Discussion

This is the first study among the Polish population to use the NOT-S questionnaire. The questionnaire was conducted to assess orofacial dysfunction in children with UCLP in comparison with the control group. Both hypotheses have been confirmed.

Disorders in the cleft group mainly concerned breathing, chewing and swallowing, drooling, face at rest, facial expression, and speech. These results are consistent with data published by Hairfield et al.,[18] who showed that people with UCLP statistically more often have respiratory problems. This may be directly due to the narrowing of the upper respiratory tract within the nasal cavity among patients with UCLP.[19] However, it is worth emphasizing that the paranasal sinuses remain well-developed.[20] Respiratory plethysmography in combination with an integrated pneumotachograph, to measure the percentage of nasal breathing, and a flow pressure test showed that most people had less than 0.4 cm^2 of airway, which is less than normal.[21]

Chewing and swallowing disorders affect 51.4% of the cleft group (n = 18; compared to the control group: 8.6%; n = 3; $p < 0.001$). Using a chewable test material, the particle size of the crushed food was determined in patients with UCLP; it was found to be larger in the cleft group than the control group. Likewise, the number of chewing cycles needed to crush the material was greater.[22] It is worth emphasizing that the orbicularis oris muscle tension measured with an electromyograph[23] was higher in the group of patients with UCLP than in the control group while swallowing and at rest.

On the other hand, the results regarding dryness of the mouth show that in the group with UCLP the problem was not statistically significantly more frequent. This confirms a study published in 2008,[24] in which sialometers and sialochemistry were used to assess these patients. There were no differences in the abovementioned parameters between patients with UCLP and those in the control group. Interestingly, cortisol[25] concentration in the saliva of UCLP patients was also checked as an expression of stress response to determine health-related quality of life (HRQoL). There was no difference in salivary cortisol levels between the patient and control groups. No correlation between cortisol concentration and HRQoL was confirmed.

In the NOT-S examination, facial disorders at rest affected 66% (n = 23) of patients, while in the control group, this figure was 11.4% (n = 4; $p < 0.001$). It has been shown that the face of patients with CLP is perceived more

negatively than that of people without the disorder. Moreover, observation of the nose and mouth area in these people lasts longer. It has also been shown that patients with CLP looking at other people with CLP spend more time looking at the nose and less time looking at the eyes than people without CLP.[26] It should also be emphasized that the intensity of asymmetry increases with a maximum smile.[27] Based on scientific reports, presurgical nasal molding improves the esthetics of the nose in patients with unilateral clefts of the lip, alveolus and palate, and distinctly flattens nasal wings.[28]

Patients with CLP undergo surgery due to the lack of tissue continuity. However, despite a significant improvement in facial symmetry after surgery, 4 years after surgery the remaining asymmetry is more visible: the philtrum of the upper lip is deviated toward the scar tissue on the cleft side, and the asymmetry of the nose is significantly worse.[29] The effects of secondary osteotomy were also compared. No significant influence was demonstrated on craniofacial growth in children with UCLP.[30]

Considering the aspects discussed above, it is understandable that they affect the QoL of patients with UCLP, which was confirmed in our study.

Conclusions

The NOT-S survey is an effective tool for assessing disorders in patients with UCLP. It has been shown that patients with UCLP have more orofacial dysfunctions and worse QoL compared to the control group. Orofacial function areas and treatment outcomes need to be continually evaluated and monitored.

ORCID iDs

Natalia Kaczorowska https://orcid.org/0000-0003-4270-6143
Patrycja Markulak https://orcid.org/0000-0002-9603-5894
Marcin Mikulewicz https://orcid.org/0000-0001-5754-0284

References

1. Worley ML, Patel KG, Kilpatrick LA. Cleft lip and palate. *Clin Perinatol*. 2018;45(4):661–678. doi:10.1016/j.clp.2018.07.006
2. Mossey P, Castilla E. *Global Registry and Database on Craniofacial Anomalies. Report of a WHO Registry Meeting on Craniofacial Anomalies*. Baurú, Brazil: World Health Organization; 2001.
3. Harikrishnan P, Balakumaran V. Analysis of intramaxillary and midface skeletal asymmetry in a three-dimensional model with complete unilateral cleft lip and palate. *J Craniofac Surg*. 2018;29(8):759–762. doi:10.1097/SCS.0000000000004718
4. Al-Jamal GA, Hazza'a AM, Rawashdeh MA. Prevalence of dental anomalies in a population of cleft lip and palate patients. *Cleft Palate Craniofac J*. 2010;47(4):413–420. doi:10.1597/08-275.1
5. Paradowska-Stolarz A, Kawala B. Occlusal disorder among patients with total clefts of lip, alveolar bone and palate. *Biomed Res Int*. 2004; 2014:583416. doi:10.1155/2014/583416
6. Van Lierde KM, Dhaeseleer E, Luyten A, Van De Woestijne K, Vermeersch H, Roche N. Parent and child ratings of satisfaction with speech and facial appearance in Flemish pre-pubescent boys and girls with unilateral cleft lip and palate. *Int J Oral Maxillofac Surg*. 2012; 41(2):192–199. doi:10.1016/j.ijom.2011.10.030
7. Sharma RN, Nanda V. Problems of middle ear and hearing in cleft children. *Indian J Plast Surg*. 2009;42(3):144–148. doi:10.4103/0970-0358.57198
8. Hirschberg J. Functional consequences of cleft palate and its management [in Hungarian]. *Orv Hetil*. 2001;142(24):1259–1263.
9. Queiroz Herkrath AP, Herkrath FJ, Rebelo MA, Vettore MV. Measurement of health-related and oral health-related quality of life among individuals with nonsyndromic orofacial clefts: A systematic review and meta-analysis. *Cleft Palate Craniofac J*. 2015;52(2):157–172. doi:10.1597/13-104
10. Rando GM, Jorge PK, Vitor LLR et al. Oral health-related quality of life of children with oral clefts and their families. *J Appl Oral Sci*. 2018;26: e20170106. doi:10.1590/1678-7757-2017-0106
11. Zeraatkar M, Ajami S, Nadjmi N, Golkari A. Impact of oral clefts on the oral health-related quality of life of preschool children and their parents. *Niger J Clin Pract*. 2018;21(9):1158–1163. doi:10.4103/njcp.njcp_426_17
12. Bos A, Prahl C. Oral health-related quality of life in Dutch children with cleft lip and/or palate. *Angle Orthod*. 2011;81(5):865–871. doi:10.2319/070110-365.1
13. Brand S, Blechschmidt A, Müller A, Sader R, Schwenzer-Zimmerer K, Zeilhofer HF, Holsboer-Trachsler E. Psychosocial functioning and sleep patterns in children and adolescents with cleft lip and palate (CLP) compared with healthy controls. *Cleft Palate Craniofac J*. 2009; 46(2):124–135. doi:10.1597/07-165.1
14. Bakke M, Bergendal B, McAllister A, Sjögreen L, Asten P. Development and evaluation of a comprehensive screening for orofacial dysfunction. *Swed Dent J*. 2007;31(2):75–84.
15. Montes ABM, Oliveira TM, Gavião MBD, Barbosa TS. Orofacial functions and quality of life in children with unilateral cleft lip and palate. *Braz Oral Res*. 2019;33:e0061. doi:10.1590/1807-3107bor-2019.vol33.0061
16. Alaçam A, Çalık Yılmaz BC, Incioğlu AS. Assessment of orofacial dysfunction using the NOT-S method in a group of Turkish children with cerebral palsy. *Eur Arch Paediatr Dent*. 2019;21(2):215–221. doi:10.1007/s40368-019-00475-z
17. Bergendal B, McAllister A, Stecksén-Blicks C. Orofacial dysfunction in ectodermal dysplasias measured using the Nordic Orofacial Test-Screening protocol. *Acta Odontol Scand*. 2009;67(6):377–381. doi:10.1080/00016350903160571
18. Hairfield WM, Warren DW, Seaton DL. Prevalence of mouth breathing in cleft lip and palate. *Cleft Palate J*. 1988;25(2):135–138.
19. Liu H, Warren DW, Drake AF, Davis JU. Is nasal airway size a marker for susceptibility toward clefting? *Cleft Palate Craniofac J*. 1992;29(4): 336–339. doi:10.1597/1545-1569_1992_029_0336_inasam_2.3.co_2
20. Koppe T, Weigel C, Bärenklau M, Kaduk W, Bayerlein T, Gedrange T. Maxillary sinus pneumatization of an adult skull with an untreated bilateral cleft palate. *J Craniomaxillofac Surg*. 2006;34(Suppl 2):91–95. doi:10.1016/S1010-5182(06)60020-6
21. Warren DW, Hairfield WM, Dalston ET. The relationship between nasal airway size and nasal-oral breathing in cleft lip and palate. *Cleft Palate J*. 1990;27(1):46–52. doi:10.1597/1545-1569(1990)027<0046:trbnas>2.3.co;2
22. Montes ABM, de Oliveira TM, Gavião MBD, de Souza Barbosa T. Occlusal, chewing, and tasting characteristics associated with orofacial dysfunctions in children with unilateral cleft lip and palate: A case-control study. *Clin Oral Investig*. 2018;22(2):941–950. doi:10.1007/s00784-017-2173-4
23. Ravera MJ, Miralles R, Santander H, Valenzuela S, Villaneuva P, Zúñiga C. Comparative study between children with and without cleft lip and cleft palate, part 2: Electromyographic analysis. *Cleft Palate Craniofac J*. 2000;37(3):286–291. doi:10.1597/1545-1569_2000_037_0286_csbcwa_2.3.co_2
24. Aizenbud D, Peri-Front Y, Nagler RM. Salivary analysis and antioxidants in cleft lip and palate children. *Arch Oral Biol*. 2008;53(6):517–522. doi:10.1016/j.archoralbio.2007.12.006
25. Sundell AL, Marcusson A, Törnhage CJ. Salivary cortisol rhythms in children with cleft lip and/or palate: A case-control study. *Cleft Palate Craniofac J*. 2018;55(8):1072–1080. doi:10.1177/1055665618767425
26. Meyer-Marcotty P, Gerdes AB, Reuther T, Stellzig-Eisenhauer A, Alpers GW. Persons with cleft lip and palate are looked at differently. *J Dent Res*. 2010;89(4):400–404. doi:10.1177/0022034509359488

27. Al Rudainy D, Ju X, Mehendale F, Ayoub A. The effect of facial expression on facial symmetry in surgically managed unilateral cleft lip and palate patients (UCLP). *J Plast Reconstr Aesthet Surg*. 2019;72(2):273–280. doi:10.1016/j. bjps.2018.10.004
28. Kirbschus A, Gesch D, Heinrich A, Gedrange T. Presurgical nasoalveolar molding in patients with unilateral clefts of lip, alveolus and palate: Case study and review of the literature. *J Craniomaxillofac Surg*. 2006; 34(Suppl 2):45–48. doi:10.1016/S1010-5182(06)60010-3
29. Al Rudainy D, Ju X, Mehendale FV, Ayoub A. Longitudinal 3D assessment of facial asymmetry in unilateral cleft lip and palate. *Cleft Palate Craniofac J.* 2019;56(4):495–501. doi:10.1177/1055665618780108
30. Gesch D, Kirbschus A, Mack F, Gedrange T. Comparison of craniofacial morphology in patients with unilateral cleft lip, alveolus and palate with and without secondary osteoplasty. *J Craniomaxillofac Surg*. 2006;34(Suppl 2):62–66. doi:10.1016/S1010-5182(06)60014-0

Paclitaxel inhibits proliferation and invasion and promotes apoptosis of breast cancer cells by blocking activation of the PI3K/AKT signaling pathway

*Gang Li[1,A–D], *Dongxin Xu[2,A–D], Jinju Sun[3,C,D], Shiyun Zhao[4,A,C,D], Dan Zheng[5,E,F]

[1] First Department of Oncology Surgery, Hangzhou Cancer Hospital, China
[2] Fourth Department of Internal Medicine, Zibo City Traditional Chinese Medicine Hospital, China
[3] Department of Pharmacy, The Second People's Hospital of Liaocheng, China
[4] Disinfection Supply Center, Maternal and Child Health Care of Zaozhuang, China
[5] Department of Pharmacy, Hangzhou Cancer Hospital, China

A – research concept and design; B – collection and/or assembly of data; C – data analysis and interpretation; D – writing the article; E – critical revision of the article; F – final approval of the article

Advances in Clinical and Experimental Medicine, ISSN 1899–5276 (print), ISSN 2451–2680 (online) *Adv Clin Exp Med*. 2020;29(11):1337–1345

Address for correspondence
Dan Zheng
E-mail: zhengdanqazx12@163.com

Funding sources
None declared

Conflict of interest
None declared

*Gang Li and Dongxin Xu contributed equally to this work.

Received on September 20, 2019
Reviewed on June 13, 2020
Accepted on September 20, 2020

Cite as
Li G, Xu D, Sun J, Zhao S, Zheng D. Paclitaxel inhibits proliferation and invasion and promotes apoptosis of breast cancer cells by blocking activation of the PI3K/AKT signaling pathway. *Adv Clin Exp Med*. 2020;29(11):1337–1345. doi:10.17219/acem/127681

DOI
10.17219/acem/127681

Abstract

Background. Breast cancer has the highest incidence and mortality among all cancers in women. Paclitaxel (PTX) has a notable therapeutic effect on cancer in clinical practice.

Objectives. To explore the effect and mechanism of PTX on the proliferation, apoptosis and invasiveness of breast cancer cells.

Material and methods. MCF-7 cells were treated with PTX (0 μM, 0.01 μM, 0.1 μM, 1 μM) for 48 h. Cell viability was detected using MTT assay and lactate dehydrogenase (LDH) assay; the cell proliferation rate was detected using 5-ethynyl-2′-deoxyuridine (EdU) assay to screen the most effective concentration of PTX. MCF-7 cells were then divided into 5 groups: control group, PTX group, oe-PI3K group, NC-PI3K group, and oe-PI3K+PTX group. Cell apoptosis and cell cycles were detected with flow cytometry; cell invasion was determined using a transwell assay; western blot and quantitative reverse-transcription polymerase chain reaction (qRT-PCR) were used to measure the mRNA and protein expression level of cleaved caspase-3, Bax, Bcl-2, matrix metalloproteinase 9 (MMP-9), vascular endothelial growth factor (VEGF), p-AKT (Thr308), and p-AKT (Ser473).

Results. Paclitaxel inhibited cell viability and proliferation in a dose-dependent manner. In the PTX group, the apoptosis rate, the number of cells arrested in the G2/M phase and the expression levels of Cleaved caspase-3 and Bax were increased, but the number of invasive cells and the expression levels of Bcl-2, MMP-9, vascular endothelial growth factor (VEGF), p-AKT (Thr308), and p-AKT (Ser473) were decreased. However, PI3K upregulation can reverse the effects of PTX.

Conclusions. Paclitaxel could inhibit MCF-7 cell proliferation and invasion, and promote MCF-7 cell apoptosis by downregulating the expression of p-AKT (Thr308) and p-AKT (Ser473) in the PI3K/AKT signaling pathway.

Key words: apoptosis, breast cancer, proliferation, paclitaxel, PI3K/AKt signaling pathway

Introduction

Breast cancer is the most common gynecological cancer, with the highest mortality rate. More than 1.5 million women are diagnosed with breast cancer each year worldwide, and this number is rising.[1,2] The common classification of breast cancer is based on the expression of estrogen receptor (ER), progesterone receptor (PR) and human epidermal growth factor receptor (HER2).[3] There are many factors affecting the prevalence of breast cancer, including family history, age, smoking and drinking, early amenorrhea, delayed menarche, obesity, and high-fat diet; oral contraceptives or other exogenous estrogens can also increase the incidence of breast cancer.[4–6] It is a highly heterogeneous disease – its clinical characteristics and biological behavior vary widely among patients; therefore, survival also varies from person to person.[7] At present, radiotherapy and chemotherapy are the main methods of inhibiting the growth of breast cancer in order to prolong survival. However, the outcomes of current treatment regimens are often unsatisfactory due to recurrences of the disease caused by chemotherapy drug resistance.[8–10] Therefore, fully understanding the mechanism of action of chemotherapy drugs may help improve the therapeutic outcome of breast cancer.

Paclitaxel (PTX) is a common chemotherapy drug that is widely used in clinical practice due to its remarkable therapeutic effect.[11] It can hinder cell mitosis by maintaining tubulin stability.[12] Paclitaxel can be used alone or in combination with other drugs to treat a variety of malignancies, including cervical cancer, head and neck cancers, and lung cancer.[13–17] Paclitaxel is also the first-line chemotherapy for breast cancer.[18]

PI3K/AKT is one of the most frequently activated signaling pathways in cancer, which regulates cell proliferation and invasion by targeting multiple proteins.[19] It has been reported that activation of the PI3K/AKT pathway can promote growth, invasion and metastasis of breast cancer cells.[20]

However, the relationship between PTX and the PI3K/AKT signaling pathway, and the mechanism of their interaction in the treatment of breast cancer have not been elucidated. Therefore, this study explored the relationship between PTX and the PI3K/AKT signaling pathway, with the hope of providing more insights for improving the therapeutic outcome of PTX in breast cancer patients.

Material and methods

Cell culture and transfection

Human breast cancer cell lines MCF-7, BT-549, MDA-MB-231, and T47D, and immortalized human mammary epithelial cell line MCF-10A were purchased from the Shanghai Cell Bank of the Chinese Academy of Sciences (Beijing, China). The cells were cultured in minimal essential medium (MEM) containing 10% fetal bovine serum (FBS) and 100 IU/mL penicillin in 5% CO_2 at 37°C. The PI3K overexpression plasmid pcDNA3.1-PI3K and the negative control plasmid pcDNA3.1-NC were purchased from Vigene Biosciences Inc. (Jinan, China). Transfection was performed using a lipofectamin 2000 kit (Invitrogen, Carlsbad, USA). Briefly, 250 µL of Opti-MEM (Gibco, Thermo Fisher Scientific, Waltham, USA) was used to dilute 4 µg of the desired plasmid and 10 µL of Lipofectamin 2000. The plasmid and Lipofectamin 2000 were allowed to stand at room temperature for 5 min before being gently mixed together. The mixture was allowed to stand for 20 min and then was added dropwise to the MCF-7 cell culture plate. The plate was gently shaken and put in an incubator for 6 h before the medium was changed. Cells were harvested at 48 h after transfection for later use.

MTT assay

When the MCF-7cells reached 80–90% confluency, cells were digested and seeded into 96-well plates. The cells were treated with gradient concentrations of PTX for 48 h. After the medium was gently removed, 100 µL medium containing 10% MTT solution (Solarbio Science & Technology Inc., Beijing, China) was added. After 4 h, the supernatant was discarded; 110 µL of dimethyl sulfoxide (DMSO) was then added to dissolve the crystal precipitate, and the absorbance value (optical density – OD) of each well at a wavelength of 490 nm was obtained using a microplate reader. Each group had 3 duplicate wells.

Lactate dehydrogenase cytotoxicity assay

The cell treatment was as described for the MTT assay (above). Cell culture medium was used as a blank control. Untreated MCF-7 cells were used as a spontaneous release control. Normal MCF-7 cells treated with Triton X-100 (Sigma-Aldrich, St. Louis, USA) were used as a maximum release control. In accordance with the instructions of the lactate dehydrogenase (LDH) cytotoxicity kit (Beyotime Biotechnology, Shanghai, China), 120 µL of supernatant from each well was collected and transferred to a new 96-well plate. Then 60 µL of LDH working reaction mixture was added to each well and incubated in the dark at room temperature for 30 min. The absorbance of each well was measured at a wavelength of 490 nm. Each sample had 3 replicate wells. For each test sample the cytotoxicity (%) = (experimental value – spontaneous release)/(maximum release – spontaneous release) × 100%.

EdU cell proliferation assay

The ×2 EdU working solution was made by diluting 10 µM of EdU (Beyotime) with MEM medium (1:500) and

warmed to 37°C. An equal volume of ×2 EdU working solution was added to each well and the plate was incubated at room temperature for 2 h, washed with PBS and fixed with 4% paraformaldehyde for 15 min. The plates were then washed twice with PBS containing 3% bovine serum albumin (BSA) to remove the permeabilization solution. Click-iT® cell buffer additive solution (Thermo Fisher Scientific) was added and each plate was incubated at room temperature for 30 min in the dark. Hoechst 33342 reaction solution was added, and the plates were incubated at room temperature for 10 min in the dark. The plates were washed 3 times before being observed under CKX53 inverted fluorescence microscope (Olympus, Tokyo, Japan). The red fluorescence was counted as proliferating cells, and the blue fluorescence showed nuclei. We chose 3 random ×200 fields to count the proliferating cells with nuclei. The cell proliferation rate = the number of proliferating cells/total cell number × 100%.

Flow cytometry

Cell apoptosis

A cell apoptosis detection kit was purchased from Beyotime. Cells in each group were harvested and resuspended with PBS. A cell suspension containing 10^4 cells was centrifuged and resuspended using working buffer. Then a staining solution was made by mixing Annexin V-FITC (Beyotime) and propidium iodide (PI) at a ratio of 1:2. The cells were mixed with the staining solution and incubated at room temperature for 20 min. Cell apoptosis was measured in a flow cytometer; the experiment was repeated 3 times.

Cell cycle

A cell cycle detection kit was purchased from Beyotime. Cells were harvested, fixed with 1 mL of pre-cooled 75% ethanol (–20°C) and stored overnight at 4°C. The PI staining solution, staining buffer and Rnase A were made according to the instruction manual. The cells were washed twice with pre-cooled PBS, resuspended with PI staining solution and incubated at 37°C for 30 min. The cell cycle was then detected using flow cytometry in the dark at 4°C. The experiment was repeated 3 times.

Transwell invasion assay

Cells were starved for 12 h before the invasion assay. A 24-well plate with 8 μm Transwell inserts (Corning Inc., Corning, USA) was used in this experiment; each group had 3 replicate inserts. The upper surface of each insert was coated with 50 μL of Matrigel (Sigma-Aldrich) and air-dried at 4°C. We added 200 μL of cell suspension to the upper chamber at a density of 1×10^5 cells/mL, and 500 μL of Dulbecco's modified Eagle's medium (DMEM) medium containing 10% bovine serum to the lower chamber. After 48 h, the inserts were taken out and the cells on the inserts were fixed with 4% paraformaldehyde for 30 min. Then the insert was placed in 0.2% Triton X-100 for 15 min and stained with 0.05% gentian violet for 5 min. We selected 5 random fields to count the number of transmembrane cells under an inverted microscope. The assay was repeated 3 times.

Western blot

Cells were harvested and resuspended with RIPA lysis buffer (Beyotime) containing phenylmethylsulfonyl fluoride (PMSF) and protein phosphatase inhibitors. The mixture was incubated on ice for 30 min, and then centrifuged at 12,000 rpm for 10 min at 4°C. The supernatant was collected as total cell protein. The protein concentration was determined using the BCA Protein Quantitation Kit (Thermo Fisher Scientific). A total of 20 μg of the protein in each sample was subjected to SDS-PAGE, and then the protein was wet transferred to a nitrocellulose (NC) membrane. The membrane was blocked with 5% BSA for 90 min and incubated with rabbit primary antibodies, including 1:1000 anti-AKT (Cell Signalling Technology (CST) Inc., Danvers, USA), 1:1000 anti-p-AKT (Ser473) (CST), 1:1000 anti-p-AKT(Thr308) (CST), 1:1000 anti-matrix metalloproteinase 9 (anti-MMP-9) (Proteintech Group Inc., Rosemont, USA), 1:1000 anti-vascular endothelial growth factor (anti-VEGF) (Proteintech Group Inc.), 1:1000 anti-cleaved caspase-3 (CST), 1:1000 Bax (CST), 1:10,000 anti- glyceraldehyde-3-phosphate dehydrogenase (anti-GAPDH) (Abcam, Cambridge, UK), and 1:2000 mouse primary antibody anti-Bcl-2 (CST) at 4°C overnight. The membrane was rinsed 3 times with Tris-buffered saline with Tween 20 (TBST) for 10 min each time. Then the membrane was incubated with horseradish peroxidase (HRP)-conjugated goat anti-rabbit or goat anti-mouse antibody (1:10,000; Jackson Immunoresearch Laboratories Inc., West Grove, USA) at room temperature for 90 min. The membrane was rinsed 3 times with TBST for 15 min each time, then developed using ECL solution and photographed using a SmartView Pro 2000 imager system (Major Science, Saratoga, USA). Relative protein expression was calculated using ImageJ software (National Institutes of Health (NIH), Bethesda, USA) with *GAPDH* as an internal reference. Relative protein expression = the grey value of each sample/the grey value of the internal reference.

qRT-PCR

Total RNAs were extracted from cells using Trizol (Invitrogen) and quantified using Nanodrop 2000 (Thermo Fisher Scientific). A PrimeScript™ RT reagent kit with gDNA Eraser (TaKaRa Bio Inc., Kusatsu, Japan) was used for reverse transcription following the manufacturer's instructions. The reaction mixture was prepared using

Table 1. qRT-PCR primer sequences

Gene	Forward primer (5′-3′)	Reverse primer (5′-3′)
MMP-9	AGACACCTCTGCCCTCACCATGAGC	TCTGTGGAGACGGGAGTGGTACTCG
VEGF	CGGTGCTGGAATTGATA	GGCGGTGTCTGTCTGTCT
GAPDH	GGGTGTGAACCATGAGAAGTATG	GATGGCATGGACTGTGGTCAT

VEGF – vascular endothelial growth factor; *MMP-9* – matrix metallopeptidase 9; *GAPDH* – glyceraldehyde-3-phosphate dehydrogenase.

a SYBR® Premix Ex Taq™ kit (TaKaRa Bio Inc.), and quantitative reverse-transcription polymerase chain reaction (qRT-PCR) was performed using an ABI7500 PCR system (Thermo Fisher Scientific). The reaction condition was as follows: pre-denaturation at 95°C for 10 min, denaturation at 95°C for 15 s and annealing at 60°C for 30 s; this cycle was repeated 40 times followed by extension at 72°C for 1 min. Relative expression was calculated using the formula:

$$\Delta\Delta Ct = (Ct_{\text{target gene}} - Ct_{\text{GAPDH}}) - (Ct_{\text{control group}} - Ct_{\text{GAPDH}})$$

with *GAPDH* as the internal reference. All the primers (Genepharma, Shanghai, China) are listed in Table 1.

Statistical analysis

All data was analyzed with SPSS v. 21.0 software (IBM Corp., Armonk, USA). Quantitative values were expressed as mean ± standard deviation (SD). A one-way analysis of variance (ANOVA) followed by the Bonferroni post hoc test was used to compare the differences between groups. A p-value less than 0.05 was considered statistically significant.

Results

Expression of the PI3K/AKT signaling pathway-related protein p-AKT in breast cancer cell lines

The expression of PI3K/AKT signaling pathway-related protein p-AKT/AKT in the MCF-7, BT-549, MDA-MB-231, T47D, and MCF-10A cell lines was detected with western blot (Fig. 1A). The results showed that p-AKT (Thr308) and p-AKT (Ser473) were most significantly expressed in the MCF-7 cell line compared with MCF-10A ($p < 0.05$). Therefore, the MCF-7 cell line was used for the subsequent experiments.

Effects of different concentrations of PTX on the viability of MCF-7 cells

The MCF-7 cells were treated with different concentrations of PTX for 48 h, and cell viability was measured using MTT assay (Fig. 2A). The results showed that cell viability decreased significantly as the concentration of PTX increased ($p < 0.05$). When the PTX concentration reached 1 μM, cell viability was 50%. The LDH cytotoxicity assay showed that cell death increased significantly as the PTX concentration increased ($p < 0.05$). When the PTX concentration was 1 μM, cell mortality was about 40% (Fig. 2B).

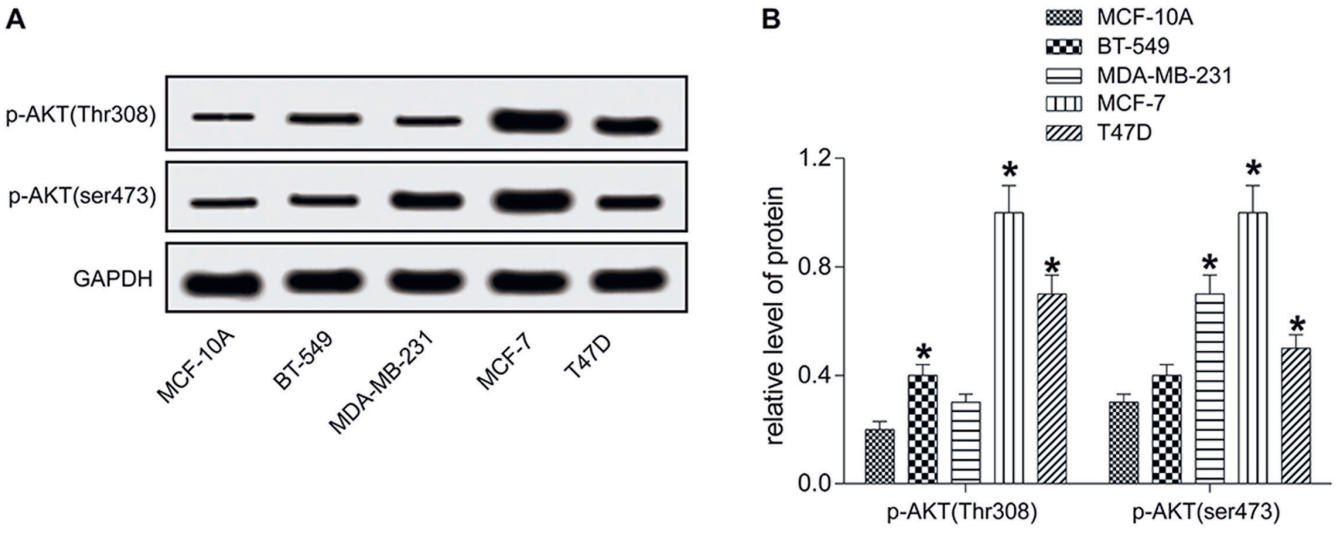

Fig. 1. Expression levels of the PI3K/AKT signaling pathway-related proteins in various cell lines. A. Expression of p-AKT (Thr308) and p-AKT (Ser473) detected with western blot in cell lines. B. Quantification of the western blot results

*$p < 0.05$, compared with the MCF-10A cell line.

Effects of different concentrations of PTX on the proliferation of MCF-7

Cell proliferation at different concentrations of PTX was measured using EdU assay (Fig. 3). The results showed that cell proliferation was inhibited by PTX in a dose-dependent manner. Cell proliferation was significantly decreased as the concertation of PTX increased ($p < 0.05$). Therefore, PTX at the concentration of 1 μM was used for the subsequent experiments.

Comparison of cell apoptosis and cell cycle after PI3K overexpression and PTX treatment

Based on the results outlined above, MCF-7 cells were selected and divided into 5 groups in the subsequent experiments: the control group (normal MCF-7 cells); the PTX group (treated with 1 μM of PTX); the oe-PI3K group (transfected with PI3K overexpression plasmid pcDNA3.1-PI3K); the NC-PI3K group (transfected with the negative control of pcDNA3.1-PI3K); and the oe-PI3K+PTX group (transfected with pcDNA3.1-PI3K and treated with 1 μM of PTX).

Apoptosis and cell cycles were detected using flow cytometry (Fig. 4A,B). Compared with the control group, the NC-PI3K group had similar results, while the PTX group had a significantly higher cell apoptosis rate and a significantly higher number of cells in the G2/M phase ($p < 0.05$). Compared with the PTX group, the cell apoptosis rate in the oe-PI3K group was significantly decreased, but the number of cells in the G2/M phase was increased ($p < 0.05$). In the oe-PI3K+PTX group, the cell behaviors in the PTX group were partly reversed ($p < 0.05$).

The expression levels of the apoptosis-related proteins Bax, Bcl-2 and cleaved caspase-3 were detected using western blot in MCF-7 cells (Fig. 4C). Compared with the control group, the NC-PI3K group had similar results, while the expression levels of Bax and cleaved caspase-3 were upregulated in the PTX group; however, the expression

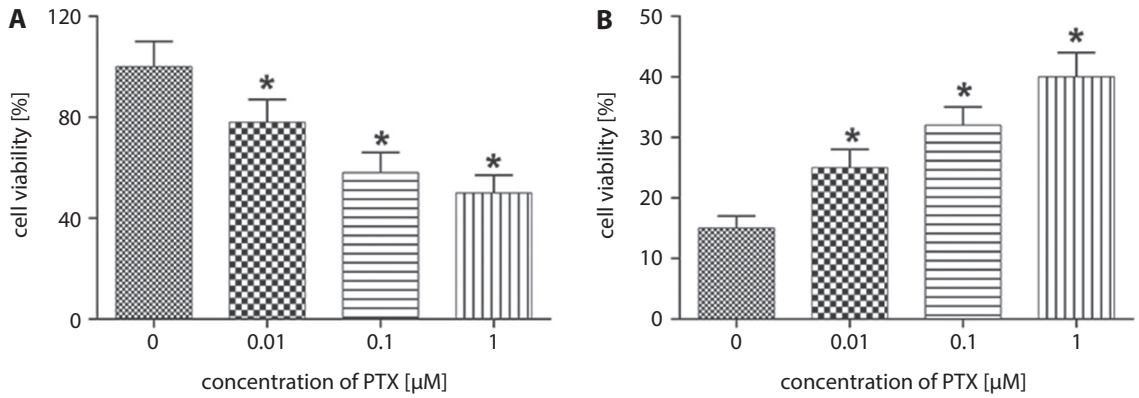

Fig. 2. Effects of different concentrations of PTX on the viability of MCF-7 cells. A. Cell viability detected with MTT assay. B. Cell death detected with LDH cytotoxicity assay

*$p < 0.05$, compared with when the PTX concentration is 0 μM.

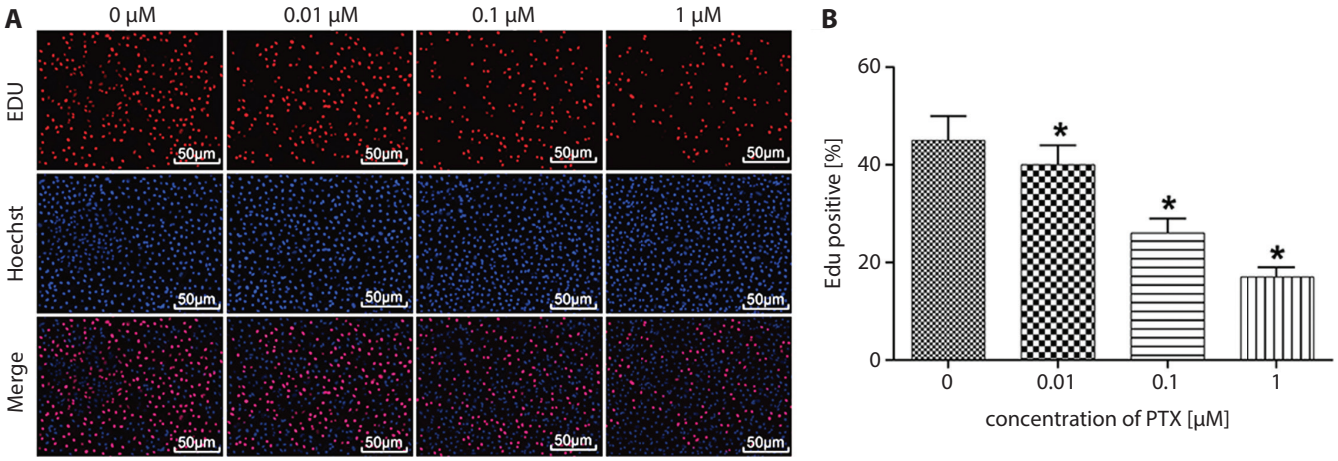

Fig. 3. Effects of different concentrations of PTX on the proliferation of MCF-7 cells. A. Cell proliferation detected with EdU proliferation assay. B. Percentage of EdU positive cells

*$p < 0.05$, compared with cells without PTX treatment.

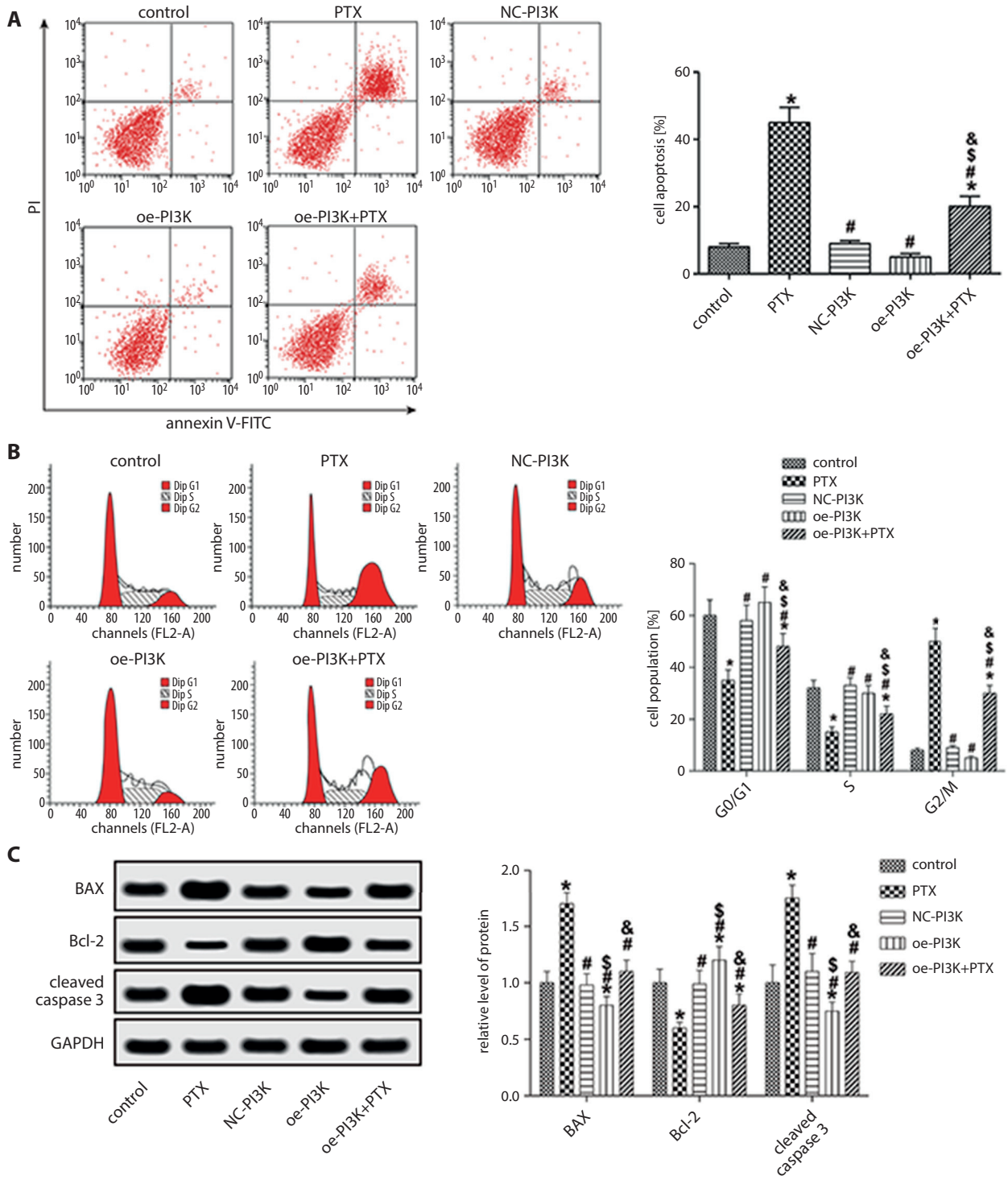

Fig. 4. Detection of apoptosis rate and cell-cycle distribution after PI3K overexpression and PTX treatment in MCF-7 cells. A. Cell apoptosis rate detected with flow cytometry. B. Cell-cycle distribution detected with flow cytometry. C. Expression level of apoptosis-related proteins detected with western blot

*$p < 0.05$ compared with the control group; #$p < 0.05$ compared with the PTX group; $^{\$}p < 0.05$ compared with the NC-PI3K group; $^{\&}p < 0.05$ compared with the oe-PI3K group.

level of Bcl-2 was decreased in the PTX group ($p < 0.05$). The expression levels of these proteins showed opposite trends in the oe-PI3K group when compared with the PTX group ($p < 0.05$). In the oe-PI3K+PTX group, the expression levels of related proteins in the PTX group was partly reversed (all $p < 0.05$).

Comparison of cell invasion after PI3K overexpression and PTX treatment

The invasive ability of MCF-7 cells in each group was detected with a Transwell invasion assay (Fig. 5A). The qRT-PCR and western blot were used to detect mRNA and

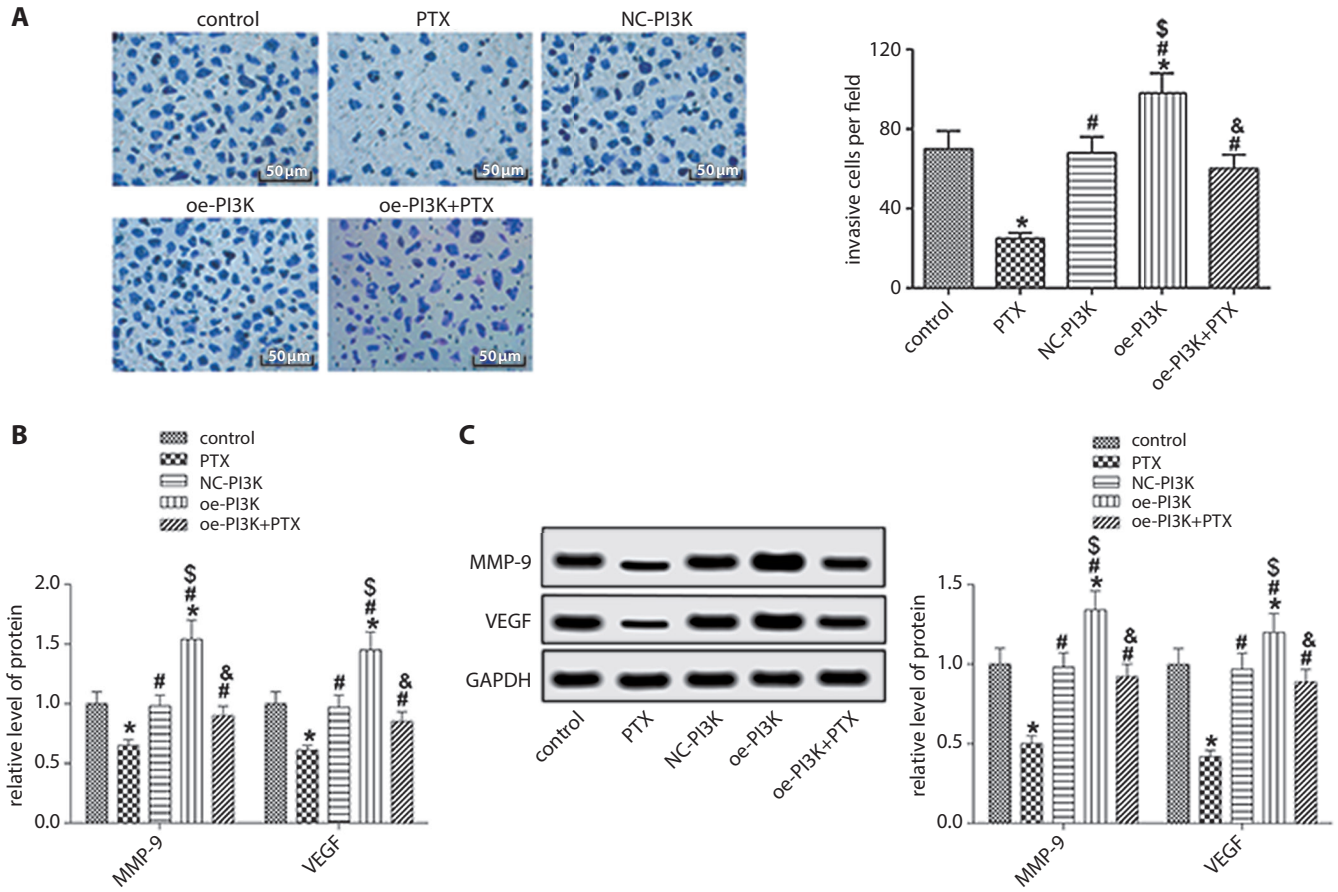

Fig. 5. Invasion assay after PI3K overexpression and PTX treatment in MCF-7 cells. A. Transwell invasion assay and transmembrane cell count. B. mRNA expression level of MMP-9 and VEGF detected with qRT-PCR. C. Protein expression level of MMP-9 and VEGF detected with western blot

*p < 0.05 compared with the control group; #p < 0.05 compared with the PTX group; $p < 0.05 compared with the NC-PI3K group; &p < 0.05 compared with the oe-PI3K group.

protein expression levels of cell invasion-related factors MMP-9 and VEGF (Fig. 5B).

The control group and the NC-PI3K group had similar results, while the PTX group had significantly decreased cell invasion ability and lower MMP-9 and VEGF expression levels ($p < 0.05$). However, the oe-PI3K group had significantly increased cell invasion ability and higher MMP-9 and VEGF expression levels when compared with the PTX group ($p < 0.05$). In the oe-PI3K+PTX group, the cell behaviors and the expression levels of related proteins in the PTX group were partly reversed (all $p < 0.05$).

Paclitaxel inhibited activation of the PI3K/AKT signaling pathway in MCF-7 breast cancer cells

Western blot was used to detect the expression of PI3K/AKT signaling pathway-related protein p-AKT in each group (Fig. 6). Compared with the control group, the expression levels of p-AKT (Thr308) and p-AKT (Ser473) were significantly downregulated in the PTX group, but significantly upregulated in the oe-PI3K group (all $p < 0.05$). Compared with the PTX group, the expression of p-AKT (Thr308) and p-AKT (Ser473) was significantly upregulated in the oe-PI3K+PTX group (both $p < 0.05$). Compared with the oe-PI3K group, the p-AKT (Thr308) and p-AKT (Ser473) expression levels were significantly downregulated in the oe-PI3K+PTX group (both $p < 0.05$).

Discussion

Currently, chemotherapy is the mainstream treatment for breast cancer, and PTX has been widely used as a first-line treatment.[21] This study confirmed the in vitro therapeutic effect of PTX on breast cancer. At the same time, we conducted a preliminary exploration of the underlying mechanism, and found that PTX can inhibit the proliferation of breast cancer cells by inhibiting the activation of the PI3K/AKT pathway.

Our study found that PTX could decrease the activity of breast cancer cells and inhibit proliferation in a dose-dependent manner. Paclitaxel has been shown to inhibit the development of a variety of cancer cells, including oral squamous cell carcinoma and breast cancer cells.[22,23] Meanwhile, we also found that PTX can induce cell-cycle arrest and promote apoptosis by regulating the expression level

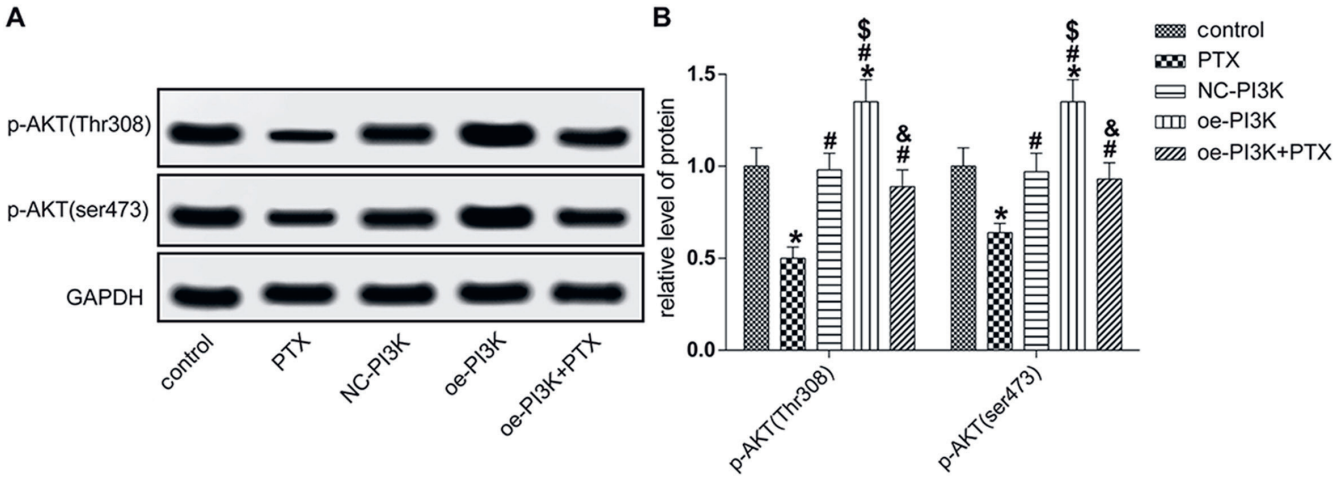

Fig. 6. Expression of p-AKT (Thr308) and p-AKT (Ser473) after PI3K overexpression and PTX treatment in MCF-7 cells. A. Expression level of p-AKT (Thr308) and p-AKT (Ser473) detected with western blot. B. Quantification result of western blot

*p < 0.05 compared with the control group; #p < 0.05 compared with the PTX group; $p < 0.05 compared with the NC-PI3K group; &p < 0.05 compared with the oe-PI3K group.

of Bax, cleaved caspase-3 and Bcl-2. Kumari et al. discovered that coralyne and PTX have a synergistic effect on enhancing apoptosis in MDA-MB-231 cell line by arresting cells in the G1/S phase, inducing DNA fragmentation and changing the mitochondria membrane potential.[24] Bax, cleaved caspase-3 and Bcl-2 are all apoptosis-related proteins that have a great impact on the development of many diseases. caspase-3 and Bax are common pro-apoptotic proteins, while Bcl-2 is an anti-apoptotic protein[25,26]; Bcl-2 regulates mitochondrial membrane permeability, while Bax destroys mitochondrial outer membranes to promote apoptosis.[27,28] The results of our study are consistent with the studies mentioned above, indicating that PTX could exert its therapeutic effect by inhibiting the proliferation of breast cancer cells and promoting their apoptosis.

In addition, PTX could also reduce the invasive ability of breast cancer cells, and the expression of invasion-related proteins MMP-9 and VEGF was inhibited in a dose-dependent manner. Ismail et al. also found that PTX inhibited breast cancer cell invasion through the DJ-1/KLF17 signaling pathway.[29] The VEGF is an angiogenic protein that strongly promotes mitosis of vascular endothelial cells and is an important angiogenic cytokine. Miller et al. confirmed that VEGF was an important factor in the development and progression of breast cancer, and its overexpression could increase the resistance of breast cancer cells to PTX.[30] The MMP-9 is a zinc-containing enzyme that participates in the regulation of the tumor microenvironment.[31] Jiang et al. reported that PTX reduced MMP-9 expression and inhibited cell proliferation in ovarian cancer cells.[32] The results of our study are consistent with these studies. Therefore, we confirmed the inhibitory effect of PTX on the invasion of breast cancer cells.

To further investigate the mechanism of PTX in the treatment of breast cancer, we examined the expression of p-AKT, which is a member of the PI3K/AKT signaling pathway. The PI3K/AKT signaling pathway has been shown to be critical for cell growth and survival.[33] Activation of the PI3K/AKT pathway could lead to increased proliferation and metastasis of various malignancies, including non-small cell lung cancer, ovarian cancer and gastric cancer.[34–36] Similarly, in breast cancer, inhibition of the PI3K/AKT signaling pathway could decrease cell proliferation and resistance to chemotherapeutic drugs.[37,38] We found that the p-AKT (Thr308) and p-AKT (Ser473) expression levels in breast cancer cells were significantly reduced after PTX treatment. Moreover, after PI3K overexpression, the inhibitory effect of PTX on the growth of breast cancer cells was partly reversed. All these findings suggested that PTX could inhibit the proliferation and development of breast cancer by inhibiting the activity of the PI3K/AKT signaling pathway, which is the fundamental mechanism of its anti-cancer effect.

Conclusions

This study validated the potent efficacy of PTX as an anticancer chemotherapeutic drug in the treatment of breast cancer, and further found that it inhibited the development of malignancies by inhibiting the activation of the PI3K/AKT signaling pathway. Therefore, PTX combined with other drugs that can target the PI3K/AKT signaling pathway may further enhance its efficacy in the treatment of breast cancer. However, these results still need to be confirmed by further clinical trials, which we are planning to carry out in the future.

ORCID iDs

Gang Li https://orcid.org/0000-0002-1300-2449
Dongxin Xu https://orcid.org/0000-0002-8728-0898
Jinju Sun https://orcid.org/0000-0002-4277-5686
Shiyun Zhao https://orcid.org/0000-0001-6883-6646
Dan Zheng https://orcid.org/0000-0002-4206-8623

References

1. Shamsi M, Pirayesh Islamian J. Breast cancer: Early diagnosis and effective treatment by drug delivery tracing. *Nucl Med Rev Centr East Eur.* 2017;20(1):45–48.
2. Zhang Y, Li H, Zhang J, et al. The combinatory effects of natural products and chemotherapy drugs and their mechanisms in breast cancer treatment. *Phytochem Rev.* 2019;19(6):1179–1197.
3. Shawky MS, Huo CW, Henderson MA, Redfern A, Britt K, Thompson EW. A review of the influence of mammographic density on breast cancer clinical and pathological phenotype. *Breast Cancer Res Treat.* 2019; 177(2):251–276.
4. Miles RC, Lehman CD, Mercaldo SF, Tamimi RM, Dontchos BN, Narayan AK. Obesity and breast cancer screening: Cross-sectional survey results from the behavioral risk factor surveillance system. *Cancer.* 2019; 125(23):4158–4163.
5. Jones ME, Schoemaker MJ, Wright LB, Ashworth A, Swerdlow AJ. Smoking and risk of breast cancer in the Generations Study cohort. *Breast Cancer Res.* 2017;19(1):118.
6. Wong G, Au E, Badve SV, Lim WH. Breast cancer and transplantation. *Am J Transplant.* 2017;17(9):2243–2253.
7. Arpino G, Milano M, De Placido S. Features of aggressive breast cancer. *Breast.* 2015;24(5):594–600.
8. Jia Y, Weng Z, Wang C, et al. Increased chemosensitivity and radiosensitivity of human breast cancer cell lines treated with novel functionalized single-walled carbon nanotubes. *Oncol Lett.* 2017;13(1): 206–214.
9. Lue X, Deng Q, Li H, Suo Z. Altered characteristics of cancer stem/initiating cells in a breast cancer cell line treated with persistent 5-FU chemotherapy. *Exp Ther Med.* 2011;2(5):821–826.
10. Kantor O, Bao J, Jaskowiak N, Yao K, Tseng J. The prognostic value of the AJCC 8th Edition Staging System for patients undergoing neoadjuvant chemotherapy for breast cancer. *Ann Surg Oncol*. 2020;27(2): 352–358.
11. Bressand D, Novell A, Girault A, et al. Enhancing Nab-paclitaxel delivery using microbubble-assisted ultrasound in a pancreatic cancer model. *Mol Pharm.* 2019;16(9):3814–3822.
12. Leung JC, Cassimeris L. Reorganization of paclitaxel-stabilized microtubule arrays at mitotic entry: Roles of depolymerizing kinesins and severing proteins. *Cancer Biol Ther.* 2019;20(10):1337–1347.
13. Ma X, Özliseli E, Zhang Y, Pan G, Wang D, Zhang H. Fabrication of redox-responsive doxorubicin and paclitaxel prodrug nanoparticles with microfluidics for selective cancer therapy. *Biomater Sci*. 2019;7(2):634–644.
14. Fukuizumi A, Minegishi Y, Omori M, et al. Weekly paclitaxel in combination with carboplatin for advanced non-small-cell lung cancer complicated by idiopathic interstitial pneumonias: A single-arm phase II study. *Int J Clin Oncol*. 2019;24(12):1543–1548.
15. Zou L, Wang D, Hu Y, et al. Drug resistance reversal in ovarian cancer cells of paclitaxel and borneol combination therapy mediated by PEG-PAMAM nanoparticles. *Oncotarget.* 2017;8(36):60453–60468.
16. Hoch MA, Cousins K, Nartey R, Riley K, Hartranft M. Two cases of combination therapy with cetuximab, paclitaxel, and cisplatin for advanced head and neck cancer. *J Oncol Pharm Pract.* 2018;24(7):553–554.
17. Xie HJ, Zhao J, Zhuo-Ma D, Zhan-Dui N, Er-Bu A, Tsering T. Inhibiting tumour metastasis by DQA modified paclitaxel plus ligustrazine micelles in treatment of non-small-cell lung cancer. *Artif Cells Nanomed Biotechnol.* 2019;47(1):3465–3477.
18. Takashima T, Kawajiri H, Nishimori T, et al. Safety and efficacy of low-dose nanoparticle albumin-bound paclitaxel for HER2-negative metastatic breast cancer. *Anticancer Res*. 2018;38(1):379–383.
19. Mendez-Pertuz M, Martinez P, Blanco-Aparicio C, et al. Modulation of telomere protection by the PI3K/AKT pathway. *Nat Commun*. 2017; 8(1):1278.
20. Qu Y, Hao C, Xu J, et al. ILK promotes cell proliferation in breast cancer cells by activating the PI3K/Akt pathway. *Mol Med Rep.* 2017;16(4): 5036–5042.
21. Zheng P, Dong L, Zhang B, et al. Long noncoding RNA CASC2 promotes paclitaxel resistance in breast cancer through regulation of miR-18a-5p/CDK19. *Histochem Cell Biol.* 2019;152(4):281–291.
22. Hu J, Zhang N, Wang R, Huang F, Li G. Paclitaxel induces apoptosis and reduces proliferation by targeting epidermal growth factor receptor signaling pathway in oral cavity squamous cell carcinoma. *Oncol Lett.* 2015;10(4):2378–2384.
23. Liu M, Gong C, Xu R, et al. MicroRNA-5195-3p enhances the chemosensitivity of triple-negative breast cancer to paclitaxel by downregulating EIF4A2. *Cell Mol Biol Lett.* 2019;24:47.
24. Kumari S, Mohan MG, Shailender G, et al. Synergistic enhancement of apoptosis by coralyne and paclitaxel in combination on MDA-MB-231, a triple-negative breast cancer cell line. *J Cell Biochem*. 2019; 120(10):18104–18116.
25. Freitas M, Alves V, Sarmento-Ribeiro AB, Mota-Pinto A. Combined effect of sodium selenite and docetaxel on PC3 metastatic prostate cancer cell line. *Biochem Biophys Res Commun.* 2011;408(4):713–719.
26. Xiang XY, Kang JS, Yang XC, et al. SIRT3 participates in glucose metabolism interruption and apoptosis induced by BH3 mimetic Si in ovarian cancer cells. *Int J Oncol.* 2016;49(2):773–784.
27. Lv J, Liang Y, Tu Y, Chen J, Xie Y. Hypoxic preconditioning reduces propofol-induced neuroapoptosis via regulation of Bcl-2 and Bax and downregulation of activated caspase-3 in the hippocampus of neonatal rats. *Neurol Res.* 2018;40(9):767–773.
28. Peng X, Chen K, Chen J, et al. Aflatoxin B1 affects apoptosis and expression of Bax, Bcl-2, and caspase-3 in thymus and bursa of fabricius in broiler chickens. *Environ Toxicol.* 2016;31(9):1113–1120.
29. Ismail IA, Ei-Sokkary GH, Saber SH. Low doses of paclitaxel repress breast cancer invasion through DJ-1/KLF17 signaling pathway. *Clin Exp Pharmacol Physiol.* 2018;45:961–968.
30. Miller K, Wang M, Gralow J, et al. Paclitaxel plus bevacizumab versus paclitaxel alone for metastatic breast cancer. *N Engl J Med*. 2007; 357(26):2666–2676.
31. Kerenidi T, Kazakou AP, Lada M, et al. Clinical significance of circulating osteopontin levels in patients with lung cancer and correlation with VEGF and MMP-9. *Cancer Invest.* 2016;34(8):385–392.
32. Jiang Z, Zhang SJ, Chen B, et al. Paclitaxel inhibited proliferation and matrix metalloproteinases (MMP-2, MMP-9) expression in ovarian cancer HO8910 cells. *Chinese Journal of Pharmaceutical Analysis*. 2002;22:458–460.
33. Ren F, Su H, Jiang H, Chen Y. Overexpression of miR-623 suppresses progression of hepatocellular carcinoma via regulating the PI3K/Akt signaling pathway by targeting XRCC5. *J Cell Biochem.* 2020;121(34): 213–223.
34. Zhu X, Jiang H, Li J, Xu J, Fei Z. Anticancer effects of Paris saponins by apoptosis and PI3K/AKT pathway in gefitinib-resistant non-small cell lung cancer. *Med Sci Monit.* 2016;22:1435–1441.
35. Meng Q, Xia C, Fang J, Rojanasakul Y, Jiang B-H. Role of PI3K and AKT specific isoforms in ovarian cancer cell migration, invasion and proliferation through the p70S6K1 pathway. *Cell Sign.* 2006;18(12): 2262–2271.
36. Sun C, Tao Y, Gao Y, et al. F-box protein 11 promotes the growth and metastasis of gastric cancer via PI3K/AKT pathway-mediated EMT. *Biomed Pharmacother.* 2018;98:416–423.
37. Liu T, Guo J, Zhang X. MiR-202-5p/*PTEN* mediates doxorubicin-resistance of breast cancer cells via PI3K/Akt signaling pathway. *Cancer Biol Ther.* 2019;20(7):989–998.
38. Li N, Miao Y, Shan Y, et al. MiR-106b and miR-93 regulate cell progression by suppression of PTEN via PI3K/Akt pathway in breast cancer. *Cell Death Dis.* 2017;8(5):e2796.

P wave duration in paroxysmal and persistent atrial fibrillation

Malte Unkell[1,A–F], Maxim Marinov[1,A–F], Peter Stephan Wolff[1,A–F], Jadwiga Radziejewska[2,B,F], Jakub Szymon Mercik[3,A–F], Jacek Gajek[4,A–F]

[1] Students' Scientific Association, Department of Emergency Medical Service, Wroclaw Medical University, Poland
[2] Klodzko County Hospital, Poland
[3] Department of Emergency Medicine, Wroclaw Medical University, Poland
[4] Department of Emergency Medical Service, Wroclaw Medical University, Poland

A – research concept and design; B – collection and/or assembly of data; C – data analysis and interpretation; D – writing the article; E – critical revision of the article; F – final approval of the article

Advances in Clinical and Experimental Medicine, ISSN 1899–5276 (print), ISSN 2451–2680 (online) *Adv Clin Exp Med*. 2020;29(11):1347–1354

Address for correspondence
Jakub Mercik
E-mail: jakub.mercik@wp.pl

Funding sources
None declared

Conflict of interest
None declared

Received on June 21, 2020
Reviewed on July 8, 2020
Accepted on September 20, 2020

Abstract

Background. Functional and structural changes in the atrial muscle constitute a substrate for atrial fibrillation (AF). The pathological changes in the left atrium decrease the conduction velocity and result in prolongation of the P wave duration.

Objectives. To assess the duration of the P wave in patients with AF in different clinical presentations of arrhythmia.

Material and methods. The study group consisted of 119 patients diagnosed with AF: 57 women and 62 men, aged 65.3 ±9.4 years. There were 65 patients with paroxysmal AF and 54 with persistent AF. In this group, electrical cardioversion was performed. The P wave duration was measured using an electrophysiological system in all leads at a paper speed of 200 mm/s.

Results. The patients did not differ in terms of age, gender or comorbidities. The patients with persistent AF had longer P wave duration (159.9 ±22.3 ms compared to 144.6 ±17.2 ms; $p < 0.001$) and higher glucose concentration (119.4 ±33.4 mg/dL compared to 108.0 ±24.6 mg/dL; $p = 0.015$). These results were not influenced by the anti-arrhythmic treatment.

Conclusions. Persistent AF shows a longer P wave duration than the paroxysmal AF, independent of age, gender and anti-arrhythmic medication. The prolongation of the P wave related to persistent arrhythmia should force physicians to restore the sinus rhythm earlier in order to more successfully maintain it in the long term.

Key words: P wave duration, atrial fibrillation, diabetes mellitus, chronic kidney disease

Cite as
Unkell M, Marinov M, Wolff PS, Radziejewska J, Mercik JS, Gajek J. P wave duration in paroxysmal and persistent atrial fibrillation. *Adv Clin Exp Med*. 2020;29(11):1347–1354. doi:10.17219/acem/127680

DOI
10.17219/acem/127680

Introduction

Atrial fibrillation (AF) is an arrhythmic consequence of multiple pathological processes leading to functional and structural changes in the atrial muscle.[1,2] Among the major pathologies leading to this arrhythmia, hypertension, coronary artery disease (CAD), and subsequent heart failure (HF) play the main roles. Despite treating both atria as a substrate of AF, it is clinically assumed that this arrhythmia occurs mainly due to left atrial pathologies, primarily due to the higher workload it needs to cope with as a consequence of the higher left ventricular resistance (LVR). These diseases cause changes in the structure of the atrial muscle through death and apoptosis of cardiomyocytes, contributing to stromal fibrosis. This affects the generation of arrhythmia foci, local potential fragmentation and possible re-entry loops. However, the main consequence visible in echocardiography is the left atrial enlargement.

Furthermore, AF is caused by other arrhythmias, such as multiple atrial extrasystole, atrial focal tachycardia or atrial flutter.[3–5] Whether they are constant or paroxysmal, they lead to electrophysiological changes in the action potential – usually a shortening of the refractory period, the local intensity of which may differ. This is manifested by the heterogeneity of the repolarization process. Repolarization disorders lead to functional conduction disturbances, which – superimposed on the structural changes and conduction slowing associated with cardiomyocyte depletion – intensify the re-entry phenomenon and promote the maintenance and persistence of arrhythmias. These pathologies have an impact on the electrocardiographic (ECG) picture of atrial muscle depolarization, depicted by the P wave of the electrocardiogram. With the duration and progression of functional and structural changes, the duration of the P wave is prolonged, making it a risk factor for AF.[6]

An interesting and clinically important issue is the positive relationship between the AF paroxysm and the tendency of the arrhythmia to persist, which was reflected in the phrase "AF begets AF" coined by Wijffels et al.[7] Rapid atrial arrhythmias affect the functional changes in the process of atrial muscular repolarization and, above all, induce heterogeneity of refraction duration by the formation of local blocks and slow conduction zones.[8] In addition, AF episodes lead to left atrial enlargement, most likely due to an increase in filling pressure, but also due to blood retention and functional mitral regurgitation. All of these processes over time lead to the paroxysmal AF becoming persistent, until finally the decision is made to leave the arrhythmia in a permanent form.[8,9]

All of these issues indicate the need for complex systemic treatment and prevention of AF paroxysms. An important aspect is to reduce the duration of individual episodes using pharmacological or electrical conversion to a sinus rhythm. Prolonged arrhythmia paroxysms lead to a deepening of functional and anatomical changes, so it is likely that patients with persistent AF after sinus rhythm restoration have a longer P wave duration than patients with the paroxysmal form of the arrhythmia.

The aim of the study was to assess P wave duration in patients with AF in different clinical presentations of the arrhythmia.

Material and methods

The study group consisted of 119 patients diagnosed with AF. The group consisted of 57 women and 62 men, aged 65.3 ±9.4 years. The essential comorbidities were reported. There were 65 patients with paroxysmal AF (AF group) who had a sinus rhythm during examination, and 54 patients with persistent AF. In this group, electrical cardioversion was performed to restore a sinus rhythm (CV group). Any antiarrhythmic medication, including β-blockers, propafenone and amiodarone (combination therapy as well), was also recorded. As the exact duration of the arrhythmia episodes was not possible to recollect, we only included those patients with persistent AF lasting 2–24 weeks.

The P wave duration was measured using a LabSystem™ Pro EP Recording System (Boston Scientific, Boston, USA), where the ECG tracings allowed the sinus P waves to be assessed. The P wave duration was measured precisely in all leads at a paper speed of 200 mm/s and an enhancement of 64–128. To avoid any influence of accidental inaccuracies, all measurements were repeated 5 times and the mean value was taken as the result.

In patients with the persistent form of AF, the direct current cardioversion was performed as a standard clinical procedure under general anesthesia using 1 mg/kg of propofol and 50 μg of fentanyl, administered intravenously. A single shock of 300 J was successful in all patients.

The study protocol was approved by the local Bioethical Committee at Wroclaw Medical University, Poland.

Statistical analysis

The statistical analysis was performed using STATISTICA v. 13.3 (StatSoft, Inc., Tulsa, USA). P-values less than 0.05 were considered statistically significant.

For quantitative variables, basic descriptive statistics were calculated (M – average, SD – standard deviation, Me – median, Q1 – lower quartile, Q3 – upper quartile, Min – minimum value, and Max – maximum value) and the compliance of their distributions with a theoretical normal distribution was checked using the Shapiro–Wilk W test. Comparisons were performed with Student's t-test or the Mann–Whitney U test for independent groups, or Kruskal–Wallis analysis of variance (ANOVA) for multiple comparisons. Each categorical variable is presented as numbers and percentages. The comparisons were performed with the χ^2 test.

The correlations between the parameters were checked using Spearman's rank correlation coefficient according to the statistical properties of the data.

The receiver operating characteristic (ROC) was used to assess the ability of P wave duration to classify disease status. Based on the results of examination and ROC analysis, a cutoff threshold for P wave duration was calculated for the AF and CV groups.

Results

The demographic and clinical characteristics of the study participants are presented in Table 1.

The P wave duration did differ significantly between the 2 groups, lasting longer in patients with the persistent form of arrhythmia. The same applied for fasting glucose concentration. The details are presented in Fig. 1. The P wave duration was significantly longer in patients with chronic kidney disease (CKD). The results are presented in Fig. 2. Moreover, there was a weak but statistically significant correlation between the mean P wave duration and creatinine concentration. The results are depicted in Fig. 3.

The upper and lower limits of 95% confidence interval (95% CI) are greater than 0, i.e., the correlation is positive and statistically significant ($p < 0.05$). The increase in creatinine concentration was accompanied by an increase in P wave duration.

However, no statistically significant relationship was observed between the dosage of propafenone and the duration of the P wave. Spearman's rank correlation cohort rho does not differ significantly from 0 (the upper and lower limits of the 95% CI differ in sign, i.e., they contain 0; $p > 0.05$). This conclusion applies to both the entire sample of patients and to the AF and CV groups separately.

There were no correlations between P wave duration and propafenone treatment (dosage) among all patients, nor in AF and CV groups. The results are depicted in Fig. 4. The basic statistics of P wave duration in the groups

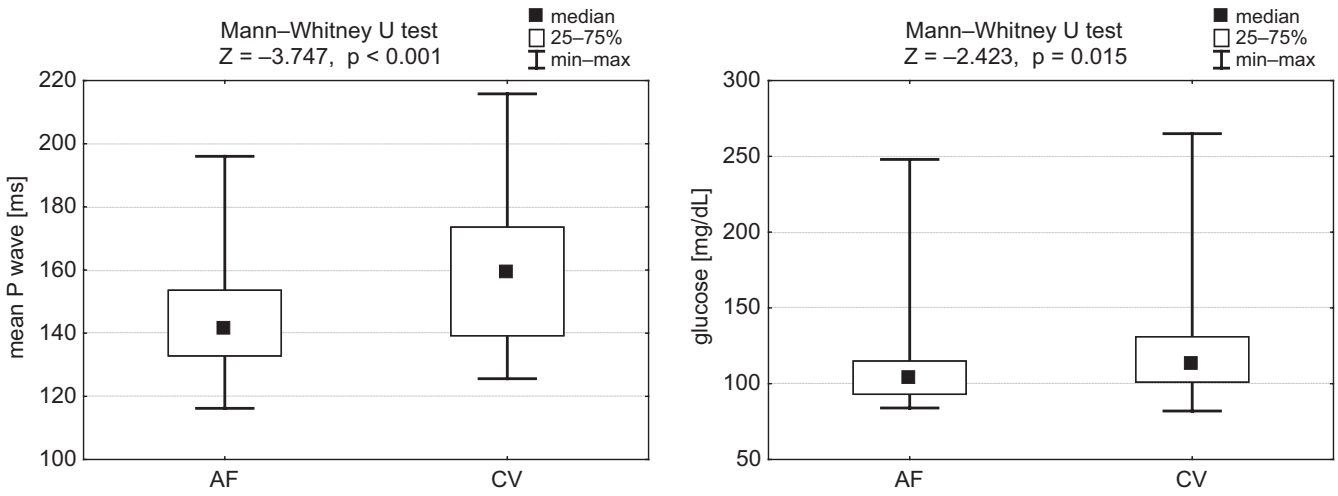

Fig. 1. Glucose level and average P wave duration in groups of patients according to the type of AF and the results of significance tests

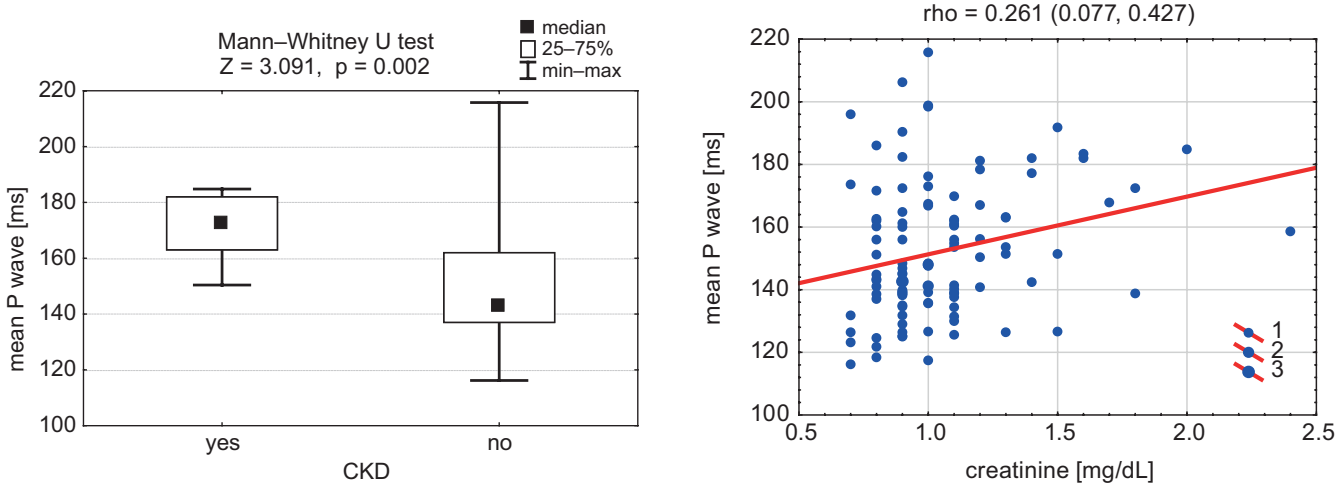

Fig. 2. The average P wave duration in groups of patients according to the presence of CKD and the results of significance tests

Fig. 3. Correlation diagram of average P wave duration with creatinine level and Spearman's rank correlation coefficient and its 95% CI

Table 1. Clinical characteristics of the total population and the comparisons of 2 groups of studied patients

Parameter	Total	AF	CV	p-value
	n = 119 (100%)	n = 65 (54.6%)	n = 54 (45.4%)	
Mean age [years]	65.3 ±9.4	65.0 ±8.9	65.6 ±10.1	0.712
Male/female	62/57	34/31	28/26	0.893
Comorbidities:				
HT	89 (74.8%)	48 (73.8%)	41 (75.9%)	0.962
DM	25 (21.0%)	12 (18.5%)	13 (24.1%)	0.601
CKD	9 (7.6%)	6 (9.2%)	3 (5.6%)	0.509
IHD	21 (17.6%)	12 (18.5%)	9 (16.7%)	0.989
HF	11 (9.2%)	3 (4.6%)	8 (14.8%)	0.065
Laboratory:				
K+ [mmol/L]	4.45 ±0.44	4.42 ±0.43	4.49 ±0.45	0.446
Glucose [mg/dL]	113.3 ±29.4	108.0 ±24.6	119.4 ±33.4	0.015
Creatinine [mg/dL]	1.05 ±0.28	1.01 ±0.22	1.09 ±0.34	0.340
Medicines:				
Propafenone	43 (36.1%)	19 (29.2%)	24 (44.4%)	0.126
Amiodarone	17 (14.3%)	9 (13.8%)	8 (14.8%)	0.910
Bisoprolol	22 (18.5%)	12 (18.5%)	10 (10.5%)	0.819
Metoprolol	86 (72.3%)	44 (67.7%)	42 (77.8%)	0.309
Mean P wave duration [ms]	151.5 ±21.0	144.6 ±17.2	159.9 ±22.3	<0.001

HT – arterial hypertension; DM – diabetes mellitus; CKD – chronic kidney disease; IHD – ischemic heart disease; HF – heart failure.

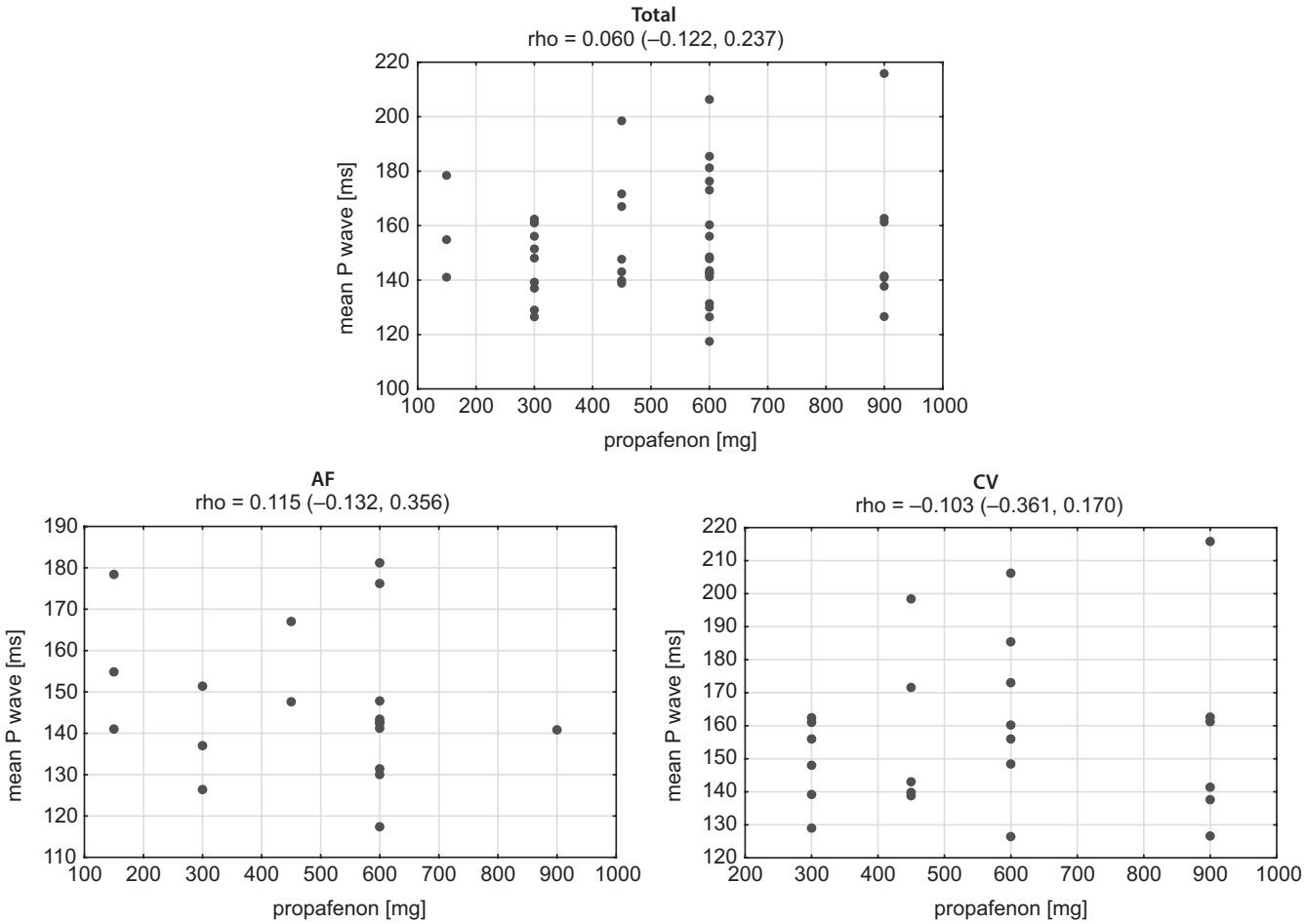

Fig. 4. Correlation diagram of average P wave duration with creatinine level and Spearman's rank correlation coefficient and its 95% CI

Table 2. Basic statistics of the average P wave duration in the study group according to the analyzed parameters and the results of significance tests

Variables	Mean P wave duration [ms]			p-value
	M ±SD	Me [Q1, Q3]	min–max	
Group				
AF (n = 65)	144.6 ±17.2	141 [133; 154]	116–196	<0.001
CV (n = 54)	159.9 ±22.3	159 [139; 174]	126–216	
Gender				
Male (n = 62)	149.4 ±20.2	147 [134; 162]	116–206	0.273
Female (n = 57)	153.8 ±21.8	145 [139; 167]	118–216	
Age [years]				
≤65 (n = 52)	149.3 ±21.7	141 [136; 161]	117–216	0.193
>65 (n = 67)	153.3 ±20.5	150 [139; 167]	116–199	
HT				
Yes (n = 89)	154.4 ±21.7	150 [139; 168]	116–216	0.008
No (n = 30)	142.9 ±16.2	139 [132; 151]	117–199	
DM				
Yes (n = 25)	151.8 ±21.9	145 [139; 172]	116–190	0.891
No (n = 94)	151.5 ±20.9	147 [138; 163]	117–216	
CKD				
Yes (n = 9)	170.6 ±13.5	172 [163; 182]	150–185	0.002
No (n = 110)	150.0 ±20.8	143 [137; 162]	116–216	
IHD				
Yes (n = 21)	154.7 ±22.8	151 [139; 177]	116–186	0.397
No (n = 98)	150.9 ±20.7	145 [137; 162]	117–216	
HF				
Yes (n = 11)	156.8 ±24.7	160 [139; 182]	116–192	0.361
No (n = 108)	151.0 ±20.7	145 [137; 163]	117–216	
Propafenone				
Yes (n = 43)	153.2 ±22.0	148 [139; 163]	117–216	0.519
No (n = 76)	150.6 ±20.5	145 [136; 164]	116–199	
Amiodarone				
Yes (n = 17)	150.3 ±17.8	150 [141; 160]	116–182	0.796
No (n = 102)	151.7 ±21.6	144 [137; 167]	117–216	
Metoprolol				
Yes (n = 86)	151.2 ±20.9	148 [138; 163]	116–216	0.974
No (n = 33)	152.3 ±21.7	141 [137; 170]	123–198	
Bisoprolol				
Yes (n = 22)	147.6 ±17.7	144 [139; 156]	125–199	0.453
No (n = 97)	152.4 ±21.7	148 [138; 167]	116–216	

HT – arterial hypertension; DM – diabetes mellitus; CKD – chronic kidney disease; IHD – ischemic heart disease; HF – heart failure.

of patients differing according to the analyzed parameters and the results of significance tests are presented in Table 2.

In ANOVA, it turned out that P wave duration has a statistically significant relationship with diagnosis (AF group = 0; CV group = 1) as well as hypertension and CKD. Due to the possibility of a strong correlation between these parameters, a multifactorial (progressive, stepwise) regression analysis was performed. As a result, the following model was obtained:

Mean P wave duration = 120.3 + 15.8 × CV + 20.2 × CKD + 9.0 × HT ± 18.5

The factors (stimulants) of longer P wave duration turned out to be membership in the CV group and the presence of CKD and hypertension. All structural parameters of the model are statistically significant ($p < 0.0001$): $F(3, 115) = 12.6$; $p < 0.001$.

The duration of the P wave can be regarded as a parameter by which patients can be classified into the CV or AF

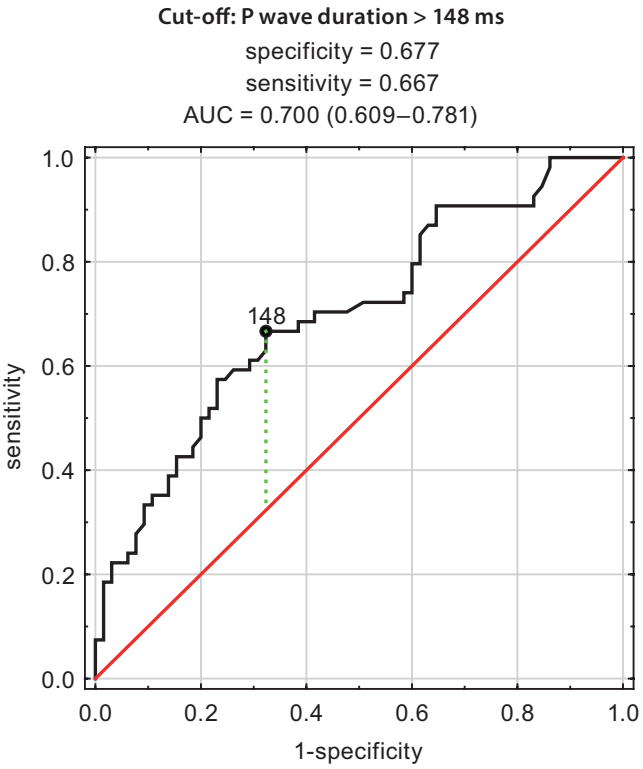

Fig. 5. ROC curve for P wave duration; cutoff value between patients from the CV and the AF groups; the sensitivity and specificity of the test and the AUC and its 95% CI

group. Analysis of the ROC curve showed that for the cut-off value of P wave, duration was lower than 148 ms, the diagnostic sensitivity of the test was 67.7%, the specificity 66.7%, and the area under the ROC curve (AUC) was 0.700. This is not a sensational result, but the lower confidence limit for AUC is 0.609 and is greater than 0.5, which indicates the diagnostic usefulness of this parameter. According to the literature, if the AUC is in the range of 0.7–0.8, the classifier is satisfactory. The graph is shown in Fig. 5.

Discussion

The duration of the P wave is a result of the conduction velocity in the atrial working myocardium and the distance the electrical activation has to travel. Functional and structural changes in the atrial muscle affect both of these parameters – they slow down conduction velocity and extend the path to be traveled due to the enlargement of the atria. This results in a longer P wave duration and a change in its morphology. The same changes in structure and function are responsible for generating atrial arrhythmias, including AF.[6] Additionally, the ongoing arrhythmia leads to a progression of the abovementioned changes. In particular, the enlargement of the left atrium is clearly associated with an increase in the filling pressure of the left ventricle and likely dependent on the ventricular rate.[10] Data on the effect of AF on muscle conduction is more scarce and less consistent.[11]

The main finding of our study is the longer duration of the P wave in patients with average long-term persistent AF compared to patients with paroxysmal arrhythmia and sinus rhythm at the time of the study. The degree to which the P wave duration was extended (about 10%) is not only statistically significant, but clinically as well. It should be emphasized that the P waves measured in both groups markedly exceed the normal values of 120 ms (144.6 ms in AF group compared to 159.9 ms in CV group). Similar comparisons are not numerous in the available literature.[12–13] As our subgroups of patients suffering from paroxysmal and persistent AF are comparable according to age and gender distribution, comorbidities and antiarrhythmic medication, it indicates that this additional prolongation was caused only by the presence of the prolonged episodes of arrhythmia. Our measurements were not performed immediately after the cardioversion shock, so the influence of direct current can be ignored. Additionally, in 1 small study, the direct current flow during cardioversion had little or no effect on the P wave duration immediately after the procedure and on the next day.[14]

Even if diabetic patients were not frequently presented in our study group, there was a noticeable difference between diabetics and non-diabetics in terms of P wave duration. Those with diabetes mellitus (DM) were observed to have a longer P wave than participants without it. This is in line with other clinical observations even the direct evidence lacks in human. Diabetes is presumed to be a risk factor for AF; the topic has been reviewed quite often. A meta-analysis of different cohort and case control studies investigating the correlation between DM and AF showed that individuals with DM had a 40% greater risk of AF than unaffected individuals.[15] There is sparse literature to be found about DM leading to electrical changes of the atrial substrate.[16] In an experimental setting of DM, it was associated with increased atrial fibrosis, interatrial conduction delay and greater inducibility of AF.[17] Another animal study confirmed those results with additional interesting observations of P wave prolongation in diabetic rats without left atrial enlargement, which the authors attributed to diabetic changes in the gap junction protein, Cx.[18] Similar outcomes were obtained in patients with impaired fasting glucose levels leading to significantly longer interatrial conduction times and, in consequence, decreased left atrial emptying volume and fraction.[19]

In another subgroup of our patients, CKD was found to be a predictor of longer P wave duration. In the literature, some studies have made an association between maximum P wave duration and an exacerbation of the renal condition until the defined endpoints of hemodialysis, death or a specified decline in estimated glomerular filtration rate (eGFR).[20,21] Based on our results, it could be assumed that a reciprocal influence of CKD on P wave duration is occurring as well, possibly because of a simple fluid overload. Referring to the patients included in our study, only a small number of patients (9 (7.6%)) presented with

CKD as a comorbidity, but it was discovered to be statistically significantly related to P wave duration. This requires further investigation in other studies which would not be distorted by the small number of CKD patients. Atrial fibrillation is frequently described together with renal dysfunction, mainly as a preceding comorbidity, but no evidence has been found supporting the notion of CKD being the cause of AF. Nevertheless, our results indicate such a possibility, making the subject worthy of study.

Anti-arrhythmic medication influences the electrophysiological properties of the working myocardium, in particular the conduction speed and refractory period, which could influence P wave duration. The results of our study do not support this idea. Amiodarone is a class III antiarrhythmic agent acting mainly as a potassium channel blocker. The drug prolongs refractory period and atrial repolarization. It has been shown to be effective in maintaining a sinus rhythm and preventing arrhythmia episodes in patients with paroxysmal AF. Although in 1 small study the researchers reported an amiodarone-related increase in P wave duration, it was a narrow, experimental animal study and the conditions were not comparable to the sinus rhythm in humans, which was present in our study.[22] The relationship between P wave duration and amiodarone administration was similarly negated in a study conducted by Sasaki et al.[23]

In contrast to amiodarone, treatment with a sodium channel blocker could theoretically influence the P wave duration. Propafenone is an IC class agent which blocks the fast sodium channels, slowing down the conduction velocity in the working myocardium. According to literature data, there is no direct relationship between the dosage of propafenone and P wave duration, though the same study confirmed a weak correlation between treatment with propafenone and a prolongation of P wave duration.[24] Our data does not confirm this finding. It should be noted, however, that our group of patients treated with propafenone was not very large.

Based on our results, the theoretical model resulting from ROC curves indicates an estimated P wave duration which differentiates patients between sinus rhythm and persistent AF groups. This approach has not been presented in the literature so far, so our value of P wave duration (148 ms) can only be referred to studies indicating the importance of this parameter in the prediction of sinus rhythm maintenance after electrical cardioversion. In 1999, Aytemir et al. investigated the P wave signal-averaged ECG in 73 patients after successful cardioversion. During the six-month follow-up period, a recurrence of AF was observed in 31 patients, while in 42 patients, a sinus rhythm was maintained. The researchers found no difference between the groups according to gender, age, presence of organic heart disease, left atrial diameter, left ventricular ejection fraction, use of antiarrhythmic drug, or duration of AF. The filtered P wave duration was statistically significantly longer in patients with a recurrence of AF (138.4 ms compared to 112.5 ms). A filtered P wave duration of 128 ms had a sensitivity of 70% and a specificity of 76% for the detection of AF recurrence.[25] On the other hand, in a study by Perzanowski et al. the maximum P wave duration did not differentiate patients who remained in sinus rhythm or experienced a recurrence of arrhythmia (142 ms compared to 145 ms; p-value not significant).[26] As the authors did not mention their methodology of P wave duration measurement, it should be assumed that they used a simple, standard 12-lead ECG without any more precise equipment. This lack of precision could have been the cause of their results. In a study by Gonna et al., a 12-lead ECG was recorded after electrical cardioversion for persistent AF in 77 patients and was repeated after 1 month. Compared with the sinus rhythm group, the group with recurrent AF had more patients with a P wave duration that exceeded 142 ms. Using a cutoff <142 ms for P wave duration, the authors showed a sensitivity of 64.6% and a specificity of 62.1% for sinus rhythm maintenance. In multiple regression analysis, a P wave duration longer than 142 ms was the only independent predictor of AF recurrence.[27] The abovementioned considerations indicate unequivocally that the prolongation of the P wave is clearly a risk factor for paroxysm of AF and for more advanced stages of arrhythmia, which is in line in our results. Moreover, we have produced evidence which supports the previous findings in different settings. Regarding the higher values of P wave duration obtained in this study, it should be remembered that the precise methodology used in our study is qualitatively different from that of other researchers.[26,27] This is because a few years ago we confirmed the lack of P wave dispersion that was reported in some of the abovementioned papers, which is related to the inaccuracy of the measurements.[28]

In summary, ongoing AF in the form of a moderately long, persistent arrhythmia has a negative impact on structural and functional atrial remodeling. This occurs independently of age, gender and type of anti-arrhythmic treatment, it but may be somewhat related to certain comorbidities.

Study limitations

An important limitation of our study is its single-center design and relatively small study group. In addition, this is not a prospective clinical study indicating the relationship between ECG parameters and long-term prognosis. As our measurement method – an electrophysiological recording system – is extremely precise, we are aware that our results cannot be directly compared to those of other authors. We previously mentioned that the duration of the persistent form of arrhythmia cannot be exactly estimated. Because our hypothesis is that the longer P wave duration is mainly related to AF itself, this should be assumed as the main limitation of our study, even if the literature data contradict the correlation between arrhythmia duration and P wave prolongation.[14]

Conclusions

Persistent AF shows a longer P wave duration than the paroxysmal form of arrhythmia, independent of age, gender and anti-arrhythmic medication. The prolongation of the P wave related to persistent arrhythmia should compel physicians to restore a sinus rhythm earlier to more successfully maintain it in the long term.

ORCID iDs

Malte Unkell https://orcid.org/0000-0003-4471-848X
Maxim Marinov https://orcid.org/0000-0001-8048-9675
Peter Stephan Wolff https://orcid.org/0000-0002-9687-8808
Jadwiga Radziejewska https://orcid.org/0000-0001-9153-9754
Jakub Szymon Mercik https://orcid.org/0000-0002-5627-7071
Jacek Gajek https://orcid.org/0000-0002-0038-1750

References

1. Thijssen VLJL, Ausma J, Liu GS, Allessie MA, van Eys GJ, Borgers M. Structural changes of atrial myocardium during chronic atrial fibrillation. *Cardiovasc Pathol*. 2000;9(1):17–28.
2. Casaclang-Verzosa G, Gersh BJ, Tsang TSM. Structural and functional remodeling of the left atrium: Clinical and therapeutic implications for atrial fibrillation. *J Am Coll Cardiol*. 2008;51(1):1–11.
3. Waks JW, Josephson ME. Mechanisms of atrial fibrillation: Reentry, rotors and reality. *Arrhythm Electrophysiol Rev*. 2014;3(2):90–100.
4. Pellman J, Sheikh F. Atrial fibrillation: Mechanisms, therapeutics and future directions. *Compr Physiol*. 2015;5(2):649–665.
5. Rosso R, Kistler PM. Focal atrial tachycardia. *Heart*. 2010;96(3):181–185.
6. Hari KJ, Nguyen TP, Soliman EZ. Relationship between P-wave duration and the risk of atrial fibrillation. *Expert Rev Cardiovasc Ther*. 2018;16(11):837–843.
7. Wijffels MC, Kirchhof CJ, Dorland R, Allessie MA. Atrial fibrillation begets atrial fibrillation: A study in awake chronically instrumented goats. *Circulation*. 1995;92(7):1954–1968.
8. Shukla A, Curtis AB. Avoiding permanent atrial fibrillation: Treatment approaches to prevent disease progression. *Vasc Health Risk Manag*. 2014;10(1):1–12.
9. Fuster V, Rydén LE, Cannom DS, et al; American College of Cardiology Foundation/American Heart Association Task Force. 2011 ACCF/AHA/HRS focused updates incorporated into the ACC/AHA/ESC 2006 guidelines for the management of patients with atrial fibrillation: A report of the American College of Cardiology Foundation/American Heart Association Task Force on practice guidelines. *Circulation*. 2011;123(10):e269–e367.
10. D'Andrea A, De Corato G, Scarafile R, et al. Left atrial myocardial function in either physiological or pathological left ventricular hypertrophy: A two-dimensional speckle strain study. *Br J Sports Med*. 2008;42(8):696–702.
11. Nattel S, Burstein B, Dobrev D. Atrial remodeling and atrial fibrillation: Mechanisms and implications. *Circ Arrhythm Electrophysiol*. 2008;1(1):62–73.
12. Censi F, Calcagnini G, Triventi M, et al. P-wave characteristics after electrical external cardioversion: Predictive indexes of relapse. *Conf Proc IEEE Eng Med Biol Soc*. 2010:3442–3445.
13. Bagliani G, Michelucci A, Angeli F, Meniconi L. Atrial activation analysis by surface P wave and multipolar esophageal recording after cardioversion of persistent atrial fibrillation. *Pacing Clin Electrophysiol*. 2003;26(5):1178–1188.
14. Sato T, Mitamura H, Kurita Y, et al. Recovery of electrophysiological parameters after conversion of atrial fibrillation. *Int J Cardiol*. 2001;79(2–3):183–189.
15. Huxley RR, Filion KB, Konety S, Alonso A. Meta-analysis of cohort and case-control studies of type 2 diabetes mellitus and risk of atrial fibrillation. *Am J Cardiol*. 2011;108(1):56–62.
16. Wang A, Green JB, Halperin, Piccini JP Sr. Atrial fibrillation and diabetes mellitus. *J Am Coll Cardiol*. 2019;74(8):1107–1115.
17. Fu H, Liu C, Li J, et al. Impaired atrial electromechanical function and atrial fibrillation promotion in alloxan-induced diabetic rabbits. *Cardiol J*. 2013;20(1):59–67.
18. Li B, Pan Y, Li X. Type 2 diabetes induces prolonged P-wave duration without left atrial enlargement. *J Korean Med Sci*. 2016;31(4):525–534.
19. Ayhan S, Ozturk S, Alcelik A, et al. Atrial conduction time and atrial mechanical function in patients with impaired fasting glucose. *J Interv Card Electrophysiol*. 2012;35(3):247–252.
20. Huang J-C, Wei S-Y, Chen S-C, et al. P wave dispersion and maximum P wave duration are associated with renal outcomes in chronic kidney disease. *PLoS One*. 2014;9(7):e101962.
21. Su H-M, Tsai W-C, Lin T-H, et al. P wave dispersion and maximum P wave duration are independently associated with rapid renal function decline. *PLoS One*. 2012;7(8):e42815.
22. Burashnikov A, Di Diego JM, Sicouri S, Ferreiro M, Carlsson L, Antzelevitch C. Atrial-selective effects of chronic amiodarone in the management of atrial fibrillation. *Heart Rhythm*. 2008;5(12):1735–1742.
23. Sasaki N, Watanabe I, Kogawa R, et al. Effects of intravenous amiodarone and ibutilide on action potential duration and atrial conduction kinetics in patients with persistent atrial fibrillation. *Int Heart J*. 2014;55(3):244–248.
24. Cheriex EC, Krijne R, Brugada P, Heymeriks J, Wellens HJ. Lack of clinically significant beta-blocking effect of propafenone. *Eur Heart J*. 1986;8(1):53–56.
25. Aytemir K, Aksoyek S, Yildirir A, Ozer N, Oto A. Prediction of atrial fibrillation recurrence after cardioversion by P wave signal-averaged electrocardiography. *Int J Cardiol*. 1999;70(1):15–21.
26. Perzanowski C, Ho AT, Jacobson AK. Increased P-wave dispersion predicts recurrent atrial fibrillation after cardioversion. *J Electrocardiol*. 2005;38(1):43–46.
27. Gonna H, Gallagher MM, Guo XH, Yap YG, Hnatkova J, Camm AJ. P-wave abnormality predicts recurrence of atrial fibrillation after electrical cardioversion: A prospective study. *Ann Noninvasive Electrocardiol*. 2014;19(1):57–62.
28. Zimmer K, Przywara W, Zyśko D, Sławuta A, Gajek J. The nature of P-wave dispersion: A clinically useful parameter that does not exist. *Int J Cardiol*. 2016;212:59–60.

Optimization of tubing method of biopsy samples during preimplantation genetic testing

Shuai Liu[A–D,F], Zhiheng Chen[A,F], Yunhao Liang[B,F], Hui Wang[C,F], Li Yang[C,F], Ling Sun[A–D,F]

Center of Reproductive Medicine, Guangzhou Women and Children's Medical Center, Guangzhou Medical University, China

A – research concept and design; B – collection and/or assembly of data; C – data analysis and interpretation;
D – writing the article; E – critical revision of the article; F – final approval of the article

Advances in Clinical and Experimental Medicine, ISSN 1899–5276 (print), ISSN 2451–2680 (online) *Adv Clin Exp Med*. 2020;29(11):1355–1361

Address for correspondence
Ling Sun
E-mail: sunling6299@163.com

Funding sources
This study was supported by the project grant from the Health Science and Technology Project of Guangzhou (grant No. 20191A011027) and Clinical Research Project of Chinese Medical Association (grant No. 18010210750).

Conflict of interest
None declared

Received on May 29, 2020
Reviewed on August 10, 2020
Accepted on September 20, 2020

Abstract

Background. Preimplantation genetic testing (PGT) is a powerful tool for patients with a high risk of transmitting a genetic abnormality to their children. Unlike other assisted reproductive technologies (ART), it has technical issues which remain unresolved.

Objectives. To develop a modified tubing method for placing biopsied samples into amplification tubes for PGT.

Material and methods. A modified tubing method was developed and applied to PGT, with the micromanipulator aiding in the fine movement of transfer pipettes, and with a microinjector to minimize the amount of medium which is transferred with the biopsy samples into the amplification tube. A total of 826 blastocysts from 222 PGT cycles performed between December 2016 and December 2019 were retrospectively analyzed. As the tubing of the cells could not always be inspected visually and they would only be detected by the presence of DNA after amplification, the main outcome measure was the amplification success rate.

Results. The amplification success rate with the modified tubing method was 99.6%.

Conclusions. The modified tubing method is efficient and simple. It is a promising technique for PGT tubing. To the best of our knowledge, this is the first report on the use of a modified micromanipulator and microinjector for improving the tubing rate in PGT cycles, and the presented method is by far the closest to actual use for PGT tubing.

Key words: trophectoderm biopsy, preimplantation genetic testing, modified tubing method, vision-based tubing system, biopsy tubing

Cite as
Liu S, Chen Z, Liang Y, Wang H, Yang L, Sun L. Optimization of tubing method of biopsy samples during preimplantation genetic testing. *Adv Clin Exp Med*. 2020;29(11):1355–1361. doi:0.17219/acem/127679

DOI
10.17219/acem/127679

Introduction

Preimplantation genetic testing (PGT) is used in early prenatal genetic diagnosis, in which abnormal embryos are identified, so that only genetically normal embryos can be used for transfer. Its indications have also been significantly extended to include common late-onset disorders and non-genetic conditions, such as testing for human leukocyte antigens (HLA) matching.[1,2] There is no doubt that PGT is a powerful tool for patients with a high risk of transmitting a genetic abnormality to their children, though the technique has its own set of specific technical issues.[3,4]

Preimplantation genetic testing requires multiple steps and manipulations of the gametes and embryos in order to select unaffected embryos for transfer and subsequent potential pregnancy. For example, the quantitative polymerase chain reaction (qPCR)-based trophectoderm biopsy for both monogenic diseases and chromosomal abnormalities consists of 32 steps in the process.[5] The main steps involved in PGT are as follows: embryo biopsy, biopsy tubing, embryo cryopreservation, diagnosis, embryo warming, and embryo transfer.[6] Placing biopsied samples into amplification tubes (tubing) without losing genetic material is a prerequisite for the ultimate success of DNA amplification.[7] Cases of DNA amplification failure are mainly due to losing the biopsy samples during the tubing process, which requires repeated moving and washing.[8] Because of these losses, there may be no biopsy samples to diagnose, which is an outcome that is unacceptable for all couples.[9]

Unfortunately, the conventional method relies on the manual control of micropipettes for transferring embryonic cells to PCR tubes with or without microscopic visualization.[10] Transferring biopsy samples into PCR tubes and precisely controlling the position of the cells within the micropipette is challenging because of the small volume and the strong adhesion force of the cells involved in the process. Due to the inherently limited manipulability offered by manual control, the outcome is heavily dependent on the operator's ability and experience. These limitations cause the need for optimization of the tubing process.

In recent years, we have seen progress in automation and novel techniques in the field of assisted reproductive technology (ART) manipulation, but there is little or no debate about the optimization of tubing techniques for placing biopsy samples into amplification tubes for PGT.[11–14] The purpose of this study was to describe a new method for biopsy sample tubing, which allows the tubing step to be precisely controlled, and minimizes the amount of medium transferred along with the cell into the PCR tube. To our knowledge, this is the first report on the use of a modified micromanipulator and microinjector for improving the tubing rate in PGT cycles, and the presented method is by far the closest to the actual use for PGT tubing.

Material and methods

Patients

This retrospective study was performed at a single in vitro fertilization (IVF) center and analyzed the PGT cycles of patients who had undergone treatment between December 2016 and December 2019. A total of 826 embryos from 139 patients were biopsied at the blastocyst stage. Only vitrified–warmed single-embryo transfers (SETs) were performed in this study. The primary outcome in this study was the amplification success rate, as the tubing of the cells could occasionally not be inspected visually and would only be detected through the presence of DNA after amplification. The study was approved by the Ethics Committee of Guangzhou Women's and Children's Hospital (China) and informed consent was obtained from all participants.

Embryo culture and biopsy

Only zygotes presenting with 2 pronuclear bodies were cultured in G1-PLUS/G2-PLUS sequential media (Vitrolife, Gothenburg, Sweden) until they reached the blastocyst stage. Blastocyst grading was performed based on the Gardner and Schoolcraft criteria.[15] Biopsies were performed on day 5 or day 6 according to the blastocyst grade on that day.

Preparation of modified transfer device

The modified transfer device assembly consists of a modified micromanipulator, a modified microinjector with a drawn Pasteur pipette, and a homemade PCR rack (Fig. 1A). It was used in conjunction with a stereomicroscope (Fig. 1B). The micromanipulator modified for the movement of the transfer micropipette could be made by dismantling part of the injection holder from a commercial micromanipulator, such as RI (Falmouth, UK), Narishige (Tokyo, Japan), or Eppendorf. The modified microinjector (Fig. 2A) was made from a commercial microinjector, where the end cap on the top of the micropipette holder was replaced with a flexible silica gel connector with an inner diameter of 200–300 µm. The rack for the PCR tube (Fig. 2B) was made from a petri dish with a notch attached to it to give it a suitable tilting angle (30–35°) for the tube. The micropipettes used to transfer the biopsy samples (Fig. 2A), with an internal diameter of 30–40 µm, were drawn using Pasteur pipettes. After being drawn, the glass pipettes were sterilized using dry heat at 160°C for 2 h.

Biopsy tubing

At any step from biopsy tubing onwards, the procedure of moving biopsy samples from the biopsy dish to a PCR tube was performed inside an IVF workstation, with the aid of a modified transfer device and

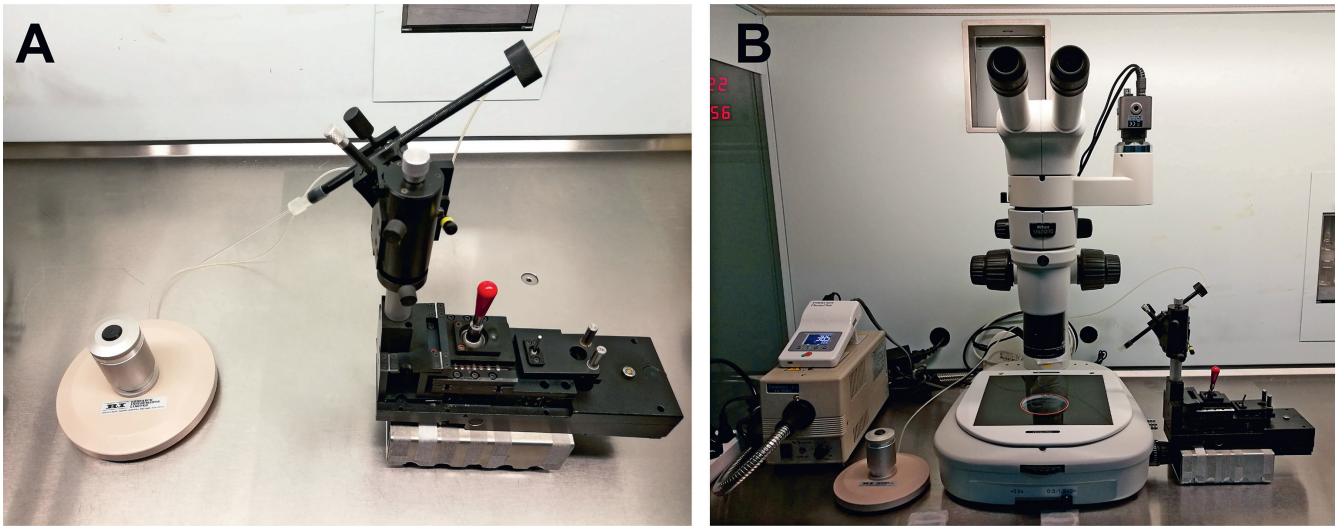

Fig. 1. Representation of the modified transfer device. A. The modified transfer device assembly. B. The modified transfer device in conjunction with stereomicroscope

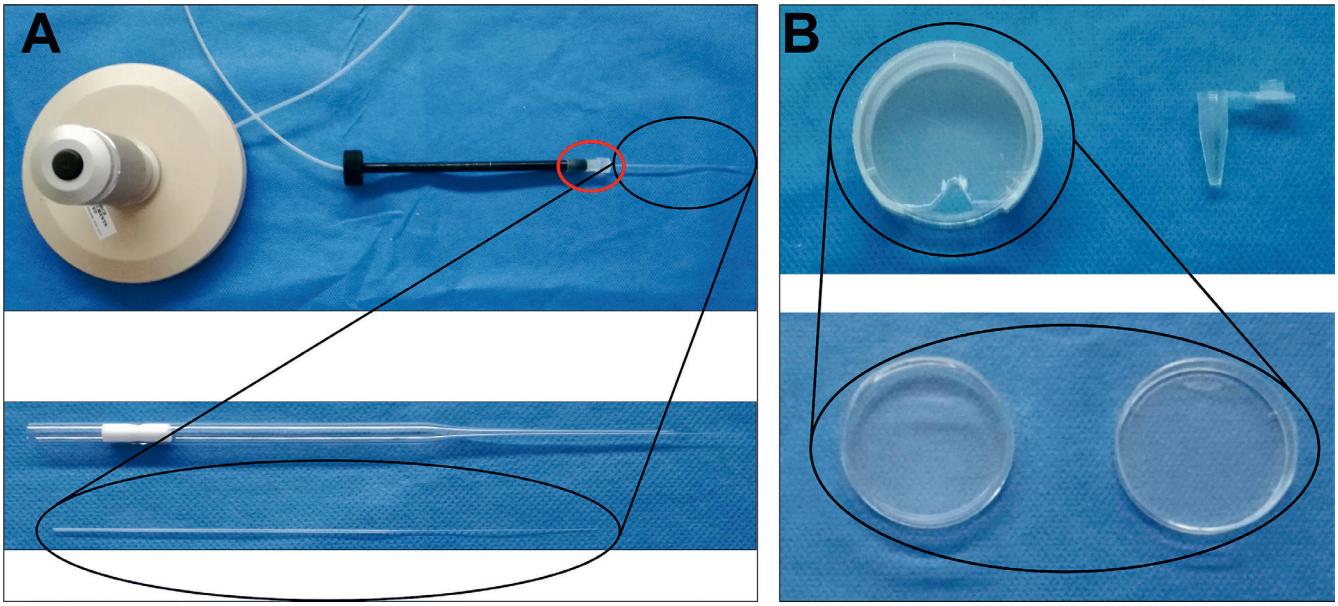

Fig. 2. Material source and construction of modified microinjector, micropipette and PCR tube rack. Inside the red oval is the flexible silica gel connector

a stereomicroscope. In brief, the biopsy dish is moved and placed under the stereomicroscope. The magnification of the stereoscope is adjusted according to the micropipette. With the aid of the modified micromanipulator and microinjector, the transfer micropipette is moved to the biopsy sample, and then the biopsy sample is drawn into the micropipette (Fig. 3A,B). The biopsied specimen is washed with a few drops of clean media to remove paraffin oil, partial sets of chromosomes and other potential contaminants. Following the same steps, the biopsy samples in the micropipette are moved into the corresponding PCR tube (Fig. 3C,D).

To avoid the biopsied cells becoming stuck to the inner wall of the transfer micropipette, the micropipette should be washed in 7% polyvinylpyrrolidone (PVP) medium before biopsy tubing.

Statistical analysis

All data analysis was performed using SPSS Statistics v. 25 software (IBM Corp., Armonk, USA). The statistics are expressed as means ± standard deviation (SD) for continuous variables, while percentages are used for categorical variables.

Results

Characteristics and embryological data of the study patients

A total of 826 blastocyst-stage biopsies from 222 PGT cycles at a single center using the modified tubing method

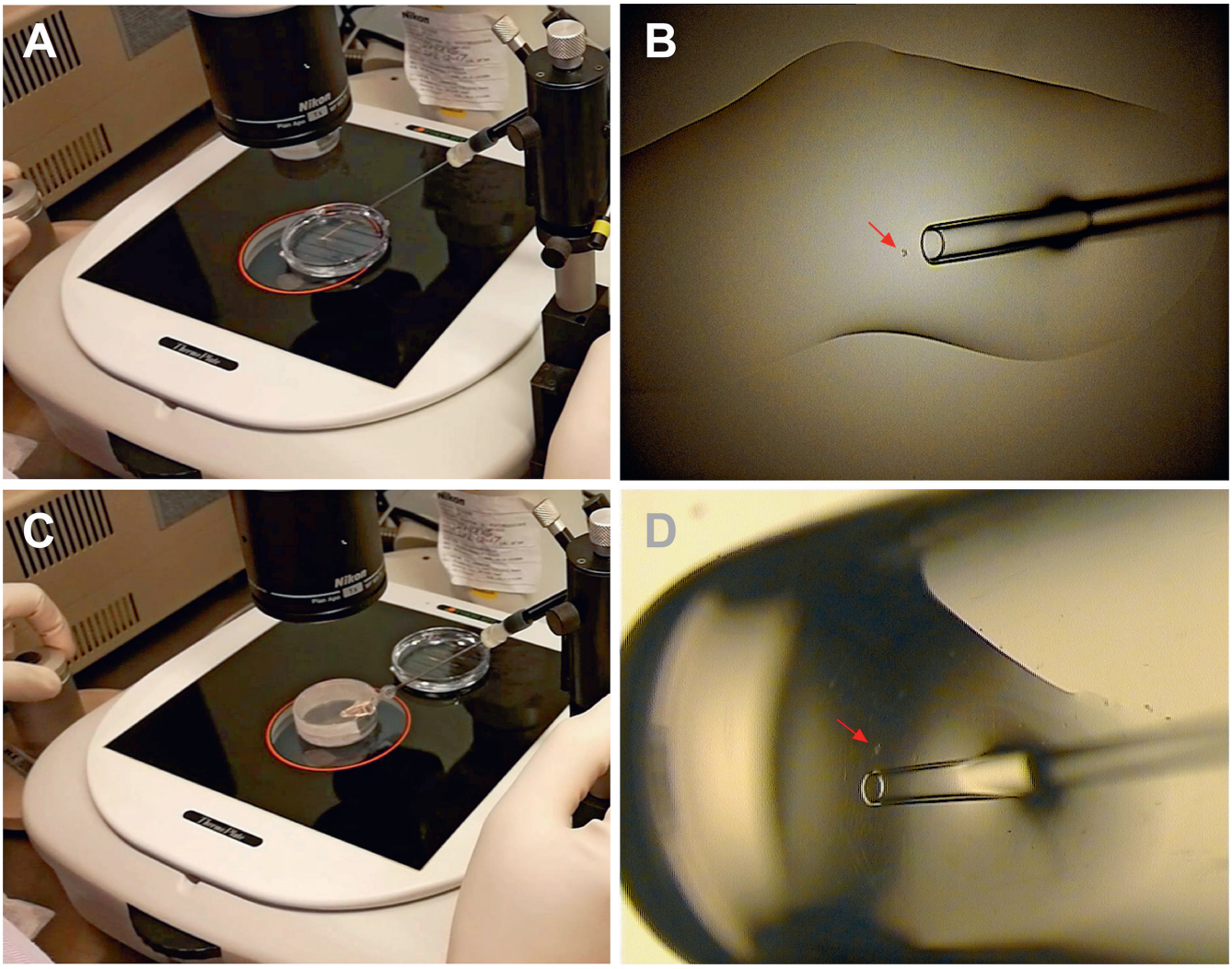

Fig. 3. Optimization of biopsy tubing procedural steps. A,B. The biopsy sample was transferred from biopsy dish. C,D. The locate the micropipette containing biopsy sample was inserted into the PCR tube, and the biopsy sample was expelled into the PCR tube. The red arrows showed the microscopic visualization of biopsy sample

for biopsy samples between December 2016 and December 2019 were included. The characteristics of the study patients are shown in Table 1. In laboratory outcomes, 2595 metaphase II (MII) oocytes were injected and cultured, 2113 were observed to have 2 pronuclear bodies and 2060 fertilized oocytes reached the cleavage stage. There were 1359 cleavage-stage embryos developed to blastocyst stage, of which 826 were usable blastocysts and 459 were high-quality blastocysts. The fertilization rate, cleavage rate, blastocyst formation rate, usable blastocyst rate, and high-quality blastocyst rate were 81.4%, 97.5%, 66.0%, 60.8%, and 33.8%, respectively (Table 2).

PGT results and clinical outcomes of modified biopsy sample tubing method

In the PGT results, of a total of 222 PGT cycles, 190 cycles achieved embryo biopsy, while 32 cycles (14.4%) did not, as no embryo developed to the available blastocyst stage. Overall, 823 out of 826 (99.6%) blastocyst biopsies resulted in successful amplification. Three (0.4%), including 2 day 5 blastocysts (Fig. 4A,B) and 1 day 6 blastocyst (Fig. 4C) from different individual patients failed to amplify. The mean number of biopsied embryos per patient was 3.7 ±3.4. Of the embryos successfully amplified, 100% had interpretable results and 38.2% were genetically transferable. The clinical pregnancy rate per transfer, live birth rate and miscarriage rate were 80.9%, 74.5% and 6.4%, respectively (Table 2).

Discussion

A key caveat for PGT is the need to prevent the loss of biopsy samples during tubing. This problem is even more pronounced in patients from whom few oocytes are retrieved. How can the loss be minimized? Conventional PGT to date has focused on embryo biopsy and diagnosis,[3,5,10] but not a single paper has been published focusing

Table 1. Characteristics of the study population

Indication	Total
Number of patients, n	139
Number of cycles, n	222
Maternal age (±SD) [years]	33.3 ±5.4
BMI [kg/m^2]	21.7 ±2.6
Infertility duration (±SD) [years]	2.3 ±2.5
Basal FSH [IU/L]	6.0 ±2.1
Basal LH [IU/L]	3.7 ±2.1
Indication to PGT (%)	
PGT-A	86/222 (38.7)
PGT-M	54/222 (24.3)
PGT-SR	78/222 (35.1)
Other	4/222 (1.8)
Retrieved oocytes, n (mean ±SD)	2087 (14.5 ±8.9)
MII oocytes, n (mean ±SD)	1707 (11.7 ±7.3)

BMI – body mass index; MII – metaphase II; PGT-A – PGT for aneuploidies; PGT-M – PGT for monogenic; PGT-SR – PGT for structural arrangements; SD – standard deviation.

Table 2. Embryological data and PGT results of modified biopsy sample transfer method

Parameter	Total
Cycle characteristics	
Oocytes injected	2595
Fertilization rate, n (%)	2113/2595 (81.4)
Cleavage rate, n (%)	2060/2113 (97.5)
Blastocyst formation rate, n (%)	1359/2060 (66.0)
Usable blastocyst rate, n (%)	826/1359 (60.8)
High-quality blastocyst rate, n (%)	459/1359 (33.8)
PGT results	
Cycles with biopsiable embryos, n (%)	190/222 (85.6)
Biopsied embryos, n (mean ±SD)	826 (3.7 ±3.4)
Amplification efficiency, n (%)	823/826 (99.6)
Not affected embryos diagnosed, n (%)	314/823 (38.2)
Clinical outcomes	
Number of embryos transferred, n (mean ±SD)	47 (1.0 ±0.0)
Implantation rate	38/47 (80.9)
Clinical pregnancy rate, n (%)	38/47 (80.9)
Miscarriage rate	3/47 (6.4)
Live birth rate (% per ET)	35/47 (74.5)

SD – standard deviation; ET - embryo transfer.

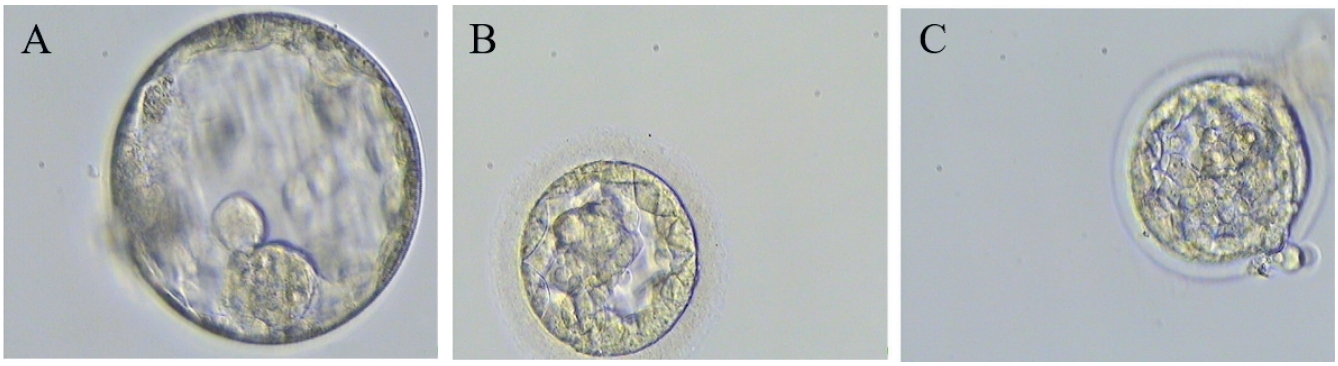

Fig. 4. Amplification failure – embryos from three different individual patients

on the optimization of the tubing method for placing biopsy samples into amplification tubes for PGT. Our center had started to advance the safety and accuracy of tubing and to encourage this technique to be adopted into clinical practice in order to improve PGT.

Precise control is required during tubing, because of the size of the biopsy samples (no more than 30 µm) and the volume of lysis buffer in the amplification tube (usually 3 µL in whole genome amplification). However, the manual control of micropipettes is notoriously imprecise. Therefore, tubing biopsy samples into PCR tubes is a challenging task for many embryologists. For European Society for Human Reproduction and Embryology (ESHRE) data collection XIV–XV,[16] 71 centers reported data on 11,481 cycles with PGT, along with 64,395 biopsies from January 2011 to December 2012; DNA amplification products were detected in 63,388 biopsies (98.4%) and 59,556 biopsies (92.5%) had interpretable results. In a study by Capalbo et al. on 2586 blastocyst-stage biopsies from 906 IVF-PGT cycles at 3 IVF centers between April 2013 and December 2014, the amplification success rate and diagnostic efficiency were 98.8% (2556/2586) and 94.2% (2,437/2,586), respectively.[17] More recently, a study that included 8990 blastocyst-stage biopsies of 6 IVF centers found that 98.0% of biopsies could be detected through the presence of DNA after amplification, but up to 97.5% of biopsied samples were able to be conclusively diagnosed.[18] This evidence suggests that diagnostic efficiency is continually improving, whereas the amplification success rate has remained unchanged. This means that with new genetic testing technology, the accuracy and sensitivity of the analysis method has increased,[19] though

no significant development has been made in the tubing or DNA amplification techniques.

In the present study, the amplification success rate was 99.6%, which was higher than the reference studies selected in it. The reasons for the outcomes were the proposed optimization approach, which included a few improvements: the modified micromanipulator aided in the fine movement of the micropipette, the modified microinjector minimized the amount of medium co-transferred with the cell, and the modified transfer device combined with a stereomicroscope provided a vision-based tubing system. These simple solutions can lead to a reduced need for an embryo re-biopsy, benefiting the amplification success rate and resulting in improved PGT results. As is well-known, the guidelines of the Preimplantation Genetic Diagnosis International Society and the ESHRE PGD consortium all recommend that the amplification success rate be no less than 90%.[20,21] Based on data from surveys and the PGD Consortium, the Vienna consensus recommends that the reference values of a successful biopsy rate be as follows: competency ≥90% and benchmark ≥95%. Additionally, the benchmark of a tubing rate of 95% was reported in the Alpha survey.[22] These recommendations confirm that this modified approach is technically solid. At the same time, the tubing procedure with the modified method was easily standardized among the operators. As the success of a PGT treatment cycle is the result of great attention to detail, the optimization of any procedural steps is a pragmatic goal.[8]

A common characteristic between all biopsy stages is the limited quantity of samples available for genetic analysis, potentially compounded by the often sub-optimal quality of the embryo cell biopsied.[23] The cell death in TE cells, damage to genomic DNA from the laser or mechanical injury during the biopsy may also affect the quality of the biopsy samples.[24,25] Damaged DNA from poor-quality biopsy samples may lead to an amplification failure or to low-confidence profiles.[26] In the present study, 3 biopsies did not produce any DNA amplification (Fig. 4). Amplification failure (AF) suggests only the absence of TE cells in the test tube or the presence of degenerated/lysed cells. The rate of AF is mainly imputable to technical aspects, and an increasing trend has been found from the most to the least experienced clinics.[18] As the control was visual and precise in this study, AF may be related not to the loss of the biopsied TE cells during the transfer from the biopsy dish to the amplification tube, but to the biopsy procedure. In fact, careful consideration is required when selecting the optimal time to perform biopsy for PGT. According to our results, as the expansion grade of blastocysts in 3 biopsies of AF was low, these blastocysts would be better with extended culturing.

In this study, biopsy and embryo transfer were performed at the blastocyst stage. The different days of biopsy turned out to be the main variable affecting both the presence and quality of the analyzed DNA. From days 3 to 5, longer culturing in vitro and wider blastocyst expansion were associated with smaller biopsy samples (i.e., with a higher DNA content and quality).[18] Also, the evidence suggests that cleavage-stage biopsy impairs the potential for human embryo implantation significantly more than blastocyst biopsy,[27–29] and embryo transfer at the blastocyst stage is accompanied by an improvement in pregnancy rates. From recently performed reviews and meta-analyses, the live birth rate of PGT ranged between 30% and 70%.[30–32] In the present study, the implantation rate, clinical pregnancy rate, live birth rate, and miscarriage rate were 80.9%, 80.9%, 74.5%, and 6.4%, respectively. These findings suggest that the PGT technique in our IVF center is stable.

The study has a few limitations. Because there is no ideal indicator for tubing, our outcome measure was the amplification success rate rather than the tubing rate. No comparative studies between the conventional method and the modified approach were performed in the same lab, and there are only few reports on amplification success rate. However, for safety assessment and training, the modified approach was evaluated both in a mouse experimental system and in a preclinical study using spare embryos from routine IVF procedures, before being applied in clinical PGT. The results were shown to be compatible with a high tubing rate of biopsy samples.

Conclusions

The present study demonstrates that the tubing method of biopsy samples can be a viable option for clinical application in PGT cycles. Instead of manual control, which requires many procedures of training to obtain proficiency, this tubing procedure is simple to perform and has a high degree of precision.

ORCID iDs

Shuai Liu https://orcid.org/0000-0003-4864-5804
Zhiheng Chen https://orcid.org/0000-0001-7421-4042
Yunhao Liang https://orcid.org/0000-0001-9314-1694
Hui Wang https://orcid.org/0000-0002-1361-0030
Li Yang https://orcid.org/0000-0003-3379-2553
Ling Sun https://orcid.org/0000-0002-4267-8210

References

1. Harper JC, Wilton L, Traeger-Synodinos J, et al. The ESHRE PGD Consortium: 10 years of data collection. *Hum Reprod Update*. 2012;18(3):234–247.
2. Kakourou G, Kahraman S, Ekmekci GC, et al. The clinical utility of PGD with HLA matching: A collaborative multi-centre ESHRE study. *Hum Reprod*. 2018;33(3):520–530.
3. Ubaldi FM, Cimadomo D, Capalbo A, et al. Preimplantation genetic diagnosis for aneuploidy testing in women older than 44 years: A multicenter experience. *Fertil Steril*. 2017;107(5):1173–1180.
4. Rubio C, Bellver J, Rodrigo L, et al. In vitro fertilization with preimplantation genetic diagnosis for aneuploidies in advanced maternal age: A randomized, controlled study. *Fertil Steril*. 2017;107(5):1122–1129.
5. Cimadomo D, Ubaldi FM, Capalbo A, et al. Failure mode and effects analysis of witnessing protocols for ensuring traceability during PGD/PGS cycles. *Reprod Biomed Online*. 2016;33(3):360–369.

6. Preimplantation Genetic Diagnosis International Society (PGDIS). Guidelines for good practice in PGD: Programme requirements and laboratory quality assurance. *Reprod Biomed Online*. 2008;16(1):134–147.
7. Harton GL, Magli MC, Lundin K, Montag M, Lemmen J, Harper JC; European Society for Human Reproduction and Embryology (ESHRE) PGD Consortium/Embryology Special Interest Group. ESHRE PGD Consortium/Embryology Special Interest Group: Best practice guidelines for polar body and embryo biopsy for preimplantation genetic diagnosis/screening (PGD/PGS). *Hum Reprod*. 2011;26(1):41–46.
8. Harper JC, Sengupta S, Vesela K, et al. Accreditation of the PGD laboratory. *Hum Reprod*. 2010;25(4):1051–1065.
9. Imudia AN, Plosker S. The past, present, and future of preimplantation genetic testing. *Clin Lab Med*. 2016;36(2):385–399.
10. Harton GL, De Rycke M, Fiorentino F, et al; European Society for Human Reproduction and Embryology (ESHRE) PGD Consortium. ESHRE PGD consortium best practice guidelines for amplification-based PGD. *Hum Reprod*. 2011;26(1):33–40.
11. Malter HE. Micromanipulation in assisted reproductive technology. *Reprod Biomed Online*. 2016;32(4):339–347.
12. Shojaei-Baghini E, Zheng Y, Sun Y. Automated micropipette aspiration of single cells. *Ann Biomed Eng*. 2013;41(6):1208–1216.
13. Zhang X, Leung C, Lu Z, Esfandiari N, Casper RF, Sun Y. Controlled aspiration and positioning of biological cells in a micropipette. *IEEE Trans Biomed Eng*. 2012;59(4):1032–1040.
14. Banerjee AG, Gupta SK. Research in automated planning and control for micromanipulation. *IEEE Transactions on Automation Science and Engineering*. 2013;10(3):485–495.
15. Gardner DK, Schoolcraft WB. In-vitro culture of human blastocyst. In: Jansen R, Mortimer D, eds. *Towards Reproductive Certainty: Infertility Genetics Beyond 1999*: *The Plenary Proceedings of the 11th World Congress*. New York NY: Parthenon Press; 1999:378–388.
16. De Rycke M, Goossens V, Kokkali G, Meijer-Hoogeveen M, Coonen E, Moutou C. ESHRE PGD Consortium data collection XIV–XV: Cycles from January 2011 to December 2012 with pregnancy follow-up to October 2013. *Hum Reprod*. 2017;32(10):1974–1994.
17. Capalbo A, Ubaldi FM, Cimadomo D, et al. Consistent and reproducible outcomes of blastocyst biopsy and aneuploidy screening across different biopsy practitioners: A multicentre study involving 2586 embryo biopsies. *Hum Reprod*. 2016;31(1):199–208.
18. Cimadomo D, Rienzi L, Romanelli V, et al. Inconclusive chromosomal assessment after blastocyst biopsy: Prevalence, causative factors and outcomes after re-biopsy and re-vitrification. A multicenter experience. *Hum Reprod*. 2018;33(10):1839–1846.
19. Xu K, Montag M. New perspectives on embryo biopsy: Not how, but when and why? *Semin Reprod Med*. 2012;30(4):259–266.
20. Thornhill AR, deDie-Smulders CE, Geraedts JP, et al; ESHRE PGD Consortium. ESHRE PGD Consortium "Best practice guidelines for clinical preimplantation genetic diagnosis (PGD) and preimplantation genetic screening (PGS)". *Hum Reprod*. 2005;20(1):35–48.
21. Preimplantation Genetic Diagnosis International Society. The Preimplantation Genetic Diagnosis International Society (PGDIS): Guidelines for good practice in PGD. *Reprod Biomed Online*. 2004;9(4):430–434.
22. ESHRE Special Interest Group of Embryology and Alpha Scientists in Reproductive Medicine. The Vienna consensus: Report of an expert meeting on the development of art laboratory performance indicators. *Hum Reprod Open*. 2017;35(5):494–510.
23. Dreesen J, Destouni A, Kourlaba G, et al. Evaluation of PCR-based preimplantation genetic diagnosis applied to monogenic diseases: A collaborative ESHRE PGD consortium study. *Eur J Hum Genet*. 2014;22(8):1012–1018.
24. Zhang S, Tan K, Gong F, et al. Blastocysts can be rebiopsied for preimplantation genetic diagnosis and screening. *Fertil Steril*. 2014;102(6):1641–1645.
25. Wininger JD, Taylor TH, Orris JJ, Glassner M, Anderson SH. Pregnancy after rebiopsy and vitrification of blastocysts following allele drop-out after day 3 biopsy. *Fertil Steril*. 2011;95(3):1122.e1–e2.
26. Parriego M, Coll L, Vidal F, et al. Inconclusive results in preimplantation genetic testing: Go for a second biopsy? *Gynecol Endocrinol*. 2019;35(1):90–92.
27. Sciorio R, Tramontano L, Catt J. Preimplantation genetic diagnosis (PGD) and genetic testing for aneuploidy (PGT-A): Status and future challenges. *Gynecol Endocrinol*. 2020;36(1):6–11.
28. Jing S, Luo K, He H, et al. Obstetric and neonatal outcomes in blastocyst-stage biopsy with frozen embryo transfer and cleavage-stage biopsy with fresh embryo transfer after preimplantation genetic diagnosis/screening. *Fertil Steril*. 2016;106(1):105–112.e4.
29. Scott RT Jr, Upham KM, Forman EJ, Zhao T, Treff NR. Cleavage-stage biopsy significantly impairs human embryonic implantation potential while blastocyst biopsy does not: A randomized and paired clinical trial. *Fertil Steril*. 2013;100(3):624–630.
30. Wei D, Liu JY, Sun Y, et al. Frozen versus fresh single blastocyst transfer in ovulatory women: A multicentre, randomised controlled trial. *Lancet*. 2019;393(10178):1310–1318.
31. Zeng M, Su S, Li L. Comparison of pregnancy outcomes after vitrification at the cleavage and blastocyst stage: A meta-analysis. *J Assist Reprod Genet*. 2018;35(1):127–134.
32. Martins WP, Nastri CO, Rienzi L, van der Poel SZ, Gracia C, Racowsky C. Blastocyst vs cleavage-stage embryo transfer: Systematic review and meta-analysis of reproductive outcomes. *Ultrasound Obstet Gynecol*. 2017;49(5):583–591.

Adaptation of endovascular technique of self-expandable metal esophageal stent implantation in palliative treatment of malignant dysphagia in the course of esophageal and bronchial cancers: A one-center study

Damian Ziaja[1,2,B], Bartłomiej Stasiów[3,B], Mariola Sznapka[2,B], Jolanta Domalik[4,B], Wacław Kuczmik[2,E], Krzysztof Ziaja[2,A,E], Jerzy Chudek[5,F]

[1] Department of Physiotherapy, Faculty of Health Sciences in Katowice, Medical University of Silesia in Katowice, Poland
[2] Department of Department of General and Vascular Surgery, Faculty of Medical Sciences in Katowice, Medical University of Silesia in Katowice, Poland
[3] Department of Radiology, Upper-Silesian Medical Centre in Katowice of Medical University of Silesia in Katowice, Poland
[4] Department of General, Vascular and Transplant Surgery, Faculty of Medical Sciences in Katowice, Medical University of Silesia in Katowice, Poland
[5] Department of Internal Diseases and Oncological Chemotherapy, Faculty of Medical Sciences in Katowice, Medical University of Silesia in Katowice, Poland

A – research concept and design; B – collection and/or assembly of data; C – data analysis and interpretation;
D – writing the article; E – critical revision of the article; F – final approval of the article

Advances in Clinical and Experimental Medicine, ISSN 1899–5276 (print), ISSN 2451–2680 (online) *Adv Clin Exp Med*. 2020;29(11):1363–1366

Address for correspondence
Jerzy Chudek
E-mail: chj@poczta.fm

Funding sources
None declared

Conflict of interest
None declared

Acknowledgements
The modification of the technique was developed without any knowledge of a similar approach being developed in Qilu Hospital of Shandong University, Jinan, China.

Received on December 22, 2018
Reviewed on March 22, 2019
Accepted on August 18, 2019

Cite as
Ziaja D, Stasiów B, Sznapka M, et al. Adaptation of endovascular technique of self-expandable metal esophageal stent implantation in palliative treatment of malignant dysphagia in the course of esophageal and bronchial cancers: A one-center study. *Adv Clin Exp Med*. 2020;29(11):1363–1366. doi:10.17219/acem/111810

DOI
10.17219/acem/111810

Abstract

Background. Esophageal stent implantation is an alternative for microjejunostomy or total parenteral nutrition in the palliative treatment of malignant dysphagia in the course of esophageal and advanced bronchial cancers infiltrating the esophagus. The procedure of implanting an esophageal self-expanding metal stent (SEMS) is performed with gastroscopic guidance under general anesthesia.

Objectives. To analyze the efficacy and safety of a simplified technique (without gastroscopic guidance in local anesthesia) of esophageal SEMS implantation in patients with malignant dysphagia in the course of esophageal and bronchial cancers.

Material and methods. This is a retrospective analysis of consecutive procedures of uncovered esophageal SEMS implantation performed with a simplified adaptation of the endovascular technique (Seldinger wire) in patients with esophageal and bronchial cancers and poor performance status. The procedures were done in a single surgical center over an 8-year period in 27 patients who were referred from oncology departments with esophageal stenosis confirmed using gastroscopy and who were being treated for malignant dysphagia. The study endpoints were effectiveness (a decrease in dysphagia from grade 3 or 4 to grade 1 after the procedure) and complications related to the procedures (including restenosis and stent migration).

Results. In all 27 patients, the SEMS were effectively implanted, enabling enteral nutrition after the procedure. No early complications related to the procedure were observed. A single patient developed restenosis 14 days after the procedure, which required re-stenting.

Conclusions. The simplified method for SEMS implantation described herein may be considered an option in the palliative treatment of patients with malignant dysphagia in the course of esophageal and bronchial cancers and poor performance status, especially in facilities with limited access to endoscopy.

Key words: esophageal cancer, bronchial cancer, self-expandable metal esophageal stent implantation, malignant dysphagia, palliative treatment

Introduction

Dysphagia caused by cancer is a common and severe complication of locally advanced, unresectable or recurring cancers of the gastro-esophageal junction, and much less frequently from infiltration of bronchial carcinomas. It is followed by the rapid development of cachexia, which affects the quality of life and overall patient survival.[1,2] At this stage of the disease, the priority is on supportive care and improving the patient's quality of life rather than curative treatment.[3]

Malnutrition can be reduced either by enteral nutrition through a jejunostomy or total parenteral nutrition. However, neither of these procedures resolves the problem of the patient's inability to swallow saliva, which leads to the severe complication of saliva aspirating into the airway. Therefore, restoration of esophageal patency is the only way to resolve this problem and improve their ability to swallow, and thus their quality of life.[4]

Currently, the most commonly used palliative treatment for dysphagia from cancer in patients with at least partial patency of the esophagus is stenting with self-expanding metal stents (SEMSs) of different types (fully covered, uncovered or partially covered).[3,5,6] The choice of stent depends on the tumor size (length of the stenosis), its location and the morphology of the stenosis.[3] A SEMS implant results in an immediate reduction in dysphagia and gives the patient the opportunity to take in fluids and food.[3,6] Stents are routinely placed over a guidewire positioned through gastroscopy and under fluoroscopic guidance during conscious sedation of the patient. In our center, this method was used until 2009.

In 2009, we introduced a simplified procedure of SEMS placement performed under local anesthesia only, without gastroscopic guidance, using a simplified adaptation of the endovascular technique (Seldinger wire).

In this paper, we describe the effective application of this modified method in a series of patients with dysphagia from cancer in the course of advanced or recurring esophageal and bronchial cancers.

Patients and methods

Between 2010 and 2017, 28 patients with esophageal stenosis and dysphagia who were in the course of advanced esophageal and bronchial cancers confirmed using gastroscopy, and who were disqualified from chemo- and radiotherapy due to poor performance status (Eastern Cooperative Oncology Group performance status 3 or 4), were referred from oncology centers to the Department General and Vascular Surgery. A SEMS implantation was performed in 27 patients with dysphagia of grade 3 or 4 unable to swallow liquids/saliva (Table 1). One patient was disqualified due to poor general clinical condition and died a few days later. Each patient gave written informed consent for the procedure. The study was conducted in accordance with the Declaration of Helsinki. The modification of the stenting procedure was reviewed by the Bioethical Committee of the Silesian Medical University in Katowice (approval No. NN-6501-53/06).

Table 1. Characteristics of patients with cancer dysphagia (n = 27)

Parameter	Value
Gender [men/women]	18/9
Age [years]	62.5 (range: 52–87)
Weight loss during the last 3–6 months [kg]	17.5 (range: 10–35)
Causes	**Number of patients**
Recurrence of gastro-esophageal junction adenocarcinoma (after initial resection and chemotherapy)	8
Progression of unresectable esophageal squamous cell carcinoma (after chemo- and radiotherapy)	14
Progression of bronchial carcinoma with esophageal infiltration (after chemotherapy)	5

Stenting procedure

The procedures were performed at the Department of Radiology.

After local anesthesia of the mouth and throat with topical xylocaine spray, A 21Fr tube was introduced into the mouth to the level of the tumor while the patient was in a supine position. After removal of residual saliva from the esophagus using a 20-milliliter syringe, 20 mL of iodine contrast was injected through the tube in order to visualize the stenotic canal and to manipulate the tumor under fluoroscopy (Fig. 1 – upper-left panel). We then withdrew the 21Fr tube by about 3 cm, introducing through it a hydrophilic standard guidewire (0.035"; Terumo Interventional Systems, Somerset, USA), followed by Van Schie Seeking Catheters (2–3Fr, Cook Medical, Bloomington, USA), gently maneuvering into the stenotic channel to reach the stomach. After replacing the Van Schie Seeking Catheters with an extra-stiff guidewire (Lunderquist® Extra-Stiff Wire; Cook Medical, Bloomington, USA), we introduced a balloon with an uncovered SEMS. Finally, X-ray control was performed with iodine contrast at the end of the procedure (Fig. 1 – upper-right panel).

Results

The modified technique of esophageal SEMS implantation was successfully performed in all 27 patients, enabling enteral nutrition (liquid diet) immediately after the procedure (decreasing dysphagia from grade 3 or 4 to grade 1). No complications related to the procedure or migration of the SEMS was observed. One patient required a second SEMS due to re-stenosis 14 days after the 1st procedure

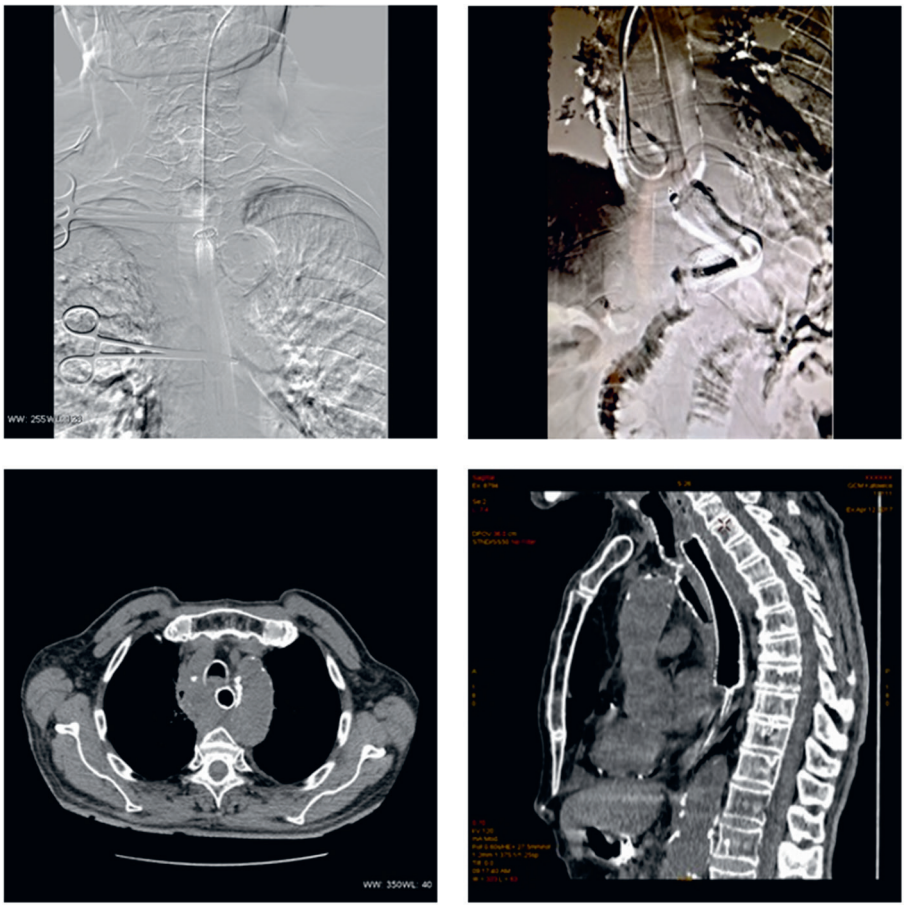

Fig. 1. The upper and lower borders of the stenotic canal are marked using metal forceps fixed to the patient's skin (upper-left panel). Fluoroscopy (upper-right panel) after stent placement in a patient with an esophageal tumor infiltrating the trachea. Computed tomography after self-expanding metal replacement in a patient with stenosis recurrence (lower-left and -right panel)

(Fig. 1 – lower-left and -right panels), and percutaneous endoscopic gastrostomy after another 28 days (40 days from the 1st procedure).

All patients expressed satisfaction with the procedure in terms of restoring enteral nutrition. Almost half of the patients (n = 13) were discharged home with the recommendation of palliative care, while the others were transferred to district hospitals (n = 11) or oncology units (n = 3). The mean post-procedure survival time was 76 days (28–117 days).

Discussion

In our opinion, this modified procedure of esophageal SEMS implantation is a convenient alternative to the traditional procedure, with sedation provided by an anesthesiologist and the use of gastroscopy, or to the more invasive microjejunostomy or gastrostomy, in patients with esophageal stenosis and dysphagia from cancer, prevoiusly confirmed using gastroscopy (performed in other clinics as a part of a diagnostic work-up), especially in centers with limited access to endoscopy.

This simplified procedure of SEMS implantation is performed without an anesthesiologist or gastroscopy, and in consequence, is less expensive for the healthcare system. The technique is quite simple for qualified vascular surgeons, angiologists and interventional radiologists. It may be utilized in medical centers with limited access to gastroscopy. A quite similar approach has recently been described by Zhang et al.[7] as a simple fluoroscopic method of SEMS insertion performed in 36 patients with dysphagia and fistula caused by esophageal carcinoma. They did not report clinically significant complications during or after the procedure.

Both our observations and those by Zhang et al.[7] have proven the efficacy and safety of this procedure. Therefore, it seems that this method may be applied in other facilities even without large prospective, multicenter studies. We do not suggest that this method is better than the traditional approach. Certainly, endoscopic control has its advantages, e.g., direct identification of the residual lumen and evaluation of the stricture, which should ensure greater safety of the procedure. It should be stressed that in all of the patients in our study, endoscopy had already been performed in clinics which were unable to perform SEMS implantation, referring the patients to our center.

Esophageal brachytherapy is considered to be a suitable alternative to SEMS implantation, possibly providing a longer duration of improvement in symptoms and better quality of life[8]; however, the improvement in narrow stenosis can be achieved faster with SEMS implantation.[9] In addition, esophageal stenting may be combined with brachytherapy[10] or stents loaded with ^{125}iodine seeds[11]

in patients with at least a three-month life expectancy in order to prevent restenosis. Nevertheless, in general, the majority of these palliatively treated patients have a short life expectancy, with a relatively low risk of restenosis. From our group of patients, with a mean period of survival of 76 days, a single patient developed restenosis and required re-stenting. We did not observe stent migration, which is more typical of covered stents,[12] or other late complications (defined as events occurring at least 2–4 weeks after stenting) such as bleeding, perforation, gastroesophageal reflux disease, or chronic thoracic pain, which were previously reported after SEMS implantation.[13]

Conclusions

The simplified method for SEMS implantation described herein may be considered an option in palliative treatment for patients with malignant dysphagia in the course of esophageal and bronchial cancers and poor performance status, especially in centers with limited access to endoscopy.

ORCID iDs

Damian Ziaja https://orcid.org/0000-0002-2348-2933
Bartłomiej Stasiów https://orcid.org/0000-0001-6184-6948
Mariola Sznapka https://orcid.org/0000-0001-7646-9997
Jolanta Domalik https://orcid.org/0000-0001-5425-3247
Wacław Kuczmik https://orcid.org/0000-0002-0927-0977
Krzysztof Ziaja https://orcid.org/0000-0003-2230-5860
Jerzy Chudek https://orcid.org/0000-0002-6367-7794

References

1. Watt E, Whyte F. The experience of dysphagia and its effect on the quality of life of patients with esophageal cancer. *Eur J Cancer Care (Engl).* 2003;12(2):183–193.
2. Anandavadivelan P, Lagergren P. Cachexia in patients with esophageal cancer. *Nat Rev Clin Oncol.* 2016;13(3):185–198.
3. Martinez JC, Puc MM, Quiros RM. Esophageal stenting in the setting of malignancy. *ISRN Gastroenterology.* 2011;2011:719575.
4. Reed CE, Marsh WH, Carlson LS, at al. Prospective, randomized trial of palliative treatment for unresectable cancer of the esophagus. *Ann Thorac Surg.* 1991;51(4):552–555.
5. Dormann AJ, Eisendrath P, Wigginghaus B, Huchzermeyer H, Devière J. Palliation of esophageal carcinoma with a new self-expanding plastic stent. *Endoscopy.* 2003;35(3):207–211.
6. Madhusudhan C, Saluja SS, Pal S, et al. Palliative stenting for relief of dysphagia in patients with inoperable esophageal cancer: Impact on quality of life. *Dis Esophagus.* 2009;22(4):331–336.
7. Zhang K, Wei S, Wu J, Li C, Ma X, Wang Q. Palliation of malignant esophageal obstruction and fistulas with covered self-expandable metallic stents: Assessment of a simple fluoroscopic method. *Int J Clin Exp Med.* 2015;8(6):8860–8865.
8. Dai Y, Li C, Xie Y, et al. Interventions for dysphagia in esophageal cancer. *Cochrane Database Syst Rev.* 2014;10:CD005048.
9. Homs MY, Steyerberg EW, Eijkenboom WM, et al. Single-dose brachytherapy versus metal stent placement for the palliation of dysphagia from esophageal cancer: Multicentre randomised trial. *Lancet.* 2004;364(9444):1497–1504.
10. Bergquist H, Johnsson E, Nyman J, et al. Combined stent insertion and single high-dose brachytherapy in patients with advanced esophageal cancer: Results of a prospective safety study. *Dis Esophagus.* 2012;25(5):410–415.
11. Zhu HD, Guo JH, Mao HW, et al. Conventional stents versus stents loaded with ^{125}iodine seeds for treatment of unresectable esophageal cancer: A multicentre, randomized phase 3 trial. *Lancet Oncol.* 2014;15(6):612–619.
12. Lee S, Osugi H, Tokuhara T, et al. Self-expandable metallic stent for unresectable malignant strictures in the esophagus and cardia. *Jpn J Thorac Cardiovasc Surg.* 2005;53(9):470–476.
13. Hindy P, Hong J, Lam-Tsai Y, Gress F. A comprehensive review of esophageal stents. *Gastroenterol Hepatol (NY).* 2012;8(8):526–532.

Experimental study on the repair of ureteral functional regeneration with highly bioactive extracellular matrix stent

*Lifeng Gu[A], *Xiaosong Fan[A], Jiancheng Lu[B], Bojun Li[B], Weijie Xia[C], Feiping He[D,E], Jie Chen[D,E], Weixing Yu[F]

Department of Urology, Shaoxing Shangyu People's Hospital, China

A – research concept and design; B – collection and/or assembly of data; C – data analysis and interpretation;
D – writing the article; E – critical revision of the article; F – final approval of the article

Advances in Clinical and Experimental Medicine, ISSN 1899–5276 (print), ISSN 2451–2680 (online) *Adv Clin Exp Med*. 2020;29(11):1367–1373

Address for correspondence
Weixing Yu
E-mail: yuweixingsy1y@163.com

Funding sources
None declared

Conflict of interest
None declared

*Lifeng Gu and Xiaosong Fan contributed equally to this work.

Received on March 11, 2020
Reviewed on March 15, 2020
Accepted on June 2, 2020

Published online on November 16, 2020

Abstract

Background. The research of extracellular matrix stent (ECM) has made some progress in the repair of urethra and bladder defects.

Objectives. To observe the effects of highly bioactive ECM scaffold on the regeneration and repair of defects in long-segment ureteral replacement.

Material and methods. An animal model of long-segment ureteral defect was established and four-layer tubular highly bioactive ECM materials were prepared. After the ureteral defect was repaired through surgery, the rabbits in the negative control group were administered a non-bioactive stent, and rabbits in the observation group were treated with an ECM stent.

Results. Comparison of macro-indicators: The negative control group had a higher infection rate, a lower survival rate and more complications than the observation group ($p < 0.05$). The frequency of ureteral peristalsis in the negative control group was lower than in the observation group. In addition, the rate of urinary dysfunction was higher, and the ratio of ureteral diameter was lower in the negative control group than in the observation group (all $p < 0.05$). Comparison of histopathology: Three months after the operation, the vascular, smooth muscle and mucous membrane of the ureter in the observation group regenerated to close to normal ureteral tissue. There was no significant difference between the ureter regeneration in the repair area and the normal ureter tissue in the observation group 3 months after the operation. The number of regenerated muscle fibers in the observation group was significantly higher than that of the negative control group. Compared with the negative control group, the fibrous capsule was thicker, the percentages of CD31, CD3, CD68, CD80+, and CD163+ were higher, the scope of new smooth muscle fiber was expanded, fusion with the host muscle fibers was higher, and the neuromuscular junction (NMJ) structure was stronger in the observation group (all $p < 0.05$).

Conclusions. A highly bioactive ECM stent can better regenerate the local anatomical structure and physiological function.

Key words: extracellular matrix, ureteral defect, high biological activity, regeneration and repair

Cite as
Gu L, Fan X, Lu J. Experimental study on the repair of ureteral functional regeneration with highly bioactive extracellular matrix stent. *Adv Clin Exp Med*. 2020;29(11):1367–1373. doi:10.17219/acem/123353

DOI
10.17219/acem/123353

Introduction

There are many factors that can lead to the defect of ureteral function and anatomical structure. At present, for ureteral defects larger than 2 cm, the colon or bladder muscle flap is mainly used as a substitute, or even directly treated with the kidney transplantation.[1] However, these treatment methods are always accompanied by many complications, so it is urgent to find other repair techniques. The main purpose of tissue engineering research is to repair and reconstruct damaged or non-functional organs. At present, great progress has been made in the reconstruction of urethras and bladders with tissue engineering scaffold materials.[2,3] With the development and maturity of bioengineering technology, the extracellular matrix (ECM) has become important in the repair of urethra and bladder defects.[4] The higher physiological requirements of the ureter than those of the bladder or urethra, a regenerated ureter should be free of urine leakage, stone formation, anastomotic stenosis, and inelasticity, and should be consistent with the host's ureteral peristalsis rhythm has largely limited the research of ECM material in ureter regeneration.

Although some studies have proposed that the ECM plays an important role in the repair of ureteral defects, research on how to make full use of its functions to promote injury repair and clinical transformation is still lacking. Our group has developed a highly bioactive ECM stent which is able to retain at least 60% of the bioactive components in the natural ECM, thus improving the anti-infectivity and reducing the loss of elasticity in the repair area.[5] The ECM stent contains a variety of bioactive factors and more than 90% type I and type III collagen. After transplantation, it can be effectively degraded to produce a large number of active peptides, which increases its antibacterial ability. Therefore, the present study further applies it to animal models, discusses the changes in histopathology microscopically and the changes of ureteral dynamic function macroscopically, and explores the influence of highly bioactive ECM materials on ureteral regeneration, striving for a breakthrough in the field of ureteral regeneration.

Material and methods

Experimental animal subjects

A total of 48 male adult New Zealand rabbits, weighing 2.0–3.0 kg (average: 2.68 kg), were provided by the experimental animal center of Zhejiang University, Shaoxing, China. During the experiment, the animals were treated according to the requirements of animal ethics.

Establishment of long-segment ureteral defect animal model

The rabbits were anesthetized using general pentobarbital sodium (30 mg/kg) through the ear vein. The related operation area was sterilized and paved with a sterile sheet. Through the posterior peritoneum channel, a blunt separation was carried out in the muscular space along a left straight incision of the spine. The upper and middle ureters were found and separated along the psoas major muscle, and sections of ureters with a length of 1.0 cm were excised.

Preparation of the highly bioactive ECM tubular stent

Fresh pig jejunum (warm ischemia time <10 min) was rinsed in phosphate-buffered saline (PBS) and added to a Hanks solution at 4°C. The serous layer, mucosal layer and muscular layer of jejunum were removed using mechanical force, and the residual cell components were washed using double-distilled water to obtain the porcine small intestinal submucosa (P-SIS). Then, the P-SIS was stirred in 0.5% pancreatin + 0.5% EDTA for 10 h, washed with PBS and double-distilled water to remove the pancreatin, immersed in phenol chloroform and methanol (volume ratio: 1:3), and immersed in the fume hood for 12 h (the liquid was changed every 3 h). Finally, PBS and double-distilled water were used to clean the residual reagent.

The P-SIS was immersed in 2.5% SDS for 16 h, then rinsed with PBS and double-distilled water to remove the SDS. After that, the P-SIS was added to 10% ethanol containing 0.8% peracetic acid (PAA), and it was rinsed with PBS and double-distilled water to remove the PAA.

An FR 3.0 double-J tube (Huasheng Medical Materials Co., Ltd., Jiangsu, China) was used as an inner support, and P-SIS was made into a tubular material with a specific diameter, which was overlapped with 4 layers using the vacuum lamination method. It was then dried completely at –120°C in a freeze-drying machine, and sterilized with ethylene oxide in sterilized paper plastic bags.[6]

Experimental grouping

A total of 48 rabbits were randomly divided into a negative control group and an observation group (24 rabbits in each group). In the negative control group, the 2.0-mm diameter silica gel double-J tube was used as a stent with one end placed in the renal pelvis and the other end placed inside the bladder. Transplantation was conducted with the same length of a non-bioactive stent. The upper and lower ends of the ureter were anastomosed with the non-bioactive stent using 9-0 absorbable sutures under microscope. In the observation group, the 2.0 mm diameter

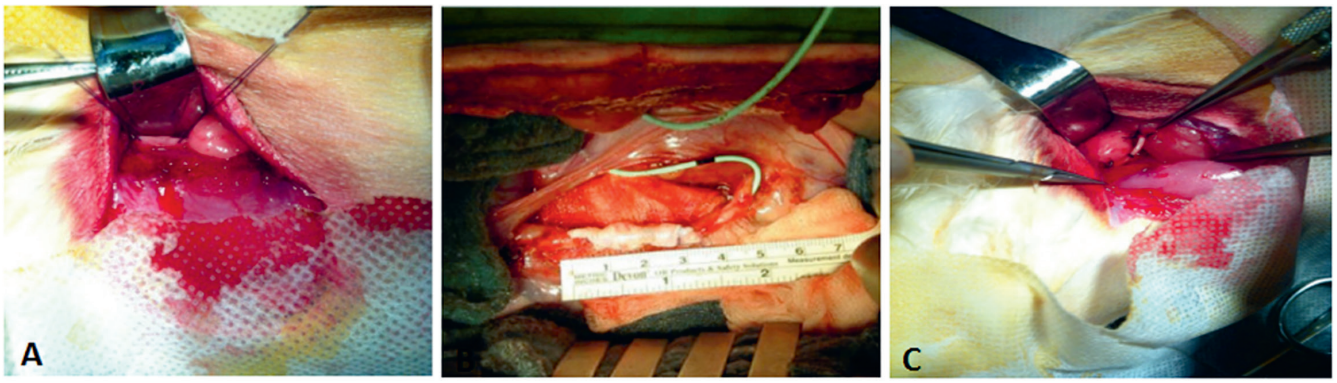

Fig. 1. Process of the operation: (A) establishment of the ureteral injury animal model; (B) implantation of the inactive stent; (C) implantation of the highly bioactive stent

silica gel double-J tube was used as a stent with one end placed in the renal pelvis and the other end placed inside the bladder. Transplantation was conducted with the same length of tubular highly bioactive ECM stent. The upper and lower ends of the ureter were anastomosed with the ECM stent using 5-0 absorbable sutures under microscope. Four or 5 stitches were sutured at each end, and the subcutaneous tissue and skin were sutured intermittently with 3-0 silk thread. An intramuscular injection of 1.6 million units of penicillin was administered intraoperatively in order to prevent infection during the operation (Fig. 1).

Observation index

Macro indicators

The infection and survival rates were recorded at 2 weeks and 1, 2, 3, 4, and 6 months postoperatively. The incidence of hydronephrosis, renal function damage, ureteral stricture, and urinary leakage were studied using pyelography after removal of the double-J tube. The peristalsis and micturition functions of the ureter were also observed. The dynamic function of the ureter was evaluated by the diameter ratio of the 2 ureters at the same stage.

Histopathological index

The hematoxylin & eosin (H&E) staining results were checked at 2 weeks and 1, 2, 3, 4, and 6 months postoperatively, and the number and structure of ureteral regenerated muscle fibers were observed under electron microscope. Immunofluorescence staining was used to detect the cell–material response, including surrounding tissue wrapping (thickness of the fibrous capsule), the percentage of vascularization (CD31), infiltrating cells (CD3 and CD68), and monocyte macrophages ($CD80^+$ and $CD163^+$). The material remodeling and regeneration of intima and smooth muscle innervation were detected. Each group had 4 animal subjects at each time point.

Detection methods

Intravenous pyelography

The double-J tube was removed and intravenous pyelography was conducted. After the anesthesia took effect, the rabbits were fixed on the X-ray examination table to establish the venous access. An injection of 20 mL of 60% meglumine diatrizoate was made intravenously and an abdominal flat film was taken 5 min, 10 min and 20 min later. The incidence of hydronephrosis, renal function damage (serum creatinine level at least 2 times higher than the baseline value), ureteral stenosis, and urinary leakage was examined. The peristalsis and micturition functions of the ureter were observed, and the dynamic function of the ureter was evaluated by the ratio of the diameter of the 2 ureters at the same stage.

Examination of ureteral dynamic function

The whole ureter of both sides was excised, the distal side was ligated and the proximal one was connected with the infusion tube perfusion system. The ureter was perfused with 60 cm H_2O pressure, and the ratio of the diameters of the 2 ureters at the same stage was used as the observation index. The results were automatically read out using the own software of the system (Urodynamic Analyzer; MMS, Enschede, the Netherlands).

Tissue section and pathological analysis

The normal ureteral tissue and ureteral tissue repaired using ECM were made into paraffin sections. For H&E staining, the sections were washed with distilled water, stained with hematoxylin solution for several minutes, decolorized with acid water and ammonia water, dehydrated with an alcohol gradient, stained with eosin, sealed with xylene, and observed under a microscope. For immunofluorescence staining, the sections were washed in PBS and incubated in Tris-buffered saline (TBS) containing

0.1% Triton X-100 + 0.1% calf serum protein for 20 min. The antigen repair buffer (100 mM of Tris and 5% urea; pH: 9.5) was added and heated at 95°C for 10 min, then washed with PBS. The cells were incubated with PBS with Tween® 20 (PBST) containing 1% bovine serum albumin (BSA) and 22.52 mg/mL of glycine for 30 min to block the antibody; then, they were washed with PBS. After being incubated with monoclonal antibody against CD31, CD3, CD68, $CD80^+$, $CD163^+$, and muscle fiber (Sigma-Aldrich, St. Louis, USA), the cells were washed with PBS and incubated with corresponding fluorescence labeled secondary antibodies (Sigma-Aldrich). Four slices were studied in each animal and 4 animals were randomly selected from each group. Four visual fields were taken from each slice and observed under laser confocal microscope. The results were calculated as average values.

Statistical analysis

The IBM SPSS v. 20.0 statistical software (IBM Corp., Armonk, USA) was used for the statistical analysis. The measurement data is expressed as means ± standard deviation (SD). The t-test of independent samples was used for intergroup comparisons. The numerical data is expressed using number of cases (percentage), and a χ^2 test was used for comparison between groups. P-values <0.05 indicated statistically significant differences.

Results

Comparison of infection and survival rate between the 2 groups

With the prolongation of the observation time, the infection rate increased and the survival rate decreased in the negative control group; there was a significant difference compared with the observation group ($p < 0.05$) (Table 1).

Comparison of ureteral function between the 2 groups

The incidence of hydronephrosis, renal function damage, ureteral stricture, and urinary leakage in the negative control group increased and was significantly higher than in the observation group ($p < 0.05$). The frequency of ureteral peristalsis and the ratio of ureteral diameter in the negative control group were lower than in the observation group; the incidence of urinary dysfunction was higher than in the observation group ($p < 0.05$). (Table 2 and Fig. 2,3).

Hematoxylin & eosin staining

The histopathological examination revealed that, compared with the negative control group, the repair area of the ureter in the observation group covered the epithelium. Additionally, with the passage of time, the ureteral blood vessels, smooth muscle and mucosa regenerated more and were arranged more regularly (Fig. 4). The thickness of the epithelium was increased and the number of blood vessels was higher at each time point than in the negative control group.

Regenerated muscle fiber and cell–material reaction of the ureter

Compared with the negative control group, the number of regenerated muscle fibers of ureters in the observation group increased noticeably as observed under electron microscope, the fibrous capsule was thicker, the percentages of CD31, CD3, CD68, $CD80^+$, and $CD163^+$ were higher, the scope of synovium fiber was greater, fusion with host

Table 1. Comparison of infection and survival rate between the 2 groups

Groups	Negative control group (n = 24)	Observation group (n = 24)	χ^2	p-value
Six-month infection rate	6 (25.0%)	1 (4.2%)	5.400	0.020
Six-month survival rate	17 (70.8%)	22 (91.7%)	4.547	0.033

Table 2. Comparison of ureteral function between the 2 groups

Groups	Negative control group (n = 24)	Observation group (n = 24)	t/χ^2	p-value
Hydronephrosis	1	1	0.000	1.000
Renal function damage	3	1	0.000	1.000
Ureteral stricture	3	1	0.000	1.000
Urinary leakage	2	0	0.000	1.000
Total incidence	9 (37.5%)	3 (12.5%)	4.448	0.007
Ureteral peristalsis frequency [times/h]	1.2 ±0.3	1.6 ±0.4	3.452	0.003
Urethral dysfunction	7 (29.2%)	1 (4.2%)	5.365	0.015
Ureter diameter ratio	0.6 ±0.3	0.8 ±0.3	3.265	0.006

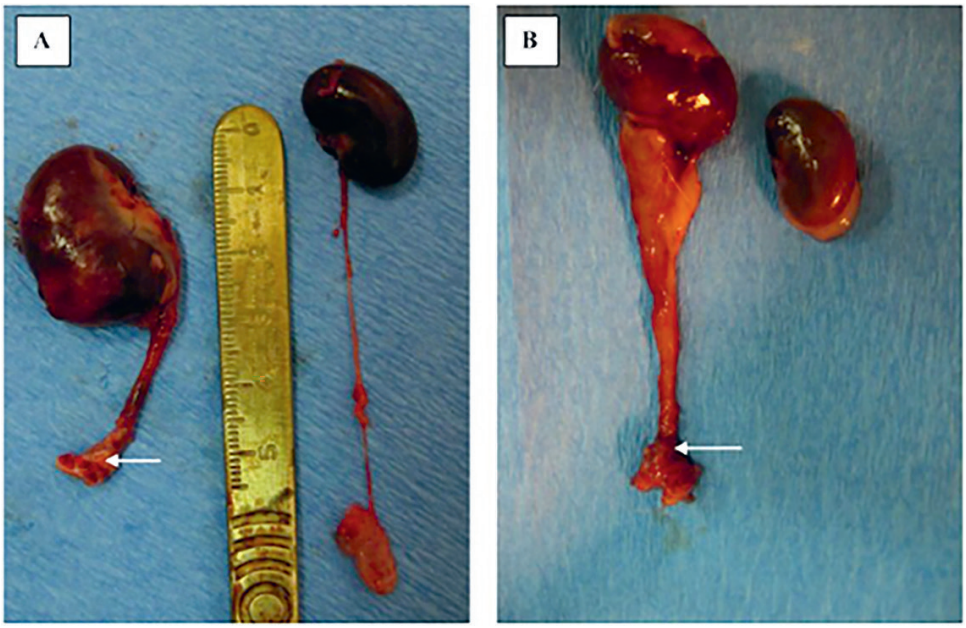

Fig. 2. Comparison of ureteral function between the 2 groups through gross observation of the kidney and ureter. (A) Negative control group: the ureter of the affected side adheres to the surrounding tissue, and the materials in the repair area are systematized. (B) Observation group: there was no difference in the appearance of the kidneys on the 2 sides; the arrow indicates the repair area

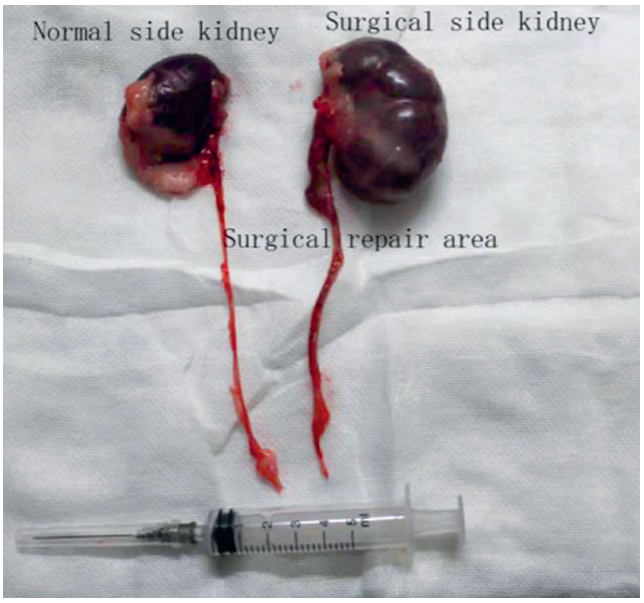

Fig. 3. General view of bilateral kidneys and ureters 3 months after operation

muscle fibers was higher, and the number of neuromuscular junction (NMJ) structure increased (all $p < 0.05$) (Table 3 and Fig. 5).

Discussion

In this study, a rabbit model of long-segment ureteral defect was established and 4 layers of tubular highly bioactive ECM materials were prepared. The results showed that the ECM material group had a lower infection rate, a higher survival rate, a lower incidence of hydronephrosis, renal function damage, ureteral stricture and urinary leakage, a higher frequency of ureteral peristalsis, a decreased incidence of ureteral dysfunction, and improved ureteral dynamic function. These results indicate that it is feasible to repair a ureteral defect with ECM material. The mechanism of action may be related to the following aspects:

Table 3. Comparative study on the cell–material reaction of ureteral regenerated muscle fibers (per high-power field)

Groups	Negative control group	Observation group	t	p-value
Cases	4	4	–	–
Number of regenerated muscle fibers	2.6 ±0.9	3.5 ±1.1	3.625	0.02
Thickness of fibrous capsule [μm]	10.8 ±5.4	12.3 ±5.6	3.321	0.024
CD31 [%]	26.7 ±8.4	35.6 ±9.4	15.632	0
CD3 [%]	24.6 ±7.9	32.4 ±8.6	10.254	0
CD68 [%]	36.9 ±13.5	41.2 ±12.3	14.528	0
$CD80^+$ [%]	23.5 ±11.3	29.8 ±10.2	9.635	0
$CD163^+$ [%]	24.5 ±12.2	30.6 ±9.5	8.524	0
Number of newborn smooth muscle fibers	2.5 ±0.8	3.2 ±0.9	3.065	0.031
Number of neuromuscular junctions	2.1 ±0.7	2.6 ±0.8	2.968	0.035

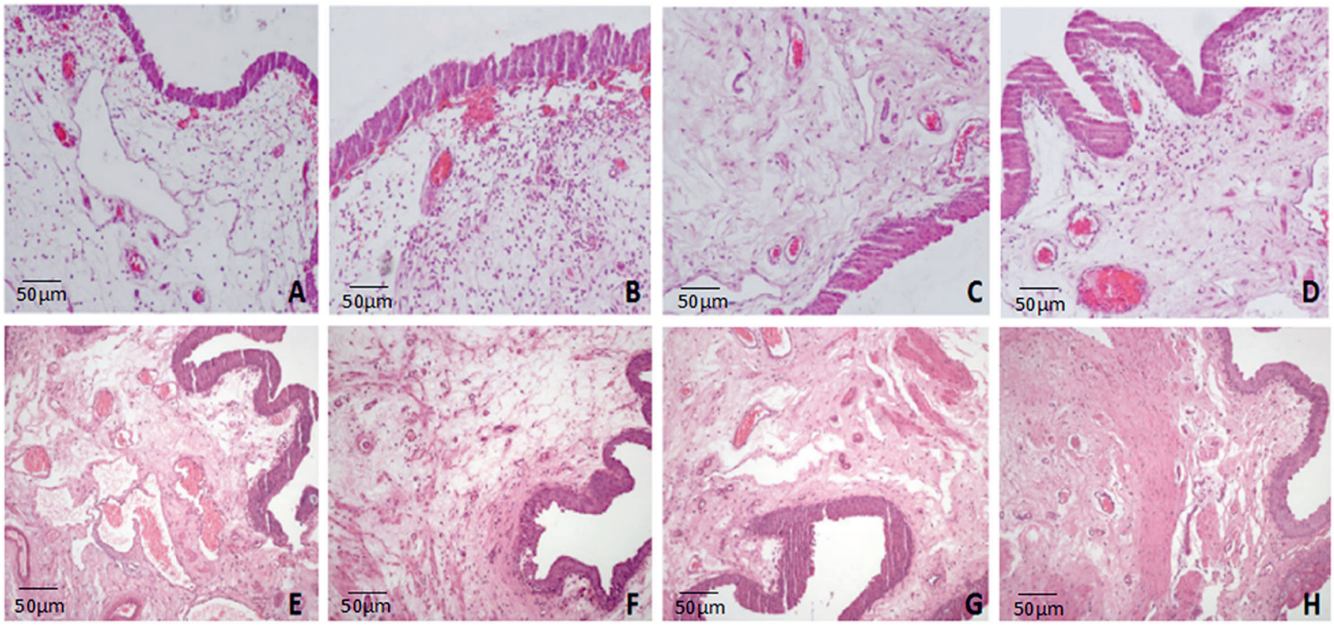

Fig. 4. H&E staining (×100); (A–D) epithelial regeneration was seen in the observation group 1, 2, 3, and 6 months after operation; (E–H) epithelial regeneration was seen in the control group 1, 2, 3, and 6 months after the operation

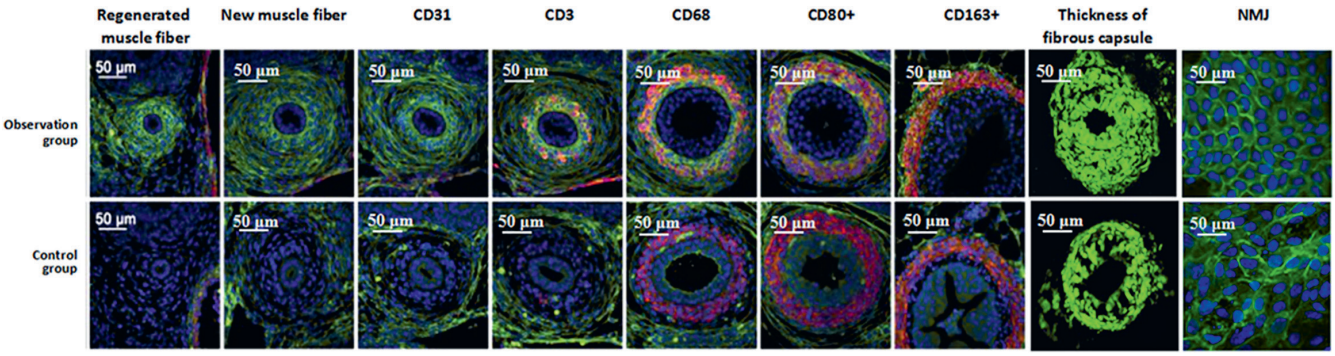

Fig. 5. Immunofluorescence detection of cell–material reaction in each group. Muscle fibers, CD31- and NMJ-positive shown in green; CD3-, CD68-, CD80$^+$-, and CD163$^+$-positive shown in red. The fluorescence intensity of the above index in the observation group was higher than that of the negative control group

1. The ECM does not contain high-antigenicity cell components obtained through special decellularization, and only retains low antigenic substances such as collagen, proteoglycan, glycoprotein, etc., which tend not to lead to rejection after transplantation.

2. This operation retains a complete three-dimensional space for cell survival and a full range of bioactive ingredients, which are conducive to cell nutrition, gas exchange and waste discharge.[6–12]

3. In addition, ECM can ensure enough biomechanical strength to meet the needs of tissue repair and reconstruction, can attract and regulate the growth and differentiation of host cells in the scaffold, and can form new self-tissue to complete the specific repair and functional recovery from defects.[13–17]

The transplanted stent needs not only to reduce the abnormal immune rejection and tissue proliferation, but also to promote a normal connection between an ECM stent and the surrounding normal ureteral tissue cells, and to increase vascularization.[18–20] The percentages of surrounding tissue wrapping, vascularization, infiltrating cells, and monocyte macrophages are commonly used to reflect the intensity of cell–material reaction between the stent and surrounding normal ureteral tissue. Our histopathological observation showed that there was no significant difference between the ureter regeneration in the repair area and the normal ureter tissue in the observation group after 3 months of treatment. Under the electron microscope, we found that the number of regenerated muscle fibers in the ureters had increased significantly, the thickness of the fibrous capsules had increased, the percentage of CD31, CD3, CD68, CD80$^+$, and CD163$^+$ had increased, the scope of new smooth muscle fibers had expanded, and the NMJ structure had increased ($p < 0.05$). Then, the stent was replaced by ureteral tissue 6 months after operation. Histological observation showed the growth

of a transitional epithelium and ureteral myometrium, a large number of blood vessels, and no inflammatory cells. These results are generally consistent with those of other studies.[21] They also show that the highly bioactive ECM scaffolds prepared by us are compatible with the surrounding tissues.

Conclusions

In conclusion, a highly bioactive ECM stent can be used to repair a ureteral defect effectively by regenerating local anatomical structure and physiological function, as an ideal material for ureteral reconstruction. However, we have not verified whether the highly bioactive ECM scaffold decomposes after replantation in vivo, and whether it also has certain promoting activity in local cells in vivo.

ORCID iDs

Lifeng Gu https://orcid.org/0000-0002-0980-4393
Xiaosong Fan https://orcid.org/0000-0002-4122-5906
Jiancheng Lu https://orcid.org/0000-0002-0093-5370
Bojun Li https://orcid.org/0000-0001-7471-7897
Weijie Xia https://orcid.org/0000-0002-6490-7483
Feiping He https://orcid.org/0000-0002-3411-9195
Jie Chen https://orcid.org/0000-0001-9388-2695
Weixing Yu https://orcid.org/0000-0002-9739-6659

References

1. Siddighi S, Yune JJ, Kwon NB, Hardesty JS, Kim JH, Chan PJ. Perioperative serum creatinine changes and ureteral injury. *Int Urol Nephrol.* 2017;49(11):1915–1919.
2. Choi YS, Lee SH, Cho HJ, Lee DH, Kim KS. Outcomes of ureteroscopic double-J ureteral stenting for distal ureteral injury after gynecologic surgery. *Int Urogynecol J.* 2018;29(9):1397–1402.
3. Ordorica R, Wiegand LR, Webster JC, Lockhart JL. Ureteral replacement and onlay repair with reconfigured intestinal segments. *J Urol.* 2014;191(5):1301–1306.
4. Tokhmafshan F, Brophy PD, Gbadegesin RA, Gupta IR. Vesicoureteral reflux and the extracellular matrix connection. *Pediatr Nephrol.* 2017;32(4):565–576.
5. Zhao Z, Liu D, Chen Y, et al. Ureter tissue engineering with vessel extracellular matrix and differentiated urine-derived stem cells. *Acta Biomater.* 2019;88:266–279.
6. Yi S, Ding F, Gong L, Gu X. Extracellular matrix scaffolds for tissue engineering and regenerative medicine. *Curr Stem Cell Res Ther.* 2017;12(3):233–246.
7. Lazica DA, Ubrig B, Brandt AS, von Rundstedt FC, Roth S. Ureteral substitution with reconfigured colon: Long-term follow-up. *J Urol.* 2012;187(2):542–548.
8. Kloskowski T, Kowalczyk T, Nowacki M, Drewa T. Tissue engineering and ureter regeneration: Is it possible? *Int J Artif Organs.* 2013;36(6):392–405.
9. Simaioforidis V, de Jonge P, Sloff M, Oosterwijk E, Geutjes P, Feitz WFJ. Ureteral tissue engineering: Where are we and how to proceed? *Tissue Eng Part B Rev.* 2013;19(5):413–419.
10. Sapora JA, Hardie RJ, Evans N. Use of a subcutaneous ureteral bypass device for treatment of bilateral proximal ureteral injury in a 9-month-old cat. *JFMS Open Rep.* 2019;5(1):2055116919831856.
11. Zhang J, Hu Z, Billiar TR, Badylak SF. Preparation of volumetric skeletal muscle whole organ acellular matrix to regenerate contractile, vascularized, innervated muscle in rodent and canine model. *J Am Coll Surg.* 2013;217(3):S145.
12. Song JJ, Guyette JP, Gilpin SE, Gonzalez G, Vacanti JP, Ott HC. Regeneration and experimental orthotopic transplantation of a bioengineered kidney. *Nat Med.* 2013;19(5):646–651.
13. Versteegden LR, van Kampen KA, Janke HP, et al. Tubular collagen scaffolds with radial elasticity for hollow organ regeneration. *Acta Biomater.* 2017;52:1–8.
14. Xiao S-W, Wang P-C, Fu W-J, Wang Z-X, Li G, Zhang X. Novel perfusion-decellularized method to prepare decellularized ureters for ureteral tissue-engineered repair. *J Biosci Bioeng.* 2016;122(6):758–764.
15. Murala JSK, Sassalos P, Owens ST, Ohye RG. Porcine small intestine submucosa cylinder valve for mitral and tricuspid valve replacement. *J Thorac Cardiovasc Surg.* 2017;154(3):e57–e59.
16. Guest JF, Weidlich D, Singh H, et al. Cost-effectiveness of using adjunctive porcine small intestine submucosa tri-layer matrix compared with standard care in managing diabetic foot ulcers in the US. *J Wound Care.* 2017;26(Suppl 1):S12–S24.
17. Zhang X, Fang Z, Cho E, et al. Use of a novel, reinforced, low immunogenic, porcine small intestine submucosa patch to repair a supraspinatus tendon defect in a rabbit model. *Biomed Res Int.* 2019;2019:9346567–9346567.
18. Chai Y, Xu J, Zhang Y, Zhang J, Hu Z, Zhou H. Evaluation of decellularization protocols for production of porcine small intestine submucosa for use in abdominal wall reconstruction. *Hernia.* 2019. doi:10.1007/s10029-019-01954-4.
19. Sous Naasani LI, Rodrigues C, Azevedo JG, Damo Souza AF, Buchner S, Wink MR. Comparison of human denuded amniotic membrane and porcine small intestine submucosa as scaffolds for limbal mesenchymal stem cells. *Stem Cell Rev Rep.* 2018;14(5):744–754.
20. Nherera LM, Romanelli M, Trueman P, Dini V. An overview of clinical and health economic evidence regarding porcine small intestine submucosa extracellular matrix in the management of chronic wounds and burns. *Ostomy Wound Manage.* 2017;63(12):38–47.
21. Bryant D, Holtby R, Willits K, et al. A randomized clinical trial to compare the effectiveness of rotator cuff repair with or without augmentation using porcine small intestine submucosa for patients with moderate to large rotator cuff tears: A pilot study. *J Shoulder Elbow Surg.* 2016;25(10):1623–1633.